Slope Failure in Cretaceous Clay Shale in Western Manitoba: A Case Study

by

Jeremy Fiebelkorn

A Thesis submitted to the Faculty of Graduate Studies of

The University of Manitoba

In partial fulfillment of the requirements of the degree of

MASTER OF SCIENCE

Department of Civil Engineering

University of Manitoba

Winnipeg

Abstract

Slope instabilities have been affecting the grade slope of Provincial Trunk Highway 5 near the junction with Provincial Trunk Highway 10 in northwestern Manitoba for over 50 years. In recent years, the instabilities have resulted in significant damage to the highway pavement surface. In 2011, Manitoba Infrastructure and Transportation initiated a geotechnical investigation to gain a better understanding of the failure, identify possible failure mechanisms, and explore various remedial design alternatives in order to stabilize the slope.

The site was instrumented with slope inclinometers and vibrating wire piezometers, and monitored over a period of two years. An extensive laboratory testing program was completed to compare the results of direct shear tests and torsional ring shear tests for determining the shear strength of the underlying Cretaceous clay shale. Measured values were compared with values back analyzed using limit equilibrium analysis. A coupled finite element model was used to model the expected excess porewater pressure response, and therefore the stability of the slope, during construction of a stabilization berm. It was subsequently calibrated to agree with the measured porewater pressure responses from the instrumentation. Finally, spring flood conditions were simulated to determine the effect of multiple flash flood events on the stability of the slope.

Acknowledgements

There are many people that contributed to the success of this case study. I would first like to thank the Department of Infrastructure and Transportation for the financial support I received over the three years that I've been working toward the completion of my Master of Science degree. In particular, Jeff Tallin and Said Kass of Materials Engineering Branch gave me much of their time and support. Their assistance is greatly appreciated.

My co-advisors, Dr. Marolo Alfaro and Dr. Jim Graham were extremely supportive in the technical aspects of the case study. Dr. Graham is a patient man, and really gave me the nudges I needed to finish my writing. He dedicated many hours to make sure that the work I produced was of the highest possible quality, and I am very proud of the results.

Dr. Lee Barbour with the University of Saskatchewan, and Dr. Curtis Kelln with Geo-Slope International Ltd., got to know how persistent I can be. Both were invaluable resources in the analysis of the project, and both gave me as much of their time and advice as I needed.

My family has always been supportive in whatever endeavors I've set out to accomplish, and the completion of this thesis is no exception. I am a very lucky son and brother.

Most importantly, I would like to thank my own little family. My son, Soren, gives me the strength and motivation I need to get through anything. I may never have made my way through this work without him. And of course his mother, Jacintha, has always been incredibly supportive. I don't think anyone wanted me to accomplish this more than her. I appreciate you both.

Thanks to all.

List of Figures

List of Tables

List of Copyrighted Material

Figure 2.3 – Quaternary Deposits in Southwestern Manitoba. Matile, G. and Keller, G. 2013.

Sand & Gravel Deposits along the Assiniboine Spillway: Sand and Gravel Deposits Image 1; Manitoba Geological Survey. http://www.manitoba.ca/iem/mrd/geo/demsm/sandgravel1.html

Reproduced from the Government of Manitoba with permission from Manitoba Mineral Resources (December 04, 2014). Copyright © 2013 Government of Manitoba.

Figure 2.4 – Elastic Stress-Strain Relationship

Budhu, M. 2007. Soil Mechanics and Foundations. 2nd Ed. John Wiley & Sons Inc. Hoboken, N.J.

Reproduced with permission from John Wiley & Sons Inc. (October 17, 2014). Copyright © 2007, 2000 John Wiley & Sons Inc.

Figure 2.5 – Elastic Perfectly Plastic Constitutive Relationship

Geo-Slope International Ltd. 2010. Stress-Deformation Modeling with Sigma/W: An engineering methodology. 4th ed.

Reproduced with permission from Geo-Slope International Ltd. (October 16, 2014). Copyright © 2008 by Geo-Slope International Ltd.

Figure 2.6 – Mohr Coulomb Failure Envelope

Budhu, M. 2007. Soil Mechanics and Foundations. 2nd Ed. John Wiley & Sons Inc. Hoboken, N.J.

Reproduced with permission from John Wiley & Sons Inc. (October 17, 2014). Copyright © 2007, 2000 John Wiley & Sons Inc.

Figure 2.7 – The Critical State Model

Budhu, M. 2007. Soil Mechanics and Foundations. 2nd Ed. John Wiley & Sons Inc. Hoboken, N.J.

Reproduced with permission from John Wiley & Sons Inc. (October 17, 2014). Copyright © 2007, 2000 John Wiley & Sons Inc.

Figure 2.8 – The State Boundary Surface

Graham, J., Crooks, J.H.A., Lau, S.L.K. 1988. Yield envelopes: identification and geometric properties. Geotechnique **38**: pp. 125-134.

Reproduced with Permission from ICE Publishing (December 12, 2014).

Figure 2.9 – Modified Cam-Clay Yield Surface

Geo-Slope International Ltd. 2010. Stress-Deformation Modeling with Sigma/W: An engineering methodology. 4th ed.

Reproduced with permission from Geo-Slope International Ltd. (October 16, 2014). Copyright © 2008 by Geo-Slope International Ltd.

Figure 2.10 – Soil Response to Shearing

Budhu, M. 2007. Soil Mechanics and Foundations. 2nd Ed. John Wiley & Sons Inc. Hoboken, N.J.

Reproduced with permission from John Wiley & Sons Inc. (October 17, 2014). Copyright © 2007, 2000 John Wiley & Sons Inc.

Figure 2.11 – Undrained Strength Envelope

Budhu, M. 2007. Soil Mechanics and Foundations. 2nd Ed. John Wiley & Sons Inc. Hoboken, N.J.

Reproduced with permission from John Wiley & Sons Inc. (October 17, 2014). Copyright © 2007, 2000 John Wiley & Sons Inc.

Figure 2.14 – Typical Bromhead Ring Shear Apparatus

Wykeham Farrance International. WF25850 Bromhead Ring Shear (User Manual). Berks, England. Date Unknown.

Reproduced with permission from Controls Group, Wykeham Farrance (October 21, 2014).

Figure 2.16 – Planar Failure in Infinite Slopes

Graham, J. 1984 Methods of stability analysis. Chapter 6 in "Slope Instability", Ed. D.Brunsden and D.B.Prior, Wiley Interscience, London, pp.171-215.

Figure 2.17 – Forces Acting on a Typical Isolated Slice

Graham, J. 1984 Methods of stability analysis. Chapter 6 in "Slope Instability", Ed. D.Brunsden and D.B.Prior, Wiley Interscience, London, pp.171-215.

Figure 2.18 – Parameters Used to Satisfy Force and Moment Equilibrium

Graham, J. 1984 Methods of stability analysis. Chapter 6 in "Slope Instability", Ed. D.Brunsden and D.B.Prior, Wiley Interscience, London, pp.171-215.

Figure 2.19 – Interslice Force Inclination Angle Distributions

Graham, J. 1984 Methods of stability analysis. Chapter 6 in "Slope Instability", Ed. D.Brunsden and D.B.Prior, Wiley Interscience, London, pp.171-215.

Figure 2.20 – FS vs λ for Varying f(x)

Graham, J. 1984 Methods of stability analysis. Chapter 6 in "Slope Instability", Ed. D.Brunsden and D.B.Prior, Wiley Interscience, London, pp.171-215.

Figure 2.21 – Limit Equilibrium and Finite Element Normal Stress Distributions Along a Slip Surface

Geo-Slope International Ltd. 2010. Stability Modeling with Slope/W: An engineering methodology. 4th ed.

Figure 3.8 – Cretaceous and Tertiary Geology in the Vicinity of the Study Area

Matile, G.L.D., Keller, G.R. 2012. Subsurface Phanerozoic geology of southern Manitoba, Transect 49 (5670870N). Manitoba Innovation, Energy and Mines, Manitoba Geological Survey, Stratigraphic Map SM2012-1.

Figure 3.12 – Geological Components of the Manitoba Escarpment

McNeil, D.H. 1977: The Cretaceous System in the Manitoba Escarpment; Ph.D. thesis, University of Saskatchewan.

Figure 3.13 – Study Area near the Base of the Manitoba Escarpment

Matile, G.L.D., Keller, G.R. 2007. Surficial Geology of Manitoba, Surficial Geology Compilation Map Series: SG-MB. Manitoba Science, Technology, Energy and Mines.

Figure 3.15 – Alluvial Deposits in Mineral Creek Valley

Matile, G.L.D., Keller, G.R. 2004. Surficial Geology Compilation Map Series: SG-62N. Manitoba Industry, Economic Development and Mines. Manitoba Geological Survey.

Figure 3.18 – Idealized Colluvium Deposition Following Valley Erosion

Turner, A.K., Schuster, R.L. (Transportation Research Board, National Research Council). 1996. Landslides: Investigation and Mitigation. National Academy Press. Washington, D.C.

Figure 7.6 – Interface Model Applied to a Line

Geo-Slope International Ltd. 2010. Seepage Modeling with Seep/W: An engineering methodology. 4th ed.

Chapter 1 – Introduction

1.1. Project Background

With an increasing number of slope failures affecting various forms of infrastructure on Manitoba highways, Manitoba Infrastructure and Transportation (MIT) began exploring the use of a Geohazard Management System to address the need to better prioritize respective geohazard sites and manage the associated risks to the provincial highway system. A Geographical Information Systems (GIS) model for managing this risk was presented to MIT in 2007, based on successful risk management systems used both in Alberta and Saskatchewan (Baldwin et al., 2007). While MIT has yet to adopt this GIS system, it has implemented a simpler risk management system modified from those used by Manitoba's western neighbours.

MIT currently has approximately 60 active geohazard sites. While these sites include such issues as culvert damage or highway pavement frost boils, the majority are classified as slope failures or landslides. MIT's Geohazard Management System assesses the risk of a particular site by assigning qualitative measures of probability of failure (PF) and consequence of failure (CF) based on experience and engineering judgment. An additional factor called the User Impact Rating (UIR) is determined from an assessment of such factors as annual average daily traffic (AADT), potential length of detour required, population affected, and the potential impact on emergency services. The UIR and PF are added, and then multiplied by the CF to assign a level of risk with respect to stability. This measure of risk assigns a numerical value that allows a particular site to be ranked, and therefore prioritized in relation to other geohazard sites in a particular region of the province. The site chosen for this case study has been ranked among those with the highest priority in northwestern Manitoba.

The site is located approximately 15 km west of Dauphin, MB (Figure 1.1), where Provincial Trunk Highway (PTH) 5 crosses the Mineral Creek valley. In late fall of 2007, a grade slope[1] failure was reported on PTH 5 near the junction of PTH 10, referred to herein as the Ashville Junction (Figure 1.2). At that time, the failure consisted of shoulder slumps affecting the pavement at two discreet locations (Figure 1.3). These slumps were re-graded and the pavement was patched intermittently as slope movements continued to occur. By late fall 2010, the area of pavement affected by the slope movements had grown considerably larger as cracks progressed in the pavement between the two slump locations and into the east bound travel lane (EBL) and southbound turning lane (Figure 1.4). In the spring of 2011, after extended periods of rainfall and subsequent flooding of the valley, the failure expanded into the EBL and resulted in partial lane closures of PTH 5 at the Ashville Junction (Figure 1.5). The failure had progressed such that re-grading and patching of the slumps was no longer feasible. Manitoba Infrastructure and Transportation initiated a geotechnical investigation of the site in order to better understand the failure.

Upon review of the site history, it was discovered that the Ashville Junction slide has been affecting PTH 5 for over 50 years. In 1964, four test holes were drilled at the site when Regional staff reported slope movements. At that time, it was noted that a saturated layer of blue-white bentonite may have led to the instabilities. Figure 1.6 is a sketch of the cross section at the failure area prepared at that time and shows the relative test hole locations. The location of this cross section relative to the current study area is unclear, as there is no available reference point for the stationing used at that time. Following the site investigation, several geotechnical recommendations were made to improve the stability of the slope. In 1965, surface drainage works were completed in an attempt to divert runoff from the site into Mineral Creek a few hundred metres west of the reported failure (Figures 1.7 and 1.8).

[1] Grade slope refers to slopes below the grade of an existing roadway

Recommendations were also made to bench cut and re-compact disturbed soils, construct a toe berm, and install subsurface drainage, but records do not indicate that any of these options were completed.

The failure was reactivated in 1974. A survey of the site revealed multiple scarp lines, consistent with retrogressive failure, along the grade slope from the south shoulder of PTH 5 down to the toe (Figures 1.9 and 1.10). Three additional test holes were drilled at the site, again revealing a blue-white layer of bentonite in the shale. Figure 1.11 is a 1974 sketch of a cross section showing some proposed stabilization options, as well as the general stratigraphy at each of the test hole locations. The bentonite was again identified as the cause of the failure and several recommendations to improve stability were made. At that time, small cracks were observed in the highway pavement surface.

In 1993, the intersection was widened to improve site lines and add the east bound through lane. In doing so, the highway was raised by up to 0.75 m in order to meet then-current MIT highway design standards, thereby loading the crest of the side slope shown in Figures 1.9 and 1.10. Figure 1.12 shows the pre and post-construction cross sections at the failure location. The toe of the slope at the most critical section of the failure now lies approximately 9 m below the existing pavement elevation, and the grade slope varies between 5H:1V and 7H:1V. Following reconstruction of the intersection, the failure continued to expand until it was observed in the fall of 2007 that the pavement was being significantly affected.

1.2. Hypothesis

Intermittent flash flooding of the Mineral Creek valley, associated increases in porewater pressures, and subsequent drawdown of the floodwaters led to down slope creep movements that caused a reduction in shear strength in the grade slope. Over a period of approximately 50 years, repeated shear straining following flood events reduced the shear strength to residual values and caused the grade slope to fail retrogressively toward PTH 5.

1.3. Objectives

An investigation to determine the cause of failure was initiated by MIT in 2010. Following the investigation, MIT's regional office in Dauphin, MB requested remedial design alternatives to repair the failure. The objective of the case study reported in this document is to examine the effect of cyclic flash flood events as a slope failure mechanism, and provide an effective design alternative to prevent further failure and damage to PTH 5.

The case study of the Ashville Junction Slide involved an extensive review of relevant publications on slope stability analysis, particularly involving the use of finite elements for establishing internal stress distributions in the slope. The study examined changing porewater pressures caused by the transient effects of flooding at the toe of the slope, and how this may have influenced the failures observed at the site. The author was responsible for a program of drilling, sampling, instrumentation and construction at the site. A laboratory testing program was undertaken that included the use of a torsional ring-shear device for measuring residual strength on the slide surface; an apparatus that had not been used at the University of Manitoba

prior to this study. The project also involved extensive informal discussions with independent researchers on the hydrogeology of the site. These discussions lead to what is believed to be the first application in Manitoba of using field piezometer data to identify not only porewater pressures, but also estimates of elastic stiffness properties in the geological materials in the slope.

Stabilizing measures were identified and constructed on the basis of the author's studies. Construction was completed in November, 2013, and the stabilizing measures have performed well since that time.

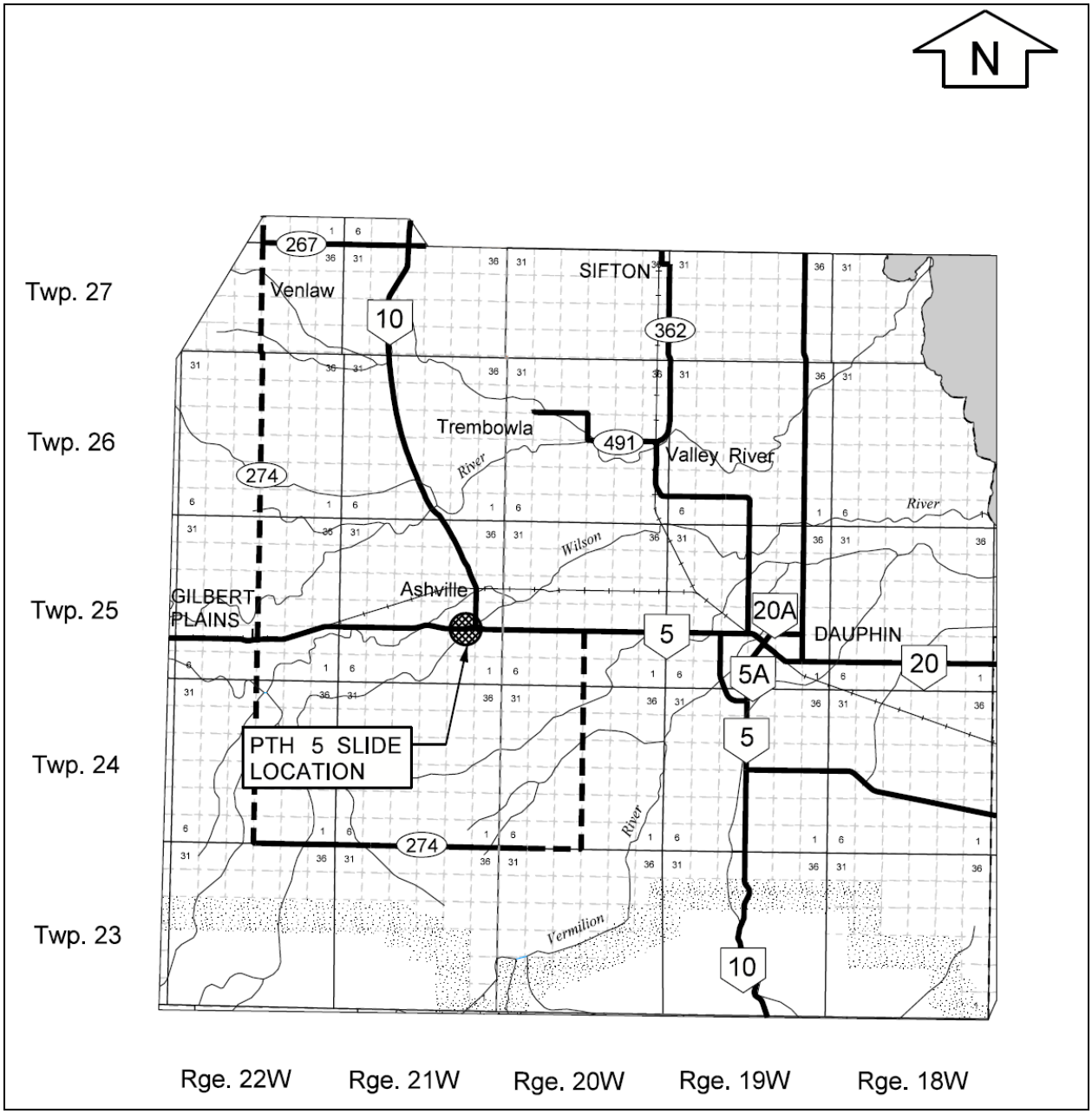

Figure 1.1 – Project Site Location

Figure 1.2 – Ashville Junction Site Plan

Figure 1.3 – October 2007, Shoulder Slumps in Shoulder of EBL

Figure 1.4 – November 2010, Progression of Pavement Cracking in EBL

Figure 1.5 – June 2011, Partial Lane Closure of PTH 5 EBL

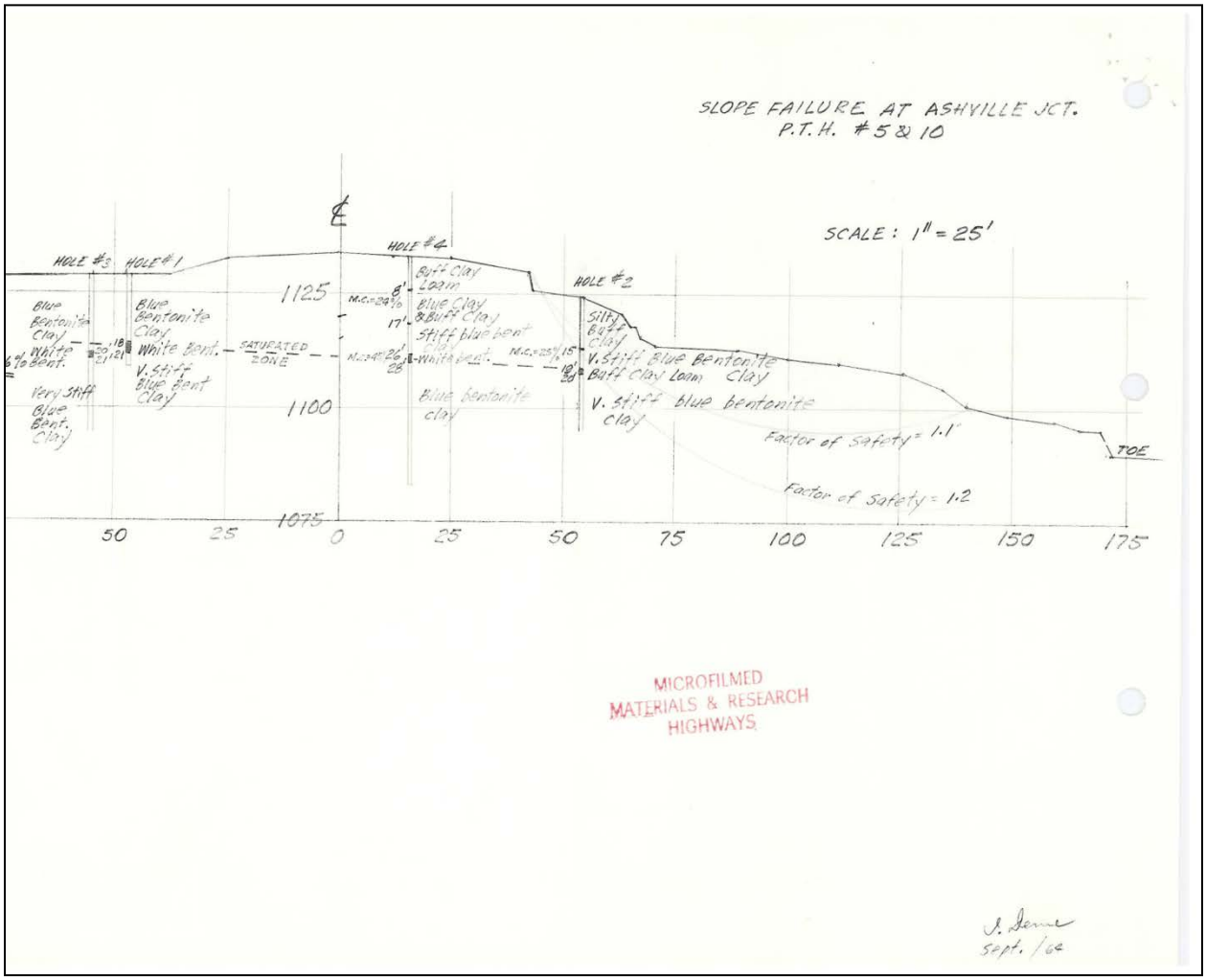

Figure 1.6 – 1964 Sketch of Cross Section at Failure Area

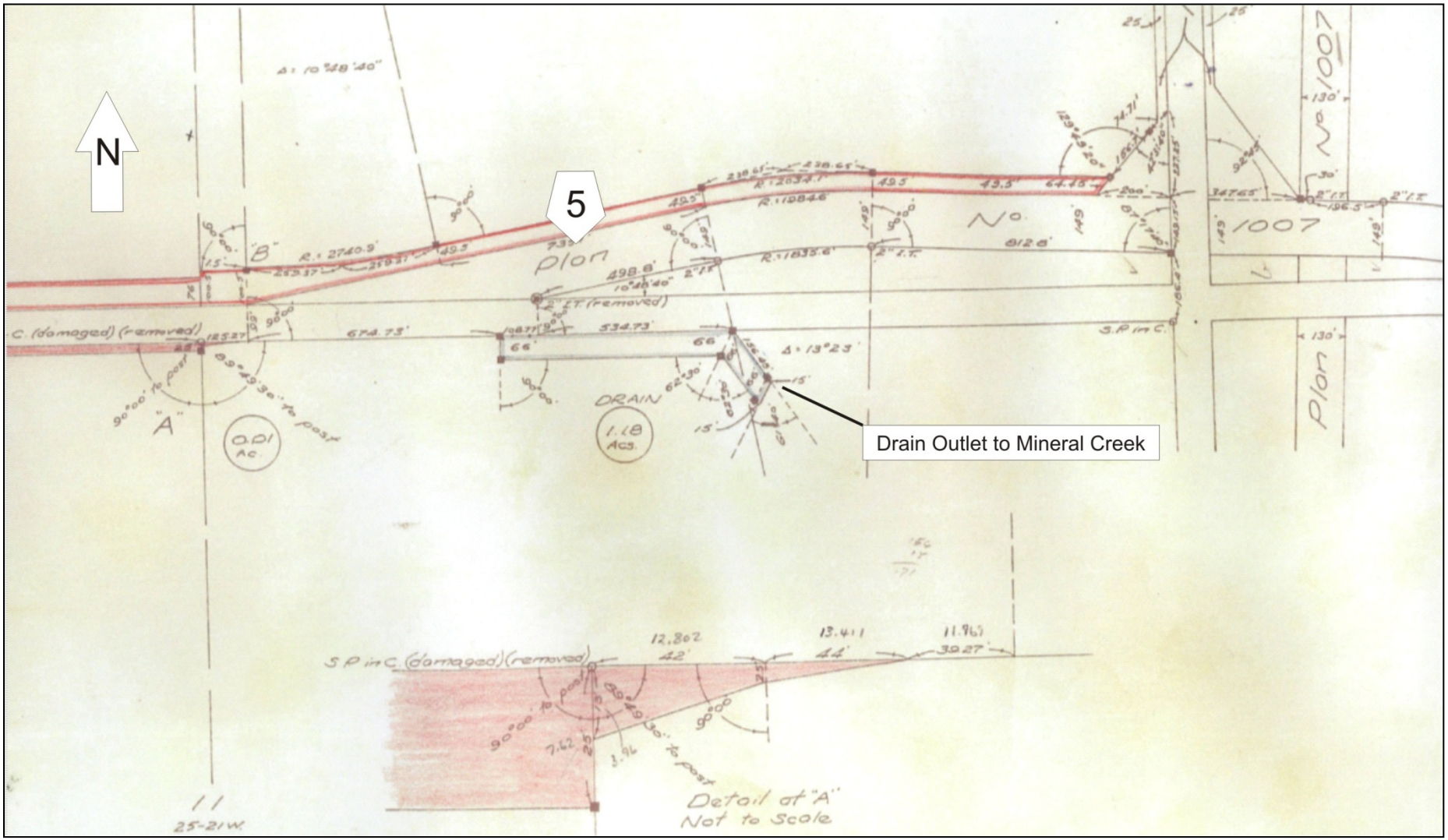

Figure 1.7 – 1965 Proposed Drainage Works West of Existing Failure (See Figure 1.2 for drain location)

Figure 1.8 – 1965 Drain Eroded into Mineral Creek Valley Wall (North from drain outfall at Mineral Creek)

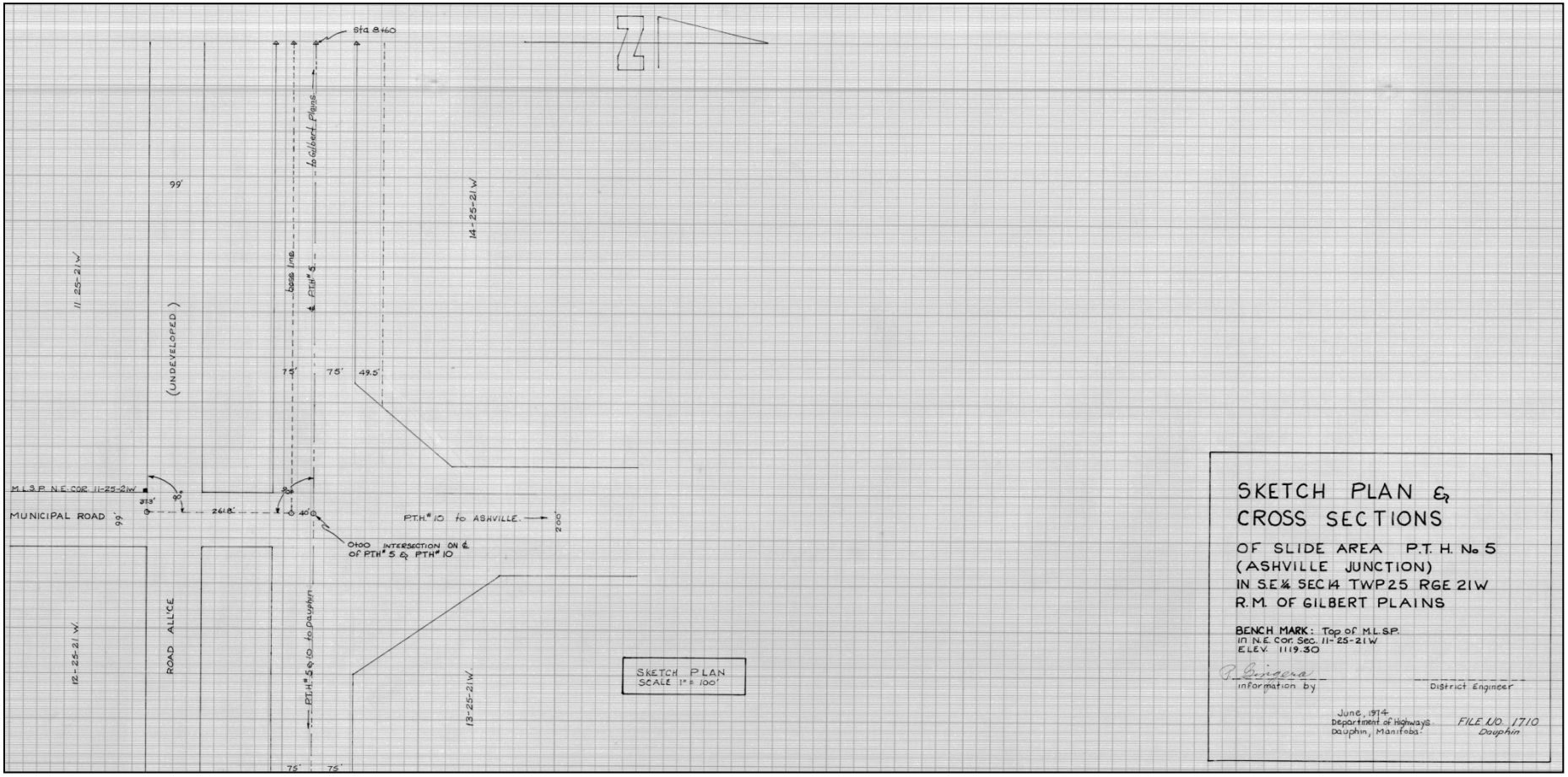

Figure 1.9 – 1974 Ashville Junction Site Plan (Note - scale is in feet)

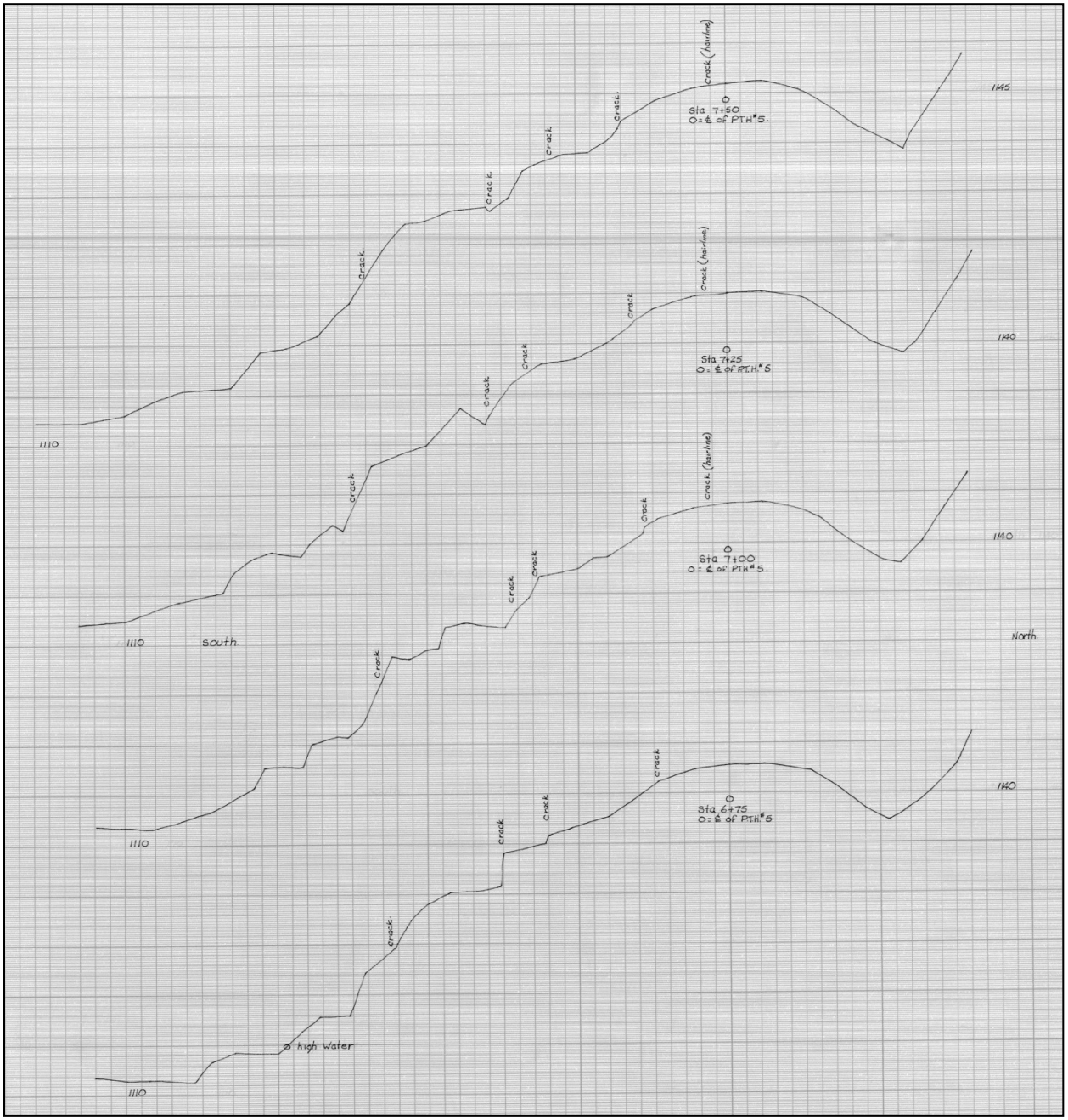

Figure 1.10 – 1974 Ashville Junction Cross Sections (Note – station 0+00 at centerline of intersection between PTH 5 and PTH 10)

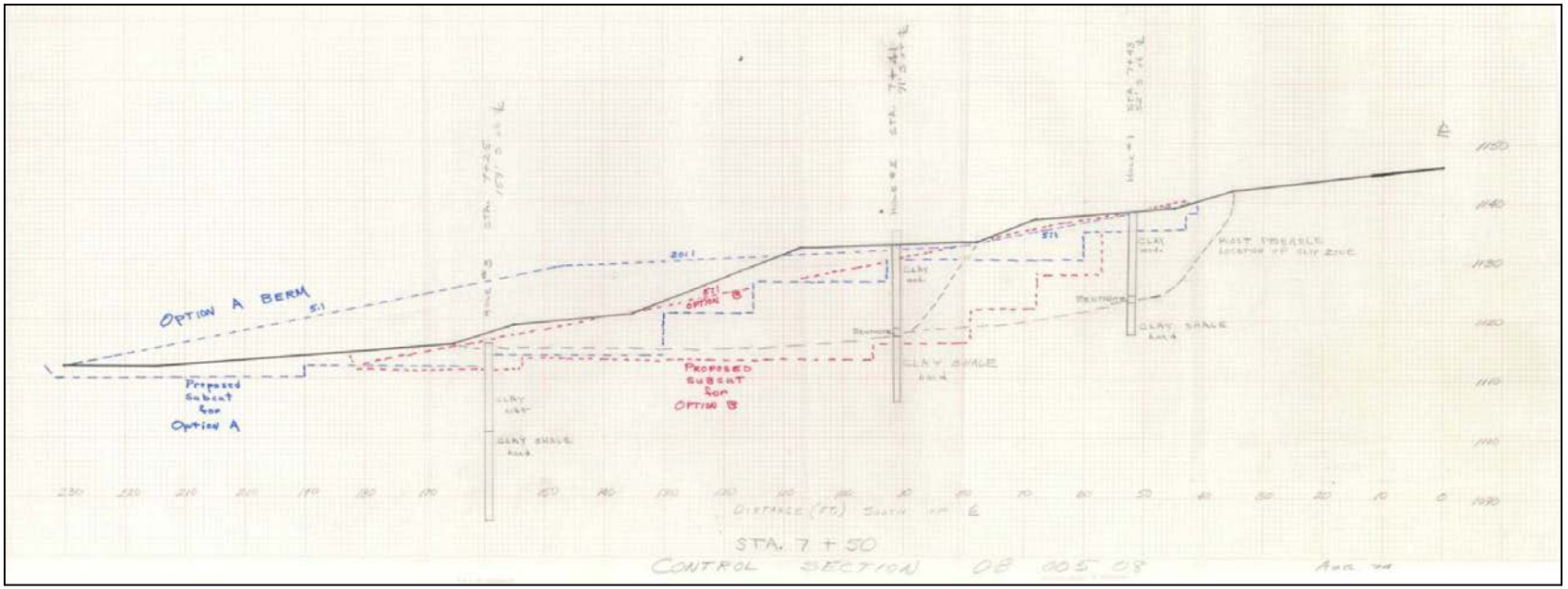

Figure 1.11 – 1974 Cross Section with Proposed Stabilization Options

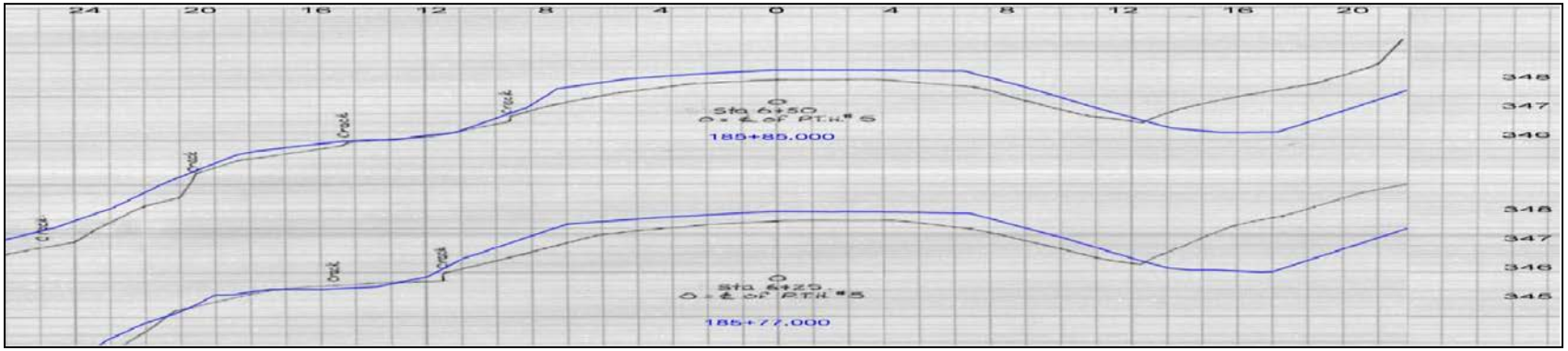

Figure 1.12 - 1993 Pre and Post-Construction Cross Section at Failure Area (Post-construction shown in blue)

Chapter 2 – Literature Review

2.1. Slope Instabilities in the Prairie Landscape

Analysis of landslides in the prairie provinces involves the evaluation of varying porewater pressure distributions and changing climatic conditions, as well as investigating the potentially complex geological history of a particular site in order to understand the various mechanisms that may lead to failure in natural slopes. Whereas a degree of engineering control is inherent in engineered slopes, there is none in a naturally occurring slope. As such, the remediation of these natural slopes is a significant aspect of geotechnical engineering practice.

While similarities in landscape exist among the three prairie provinces, there are also some marked differences in the geology and geomorphology between them. These must be identified and understood in order to effectively analyze landslides in various regions. In Alberta, east of the Rocky Mountains, deep and relatively steep valleys have been cut into till or glacio-fluvial deposits. The valley walls are subject to significant slope movements, particularly when the valley is cut into clay shale deposits containing bentonite or coal through erosion or construction processes (Moe et al., 2009). There are more obvious similarities between the landscapes of southern Saskatchewan and Manitoba. The discussion of landslides in the prairie landscape will therefore concentrate on these two provinces.

Following the retreat of the pro-glacial lakes in western Canada, much of southern Saskatchewan and western Manitoba was marked with broad, deep valleys as remaining glacial melt-water eroded significant portions of the prairie landscape. The valleys of the North and

South Saskatchewan Rivers have been eroded into deposits of Cretaceous clay shale, and continuous irregularities occur along the slopes of the valley walls (Kelly et al., 1995). While these irregularities were once thought to be the result of glacial or colluvial deposition over the valley walls, it is now understood that they are in fact the result of post-glacial slope movements[2]. Shearing of these deposits during glaciation, as well as earlier regional tectonism, has created "gouge zones" that often contain thin layers of bentonite. These gouge zones are irregularities along which the soil strength parameters have been reduced from peak values to residual values. The residual strength friction angles (ϕ'_r) of the Cretaceous (Bearpaw) clay shales in this region have been back analyzed to values as low as 6.5° at the Deer Creek Bridge Landslide (Kelly et al., 1995), or 6.8° at the Denholm Landslide (Sauer, 1983).

Many of the landslides along the valley walls of this region occur retrogressively as a result of erosion at the toe of the slope dating back as far as 11, 500 years ago (Sauer et al., 1986). While many of these slides are currently inactive, or have rates of movement that cannot be detected through visual observation, they are only marginally stable and could be reactivated with minimal disturbance (Sauer, 1982). Failures occurring at the interface of Cretaceous and Quaternary deposits are relatively common in this region (Kelly et al., 1995).

In Manitoba, west of the Manitoba Escarpment, the landscape is quite similar to that of southern Saskatchewan. The prairies here are scarred with relatively large valleys left by post-glacial river erosion, many of which have been cut into Cretaceous clay shale. Concerns about slope instability have been reported in the clay shales of this region of Manitoba, although none have been studied in as much detail as those in southern Saskatchewan. There are, however, some relatively large valleys in this region that are not cut into shale, but have been eroded only into

[2] Personal Communication, J. Graham, 2013

the Quaternary deposits overlaying the shale. The Shell River valley is one such occurrence in which the valley has been eroded into very dense clay till deposits, interlayered with alluvial sediments, overlaying Cretaceous sediments (Manitoba Infrastructure and Transportation, 2013).

The Shell River Slide at the intersection of PTH 83 and the Shell River valley is one of Manitoba's largest active landslides affecting highway infrastructure. Manitoba Infrastructure and Transportation has estimated that the most recent landslide at this location displaced approximately 4,000,000 cubic metres (m^3) of the valley wall (Figures 2.1 and 2.2)[3]. Although it is likely that the slope first failed many years before construction of PTH 83, its continued movement is believed to be the result of fluctuations in porewater pressures within the complex geology of the slope. Manitoba Infrastructure and Transportation is currently working on the feasibility of stabilization measures for this large landslide.

Many of the valley walls in this region are comprised of till or till-like Quaternary deposits (colluvium), which are generally clay rich west of the escarpment and originate from Mesozoic clay shale (Matile et al., 2004; Klassen, 1979). Shallow slope instabilities may also occur in this region due to a loss in matric suction following periods of prolonged precipitation (Blatz et al., 2004). Transient numerical analysis of such sites in this region has shown that slopes which have remained stable for many years can become marginally stable or fail when the suction component of soil shear strength is lost due to elevated porewater pressures induced by extended periods of precipitation.

[3] Personal Communication, J. Tallin, 2013

The Assiniboine “spillway” crosses the Manitoba Escarpment in southwestern Manitoba. Figure 2.3 illustrates that much of western Manitoba east of the escarpment is covered in deltaic deposits (the Assiniboine Delta) through which relatively broad valleys have been cut (Manitoba Geological Survey, 2013). Instabilities in the walls of these valleys may occur as a result of changes in porewater pressure, erosive processes following low frequency precipitation events, or in over-steepened cuts made during highway construction. The till originates from dolomitic limestone from the north-east and is generally silt rich and calcareous. (Matile et al., 2004; Klassen, 1979).

Near the base of the escarpment, till-like colluvium covers many of the valley walls and overlays Cretaceous sedimentary deposits which outcrop at various locations. The Ashville Junction study area lies within this region. Instabilities on or near the Manitoba Escarpment have been observed to occur in weakened layers within Cretaceous clay shale deposits; in shear zones well defined by the presence of thin layers of bentonite; at the interface of Cretaceous and Quaternary deposits; or within the Quaternary deposits alone as a result of changing porewater or climatic conditions.

Much of southern Manitoba outside the Assiniboine Delta consists of glacio-lacustrine deposits of high plastic clay. Many instabilities have occurred in riverbank slopes cut into these deposits. These failures are largely retrogressive in nature, occurring as a result of erosion at the toe of the riverbank, or possibly the deposition of sediment causing additional crest loading to marginally stable slopes (Pauls et al., 1999). Transient porewater pressures and aquifer potentials have also been reported to cause instabilities in such riverbank deposits (Tutkaluk et al., 2002). While slope failures in highly plastic clay are an important geotechnical

consideration, particularly in Manitoba, this case study will focus only on failures in the Cretaceous clay shales and Quaternary deposits of western Manitoba.

2.2. Strength Properties of Soils

2.2.1. Constitutive Models

There are several common constitutive models available to predict soil behavior. The linear elastic, elastic plastic, Cam-Clay, Modified Cam-Clay and hyperbolic constitutive models are some of the more common methods used in geotechnical software for numerical modeling purposes. This study will focus on the linear elastic, elastic-plastic, and modified Cam-Clay constitutive models, as these are the most suitable models for the types of analyses that are required.

The selection of an appropriate model for a particular geotechnical problem depends on the stress state of the soil. That is, the stresses that are applied to an element of soil at a given point (Budhu, 2007). It is good practice to begin an analysis with a relatively simple, linear elastic constitutive model, and then add complexity to the model if the analysis warrants it (Geo-Slope International Ltd., Sigma/W, 2010). Linear elasticity implies that the relationship between stress, σ, and strain, ε, is linear, and that all strains induced by some applied stress are elastic, and therefore completely recoverable. Stress and strain are therefore proportional, and related by a constant; Young's Modulus, E. Figure 2.4 graphically illustrates the relationship between σ and ε for both linear and non-linear elastic materials under some applied stress. Mathematically, the relationship can be shown as:

$$\begin{Bmatrix} \sigma x \\ \sigma y \\ \sigma z \\ \tau xy \end{Bmatrix} = E / [(1 + \nu)(1 - 2\nu)] \begin{bmatrix} 1-\nu & \nu & \nu & 0 \\ \nu & 1-\nu & \nu & 0 \\ \nu & \nu & 1-\nu & 0 \\ 0 & 0 & 0 & (1-2\nu)/2 \end{bmatrix} \begin{Bmatrix} \varepsilon x \\ \varepsilon y \\ \varepsilon z \\ \gamma xy \end{Bmatrix} \quad \text{Eq. 2.1}$$

Here, the stress tensor is made up of the normal stresses, σ_x, σ_y, and σ_z in the x, y, and z directions, respectively, and the shear stress, τ_{xy} in the x and y directions. The strain tensor is made up of normal strains in the x, y and z directions, denoted by ε_x, ε_y, and ε_z, respectively, and the shear strain, γ_{xy} in the x and z directions. The ratio of the lateral and vertical strains, Poisson's ratio, is denoted by ν in the stiffness matrix (Geo-Slope International Ltd., Sigma/W, 2010). Finite elements can be used to model the relationship between stress and strain. Sigma/W from Geo-Slope International Ltd., uses a two dimensional plane strain analysis, and ε_z in Equation 2.1 is therefore zero.

The linear elastic model is simplistic, but can be applied to many geotechnical problems, particularly for overconsolidated soils that have a preconsolidation pressure, σ'_c, much greater than the anticipated stresses due to loading. For lightly overconsolidated or normally consolidated soils, yielding may occur and a more rigorous constitutive model that incorporates plastic deformations following yielding may be necessary.

When yielding occurs in a soil, the induced strains are made up of two components; elastic, recoverable strains, and plastic, non-recoverable strains. Among other options, Sigma/W uses an elastic-perfectly plastic constitutive model, in which the soil behaves as a linear elastic material until yielding, or failure, is reached. Once failure occurs, large strains can be incurred with no increase in stress, and thus the soil behaves as a perfectly plastic material with no strain

hardening or strain softening (Geo-Slope International Ltd., Sigma/W, 2010). Figure 2.5 graphically illustrates this constitutive relationship.

The condition of yielding in the elastic-perfectly plastic model is represented by the Mohr-Coulomb failure criterion (Craig, 2004):

$$\tau_f = \sigma'_f \tan\phi' + c' \qquad \text{Eq. 2.2}$$

Here, σ'_f represents the normal stress on a failure plane, τ_f is the shear stress on the failure plane, ϕ' is the friction angle, and c' is the effective cohesion. Stresses on this failure plane are written mathematically as (Budhu, 2007):

$$\sigma'_f = [(\sigma_1' + \sigma_3')/2] - [(\sigma_1' - \sigma_3')/2]\sin\phi' \qquad \text{Eq. 2.3}$$

$$\tau_f = [(\sigma_1' - \sigma_3')/2]\cos\phi' \qquad \text{Eq. 2.4}$$

Here, σ_1' and σ_3' are the principal stresses at failure. In an elastic-plastic constitutive model, these are the stresses at which yielding occurs and plastic strain increments begin to develop. Figure 2.6 graphically illustrates the Mohr-Coulomb strength envelope. Stress states beyond the failure states required by the Mohr-Coulomb failure criterion, are inaccessible stress states, as, noted in the shaded area in the figure.

Regardless of the current stress state in a soil, yielding will occur at a defined boundary, called a yield locus (Budhu, 2007, Wood, 2004). This yield locus is defined by the preconsolidation

pressure, σ'_c. If a soil is normally consolidated, its current stress state lies on this boundary and any additional stress will cause the soil to behave as an elastic-plastic material. For an overconsolidated soil, the in-ground stress state lies within this boundary, and the soil behaves initially as an elastic material until loading takes the in-ground stress to the yield locus. The Critical State Model can be used to explain yielding in this way (Wood, 1990). The principal stresses, σ_1', σ_2' and σ_3' can be expressed in terms of:

$$p' = (\sigma_1' + \sigma_2' + \sigma_3')/3 \qquad \text{Eq. 2.5}$$

$$q = \sigma_1' - \sigma_3' \qquad \text{Eq. 2.6}$$

Here, p' is the mean effective stress and q is the deviatoric stress. The preconsolidation pressure is then written as p'_c. The stress state can then be defined in p', q, V space, where V is the specific volume written in terms of the voids ratio, e, as:

$$V = 1 + e \qquad \text{Eq. 2.7}$$

Figure 2.7 shows the Critical State Model expressed in p', q, V space. The non-linearity observed in natural soils is demonstrated in V, p' space (shown in the figure as e, p' space), but plots linearly in V, lnp' space. Soil behavior can then be described by a three dimensional yield surface relating stress changes to volumetric strain, called the state boundary surface (Figure 2.8). In the Critical State Model, failure is defined by the critical state line (CSL) and is shown mathematically as:

$$q_f = Mp'_f \qquad \text{Eq. 2.8}$$

In the elastic perfectly plastic constitutive model, failure occurs when the stress state of a soil element reaches the boundary defined by the critical state line. In q, p' space, the Mohr-Coulomb failure envelope is defined by M, which is the slope of the critical state line and is defined in terms of the critical state friction angle, ϕ'_{cs}, as:

$$M = (6\sin\phi'_{cs}) / (3 - \sin\phi'_{cs}) \qquad \text{Eq. 2.9}$$

Figure 2.7 shows that the Critical State Model can be used to predict changes in volume, or volumetric strains, ε_v. However, plastic strains that develop when yielding occurs are comprised of two components; ε_v, and shear strains, ε_s. Plastic strains can be defined incrementally by vectors with the Associated Flow Rule. In Associated Flow, the resultant vector of the plastic strain increments, $\delta\varepsilon_v$ and $\delta\varepsilon_s$, occurs in a direction normal to the yield locus. The Modified Cam-Clay constitutive model is formulated to predict soil deformations comprised of both volumetric and shear strain components using this rule (Wood, 1990).

Modified Cam-Clay is a Critical State Model that incorporates strain hardening, or the expansion of the elastic region, in the prediction of soil behaviour. The model can be used to simulate strain softening, but generally seems to under-predict the strain softening observed in natural clays and is therefore generally used for normally consolidated or lightly overconsolidated soils[4]. The formulation of the Modified Cam-Clay model is based on several assumptions. Firstly, the model uses the Associated Flow Rule, as described above. Additionally, elastic materials behave isotropically and straining is uncoupled as shown by the following relationship:

[4] Personal Communication, J. Graham, 2014

$$\begin{bmatrix}\delta p' \\ \delta q\end{bmatrix} = \begin{bmatrix}K' & - \\ - & 3G\end{bmatrix}\begin{bmatrix}\delta \varepsilon v \\ \delta \varepsilon s\end{bmatrix} \quad \text{Eq. 2.10}$$

Here, K' is the bulk modulus and G is the shear modulus. Equation 2.10 implies that only changes in mean effective stress induce changes in volumetric strain, and only changes in deviatoric stress induce changes in shear strain (Graham and Houlsby, 1983).

The third assumption in this model is that for a particular preconsolidation pressure, the yield locus is elliptical. Figure 2.9 graphically illustrates the assumed yield surface in p', q space for the Modified Cam-Clay model. Because the elasticity is assumed to be isotropic, the assumed ellipse plots as a straight line in lnp', V space with slope, κ (Figure 2.7). The model also assumes that plastic hardening can be defined by the normal consolidation line, which plots linearly in lnp', V space with slope, λ (Figure 2.7). The yield surface shown in Figure 2.9 is defined mathematically as:

$$q^2 = M^2 p' p'_c - M^2 p'^2 \quad \text{Eq. 2.11}$$

Finally, peak, or large strain failure is defined by the critical state line with slope, M, as described above. In Modified Cam-Clay, critical state is reached when shear straining produces no changes in mean effective stress, deviatoric stress, volume, or porewater pressure. This is shown mathematically as:

$$\delta p'/\delta \varepsilon_s = \delta q/\delta \varepsilon_s = \delta \varepsilon_v/\delta \varepsilon_s = \delta u/\delta \varepsilon_s = 0 \quad \text{Eq. 2.12}$$

Sigma/W allows use of the above constitutive relationships to satisfy the condition of equilibrium in the finite element model. The general equation for equilibrium used by Sigma/W is:

$$[K]\{\delta d\} = \{F\} \quad \text{Eq. 2.13}$$

where:

$$[K] = [B]^T[D][B] \quad \text{Eq. 2.14}$$

Here, $\{\delta d\}$ is the incremental displacement tensor and $\{F\}$ is the external force tensor. The stiffness matrix, [K], is comprised of the strain matrix, [B], and the drained constitutive matrix, [D]. A more detailed description of the mathematics used by Sigma/W for the constitutive relationships described above can be found in Geo-Slope International, Ltd, Sigma/W 2010.

2.2.2. Shear Strength of Soils

The concept of shear strength was discussed briefly in the previous section, and will be discussed in more detail here. The shear strength measured for a particular soil is not an exclusive parameter, but is dependent on such factors as the type of test completed, the stress level, the strain rate, and if the soil is in drained or undrained conditions. Shear strength is largely influenced by soil type, stress history and water content. It is described by the Mohr-Coulomb relationship in Equation 2.2, which shows that a reduction in effective stress due to increases in porewater pressure will result in a reduction in shear strength. However, this relationship must be modified to reflect the soil type or the loading conditions required (Graham, 2006). Figure 2.10 illustrates the stress strain behavior of various soil types.

Cohesionless soils, such as sands, can be described by the Mohr-Coulomb relationship, but shear stress is solely a function of the normal stress, σ'_n, and effective friction angle as:

$$\tau_f = \sigma'_n \tan\phi' \qquad \text{Eq. 2.15}$$

The strength envelope for the above condition can be represented by line AG in Figure 2.6. Conversely, if the required conditions are for quick, undrained loading, the soil is considered frictionless and the friction term in Equation 2.2 goes to zero, giving:

$$\tau_f = c_u \qquad \text{Eq. 2.16}$$

Here, the shear strength is represented by a constant value, c_u, and is interpreted as the undrained shear strength[5]. Figure 2.11 illustrates the strength envelope for a soil in undrained conditions from a constant depth. The undrained shear strength in a given soil stratum generally varies with depth and water content (Budhu, 2007). As modern analysis, particularly in numerical modeling, generally uses effective stresses for reliability, undrained shear strength will not be discussed in further detail.

As mentioned, shear strength is largely dependent on stress history and porewater pressure. Consolidated, undrained (CIŪ) triaxial tests directly measure soil strength with varying porewater pressure, and can provide information on the stress history in terms of effective stress parameters. Post-peak strength (Fig 2.12) occurs when any cementation bonds have been broken, but the orientation of soil particles is still relatively random. Once large strains

[5] J. Graham, Unpublished Course Notes - Soil Properties and Behaviour, 2013

have occurred and the soil particles become aligned, the residual shear strength of the soil is reached.

Figure 2.13 illustrates typical strength envelopes for overconsolidated, normally consolidated and residual strength conditions. The overconsolidated line represents the peak strength of an overconsolidated soil prior to strain softening toward critical state. The peak strength in soil is attributed to the random orientation of the particles of which it is comprised, as well as cementation of these particles through natural processes (Graham, 2006). Peak strength envelopes determined from samples of overconsolidated soils taken at different depths will plot parallel to one another. Once the stresses have reached critical state, the overconsolidated lines meet the normally consolidated line, which defines the normally consolidated, or post-peak strength envelope. The post-peak strength envelope represents critical state in the Critical State Model.

The residual strength envelope defines the minimum strength that can be relied on, particularly when engineering previously failed slopes[6]. Work by Skempton (1964) showed that the cohesion term in the shear strength equation, c'_r, was negligible, and residual strengths rely primarily on the friction component, ϕ'_r. Locally however in Manitoba, a relatively small cohesion component is generally included, particularly in the analysis of deep seated failures. Without this term, critical slip surfaces determined through slope stability analysis may appear more shallow and planar than what may be observed through instrumentation (Graham, 1984). Slope stability analysis will be discussed in more detail in Section 2.7. Figure 2.12 illustrates a typical stress-strain relationship for the peak, post-peak (critical state) and residual strengths for a given soil.

[6] J. Graham, Unpublished Course Notes, Soil Properties and Behaviour, 2013

There are several common methods used for determining residual strength parameters. Back analyzing previously failed slopes is a common method made relatively easy with modern numerical analysis. Once the geology and geometry of the slope, as well as a reasonable estimate of the porewater pressure distribution have been established, the solution for a known failure surface is searched until a state of limiting equilibrium is reached (Graham, 1984). Limit equilibrium will be discussed in more detail in Section 2.7. While back analysis of residual shear strength parameters is useful, it is always prudent to augment the results with laboratory test results. This is especially true because of the need to estimate porewater pressures in the failing slope.

Direct shear testing is the oldest test method used, and is especially suitable for testing stiff clays and shales (Terzaghi et al., 1996). However, determining residual shear strength parameters requires large strains which, in the direct shear test, requires multiple reversals of the shearing apparatus and this may not truly represent the displacements along a failure plane. The torsional ring shear test has the advantage of continuous, unidirectional straining of a specimen, although obtaining an intact specimen to fit the ring apparatus is difficult. Stark and Vettel (1992) and Stark and Eid (1994), successfully used the torsional ring shear apparatus with reconstituted specimens for determining residual shear strength values. As clay shale can be extremely difficult to trim, and local sampling methods do not facilitate the required geometry for an intact sample, only reconstituted specimens are suitable for the torsional ring shear tests in this study. Testing reconstituted specimens is acceptable for determining residual strengths[7].

The ring shear apparatus (Figure 2.14) is relatively rare in Canadian universities. The machine at the University of Manitoba is being used for the first time in this project. It tests a confined

[7] Personal Communication, J. Graham, 2014

annular specimen with an inner diameter of 70 mm and an outer diameter of 100 mm. A 5 mm thick, reconstituted specimen is radially confined within this area, and is vertically compressed between loading platens by way of a load hanger. The load hanger transfers the desired normal stress to the specimen through a loading arm. Consolidation is measured by a linear variable displacement transducer (LDVT) positioned on top of the loading hanger. The loading platens are porous to facilitate drained conditions. When the base plate of the apparatus is independently rotated by an electric motor, shear force is applied to the specimen. The force induced by the radial motion is read by two load cells, and is then converted into a measurement of shear stress (Wykeham Farrance International).

The shear stress on the specimen is calculated as:

$$\tau = [3(F_1 + F_2)L] / [4\pi(R_2^3 - R_1^3)] \qquad \text{Eq. 2.17}$$

Here, F_1 and F_2 are the forces read by the load cells, and R_1 and R_2 are the inner and outer radii, respectively. The normal effective stress is written as:

$$\sigma' = P / [\pi(R_2^2 - R_1^2)] \qquad \text{Eq. 2.18}$$

Here, P is the load applied to the sample. The load is applied through a counter balanced lever with a 10:1 ratio. The load P is then multiplied by 10 times the load applied to the load hanger and added to the weight of the top platen (Figure 2.14). The residual friction angle, ϕ'_r, is then:

$$\phi'_r = \tau/\sigma' = [3(F_1 + F_2)(R_2^2 - R_1^2)L] / [4(R_2^3 - R_1^3)P] \qquad \text{Eq. 2.19}$$

2.3. Soil Suction

2.3.1. Introduction

The water retention curve, also called the soil water characteristic curve (SWCC), describes the effect of volumetric water content, θ, on suction, ψ. There are two components to the suction term, ψ; osmotic suction and matric suction. However for the purpose of this study, only matric suction has been considered and is written as:

$$\psi = (u_a - u_w) \qquad \text{Eq. 2.20}$$

Here, u_a is the pore air pressure and u_w is the porewater pressure. As the water content in a soil is increased toward saturation, that is, $S_r = 1$, the soil suction decreases. Conversely, as a soil becomes less saturated, ψ increases and groundwater flow through the soil becomes more difficult as a result of reducing hydraulic conductivity (Aubertin et al., 2003). In numerical modeling, it is necessary to define the SWCC function in order to identify an appropriate hydraulic conductivity function. Without the SWCC, only the saturated hydraulic conductivity can be applied to a particular material. In the context of groundwater flow, this may result in an overestimation of flow through the unsaturated zone and incorrect porewater pressures (Geo-Slope International Ltd., Seep/W, 2010).

In an unsaturated soil, the principle of effective stress can be defined (Bishop and Blight 1953) using a highly variable χ-function as:

$$\sigma' = (\sigma - u_a) - \chi(u_a - u_w) \qquad \text{Eq. 2.21}$$

Here, σ' is the effective stress, σ is the total stress and χ is a variable describing the degree of saturation for a particular soil type (Fredlund, D.G., Morgenstern, N.R., 1977, Budhu, 2007). The χ-parameter is still well known and, in some cases, actively promoted for use in practice. Unfortunately it is not particularly useful as χ is strongly non-linear and varies with many parameters, including σ, $(u_a - u_w)$, OCR, and S_r. The χ-parameter can therefore not be easily calibrated for use in practice. The author notes that most work with unsaturated soils now uses the independent stress state variables $(\sigma - u_a)$ and $(u_a - u_w)$.

For a saturated soil, $\chi = 1$ and Equation 2.21 simplifies to:

$$\sigma' = \sigma - u_w \qquad \text{Eq. 2.22}$$

In the context of stress state, the suction can therefore have a significant impact on the effective stress in determining the available shear strength for a particular soil. Considering suction as negative porewater pressure, an increase in suction then gives an increase in effective stress, and therefore an increase in shear strength given the Mohr-Coulomb relationship described by Equation 2.2. Conversely, this relationship shows that increases in porewater pressure, due to such occurrences as flood events or precipitation, can lead to a reduction in shear strength for a particular soil element.

This study does not explicitly analyze the effects of soil suction on shear strength and slope stability. However, the above relationships demonstrate that the inclusion of the SWCC is important for the analysis of unsaturated soils in numerical modeling of slope stability. For coupled stress-porewater pressure analyses, the SWCC is a required parameter, and is

therefore critical in considering changes in volumetric water content under loading and subsequent soil consolidation (Geo-Slope International Ltd., Sigma/W, 2010). This aspect of the SWCC will be discussed in Chapter 7.

2.3.2. Estimation of the Soil Water Characteristic Curve using the Modified Kovács Method

In-situ measurements of soil suction can be difficult to determine, but there are a number of predictive methods available to determine the SWCC. The Modified Kovács Method was selected for this study, as it is based on physical soil characteristics that are relatively easy to obtain (Aubertin et al., 2004). The method has also been shown to compare reasonably well with in-situ measurements of soil suction (Blatz et al., 2004).

The theory in the Modified Kovács Method is based on capillary rise of water in a capillary tube, given by the following equation:

$$h_c = (4\sigma_w \cos\beta_w) / (\gamma_w d) \qquad \text{Eq. 2.23}$$

Here, h_c is the rise of water in a tube of diameter, d, σ_w is the surface tension of water, β_w is the contact angle between the capillary tube and the water surface, and γ_w is the unit weight of water. The method uses a parameter called the equivalent capillary rise, h_{co}, which requires some modifications to Equation 2.23. The pore spaces in a given soil are considered analogous to the diameter of the capillary tube, and the equivalent diameter is written as:

$$d_{eq} = 4e/(\rho_s S_m) \qquad \text{Eq. 2.24}$$

Here, e is the voids ratio, ρ_s is the solid grain density, and S_m is the specific surface area of the soil grains. For plastic, cohesive soils, S_m is written as:

$$S_m = \lambda w_L^{\chi} \quad \text{Eq. 2.25}$$

Here, λ and χ are material parameters established at values of 0.2 m^2/g and 1.45 (unitless), respectively, and w_L is the liquid limit. Replacing d with d_{eq} in Equation 2.23 then gives the expression of equivalent capillary rise:

$$h_{co} = [(\sigma_w \cos\beta_w) / (\gamma_w e)] \lambda \rho_s w_L^{1.45} \quad \text{Eq. 2.26}$$

The equation for the SWCC proposed by Aubertin et al. (2004) is as follows:

$$S_r = \theta/n = S_c + S_a*(1 - S_c) \quad \text{Eq. 2.27}$$

Here, S_r is the degree of saturation, θ is the volumetric water content, n is the soil porosity, and S_c and S_a represent the capillary and adhesion components of the total degree of saturation, respectively. These components are then written as functions of h_{co} and ψ as:

$$S_c = 1 - [(h_{co}/\psi)^2 + 1]^m \exp[-m(h_{co}/\psi)^2] \quad \text{Eq. 2.28}$$

$$S_a = a_c C_\psi (h_{co}^{2/3}) / (e^{1/3} \psi^{1/6}) \quad \text{Eq. 2.29}$$

$$C_\psi = 1 - [\ln(1 + \psi/\psi_r)] / [\ln(1 + \psi_0/\psi_r)] \quad \text{Eq. 2.30}$$

Here, m and a_c are fitting parameters that have values of 3×10^{-5} and 7×10^{-4}, respectively, for plastic, cohesive soils. The parameter, ψ_0, is a constant value equal to 10^7 cm of water (9.8×10^5 kPa). This is the suction corresponding to a volumetric water content of $\theta = 0$. The residual suction, ψ_r, is the suction value at the residual water content for which no significant quantity of water will be drawn from the soil by an increase in suction (Geo-slope International Ltd., Seep/W, 2010). For plastic, cohesive soils, the residual suction is written as:

$$\psi_r = 0.86(\xi/e)^{1.2} w_L^{1.74} \qquad \text{Eq. 2.31}$$

where:

$$\xi = 0.15\rho_s \qquad \text{Eq. 2.32}$$

Once the capillary and adhesion components of the total degree of saturation are solved, the SWCC can be plotted. The SWCC is obtained by plotting S_r over a defined range of suction values. It should be noted that the Modified Kovács Method does not yet present a method of directly obtaining the air entry value, ψ_a, for plastic, cohesive soils based on geotechnical properties. Values of ψ_a can be determined from the resulting SWCC plots, but are not considered critical for the purpose of this study. Figure 2.15 shows a typical plot of the SWCC, as well as the capillary and adhesion components of the curve for a particular soil.

2.4. Hydraulic Conductivity

The saturated hydraulic conductivity, k_s, is an important parameter when trying to quantify sub-surface flow and the time required for the dissipation of excess porewater pressures. The accurate determination of k_s for a given soil unit can be difficult, and laboratory measurements have been criticized for their inability to predict the effects of heterogeneity from factors such as deposition structure or fracturing (Neuzil, 1994). In-situ tests of k_s have produced results of up to three orders of magnitude different than those produced by laboratory tests (Keller et al., 1989). However, large scale field testing of hydraulic conductivity can often be impractical for many geotechnical projects. Laboratory determined values can therefore be valuable in comparing with an established range of values, as determined from literature, and can provide a point of reference in calibrating a finite element model.

The hydraulic conductivity ratio is the ratio of vertical hydraulic conductivity (k_v) to horizontal hydraulic conductivity (k_h). It describes the variability in k with direction, or anisotropy. Anisotropy is rarely shown to be greater than one order of magnitude in tests on small scale core or Shelby tube samples. The anisotropy in such a scale is attributed to the layered orientation of soil particles within a soil unit (Freeze et al., 1979). On a larger scale, the macrostructure of a soil unit has been shown to affect the hydraulic conductivity ratio by more than two orders of magnitude. This difference can be attributed to layered heterogeneity (Freeze et al., 1979) or transmissive fractures separated by relatively large distances (Neuzil, 1994). It is therefore an important parameter to consider in conjunction with k_s when analyzing a regional groundwater flow regime. The laboratory methods and typical ranges of values used to determine k_s in this study are discussed in the following paragraphs.

Published values of k_s for shale vary widely, with values shown between approximately 10^{-16} and 10^{-9} m/s (Freeze et al., 1979; Neuzil, 1994; Josh et al., 2012). Neuzil (1994) showed that laboratory and regional analyses of k_s yield values between approximately 10^{-16} and 10^{-10} m/s over a range in porosity (n) of 0.1 to 0.4, respectively. In addition to n, factors affecting heterogeneity, as described above, can also contribute to the variability observed in k_s. Accurate laboratory values can be difficult to determine due to the challenge of obtaining suitable undisturbed samples, as well as trimming the sample to obtain a specimen of the required dimensions for a particular test. As such, this study relies on the applicable range of values for k_s described above.

A comparison of laboratory hydraulic conductivity tests and various empirical methods on sandy alluvial sediments has shown that k_s can vary over several orders of magnitude (Pliakas et al., 2011). For the sediments described, the values are shown to range between approximately 10^{-4} and 10^{-1} m/s. This variability is primarily attributed to the grain size of the sediments, as k_s generally increases with increasing grain size. The alluvial sediments observed in the Ashville Junction study area vary from silts and fine sands to gravel sized particles, and the range of values described above are considered suitable for these material types.

Limited information is available for k_s values for clay rich till. Further complications may arise in determining suitable values when till or till-like soils are re-deposited as colluvium, as they have been at the Ashville Junction site. Tension cracks, fractures and roots can significantly alter the macrostructure, causing k_s to vary considerably from laboratory tests on samples taken at discrete locations over the depth of the soil layer. Keller et al. (1989) note that in-situ measurements of k_s, which can capture the effects of heterogeneity, on clay rich tills of the interior plains are typically one to three orders of magnitude greater than measurements

determined in laboratory tests. While it is recognized that the results of laboratory tests may not be representative of k_s for the colluvium encountered at the Ashville Junction site, values were determined using flexible wall permeameter tests and back calculation using the coefficient of consolidation (C_v) values determined from oedometer tests. The results of these tests provide a point of reference as described above. The hydraulic conductivity can be written in terms of C_v as:

$$k_z = C_v m_v \gamma_w \qquad \text{Eq. 2.33}$$

Here, k_z is the vertical hydraulic conductivity, m_v is the coefficient of volume compressibility, and γ_w is the unit weight of water.

As discussed in the previous section, changes in volumetric water content will result in changes in hydraulic conductivity. A hydraulic conductivity function is therefore required to reflect these changes. Seep/W offers two predictive methods for producing a hydraulic conductivity function based on the SWCC; the method proposed by Fredlund et al. (1994) and the method proposed by Van Genuchten (1980). The Van Genuchten method was arbitrarily selected for this study.

2.5. Estimation of Elastic and Hydraulic Properties Using Vibrating Wire Piezometer Data

With the use of vibrating wire piezometers and data loggers, certain elastic and hydraulic properties of soils can be measured. Anochikwa et al. (2012) describe a method in which barometric pressure loading, water table effects and moisture loading effects are analyzed to

determine in-situ measurements of the elastic modulus and vertical hydraulic conductivity for relatively shallow aquitards. This method can therefore be used to evaluate elastic stiffness for use in a finite element coupled stress-porewater pressure analysis. The Ashville Junction site has not been instrumented for precipitation and evapotranspiration data collection which, for the method described, is required for the determination of in-situ hydraulic properties, that is, specific storage, S_s, or k_v. As such, only barometric loading effects have been analyzed for the determination of in-situ elastic properties.

Because they are affected by changes in barometric pressure, observed pore-water pressure responses may generally appear irregular. An on-site barometric piezometer can be used to apply a correction to this data to eliminate barometric effects. Changes in barometric pressure can be multiplied by this correction factor, which may be adjusted until barometric effects have been eliminated from a plot of the data. As described in this method, the applied correction factor represents the loading efficiency, commonly referred to as B-bar (here written as B) in geotechnical engineering. Changes in pore-water pressure in response to an applied surface load are described by:

$$B = \Delta u / \Delta \sigma_B \qquad \text{Eq. 2.34}$$

The B term describes the loading efficiency, u is the pore-water pressure and σ_B is the barometric pressure. If the soil is considered a saturated, linearly elastic and isotropic material, B can also be described by:

$$B = (1/E_c) / (1/E_c + n/E_w) \qquad \text{Eq. 2.35}$$

Here, E_c is the constrained elastic modulus, E_w is the bulk modulus of elasticity of water (~2.2 x 10^9 Pa), and n is the soil porosity. Assuming that the measured barometric response is undrained, E_c can be shown as:

$$E_c = (E_w - BE_w) / (Bn) \quad \text{Eq. 2.36}$$

Young's modulus E, can be determined using the relationship between E, Poisson's ratio, ν, and E_c:

$$E = E_c(1+\nu)(1-2\nu) / (1-\nu) \quad \text{Eq. 2.37}$$

It is common to assume $\nu = 1/3$. As such, E can then be defined as:

$$E = 2/3\ E_c \quad \text{Eq. 2.38}$$

This method has only been shown to be suitable for saturated, linear elastic, isotropic materials, and may therefore be unsuitable for the surficial till-like soils encountered above the clay shale. Anochikwa et al. (2012) also noted that the determination of elastic properties for softer soils (ie. $E_c < 100$ MPa) has shown to be problematic, and that in this case vented pressure transducers may be required in place of vibrating wire piezometers for more accurate results.

2.6. Finite Element Seepage Modeling

2.6.1. Introduction

Finite element modeling can be used to estimate the porewater pressure conditions at a given site. Seep/W, from Geo-Slope International Ltd., is capable of producing a distribution of porewater pressures at steady state across a given domain by iteratively calculating the pressure at each node of the elements in the model until a solution is reached. The steady state condition can then be calibrated against known values of porewater pressure as determined through on-site instrumentation by varying the applied material properties in the model. Once established, the model can use this porewater pressure distribution as a "parent analysis" to additional analyses, such as a finite element slope stability analysis in Slope/W. The steady state condition can then be extended to transient analyses, where time dependent boundary conditions or loads may be applied (Geo-Slope International Ltd., Seep/W, 2010). The following section discusses the governing equations for groundwater flow used in these analyses.

2.6.2. Governing Equations

The governing equations for groundwater flow in Seep/W are based on Darcy's Law, which is true for both saturated and unsaturated flow (Geo-Slope International Ltd., Seep/W, 2010). Darcy's Law states that:

$$q = ki \qquad \text{Eq. 2.39}$$

Here, q is the specific discharge, k is the hydraulic conductivity of the soil and i is the hydraulic gradient. In finite element analysis, the partial differential expression of this law is:

$$\delta/\delta x\,[k_x \delta H / \delta x] + \delta/\delta y\,[k_y \delta H / \delta y] + Q = \delta\theta/\delta t \qquad \text{Eq. 2.40}$$

This partial differential equation (PDE) states that at a given point in time, the sum of the rates of change in flow quantity, expressed here as a function of head, H, in both the x and y directions plus some applied flow, Q, is equal to the change in storage, expressed here as volumetric water content, θ, with time, t. Under steady state conditions, the flows entering and leaving a system are equal, and the expression simplifies to:

$$\delta/\delta x\,[k_x \delta H / \delta x] + \delta/\delta y\,[k_y \delta H / \delta y] + Q = 0 \qquad \text{Eq. 2.41}$$

For transient analyses however, changes in volumetric water content can occur as a result of changing soil properties, a flux at one or more of the boundaries, or stress state. Recall from Equation 2.21 that there are two components to stress state as it relates to either saturated or unsaturated conditions, $(\sigma - u_a)$ and $(u_a - u_w)$. In an uncoupled analysis (coupled analysis will be discussed in Section 2.8), the total stress is constant. Futhermore, the Seep/W formulations are based on constant atmospheric pressure. Therefore, the $(\sigma - u_a)$ term must remain constant and does not induce any change in the volumetric water content. Since the u_a term remains constant in the $(u_a - u_w)$ term, changes in volumetric water content are then solely a function of changes in porewater pressure, which can be expressed by:

$$\delta\theta = m_w \delta u_w \qquad \text{Eq. 2.42}$$

This states that the change in volumetric water content, θ, is equal to the product of the change in porewater pressure, u_w, and the slope of the SWCC, m_w. Expressing porewater pressure at any point as a function of total head gives the following relationship:

$$u_w = \gamma_w(H - y) \qquad \text{Eq. 2.43}$$

Here, H is the total head, γ_w is the unit weight of water and y is the elevation head. Since the elevation does not change at a given point, the expression simplifies to:

$$u_w = \gamma_w H \qquad \text{Eq. 2.44}$$

Substituting Equations 2.42 and 2.44 into Equation 2.40 then gives the PDE used for transient analyses in Seep/W:

$$\delta/\delta x\,[k_x \delta H / \delta x] + \delta/\delta y\,[k_y \delta H / \delta y] + Q = m_w \gamma_w\,(\delta H/\delta t) \qquad \text{Eq. 2.45}$$

Seep/W uses Equations 2.41 and 2.45 to satisfy the condition of continuity in the finite element model. In general, the continuity equation used by Seep/W can be described as:

$$[K_w]\{H\} = \{Q\} \qquad \text{Eq. 2.46}$$

Here, $[K_w]$ is the hydraulic conductivity matrix, {H} is the total head tensor, and {Q} is a tensor describing the flow at boundary nodes. Changes in porewater pressure, δu_w are described in terms of changes in total head, H. A more detailed description of the mathematics used by Seep/W can be found in Geo-Slope International Ltd., Seep/W, 2010.

2.7. Coupled Stress-Porewater Pressure Modeling

In some analyses, particularly when there is interest in the relationship between deformations due to some externally applied load, and the associated porewater pressure response, a coupled stress-porewater pressure model can be used. In a coupled model, Sigma/W uses both the conditions of equilibrium, and continuity described by Equations 2.13 and 2.46, respectively. In analyses involving consolidation, that is, time-based equilibration of porewater pressures, the displacements cause volume changes that affect the porewater pressure response. The SWCC discussed previously is therefore an integral parameter in a coupled analysis. In turn, the induced changes in porewater pressure will alter the effective stress. In order to account for these changes, Sigma/W solves the equations of equilibrium and continuity simultaneously using a coupling matrix, [L]. The equation for a coupled analysis is then written as:

$$[([K])/([L]^T)\ ([L])/([K_w])]\ \{\delta d/\delta H\} = \{\delta F/\delta Q\} \qquad \text{Eq. 2.47}$$

A more detailed description of the coupling matrix and the mathematics used by Sigma/W in coupled stress-porewater pressure analyses can be found in Geo-Slope International, Sigma/W, 2010.

2.8. Slope Stability Analysis

2.8.1. Introduction

As discussed in Section 2.1, there are many variables to consider in slope stability analysis. Soil and groundwater behavior have been discussed in detail, and both contribute largely to the types of stability analyses that may be performed. However the selected method of analysis also requires knowledge of the site history, geology and geometry; and the material properties and porewater pressures require verification through extensive laboratory tests and site instrumentation. Consideration of all of these variables is necessary to establish potential failure mechanisms and select the most appropriate method to model a particular site (Graham, 1984). Some of the common methods of stability analysis are discussed in detail in the following sections.

2.8.2. Infinite Slope Analysis

Infinite slope stability analysis assumes that a failure is planar over some infinite extent of a constant slope. These types of failures are generally the simplest to analyze, as the mechanics are described by a determinate, static solution requiring no simplifying assumptions. However, the linearity assumed in the mechanics may require assumptions with respect to the geometry, stratigraphy or groundwater conditions for a natural or engineered slope (Graham, 1984).
As infinite slope stability analysis assumes the failure is of an infinite extent, the analysis of a single slice of the section representing this failure is sufficient to model the mechanics of the entire failed soil mass. Figure 2.16 illustrates the static forces acting on an arbitrary slice of width, b, and height, z, in a slope at an angle, β. In this figure, P is the reaction force acting across the width of the slice, W is the weight of the slice, T is the shear force across the base of

the slice, and Q_l and Q_r are the interslice forces. As the slice is assumed to represent the mechanics of the entire slope, all slices will have the same interslice forces acting in equal and opposite directions. The stresses acting on a slice of length JK in a soil with unit weight, γ, are then described by:

$$\sigma_n = \gamma z \cos^2\beta \qquad \text{Eq. 2.48}$$

$$\tau_n = \gamma z \sin\beta \cos\beta \qquad \text{Eq. 2.49}$$

where:

$$JK = b \sec\beta \qquad \text{Eq. 2.50}$$

The porewater pressure in the slice acts at a depth of (1 – m)z from the top of the slice, where m represents the portion of z that is saturated. The porewater pressure is then written as:

$$u = \gamma_w (1 - \sin^2\beta) m z \qquad \text{Eq. 2.51}$$

The factor of safety is the ratio of the required shear strength to the mobilized shear strength. Using the Mohr-Coulomb failure criterion with Equations 2.49 to 2.51, the factor of safety, FS, against sliding in an infinite slope is then:

$$FS = [c' + (\gamma - m\gamma_w) z \cos^2\beta \tan\phi'] / [\gamma z \sin\beta \cos\beta] \qquad \text{Eq. 2.52}$$

As the Ashville Junction slide is a previously failed slope, ϕ' becomes ϕ'_r and c' goes to zero in Equation 2.52. The observed failure mechanism and geometry of the Ashville Junction slide suggest that an infinite slope analysis may be appropriate as an initial approximate solution.

2.8.3. Limit Equilibrium Analysis

A common method of slope stability analysis involves discretizing a soil mass into slices. The individual slices can then be analyzed to determine the forces and moments acting on a particular slice (Graham, 1984). Figure 2.17 illustrates a typical slice through a soil mass and the forces acting on the slice. In this figure, W is the weight of the slice, Q_l and Q_r are the interslice forces acting at angles θ_l and θ_r, respectively, and U_l and U_r are the porewater forces acting on each side of the slice. Acting on the base of the slice is the normal force, P, the porewater force, U, and the mobilized shear force, S_m.

For a given soil mass discretized into n slices, there are a total of (3n – 2) unknowns for force equilibrium, and (2n – 1) unknowns for moment equilibrium. These unknowns are summarized as:

Forces:

n	normal forces, P
(n – 1)	interslice forces, Q, acting on the slice interfaces
(n – 1)	obliquities of Q, represented by the angle, θ

Moments

n	distances, e, of the resultant normal force, P

(n – 1) distances, f, of the resultant interslice forces, Q

The forces acting on the slice give two equations to solve for force equilibrium; one horizontal and one vertical, and one equation to solve for moment equilibrium. This then leaves 3n equations to solve for (5n – 3) unknowns. The solution is then statically indeterminate, requiring some simplifying assumptions to be made. If the slices are thinly discretized, such that P essentially acts at the centre of the base of the slice, the n unknown distances, e, can be removed. Furthermore, if assumptions are made with respect to the obliquities of Q, (n – 1) unknown angles, θ, can be removed. This would give a total of (2n – 1) assumptions, suggesting that the solution is then over specified, as only (2n – 3) assumptions are necessary to make the solution statically determinate. This over specification of assumptions then gives two separate solutions for the factor of safety: FS_f for force equilibrium and FS_m for moment equilibrium. With FS being dependent on assumptions with respect to θ, an infinite number of solutions are possible from the range of specified θ assumptions. Fortunately, the assumed values for θ do not have a major impact on FS, particularly if FS_m is being used (Fredlund and Krahn, 1977).

Limiting equilibrium implies that a system of forces is on the verge of failing, with FS equal to unity, and assumes a constant FS over the entire slide surface (Graham, 1984). The state of limiting equilibrium requires that the sum of the driving forces is equal to the sum of the resisting forces. From this force system, the sum of the moments of these forces about an arbitrary point must then be zero. Figure 2.18 illustrates the forces required for a limit equilibrium slope stability analysis.

Summation of the vertical forces in a slice gives:

$$W - S_m \sin\alpha - P\cos\alpha - (X_l - X_r) = 0 \qquad \text{Eq. 2.53}$$

Here, X_l and X_r are the interslice shear forces. The mobilized shear force, S_m, at the base of the slice is proportional to the required shear strength, τ_{req} by $1/FS_f$. The mobilized shear force is then written as:

$$S_m = l\tau_{req} = [c'l + (P - ul)\tan\phi'] / FS_f \qquad \text{Eq. 2.54}$$

Here, l is the length of the base of the slice. Substituting Equation 2.54 into Equation 2.53 and solving in terms of the normal force, P as a function of FS_f, then gives:

$$P = [W - ((c'l\sin\alpha)/FS_f) + ((ul\tan\phi'\sin\alpha)/FS_f) - (X_l - X_r)] / [\cos\alpha + ((\tan\phi'\sin\alpha)/FS_f)] \qquad \text{Eq. 2.55}$$

For limiting equilibrium, the sum of all the horizontal forces across all slices must equal zero, which is written as:

$$\Sigma P\sin\alpha - \Sigma S_m\cos\alpha + \Sigma KW + \Sigma(E_r - E_l) + (A_r - A_l) + L\cos\omega = 0 \qquad \text{Eq. 2.56}$$

Here, KW is a horizontal force induced by an earthquake with horizontal acceleration k_g, and E_r and E_l are the horizontal interslice forces. A_l and A_r represent the porewater forces induced by partial submergence of the toe and a water filled tension crack, respectively. In Figure 2.18, a line load, L, is applied at some angle, ω, at the crest of the slope. For the purpose of this study, KW and L will not be considered in the analysis. The interslice forces, E_r and E_l, are internal forces acting equally in opposite directions, which gives:

$$\Sigma(E_r - E_l) = 0 \qquad \text{Eq. 2.57}$$

Using Equation 2.57 and the above variable exclusions, the equation for FS_f can then be shown as:

$$FS_f = [\Sigma(c'l\cos\phi\alpha + (P - ul)\tan\phi'\cos\alpha)] \ / \ [\Sigma P\sin\alpha + (A_r - A_l)] \qquad \text{Eq. 2.58}$$

As mentioned above, at limiting equilibrium for all forces within the slide mass, the sum of the moments of all forces about an arbitrary point must be zero. Figure 2.18 shows this point as the centre of moments. Considering the entire slide mass, the sum of the moments of the internal forces, E and X, is zero. Summation of moments then gives:

$$\Sigma Wx - (A_l a_l - A_r a_r) - \Sigma Pf - \Sigma S_m R = 0 \qquad \text{Eq. 2.59}$$

The equation for FS_m can then be shown as:

$$FS_m = [\Sigma(c'lR + (P - ul)R\tan\phi')] \ / \ [\Sigma Wx - (A_l a_l - A_r a_r) - \Sigma Pf] \qquad \text{Eq. 2.60}$$

Here, R is variable for a non-circular slide surface (Figure 2.18), but remains constant if the slide surface is assumed circular. In both Equations 2.58 and 2.60, it is shown that the normal force, P, is a function of FS (Equation 2.55). The required solution for limiting equilibrium then occurs when $FS_f = FS_m$, and the equations for force and moment equilibrium must therefore be solved iteratively until a solution is reached where successive iterations differ by between 0.02 to 1% (Graham, 1984).

2.8.4. Morgenstern Price Method of Slices

There are several common methods of limit equilibrium slope stability analysis, including Bishop's simplified and rigorous methods, Janbu's simplified and rigorous methods, Spencer's method, and the Morgenstern-Price method. The most notable difference between each of these methods is in the assumptions made with respect to the interslice forces, E and X, and the inclination angle for the interslice forces, θ (Graham, 1984). For previous methods, it was common to assume that the interslice forces are equal and opposite and can therefore be ignored, or that the inclinations angles are constant. The Morgenstern-Price method (1965) assumes that θ varies across all slices, as a function of the distance along the slide mass, according to a user defined function written as:

$$\tan\theta = X/E = \lambda f(x) \qquad \text{Eq. 2.61}$$

Here, λ is a scaling constant and f(x) is the function describing the variability of θ with x. Figure 2.19 illustrates the variability of θ with different scaling constants, λ, and different functions, f(x). With this method, the interslice forces are included in the evaluation of FS_f and FS_m (Graham, 1984). The interslice forces are then written as:

$$X_l = (E_l \tan\alpha_l) - (E_l - E_r)\,(f_l / b) \qquad \text{Eq. 2.62}$$

$$(E_l - E_r) = [W - (X_l - X_r)] \tan\alpha - (S_m/\cos\alpha) \qquad \text{Eq. 2.63}$$

The equations of limiting equilibrium are again solved iteratively, assuming in the first iteration that the interslice shear forces are negligible, that is, that the θ-values are zero. Following the

first iteration, E is determined with Equation 2.63, and X_l is defined with an assumed value of λ by a function, f(x), as:

$$X_l = E_l \lambda f(x) \qquad \text{Eq. 2.64}$$

The limiting equilibrium Equations 2.58 and 2.60 are solved as described previously, but the process is repeated using different assumed values of λ. A solution is reached when $FS_f = FS_m$. Figure 2.20 illustrates how FS varies with λ for both force and moment equilibrium.

As mentioned, f(x) is user defined and should be selected based on how the inclination angles may vary across a slide mass. Slope/W, by Geo-Sloe International, Ltd., offers several functions, including the half sine, trapezoidal and clipped sine functions. Further details on these functions and the mathematics used by the Slope/W can be found in Geo-Slope International Ltd., Slope/W, 2010.

2.8.5. Finite Element Method for Slope Stability

The equations of limiting equilibrium described above show that a single FS is solved for all slices across the analyzed slide mass by making assumptions with respect to the interslice forces. This can result in stress distributions across the base of the slide mass that do not necessarily reflect the actual in-ground stresses (Krahn, 2003). It should be noted that the various limiting equilibrium methods do not evaluate strains and therefore deformations. The finite element method of slope stability uses assumed stress-strain relationships to satisfy displacement compatibility and therefore gives a more realistic stress distribution. Figure 2.21 illustrates the difference in normal stress distributions in a slide mass for both the limit

equilibrium and finite element methods. The figure illustrates how shear stress concentrations, which influence the base normal stress, can be captured in the finite element method of slope stability (Geo-Slope International Ltd., Slope/W, 2010).

Slope/W has the ability to import finite element computed stresses in order to solve for the factor of safety, FS. This eliminates the need to make assumptions about the interslice forces (Krahn, 2003), although assumptions may now need to be made with respect to an appropriate constitutive relationship, most commonly the elastic properties of various soil layers. Using finite element computed stress can be particularly useful when stresses are re-distributed following loading and subsequent deformation, or if there are isolated point loads. As the stresses at the base of each slice are now inherently known (using the assumed constitutive relationship), the solution is now deterministic, rather than iterative. The mobilized and resisting shear forces can be determined for each slice and then integrated over the length of the slip surface to determine FS, where:

$$FS = \Sigma S_r / \Sigma S_m \qquad \text{Eq. 2.65}$$

Here, ΣS_r is the sum of all resisting shear forces across the slip surface, and ΣS_m is the sum of all mobilized shear forces across the slip surface (Geo-Slope International Ltd., Slope/W, 2010). This form of solution does not force a constant FS on the base of all slices. A more detailed description of the mathematics used by Slope/W for the finite element method can be found in Geo-Slope International Ltd., Slope/W, 2010.

2.9. Summary

This section attempts to chronologically describe the theory and methods required to understand, analyze and potentially remediate failed natural or engineered slopes. It is the opinion of the author that an understanding of the environment in which the instabilities have taken place, in this case the Canadian prairie landscape, is an integral first step in establishing an appropriate method of analysis to employ. With an understanding of the soil mechanics and groundwater conditions for the materials encountered at a particular site, the appropriate constitutive model and method of stability analysis can then be used to evaluate slope instabilities.

Figure 2.1 – Oblique View of PTH 83 at Shell River Slide Area (Note slump block in backslope)

Figure 2.2 – PTH 83 - Shell River Slide (July, 2012)

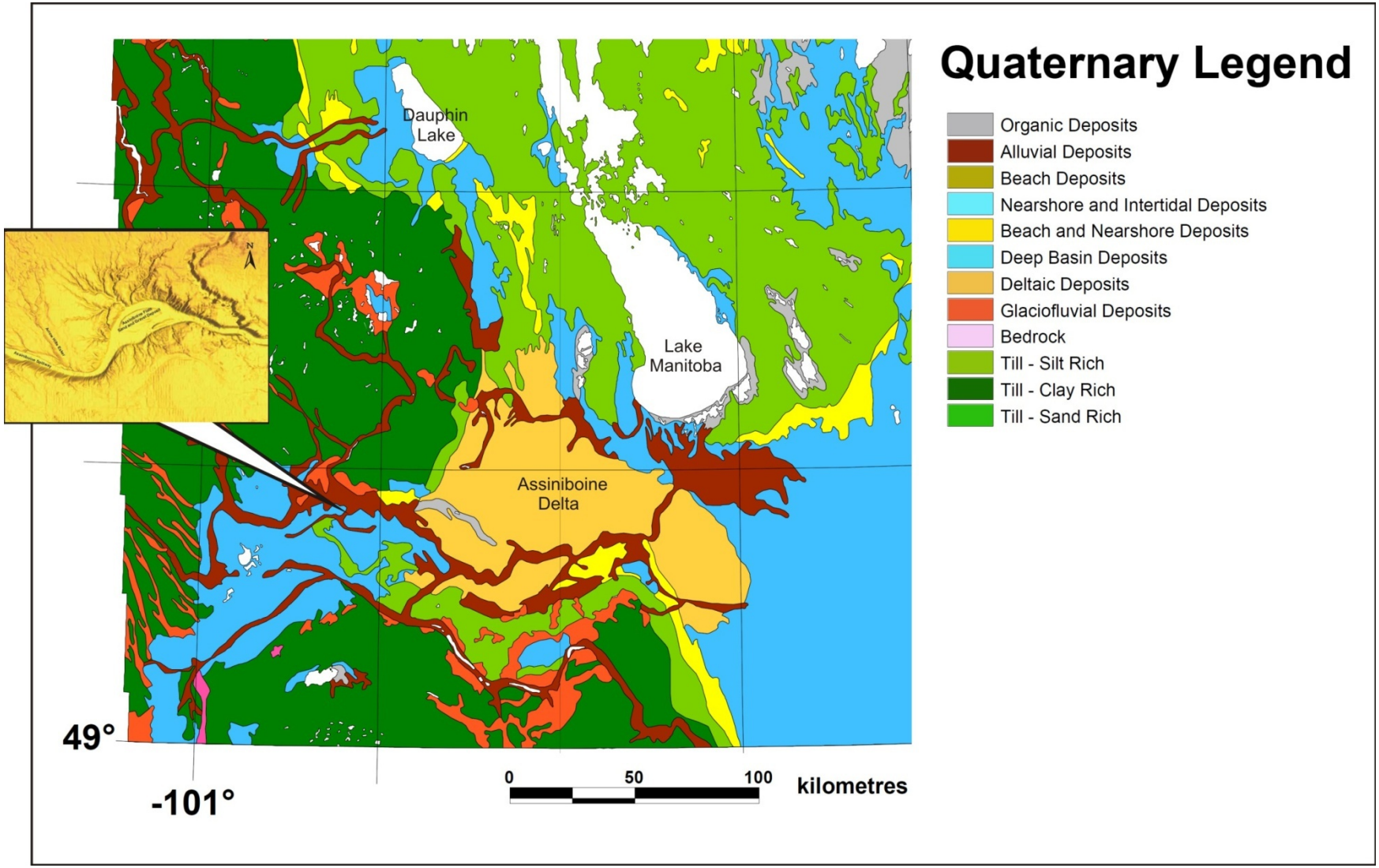

Figure 2.3 – Quaternary Deposits in Southwestern Manitoba (Assiniboine Valley inset, with permission, Matile et al., 2013)

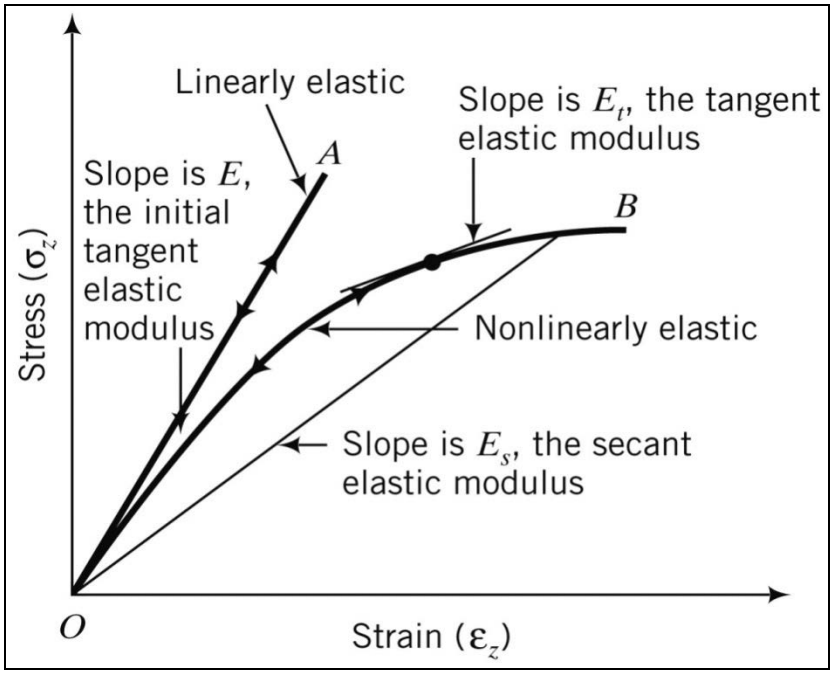

Figure 2.4 – Elastic Stress-Strain Relationship (With permission, Budhu, 2007)

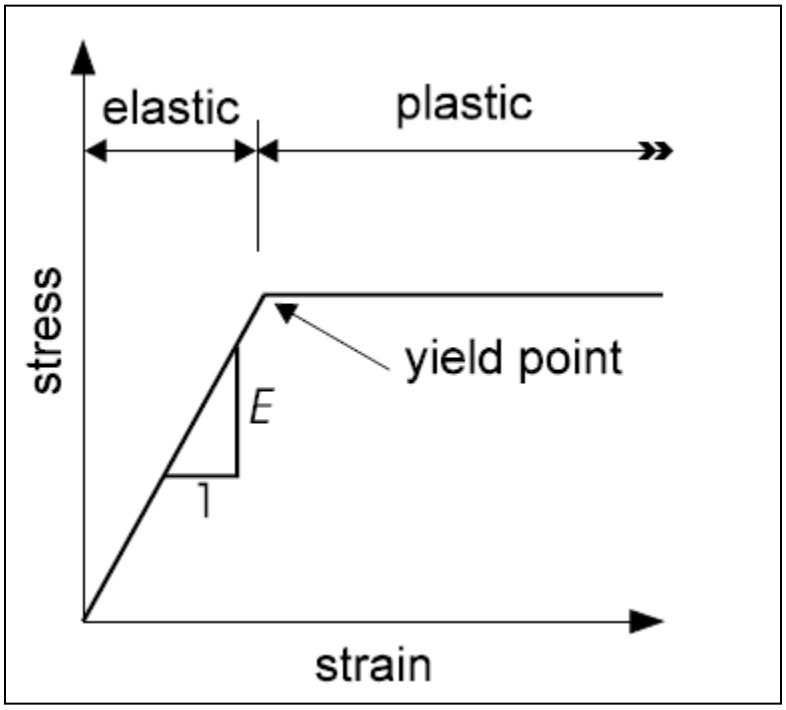

Figure 2.5 – Elastic Perfectly Plastic Constitutive Relationship (With permission, Geo-Slope International Ltd., Sigma/W, 2010)

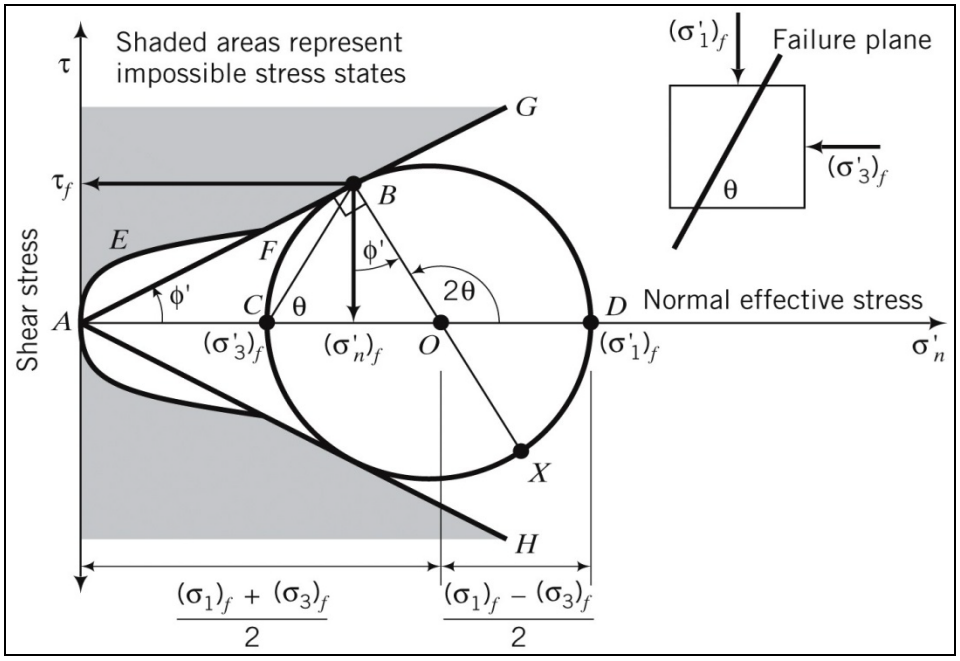

Figure 2.6 – Mohr Coulomb Failure Envelope (With permission, Budhu, 2007)

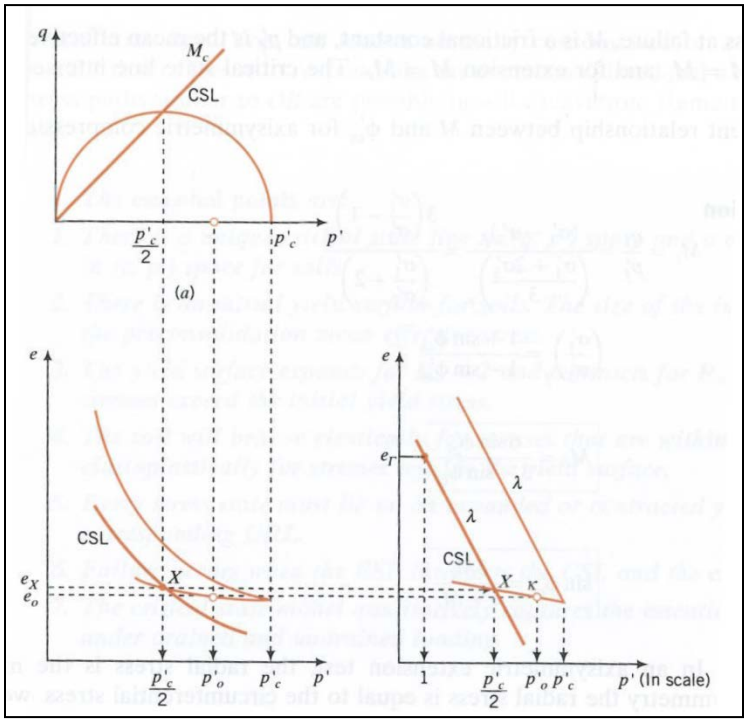

Figure 2.7 – The Critical State Model (With permission, Budhu, 2007)

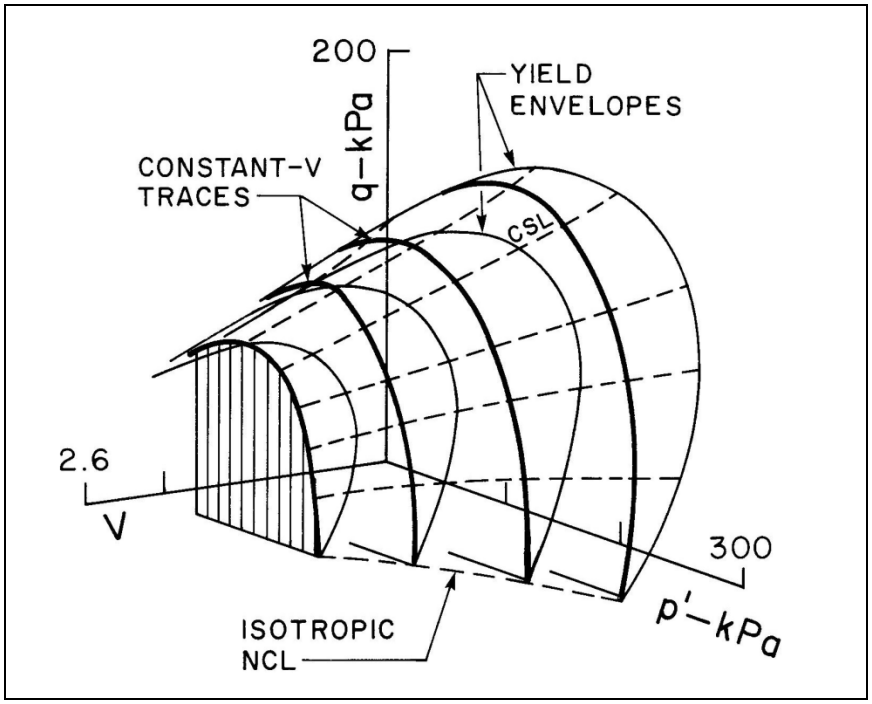

Figure 2.8 – The State Boundary Surface (With permission, Graham et al., 1988)

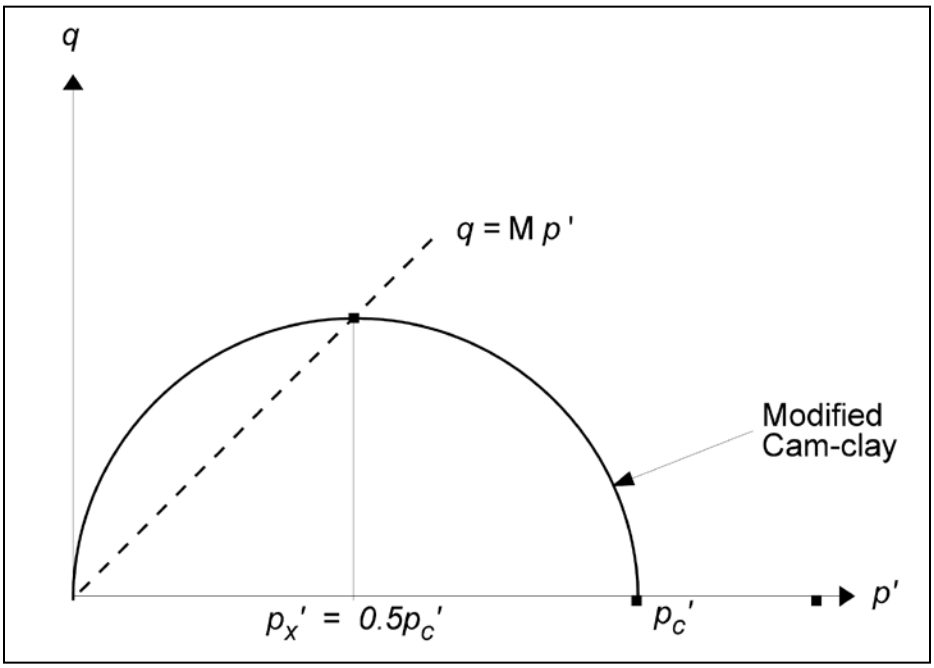

Figure 2.9 – Modified Cam-Clay Yield Surface (With permission, Geo-slope International Ltd., Sigma/W, 2010)

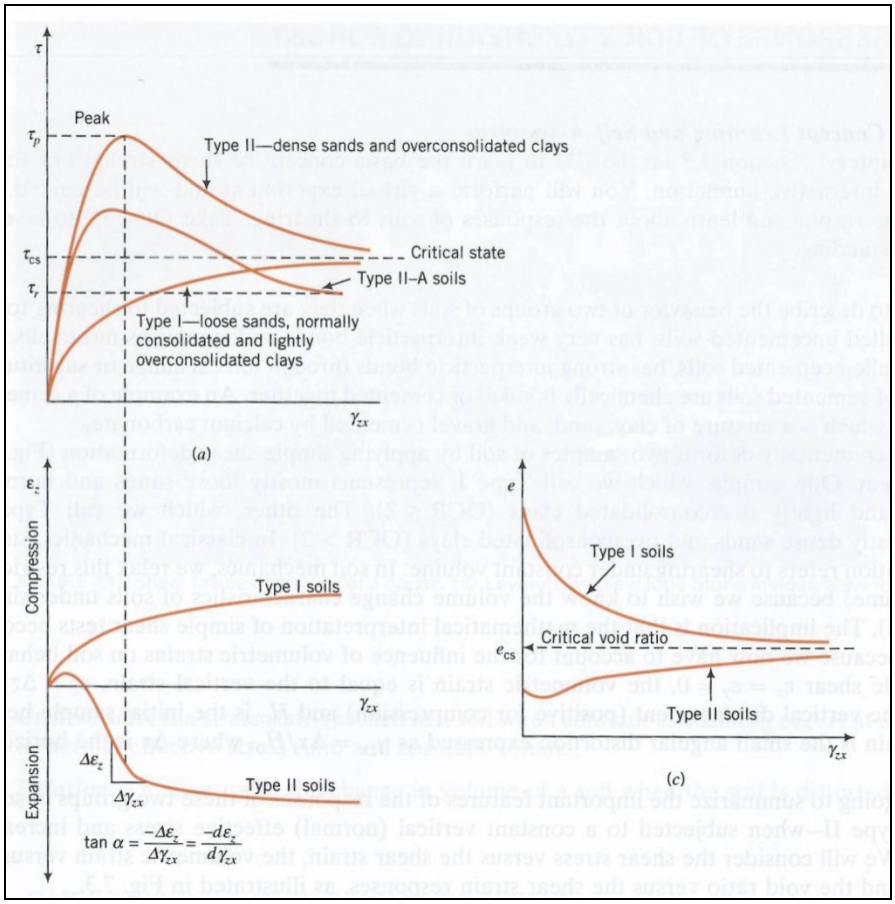

Figure 2.10 – Soil Response to Shearing (With permission, Budhu, 2007)

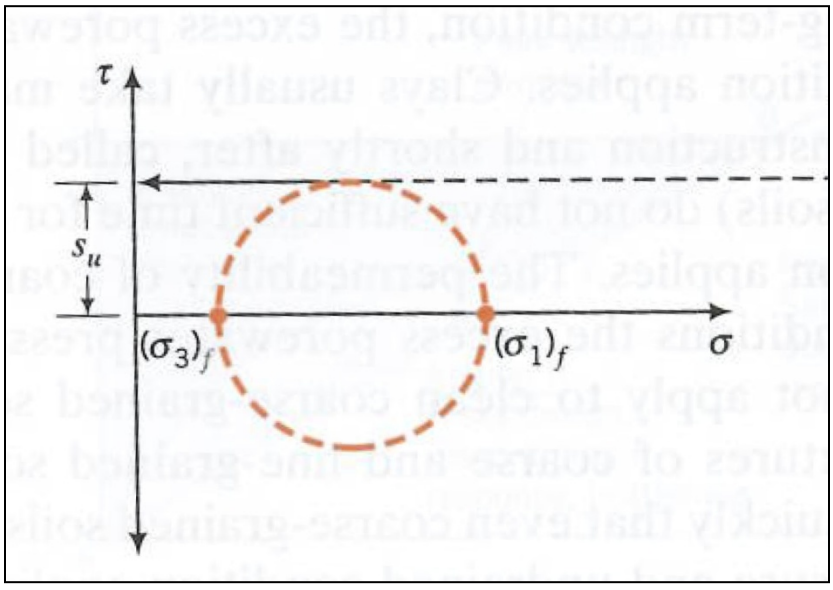

Figure 2.11 – Undrained Strength Envelope (With permission, Budhu, 2007)

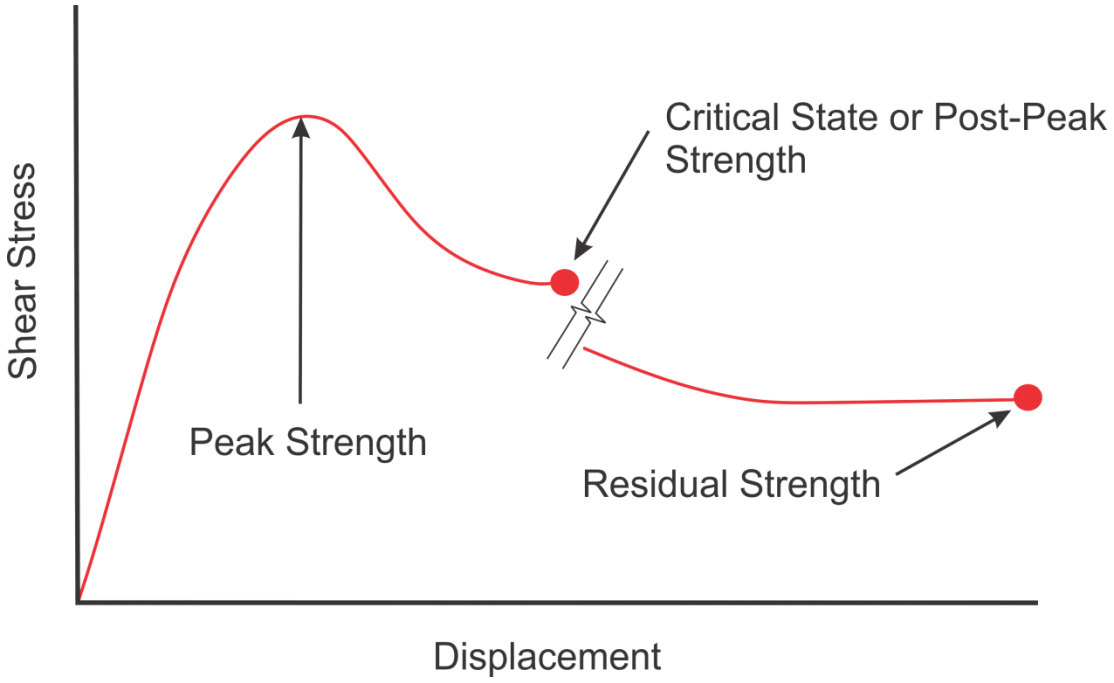

Figure 2.12 – Stress-Strain Relationship for Peak, Post-Peak and Residual

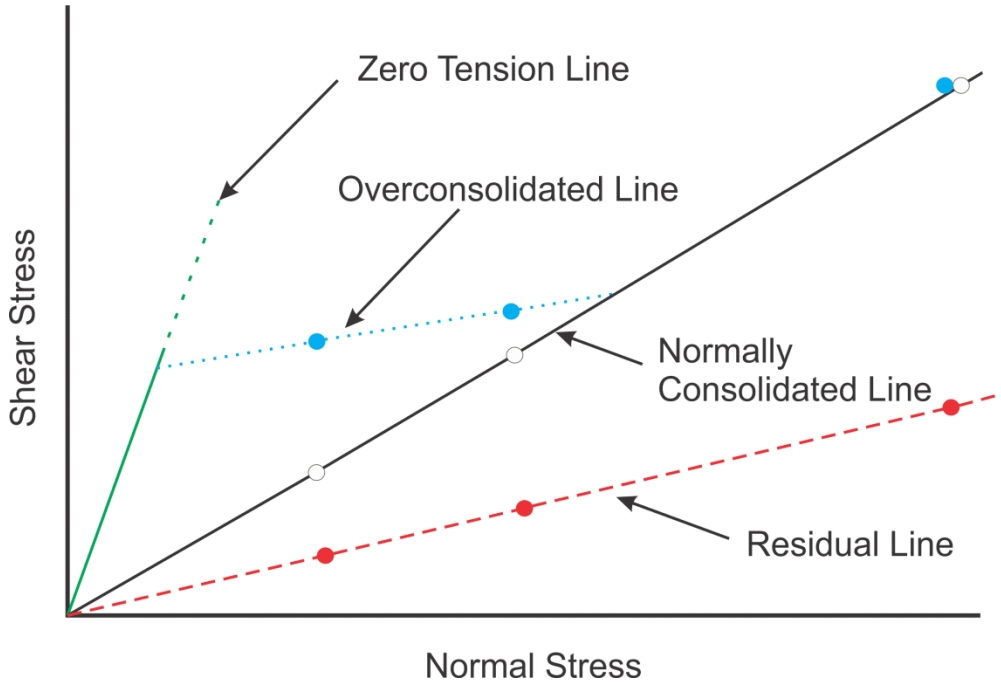

Figure 2.13 – Peak, Post Peak and Residual Strength Envelopes

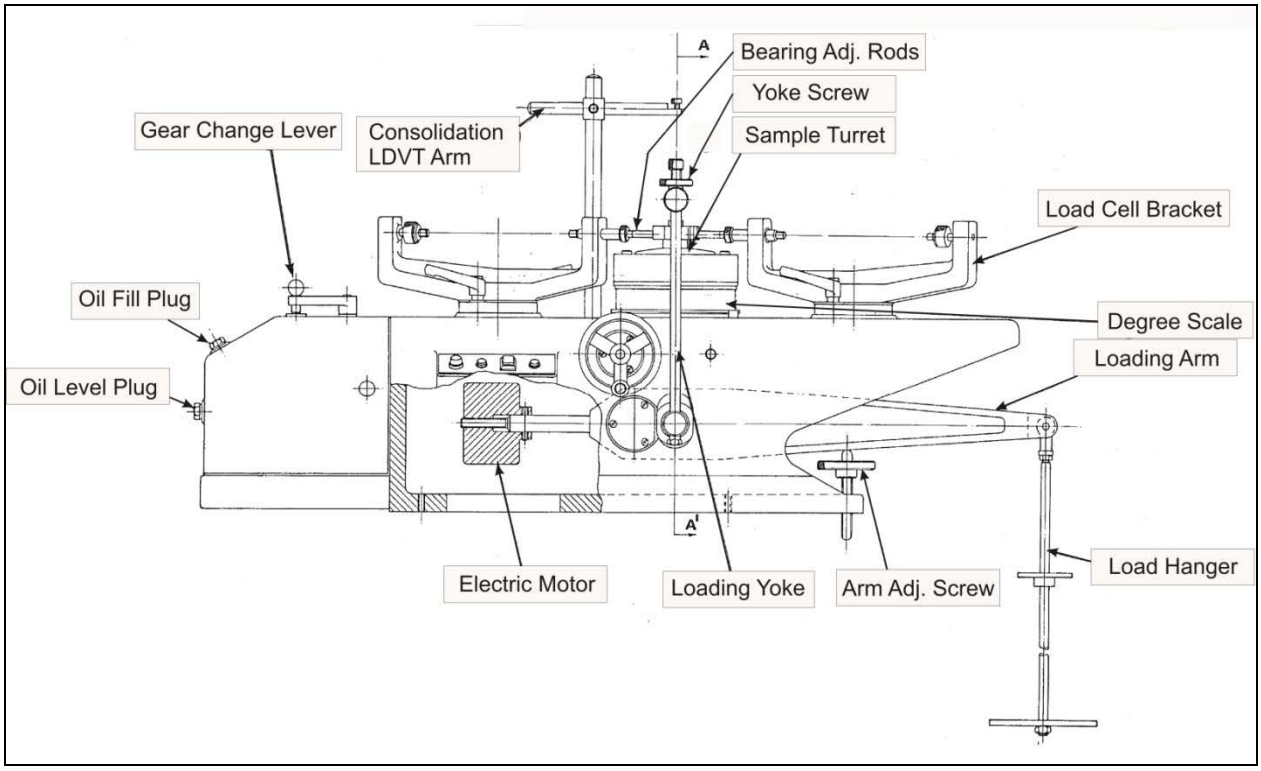

Figure 2.14 – Typical Bromhead Ring Shear Apparatus (With permission, Wykeham Farrance)

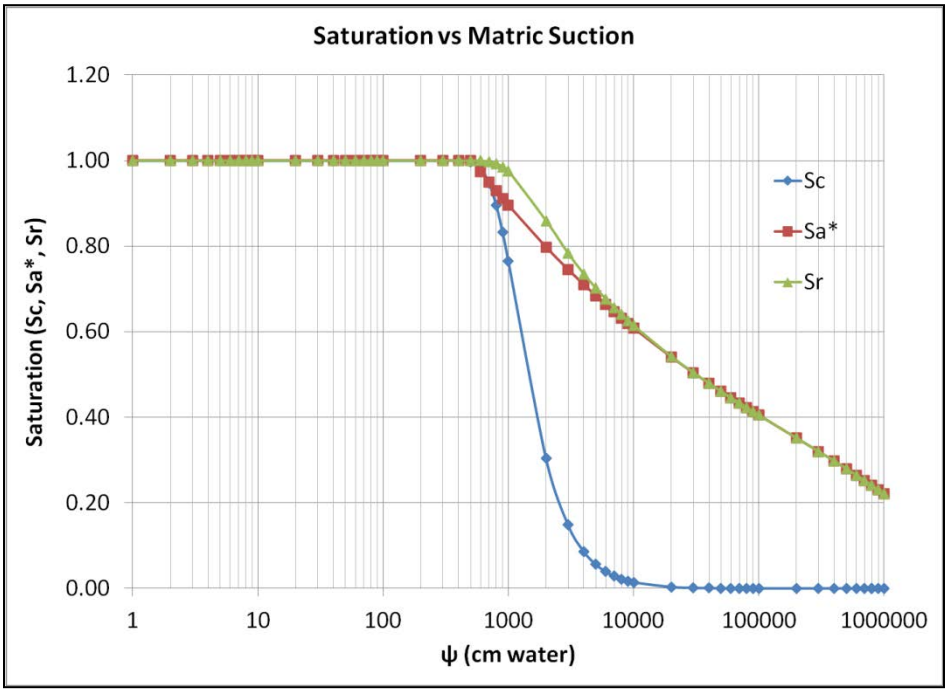

Figure 2.15 – Capillary and Adhesion Components of the SWCC

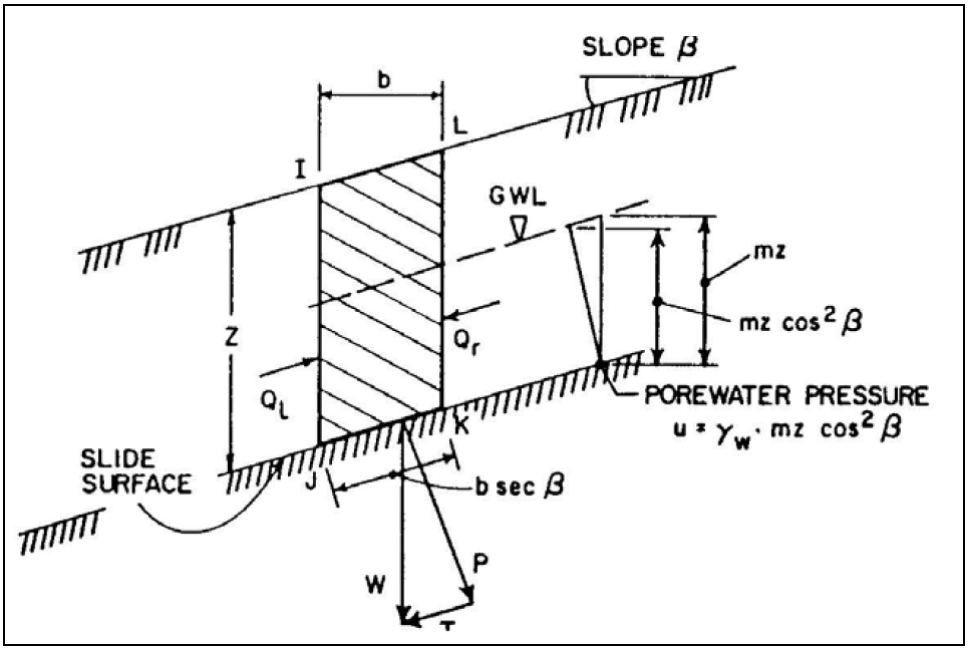

Figure 2.16 – Planar Failure in Infinite Slopes (With permission, Graham, 1984)

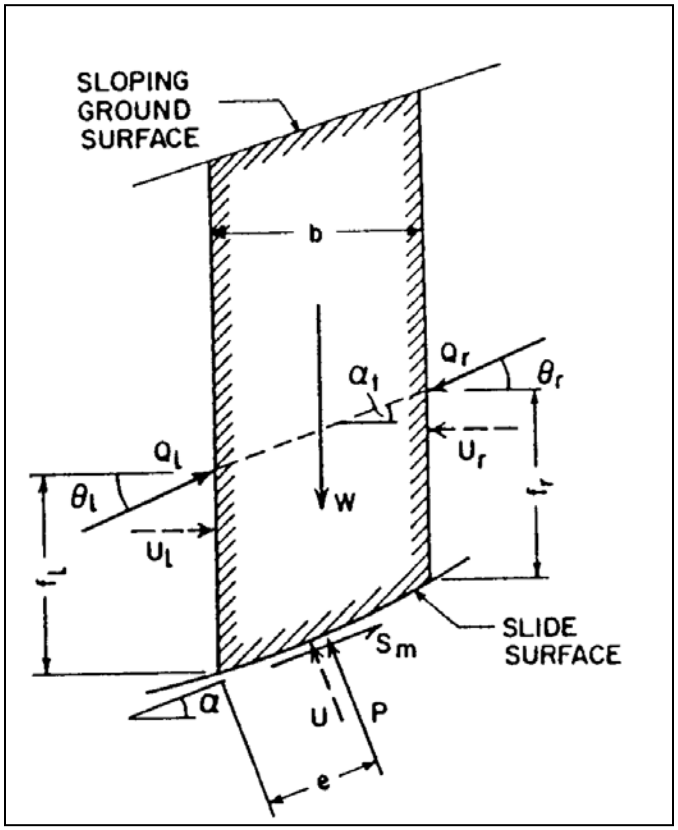

Figure 2.17 – Forces Acting on a Typical Isolated Slice (With permission, Graham, 1984)

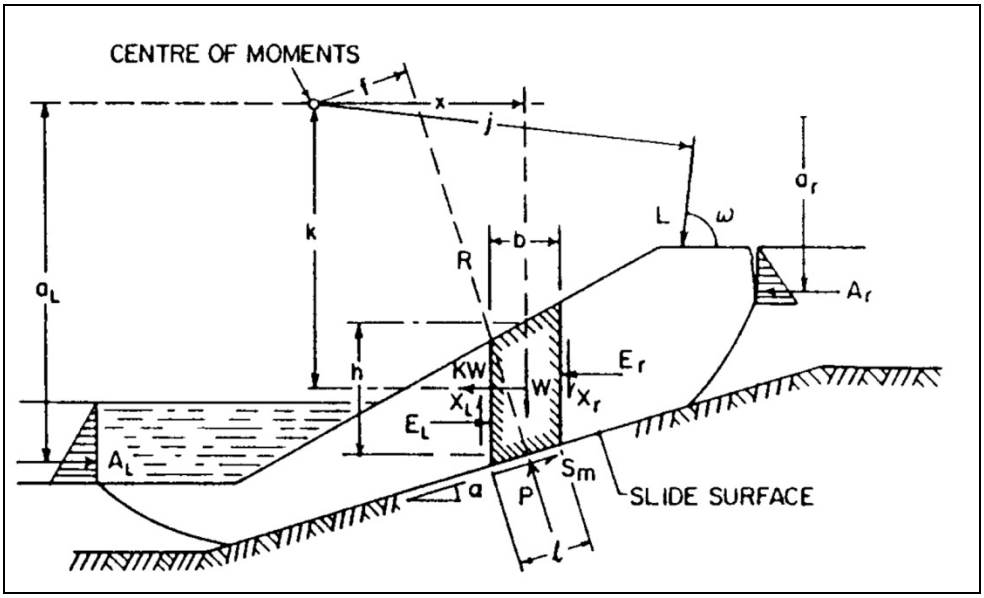

Figure 2.18 – Parameters Used to Satisfy Force and Moment Equilibrium (With permission, Graham, 1984)

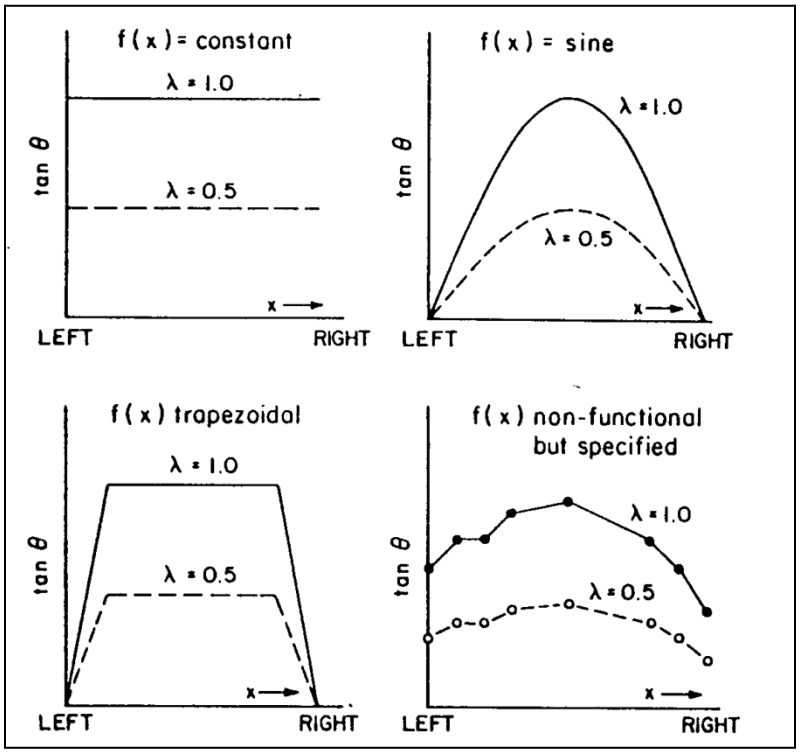

Figure 2.19 – Interslice Force Inclination Angle Distributions (With permission, Graham, 1984)

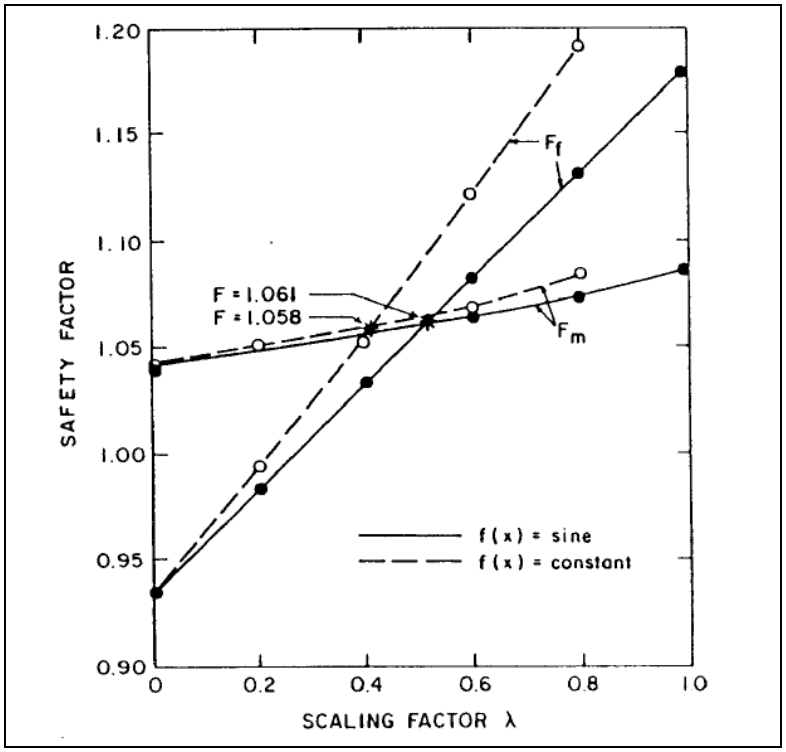

Figure 2.20 – FS vs λ For Varying f(x) (With permission, Graham, 1984)

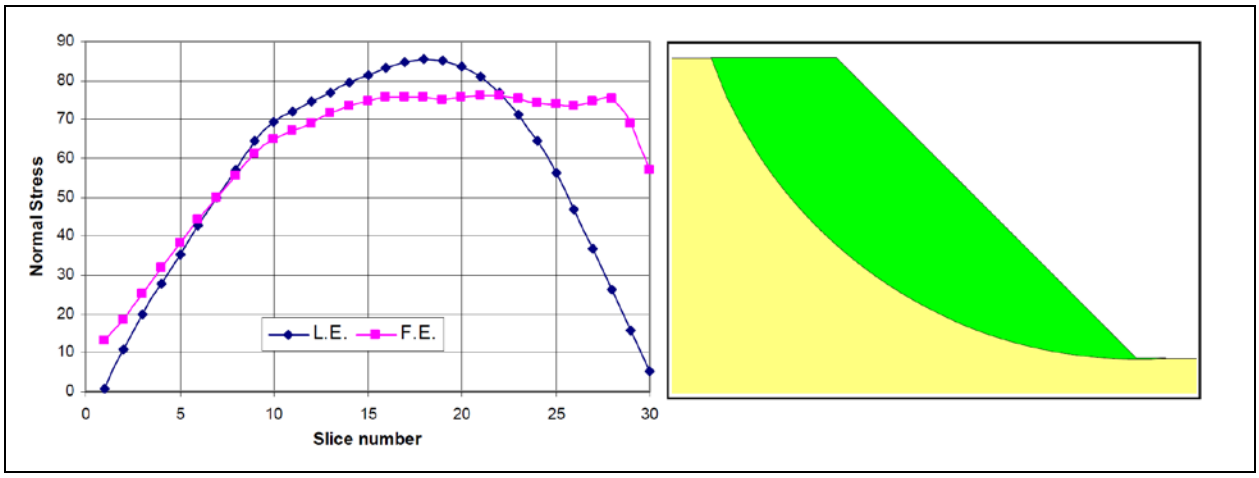

Figure 2.21 – Limit Equilibrium and Finite Element Normal Stress Distributions Along a Slip Surface (With permission, Geo-Slope International Ltd., Slope/W, 2010)

Chapter 3 – Site Conditions

3.1. General Overview

The grade slope at the Ashville Junction between PTH 5 and Mineral Creek is heavily vegetated with various trees, shrubs and grasses (Figure 3.1). Boulders left following post-glacial erosion of till soils from the Mineral Creek valley occur intermittently along the slope. As the highway crosses Mineral Creek, it cuts into the valley side slope and exposes weathered clay shale in the backslopes where the cut is most pronounced (Figure 3.2). These backslopes required re-grading following two additional failures reported by regional staff in 1988. At its lowest point within the failure area, the highway lies approximately 9 m below natural prairie level. The north side of the highway is ditched, sloping west to east toward Mineral Creek, while the south side slopes directly into the valley. Figure 3.3 shows relevant features of the site, as well as the stationing used for the project (shown along roadway centerline).

As mentioned earlier, multiple scarp lines exist on the grade slope, indicating the slope has failed retrogressively toward the highway over some time. The observed scarp lines indicate that the failure extends approximately 100 m parallel to the highway between stations 185+40 and 186+40. Shoulder slumps are affecting the pavement at the eastern extent of the failure near station 185+50, and significant cracking and slumping of the EBL has occurred near station 186+00. The total extent of the failure affecting the pavement is approximately 70 m. Cracking was also observed near the centerline in the west bound lane (WBL). It is uncertain if this is a result of slope movements as no significant change has occurred since the initial 2011 site investigation.

The municipal road (Mile Road 121W) highlighted in Figure 3.3 is subject to washouts during significant flood events on Mineral Creek (Figures 3.4 and 3.5). Local residents have claimed that the washouts appear to be increasing in frequency and magnitude since approximately 2009. The road crosses Mineral Creek approximately 200 m south of the Ashville Junction over an under-sized corrugated steel pipe (Figure 1.2). The pipe was once outfitted with a weir at the inlet (Figure 3.6), however it was washed out during flooding in June, 2013. During flood events the culvert has been observed to be overwhelmed, backing up water in the study area and washing out the road approximately 30 m south of the Ashville Junction. During periods of normal stream flow the water surface elevation of Mineral Creek is typically 337.0 m, while flood events raise the water surface elevation to approximately 340.9 m, flooding much of the study area (Figure 3.7). It is following such flood events that the most substantial slope movements have been observed to occur.

3.2. Site Geology and Geomorphology

The Manitoba Escarpment is an erosional feature of the Western Canadian sedimentary basin formed following uplift of the Western Cordillera during the Laramide Oregeny (Bamburak et al., 2004). Figure 3.8 shows a cross section of the stratigraphy over various depositional periods in the vicinity of the study area The escarpment contains primarily Cretaceous sedimentary deposits which dip southwest at approximately 0.5 m/km to 1.8 m/km. As such, the stratigraphy exposed at the face of the escarpment differs between the northwest and southeast extents. The face of the escarpment in its Pembina and Riding Mountain components in the southeast is comprised of Pierre Shale down to the Niobrara Formation. The Pasquia Hills, Porcupine Hills,

and Duck Mountain components are comprised of the Favel Formation down to the Ashville Formation (Bamburak et al., 2004).

Located approximately 2 km northwest of the Ashville Junction is an outcrop of Cretaceous clay shale, exposed through erosion of the Wilson River Valley. The Manitoba Geological Survey (2004) identifies this outcrop as the Upper Ashville Formation, and is also the deposit through which the Mineral Creek Valley has been cut in the study area. The Ashville Formation was deposited approximately 100 million years ago, and has a maximum depositional thickness of approximately 80 m. The deposit is comprised of carbonaceous shale, is dark grey to black in colour and is generally non-calcareous (not containing $CaCO_3$), although some minor bands of calcareous material have been observed. The formation also contains various relatively thin layers of bentonite. The bentonite is generally blue-grey in colour, but is observed to weather to yellow - orange (Bamburak et al., 2004). The layers of bentonite exposed at the Wilson River outcrop are consistent with this description, and are well defined at their contacts with subsequent soil layers (Figure 3.9). The Upper Ashville Formation, also called the Belle Fourche Formation, weathers into flat, chip-like pieces, may turn a brownish-grey colour when exposed, and selenite ($Ca^{2+}SO_4^{2-}$) crystals commonly occur within it. The small, exposure on the north side of PTH 5 in the study area has weathered into small fragments, with relatively large selenite crystals occurring frequently (Figures 3.10 and 3.11).

The upland components of the Manitoba Escarpment are defined by the Red Deer, Swan, Valley and Assiniboine Rivers. The corresponding river valleys separate the escarpment into the Pasquia and Porcupine Hills, and the Duck, Riding and Pembina Mountains (Figure 3.12). The Valley River separates the Duck and Riding Mountain components of the escarpment. The study area is situated in this region near the base of the escarpment, between Duck Mountain to

the northwest and Riding Mountain to the south (Figure 3.13). Like the Valley River valley, the Mineral Creek valley was formed following the retreat of glacial Lake Agassiz. While not as pronounced as many of the larger post-glacial valleys in this region, it is still relatively substantial in its depth and breadth, with relief of approximately 15 m in the study area (Figure 3.14). The base of the valley is comprised of alluvial sediments (Figure 3.15). Following flooding and subsequent washout of Mile Road 121W in the spring of 2013, these sediments were exposed as the flood waters cut into the soils beneath the road (Figures 3.16 and 3.17). In these photos, layered sands and gravels, as well as stratified silts and fine sands, are evident. These were deposited by river action from behind the escarpment following lake retreat, as well as from beach deposits formed to the west when glacial lake waters were still prevalent (Matile et al., 2004; Klassen, 1979).

The valley walls are comprised of till-like colluvium, deposited following erosion of the valley as illustrated in Figure 3.18. The colluvium is clay rich and contains variable quantities of silt, sand and gravel. Selenite crystals are common within the soil matrix, and are seen at sizes up to approximately 15 mm in diameter as shown in Figure 3.19. Large boulders of various origins deposited during glaciation are evident where erosion and weathering of the valley walls has left them exposed. The colluvium is underlain by the Ashville Formation of Cretaceous clay shale into which the Mineral Creek Valley was cut.

3.3. Site Hydrology

Mineral Creek flows into Wilson River downstream of the study area (Figure 3.20). Both watercourses make up part of the drainage basin between Duck Mountain and Riding Mountain

(Bamburak et al., 2004). The Mineral Creek watershed is within the Dauphin Lake drainage basin. Upstream of the Ashville junction, it has a tributary area of approximately 160 km^2. Mean annual precipitation in the basin varies from 508 mm per year at the Dauphin climate station to 530 mm per year at the Gilbert Plains climate station, approximately 25% of which is snowfall. In the vicinity of the eastern slopes of both the Duck and Riding Mountains, annual precipitation is generally 50 mm greater than other areas of the basin (Manitoba Water Stewardship, 2011). Between 2007 and 2013, the most recent years in which instabilities in the study area have been observed, Environment Canada reported a mean annual precipitation of 508 mm in the basin. Rainfall in the basin generally occurs as a result of convective weather systems. As such, intense storms occasionally cause flash flooding of various watercourses within the basin. Additionally, the spring snowmelt can cause flows that rise suddenly with significant peaks evident in flood hydrographs (Manitoba Water Stewardship, 2011). There are currently no active hydrometric stations along Mineral Creek. This study therefore relies on data collected at a station on the Wilson River in the vicinity of the Mineral Creek confluence. While it is understood that this data is not directly relevant to the study area, trends in the flow on the Wilson River can reasonably be applied to that of Mineral Creek.

Historically, most rainfall in the study area occurs in the months of June and July (Figure 3.21). When data from the year 2007 to 2013 is plotted however, above average precipitation events appear to have been occurring earlier in the year, particularly in the month of May, which means they then coincide with the spring freshet (Figure 3.22). In June 2013, flow in the triple box culvert, through which Mineral Creek passes beneath PTH 5, was such that the culvert was at or very near capacity (Figure 3.23). Preliminary hydrologic analysis completed by MIT shows that a flow of 73 m^3/s occurs at a frequency of 1%. This is a return period of 100 years, the

same return period for which the box culvert is designed. By comparison the upstream CSP culvert is designed with half the capacity of the box culvert, giving it a return period of 10 years.

The apparent increase in frequency of flood events of this magnitude may be the result of several factors, or any combination of them. Changes to local agricultural drainage systems, or changes to surface drainage through infrastructure development may reduce the time of concentration for a particular watercourse, thereby increasing flows more rapidly. Furthermore, climate change and, more specifically, an increase in low frequency high intensity rainfall events may be contributing to such flood events. Intense rainfalls occurring earlier in the year, when antecedent moisture contents in soils within the basin are still relatively high, may generate more runoff and higher flows than were seen in the past. Such factors are considered beyond the scope of this study and have not been explored any further in this document.

Figure 3.1 – General Terrain of Grade Slope at PTH 5 (North from mid-slope at station 185+70)

Figure 3.2 – Exposed Weathered Clay Shale in Backslope

Figure 3.3 – Study Area Site Plan

Figure 3.4 –Mile Road 121W During June, 2013 Flood Event (South from Ashville Junction)

Figure 3.5 – Washout of Mile Road 121W Following June, 2013 Flood Event (South from Ashville Junction)

Figure 3.6 – Corrugated Steel Pipe Culvert Crossing Outfitted with Weir During Normal Flow Conditions in June, 2011 (West from outlet)

Figure 3.7 – Flooding of Mineral Creek Valley in June, 2013 (Southeast from TH 2011-05)

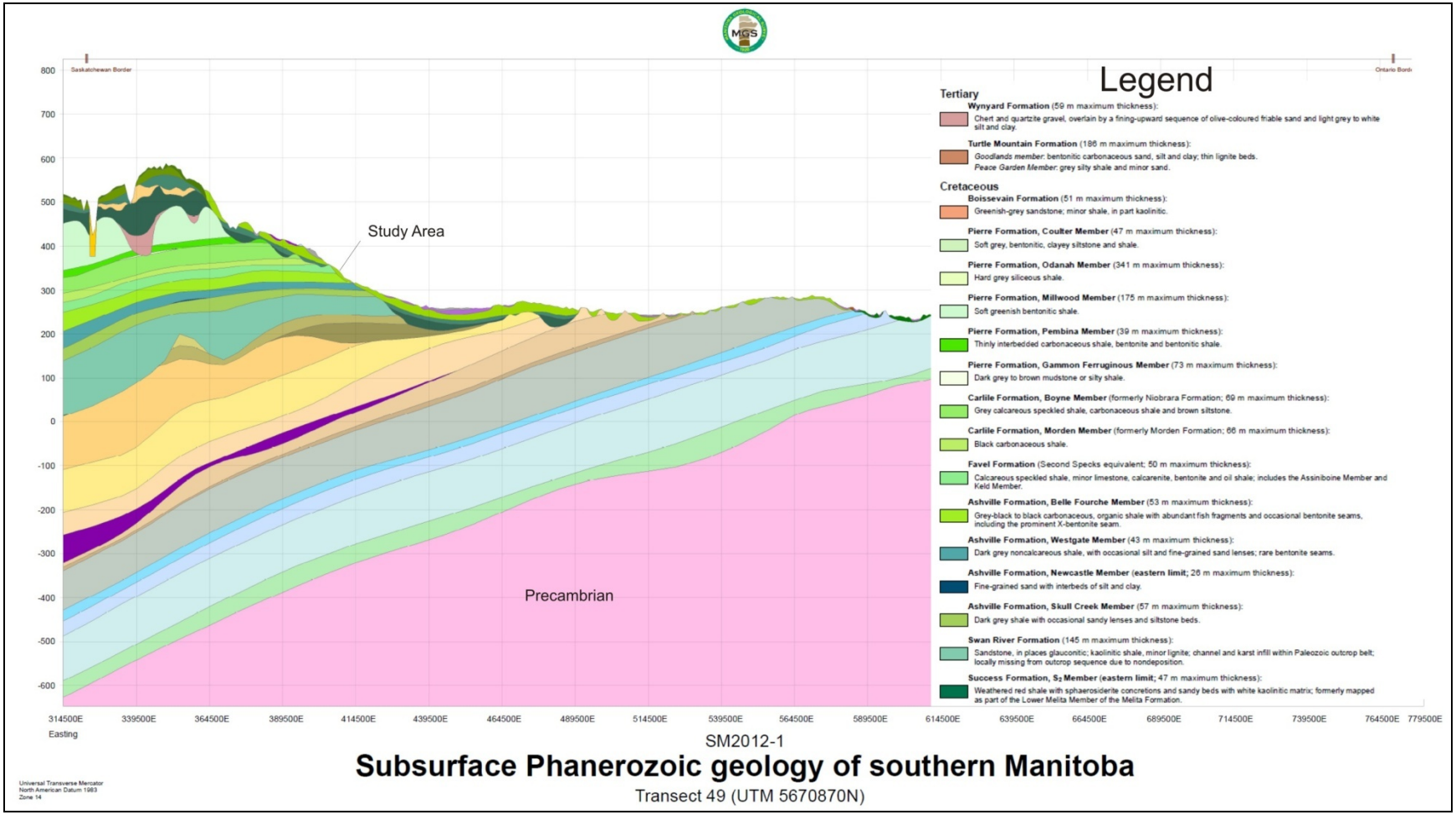

Figure 3.8 – Cretaceous and Tertiary Geology in the Vicinity of the Study Area (With permission, Matile et al., 2012)

Figure 3.9 – Ashville Formation Outcrop at Wilson River (Note - weathered bentonite seam)

Figure 3.10 – Weathered Shale Chips (Backslope of PTH 5, see Figure 3.2)

Figure 3.11 – Selenite (Gypsum) Crystals in Exposed Shale (See Figure 3.2)

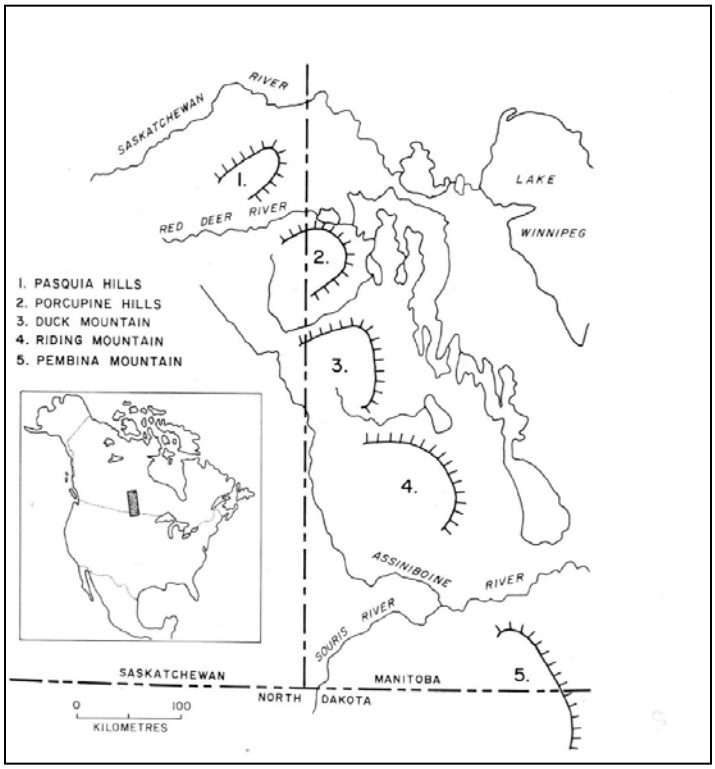

Figure 3.12 – Geological Components of the Manitoba Escarpment (With permission, McNeil, 1977)

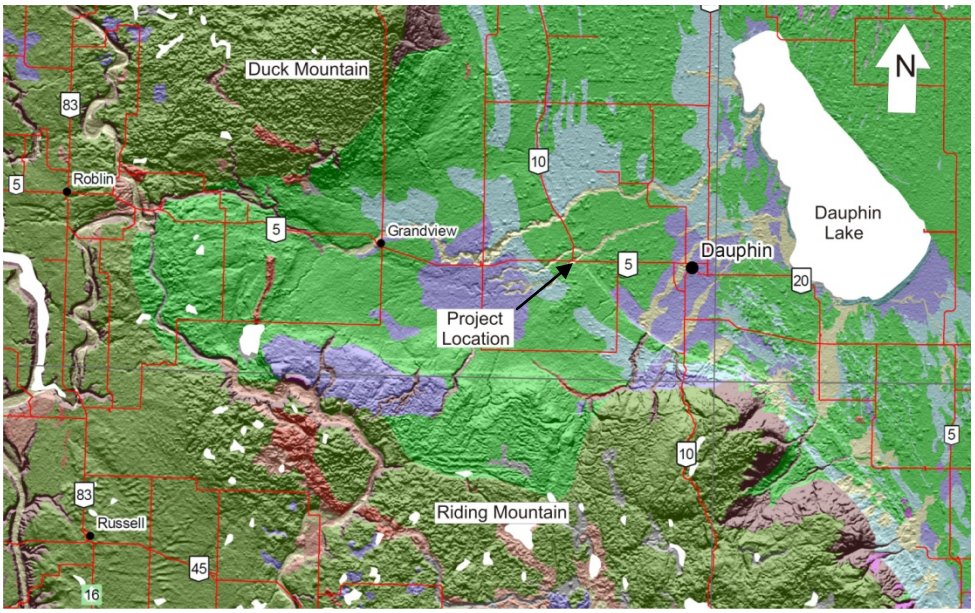

Figure 3.13 – Study Area Near the Base of the Manitoba Escarpment (With permission, Matile et al., 2007)

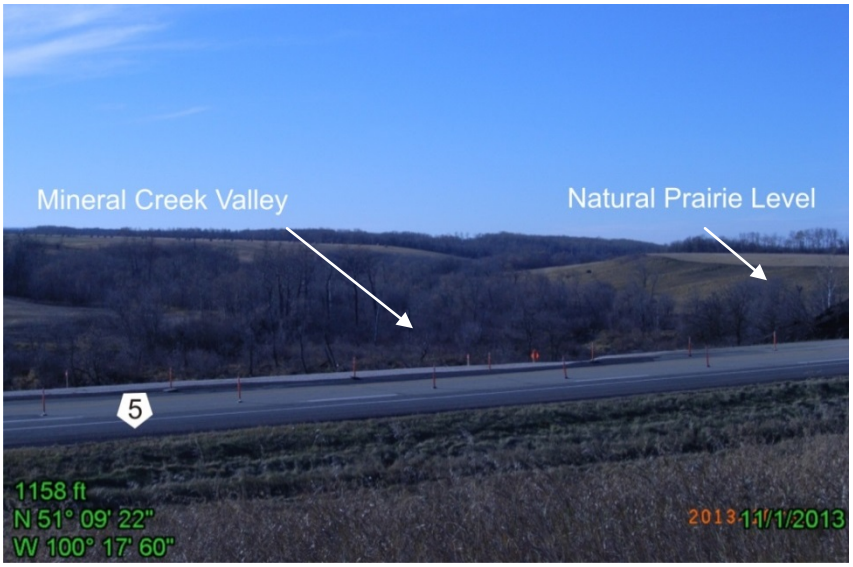

Figure 3.14 – Mineral Creek Valley (South from backslope)

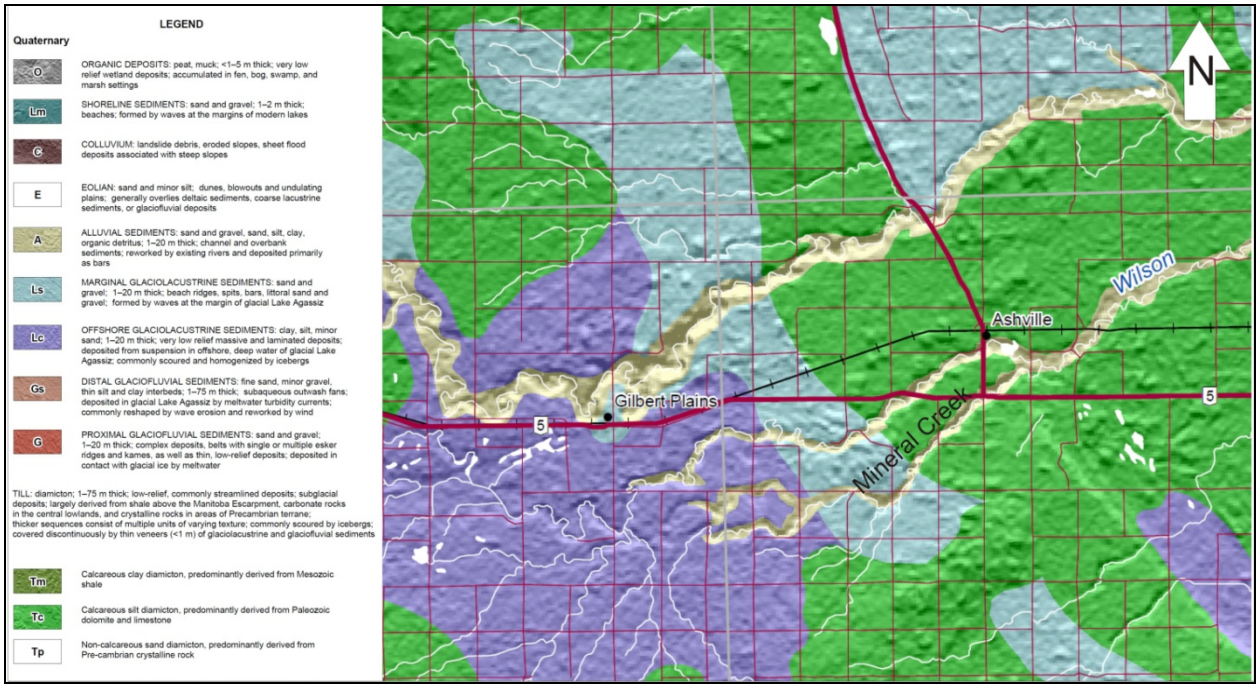

Figure 3.15 – Alluvial Deposits in Mineral Creek Valley (With permission, Matile et al., 2004)

Figure 3.16 – Stratified Alluvial Sediments Beneath Mile Road 121W

Figure 3.17 – Alluvial Sands and Gravels Beneath Mile Road 121W

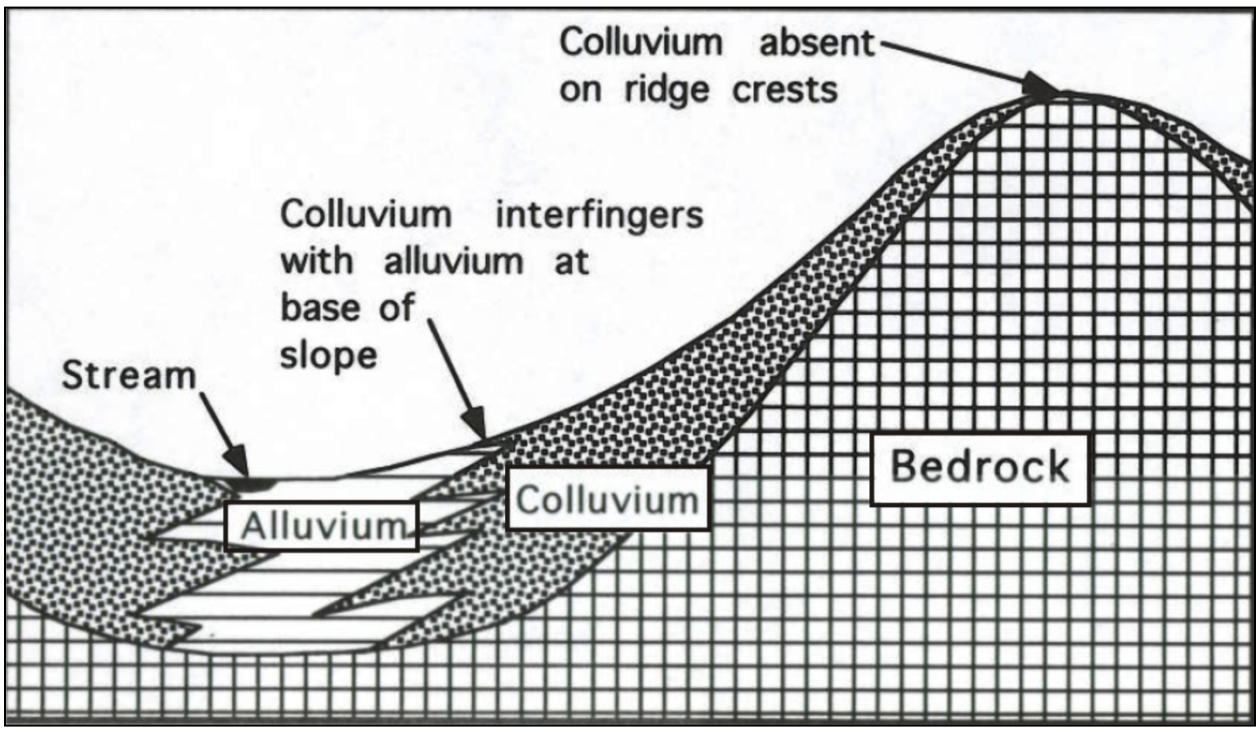

Figure 3.18 – Idealized Colluvium Deposition Following Valley Erosion (With permission, Turner et al., 1996)

Figure 3.19 – Selenite Crystals Observed in Till-Like Soils

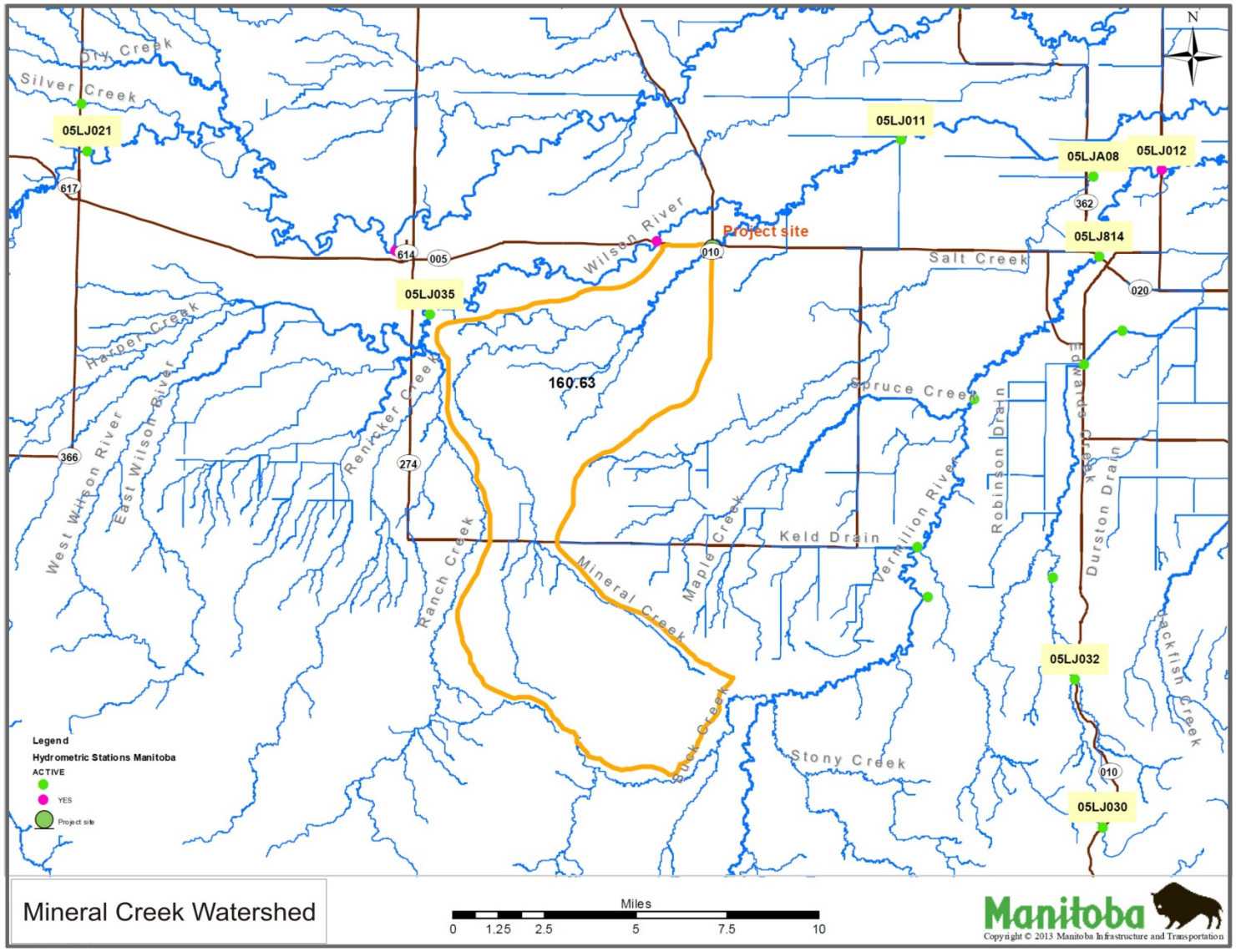

Figure 3.20 – Mineral Creek Watershed (Upstream of study area)

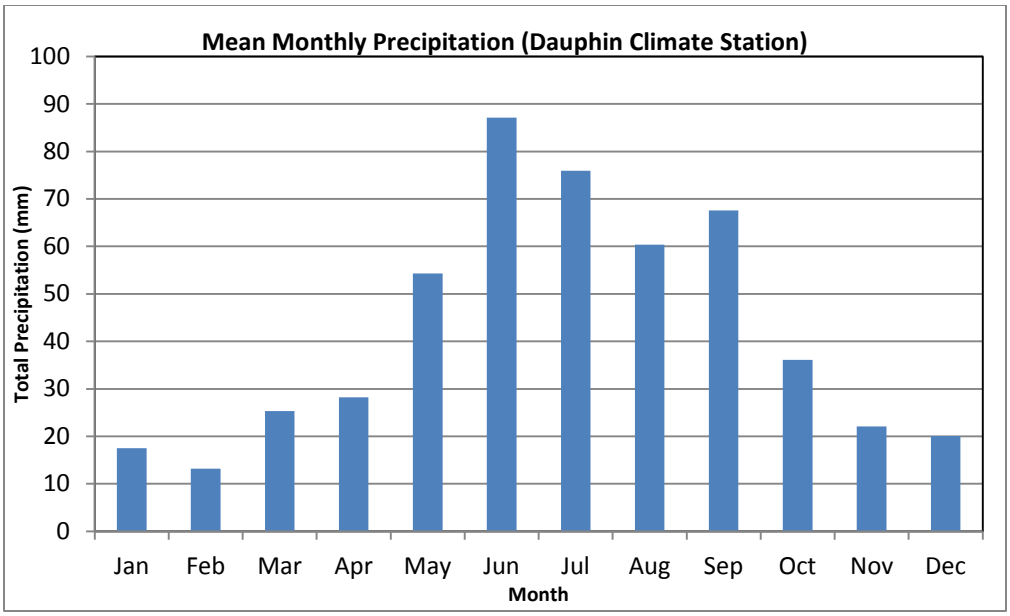

Figure 3.21 – Mean Monthly Precipitation for Study Area (Environment Canada, Climate, 2013)

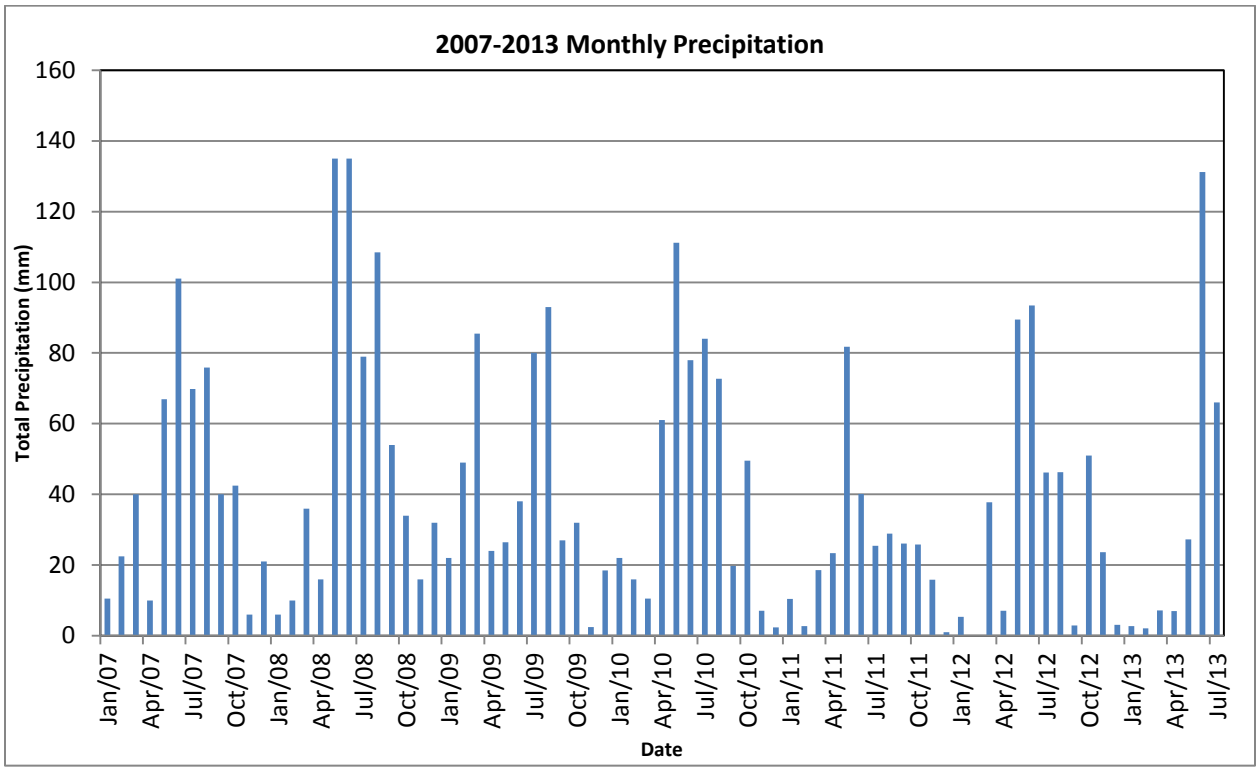

Figure 3.22 – Monthly Precipitation Between 2007 and 2013 (Environment Canada, Wateroffice2013)

Figure 3.23 – Triple Box Culvert, PTH 5 East of Slide Area (June, 2013)

Chapter 4 - Field Investigation

4.1. Introduction

Following slope movements in the spring of 2011 that heavily damaged the highway pavement, MIT initiated a geotechnical investigation to begin collecting information on the site and better understand the failure. The investigation was completed in two phases; the first in June, 2011 and the second in November, 2011. Phase I consisted of the drilling of four test holes and the installation of two slope inclinometers, three vibrating wire piezometers and one standpipe piezometer. Phase II consisted of drilling two more test holes, and installing two additional slope inclinometers and two vibrating wire piezometers. Figure 4.1 shows the locations of the instrumentation installed during both phases (white circles), as well as the positions of the test holes drilled in 1974 (blue circles) and 1989 (red circles).

4.2. Test Holes

Six test holes were drilled along the critical cross section of the failure, approximately at station 185+85 (Figure 4.1). Test holes TH2011-01 to TH2011-04 were drilled during Phase I of the investigation; test holes TH2011-05 and TH2011-06 were drilled during Phase II. During the phase I investigation, test holes were drilled with a track mounted drill rig using 125 mm solid stem augers (SSA) (Figure 4.2). All test holes during the second phase were drilled with a track mounted drill rig using 175 mm hollow stem augers (HSA) to prevent sloughing of the test hole annulus during NQ coring of the clay shale (Figure 4.3). Figure 4.4 shows a typical test hole log from the site. Detailed test hole logs, including those from 1974 and 1988, are provided in

Appendix A. The general stratigraphy encountered during both phases of the 2011 investigation is discussed in detail in following paragraphs.

TH2011-01 is located a few metres beyond the bulged toe of the slumped soil mass in the base of the valley. At this location, a relatively thin layer of organic soil was observed to be underlain by approximately 1.5 m of alluvial silty, sandy clay. The soil contains trace amounts of gravel, is of intermediate to high plasticity, and the moisture content increases with depth. Seepage was observed in this soil layer at a depth of approximately 1.7 m below existing ground level (EGL), which is relatively consistent with the normal water surface elevation of Mineral Creek. Clay content was observed to increase below a depth of approximately 2.1 m, where the soil becomes significantly stiffer, and dark grey in colour. At depths of approximately 2.1 m to 3.6 m, this clay has a blocky structure, and is likely the weathered surface of the Cretaceous clay shale below. Clay shale was encountered at a depth of approximately 3.6 m. The shale is dark grey in colour, moist, very stiff to hard, and highly plastic with occasional silt and fine sand lenses observed throughout. Standard Penetration Tests (SPT's) were completed every 3 m starting at a depth of approximately 4.5 m below EGL, and N values increase with depth from N = 60 until refusal was reached during the final two test intervals (see test hole logs in Appendix A). The test hole was terminated at a depth of 18.3 m.

TH2011-02 is located approximately 8 m south of the shoulder of the highway pavement. Approximately 1.2 m of clay road fill was observed before till-like colluvium was encountered. The colluvium consists of silty, sandy clay with trace amounts of gravel and gypsum, is brown mottled grey in colour, and of intermediate to high plasticity. Clay shale, as described above, was encountered at a depth of approximately 5.2 m, and a layer of blue-grey bentonite was encountered at a depth of approximately 5.3 m. SPT tests were completed every 1.5 m starting

at a depth of approximately 6.1 m below EGL, and N values generally increase with depth from N = 33 near the contact between colluvium and shale to N = 163 at a depth of approximately 17 m. The test hole was terminated at a depth of 18.3 m.

TH2011-04 is a relatively shallow test hole located in the ditch bottom north of PTH 5. Till-like soil, similar to that encountered in TH2011-02, was encountered to a depth of approximately 4.4 m. Blue-grey bentonite was encountered at a depth of approximately 4.3 m, and was likely displaced from the clay shale below during glaciation. Mixing of the till-like soil with clay shale near the contact between the two layers suggests that it may have been deposited glacially rather than as colluvium when the valley was formed. Clay shale, as described above, was encountered at a depth of approximately 4.4 m. Blue-grey bentonite was again encountered in the shale at a depth of approximately 7.5 m, consistent with the bentonite layer encountered in TH2011-02. This suggests that the layer may be continuous across the project area at this elevation (approximately el. 339 m). The test hole was terminated at a depth of 8.1 m.

TH2011-05 is the first test hole that was drilled during the phase II investigation, and is located approximately 18 m north of TH2011-01. A relatively thin layer of topsoil was observed to be underlain by approximately 3.2 m of till-like colluvium. The colluvium is comprised of silty clay with variable amounts of sand and gravel, is brown mottled grey in colour and of intermediate plasticity. Approximately 0.4 m of alluvial silty, clayey sand was encountered at a depth of approximately 3.2 m, and is underlain by a layer of till-like soil as described above. The location of this alluvial deposit within the slope suggests that there may have been significant slope movement occurring for many years at this location, perhaps triggered by erosion when flows in the valley were much more substantial than those even in recent years. At a depth of approximately 5.0 m, the till-like soil is underlain by clay shale as described previously. Shelby

tube samples were taken continuously from the upper contact to a depth of approximately 7.2 m, where the shale became too hard. Below 7.2 m, NQ core samples were taken to a depth of 10.8 m where the test hole was terminated (Figures 4.5 and 4.6). The shale is dark grey to black in colour, stiff becoming hard with depth and highly plastic. It has a blocky structure at its upper contact, indicating some degree of weathering has occurred. Below a depth of approximately 5.2 m the shale has a laminated structure, contains occasional silt and fine sand seems, and trace selenite crystals were observed at various depths. At the time of drilling, horizontal fracturing was observed to occur along bedding planes in intervals of 10 mm to 15 mm to a depth of approximately 5.8 m, below which the fracture interval appeared to increase to 20 mm to 40 mm. Figure 4.7 shows a typical extruded Shelby tube sample. Photos of all extruded Shelby tube and core samples can be found in Appendix B.

TH2011-06 is located on the shoulder of the EBL of PTH 5. Approximately 0.6 m of road base gravel was underlain by approximately 2.0 m of clay road fill. At a depth of approximately 2.6 m, till-like colluvium was encountered. The colluvium is comprised of silty clay with variable amounts of sand and gravel, is brown mottled grey in colour, and is of intermediate to high plasticity. Yellow-to-orange, weathered bentonite was observed at a depth of approximately 4.8 m near the contact with the clay shale below (Figure 4.8). Shelby tube samples were taken continuously over the entire depth of this soil layer. Clay shale, as described previously, was encountered at a depth of approximately 5.7 m. A layer of lightly weathered, blue-grey bentonite was encountered at a depth of approximately 5.9 m (Figure 4.9). Shelby tube samples continued into the shale to a depth of approximately 6.6 m, after which NQ core samples were taken. At a depth of approximately 8.6 m, at the beginning of the second run of coring, a 250 mm layer of blue-grey bentonite was encountered (Figure 4.10). This is relatively

consistent with the elevation this layer was encountered in other test holes. The test hole was terminated at a depth of 10.1 m.

4.3. Instrumentation

A total of four slope inclinometers (SI), five vibrating wire (VW) piezometers, and one standpipe piezometer (SP) were installed during both phases of the investigation. The instrumentation is numbered according to the test hole in which it has been installed (VW2011-01 installed in TH2011-01, etc). Table 4.1 shows a summary of all instrumentation and the depths and elevations at which they were installed. All slope inclinometers were read in imperial units using a Durham Geo Slope Indicator Inc. (DGSI)[8] probe. All vibrating wire piezometers were Model VW2100 instruments from RST Instruments[9].

4.3.1. Slope Inclinometers

Slope Inclinometer SI2011-01 was installed during the Phase I investigation, a few metres south of the toe of the slope, to a depth of approximately 18.3 m below existing ground level (el. 320.7 m) into competent clay shale. This instrument did not show any movement from the time of installation until remedial construction began, at which time all slope inclinometers were decommissioned. Figure 4.11 shows a typical slope inclinometer plot of cumulative displacement versus elevation (all plots shown in Appendix C). The “A” axis is a plot of displacement perpendicular to the roadway centerline (positive A is downslope), while the “B” axis is a plot of displacement parallel to the roadway (in this instance, positive B is west).

[8] Durham Geo Slope Indicator Inc., Mukilteo, Washington, U.S.A.
[9] RST Instruments Ltd., Coquitlam, B.C.

Slope Inclinometer SI2011-02 was installed during the Phase I investigation, south of the shoulder of PTH 5, to a depth of approximately 18.3 m below existing ground level (el. 327.6 m) into competent clay shale. Only two sets of readings were collected from this instrument before slope movements sheared the slope inclinometer pipe at an elevation of approximately 341.0 m, or a depth of 4.9 m below existing ground level. The depth of failure shows that the shear plane occurs around the interface of the till-like colluvium and the underlying clay shale.

Slope Inclinometer SI2011-05 (Figure 4.11) was installed during the Phase II investigation, around mid-slope, to a depth of approximately 10.8 m below existing ground level (el. 331.2 m) into competent clay shale. Several sets of readings were taken prior to the slope inclinometer pipe shearing in the spring of 2013. The readings indicate slope movements occurred at an elevation of approximately 338.7 m, or a depth of 3.2 m below existing ground level. The depth of failure of the SI pipe suggests that the failure surface may be exiting above the toe of the existing slope. However, “bulging” at the toe suggests that the failure surface previously exited the slope at a different location.

Slope Inclinometer SI2011-06 was installed into competent clay shale during the Phase II investigation. It was installed in the shoulder of the EBL, to a depth of approximately 10.1 m below existing ground level (el. 338.8 m). Several sets of readings were taken prior to the slope inclinometer pipe shearing in the summer of 2013. These readings indicate slope movements occurred at an elevation of approximately 342.8 m, or a depth of 5.1 m below existing ground level.

The movements observed in these slope inclinometers indicate that a shear plane exists at or near the interface between the till-like colluvium and the underlying Cretaceous clay shale. The

site was not instrumented during the geotechnical investigations conducted in 1965 and 1974, which identified weak layers of bentonite as the cause of failure. The 1974 investigation appears to assume that the failure surface follows a single weak layer of bentonite (Figure 1.11), a common mechanism of slope failure[10] in deposits of Cretaceous clay shale. The location of the shear plane observed by the instrumentation suggests that this is not the case in this study area. The 2011 investigation identified the bentonite shown in TH1974-01 and TH1974-02 as separate layers occurring approximately horizontally within the clay shale. Had TH1974-01 been drilled deeper, the separate layers might have been identified. Because of the relatively horizontal deposition of the bentonite and the location of movements observed in the slope inclinometers, these layers are not considered to be the primary cause of failure. This will be discussed in greater detail in Section 7.

4.3.2. Piezometers and Data Loggers

A single vibrating wire piezometer was installed in each of test holes TH2011-01, TH2011-02, and TH2011-04 to TH2011-06. A single standpipe piezometer with Casagrande tip was installed in TH2011-03. The piezometers were at first monitored only intermittently during site visits, but the irregular data made interpretation of the results difficult. One DGSI Quattro (four channel) Logger and one DGSI Mini (single channel) Logger were installed in February, 2013 in order to obtain a more complete data set for the interpretation of porewater pressures. Vibrating wire piezometers VW2011-01, VW2011-05 and VW2011-06 were read using the Quattro Logger, with the fourth channel dedicated to an on-site barometric piezometer. Vibrating wire piezometer VW2011-04 was connected to the Mini Logger. The data loggers were initially programmed to record in three hour intervals, but significant scatter was observed in the data

[10] Personal Communication, J. Graham, 2013

that made data interpretation for determining the soil parameters discussed in Section 2.5 difficult. It was therefore necessary to increase the reading frequency to 15 minutes[11] to reduce scatter. Figure 4.12 shows a plot of total head versus time for all data collected from the vibrating wire piezometers and the standpipe piezometer.

The data collected from the on-site barometric piezometer was compared with data obtained from Environment Canada (2013) to ensure that the barometric correction applied to the vibrating piezometer data is relatively accurate (Figure 4.13). There is significant scatter and relatively poor correlation between the data sets prior to increasing the readout frequency of the data logger in May, 2013. However, the data sets compare very well after increasing the readout frequency, with only subtle differences observed between recorded values. It should be noted that the Environment Canada climate station is located approximately 20 km from the project area, which may account for some difference between the two data sets.

Vibrating wire piezometer VW2011-01 was installed during the Phase I geotechnical investigation at a depth of approximately 17.4 m below existing ground level (el. 321.6 m) in clay shale. The piezometer was fastened to the outside of the slope inclinometer pipe, and sealed in bentonite grout to the ground surface. The raw data collected was corrected for changes in barometric pressure with the B-coefficient outlined in Section 2.5, by adjusting the coefficient until a general “smoothing” of the data occurred. In this instance, a B-coefficient of 0.9 has been selected for the clay shale observed in test hole TH2011-01. For the purpose of calibrating the steady state seepage model of the site, a piezometric elevation of 336.2 m was assumed under normal conditions for VW2011-01.

[11] Personal communication, S.L. Barbour, 2013

Figure 4.14 shows a plot of total head (m) versus time for both the raw and B-corrected data, as well as the change in barometric pressure, $\Delta\sigma_B$ (kPa), versus time. Data collected prior to the installation of the data loggers is not shown. While the corrected data in this plot still contain some irregularities, it can be seen that the effect of changes in barometric pressure has been significantly reduced. Of note on the plot of total head versus time are the two flood events; the first occurring in April, 2013 and the second in June, 2013. As vibrating wire piezometer VW2011-01 is installed at significant depth in a low permeability medium, it is unlikely that the spikes in porewater pressure have been induced by an increase in groundwater flow, but rather by the stresses induced by the flood water above.

Vibrating wire piezometer VW2011-02 was installed during the Phase I geotechnical investigation at a depth of approximately 9.8 m below existing ground level (el. 336.2 m) in clay shale. Substantial displacements of the instrumentation in test hole TH2011-02 severed the cable of VW2011-02 prior to the installation of the data loggers, and limited data was collected from this instrument. A plot of this data will be discussed later in this section. For the purpose of calibrating the steady state seepage model of the site, a piezometric elevation of 340.0 m was assumed under normal conditions for VW2011-02.

Standpipe piezometer SP2011-03 was installed during the Phase I geotechnical investigation at a depth of approximately 6.1 m below existing ground level (el. 339.7 m) in clay shale. This instrument was installed approximately 2 m east of TH2011-02. The average piezometric elevation recorded from this instrument was 340.6 m, indicating a downward hydraulic gradient of 0.17 between this instrument and VW2011-02. This observation was used in calibrating the steady state seepage model.

Vibrating wire piezometer VW2011-04 was installed during the Phase I geotechnical investigation at a depth of approximately 7.9 m below existing ground level (el. 338.6 m) in a layer of blue-white bentonite within the clay shale deposit. Figure 4.15 shows a plot of total head (m) versus time for both the raw and B-corrected data, as well as the change in barometric pressure, $\Delta\sigma_B$ (kPa), versus time. Figures 4.16 and 4.17 show plots of the corrected data for both vibrating wire piezometers VW2011-01 and VW2011-04, and demonstrate the "smoothing" of the data at a particular time interval. Data collected prior to the installation of the data loggers is not shown. It can be seen in this plot that groundwater conditions remain relatively constant between seasons and, due to the location of the instrument, the effects of flood water on porewater pressures do not appear. In this instance, a B-coefficient of 0.9 has again been selected for the bentonite and clay shale observed in test hole TH2011-04. The corrected data in Figure 4.15 still contains some irregularities, but it can be seen that the effect of changes in barometric pressure has been significantly reduced. A piezometric elevation of approximately 341.0 m was observed under normal conditions for VW2011-04.

Vibrating wire piezometer VW2011-05 was installed during the Phase II geotechnical investigation at a depth of approximately 7.0 m below existing ground level (el. 335.0 m), just below the interface between the till-like colluvium and clay shale. Figure 4.18 shows a plot of total head (m) versus time for both the raw and B-corrected data, as well as the change in barometric pressure, $\Delta\sigma_B$ (kPa), versus time. Data collected prior to the installation of the data loggers is not shown. Again, the two spring flood events are prominent in this plot. In this instance, a B-coefficient of 0.95 has been selected. However, the correction does not have the same "smoothing" effect and exhibits significantly more scatter than the data described above.

The theory for the B-correction is based on a saturated, isotropic, elastic soil. As this piezometer is located near the interface of the colluvium and shale, it is near the unsaturated zone. Furthermore, the till-like colluvium is much more heterogeneous in nature than the clay shale below, and contains relatively large roots, boulders and tensions cracks caused by slope movements. Its structure may therefore be unsuitable for the application of this theory in determining elastic and hydraulic properties. For the purpose of calibrating the steady state seepage model of the site, a piezometric elevation of 337.0 m was assumed under normal conditions for VW2011-05.

Vibrating wire piezometer VW2011-06 was installed during the Phase II geotechnical investigation at a depth of approximately 6.1 m below existing ground level (el. 341.8 m), near the interface of the till-like colluvium and clay shale. A layer of bentonite is present in the vicinity of the piezometer tip, which may also influence the observed data. Figure 4.19 shows a plot of total head (m) versus time for both the raw and B-corrected data, as well as the change in barometric pressure, $\Delta\sigma_B$ (kPa), versus time. Data collected prior to the installation of the data loggers is not shown. Of note in this plot is the general trend of increasing porewater pressure at this location, which is somewhat of an anomaly when compared with data from the other piezometers. It is possible that groundwater flow is being interrupted by the relatively impermeable bentonite. This may be causing porewater pressures to build up at this location and a perched water table to develop. Substantial displacements of the instrumentation in test hole TH2011-06 severed the cable of VW2011-06 in June, 2013, and limited data was collected from this instrument.

In this instance, a B-coefficient of 0.95 has been selected, but again, the correction does not have the same “smoothing” effect and exhibits significantly more scatter than the data described

in the paragraphs above. This is likely due to the factors described for the data collected from VW2011-05. For the purpose of calibrating the steady state seepage model of the site, a piezometric elevation of 341.0 m was assumed under normal conditions for VW2011-06.

4.4. Topographic Survey

Topcon real time kinematic (RTK) GPS equipment was used to establish control points and road lines for reference to UTM coordinates and geodetic elevations. Once the control points were established, a Topcon robotic total station and handheld data collector were used to take cross sections across the project site. The cross sections were taken in two phases, with the first phase being completed following the Phase I geotechnical investigation in July, 2011. These cross sections were taken at intervals of approximately 7.6m, between stations 185+60 and 186+40, and generally cover the failed section of the slope (Figure 3.3). A second survey was completed prior to the Phase II geotechnical investigation in the fall of 2011, and cross sections at 10 m and 20 m intervals were added to extend the survey from station 183+86.72, at the centerline of PTH 10, to 187+30 at the west-most extent. The data collected from both surveys was used to generate a digital terrain model (DTM) of the site. Figure 4.20 shows a contour plan of the plan of the project area, and Figures 4.21 and 4.22 show a three dimensional DTM of the project area.

Table 4.1 – Site Instrumentation

Test Hole #	Ground Surface Elevation (m)	SP Tip Elevation (m)	VW Tip Elevation (m)	SI Base Elevation (m)
TH2011-01	338.98	-	321.58	320.68
TH2011-02	345.90	-	336.02	327.60
TH2011-03	345.78	339.68	-	-
TH2011-04	346.52	-	338.61	338.42
TH2011-05	342.02	-	334.99	331.20
TH2011-06	347.94	-	341.84	336.94

Figure 4.1 – Test Hole and Instrumentation Plan

Figure 4.2 – Phase I Drilling, TH2011-01 (June, 2011)

Figure 4.3 – Phase II Drilling, TH2011-05 (November, 2011)

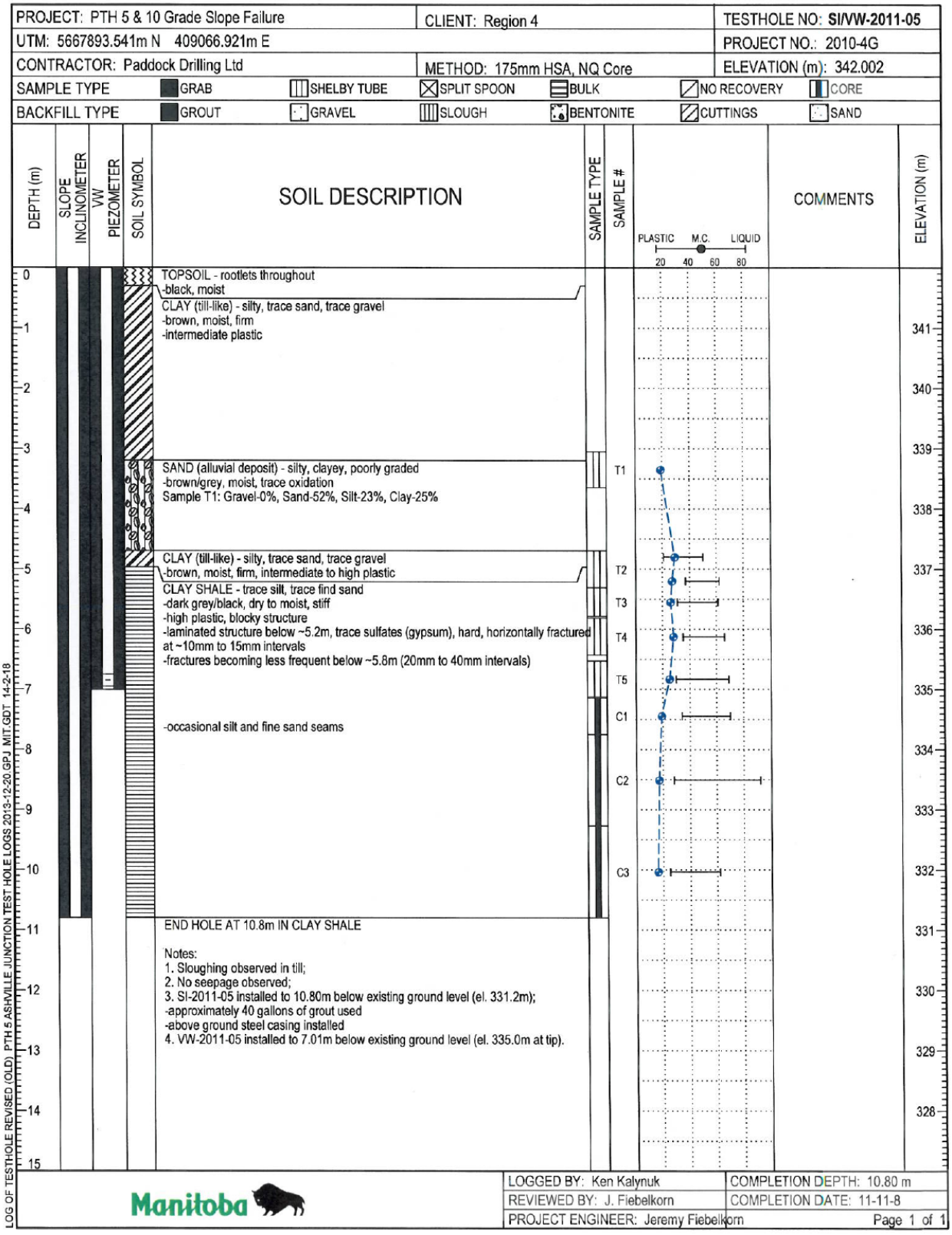

Figure 4.4 – Typical Test Hole Log, TH2011-05

Figure 4.5 – Clay Shale Core Sample During Phase II Drilling

Figure 4.6 – Clay Shale Core Sample (Lower sample shown in Figure 4.5)

Figure 4.7 – Typical Extruded Shelby Tube Sample (T07, TH2011-06)

Figure 4.8 – Weathered Bentonite Near Till/Shale Contact (TH2011-06)

Figure 4.9 – Blue-Grey Bentonite Seam, Sample T12, TH2011-06

Figure 4.10 – Blue-Grey Bentonite Seam, Sample C16, TH2011-06

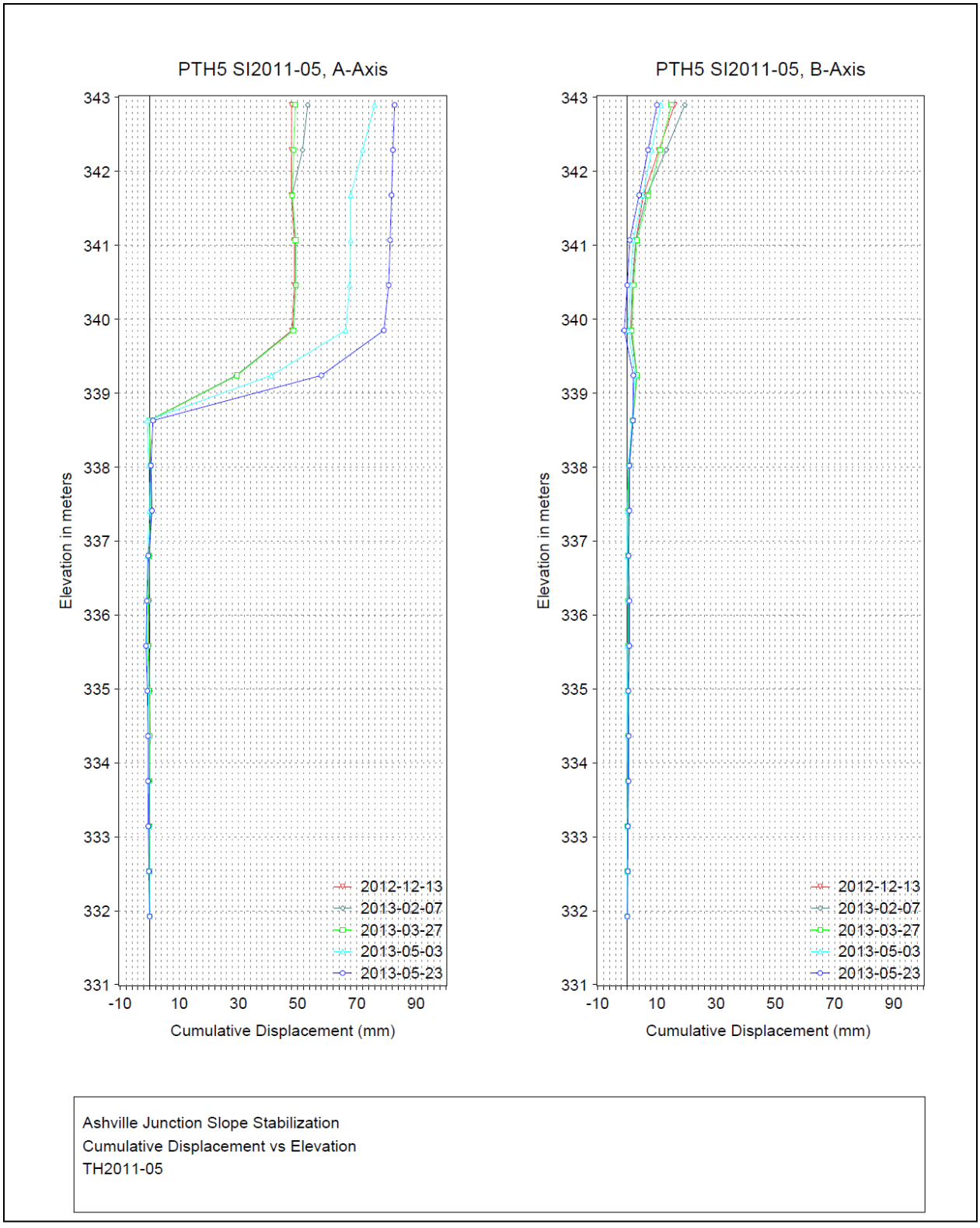

Figure 4.11 – Typical Slope Inclinometer Plot of Cumulative Displacement vs Elevation (SI2011-05)

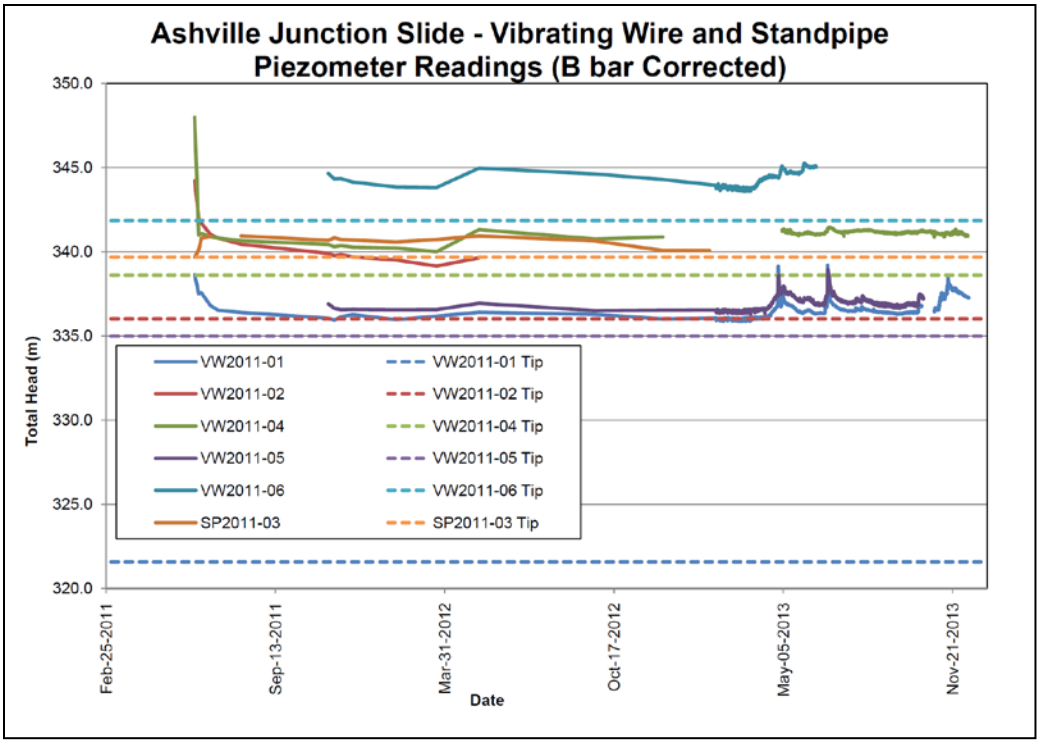

Figure 4.12 – Total Head vs Time for all Piezometer Installations

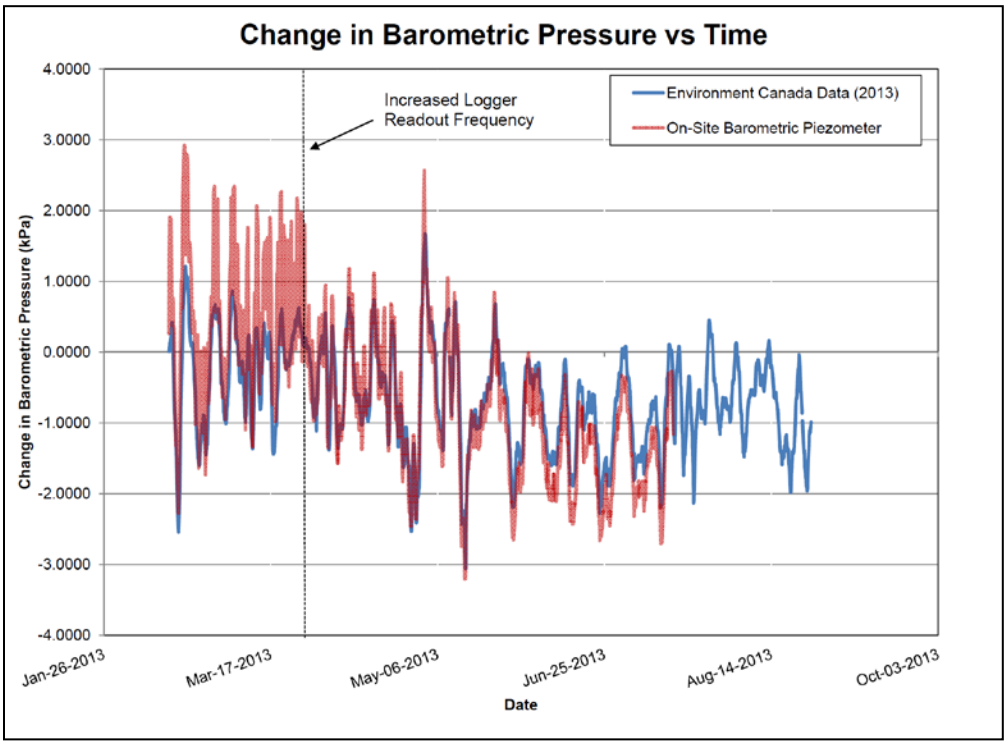

Figure 4.13 – Comparison of On-site Changes in Barometric Pressure with Environment Canada Data (Environment Canada, Climate, 2013)

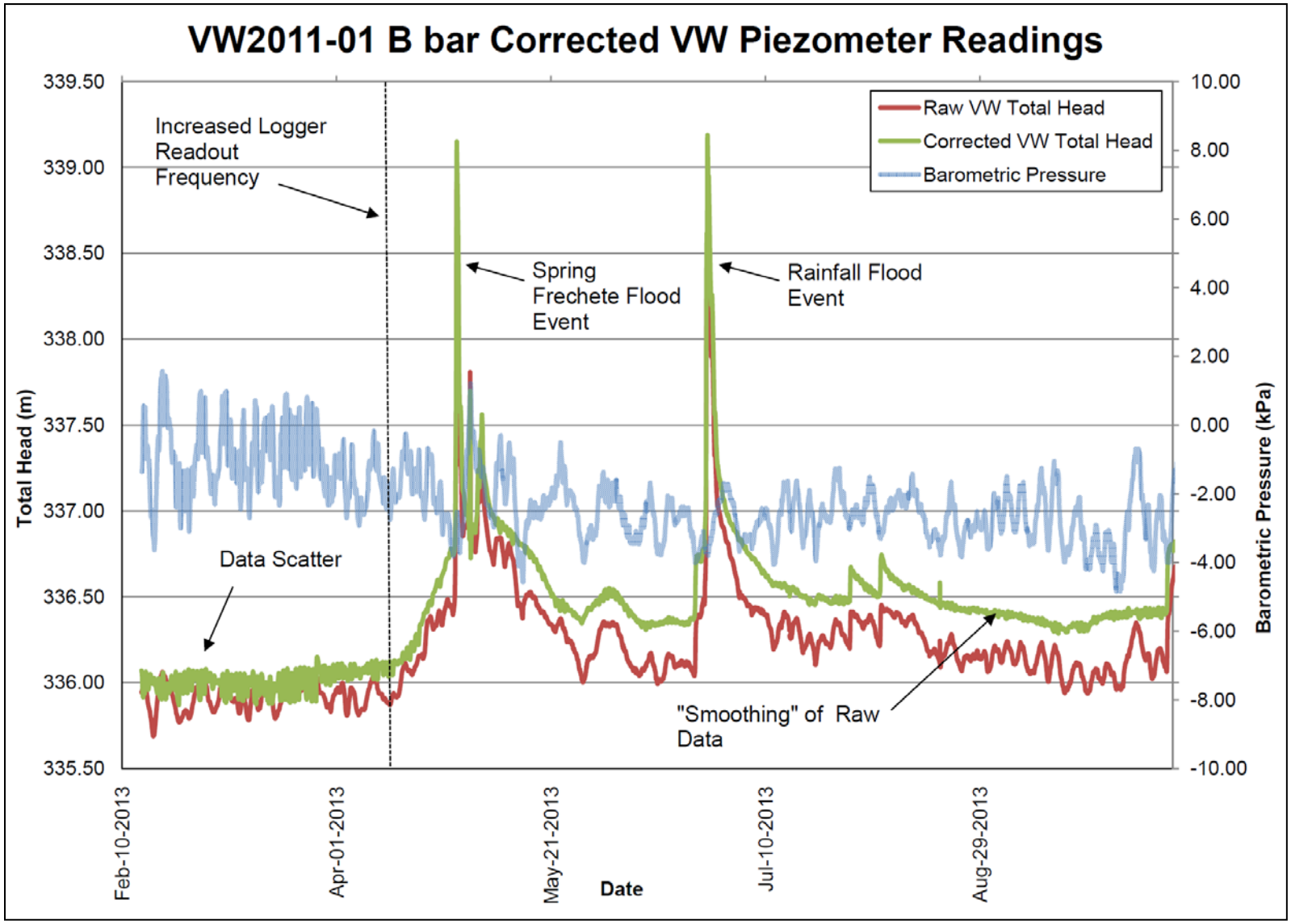

Figure 4.14 – VW2011-01 B-Corrected Piezometer Data

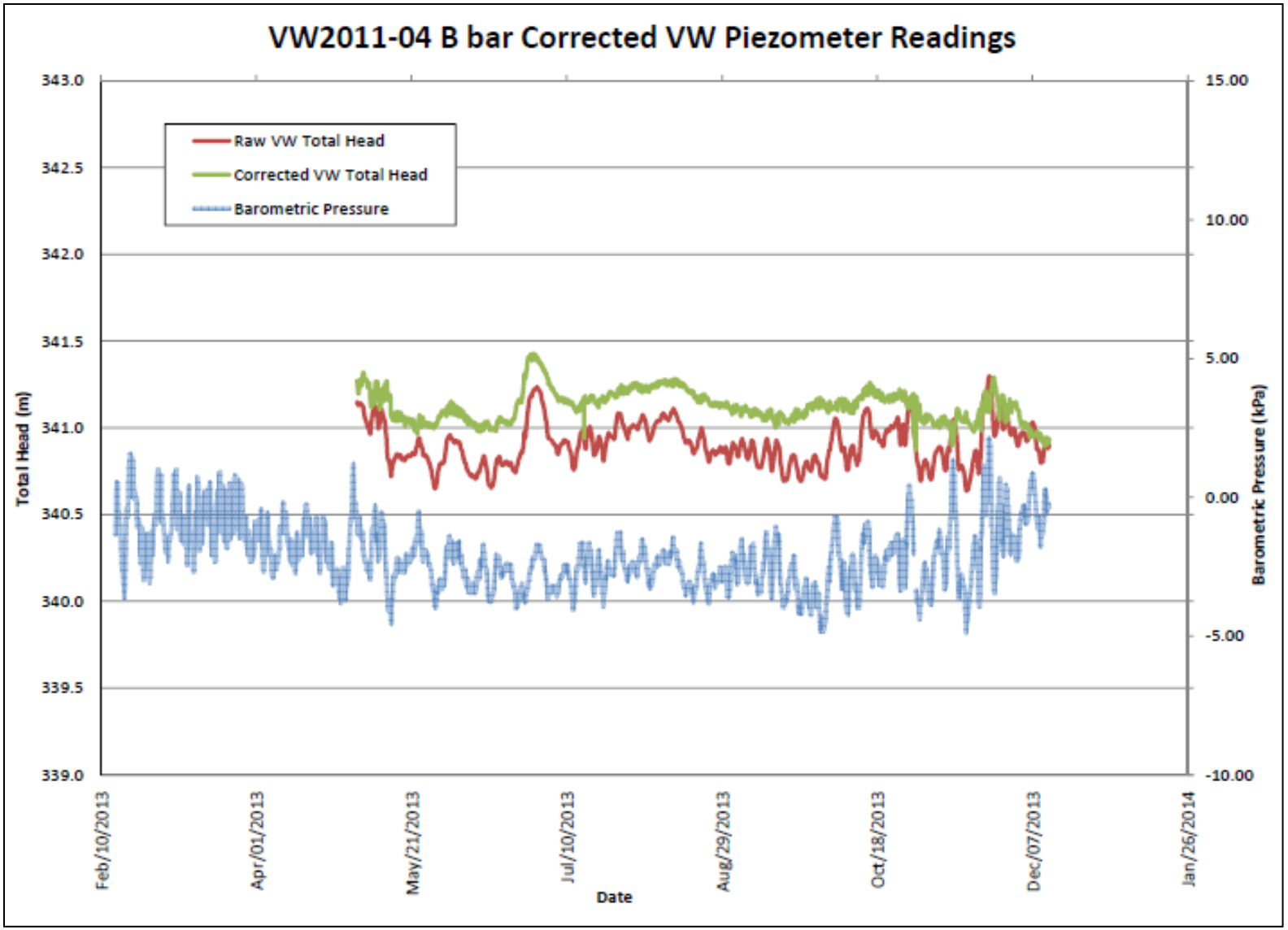

Figure 4.15 - VW2011-04 B-Corrected Piezometer Data

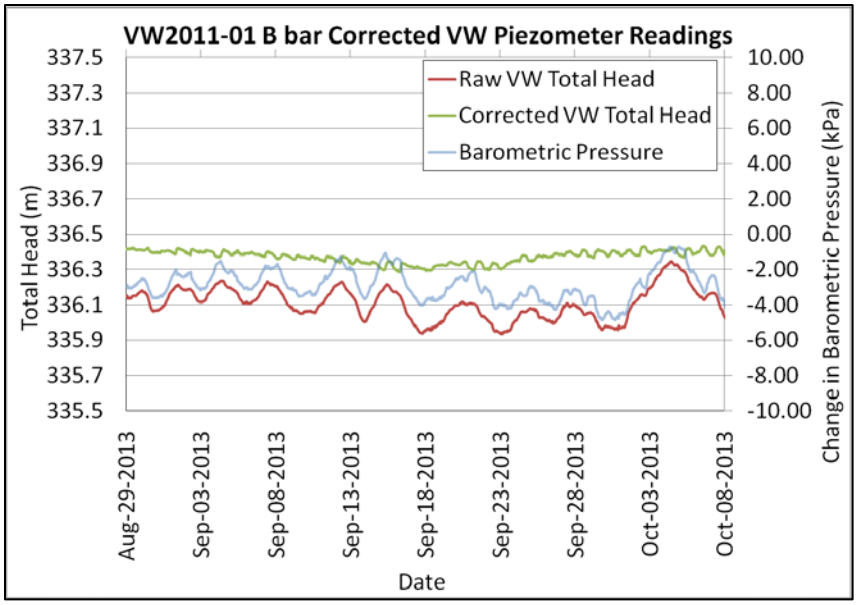

Figure 4.16 – VW2011-01 Time Interval Correction

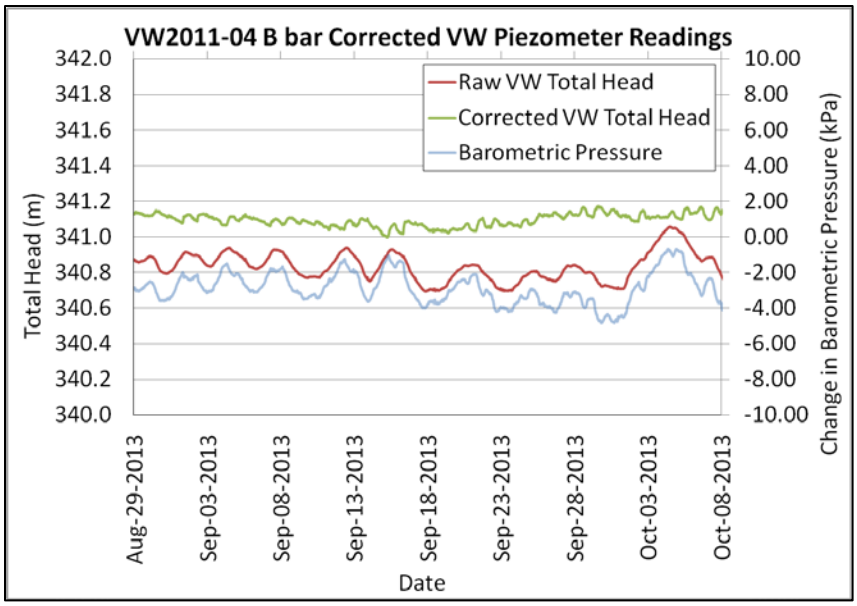

Figure 4.17 – VW2011-04 Time Interval Correction

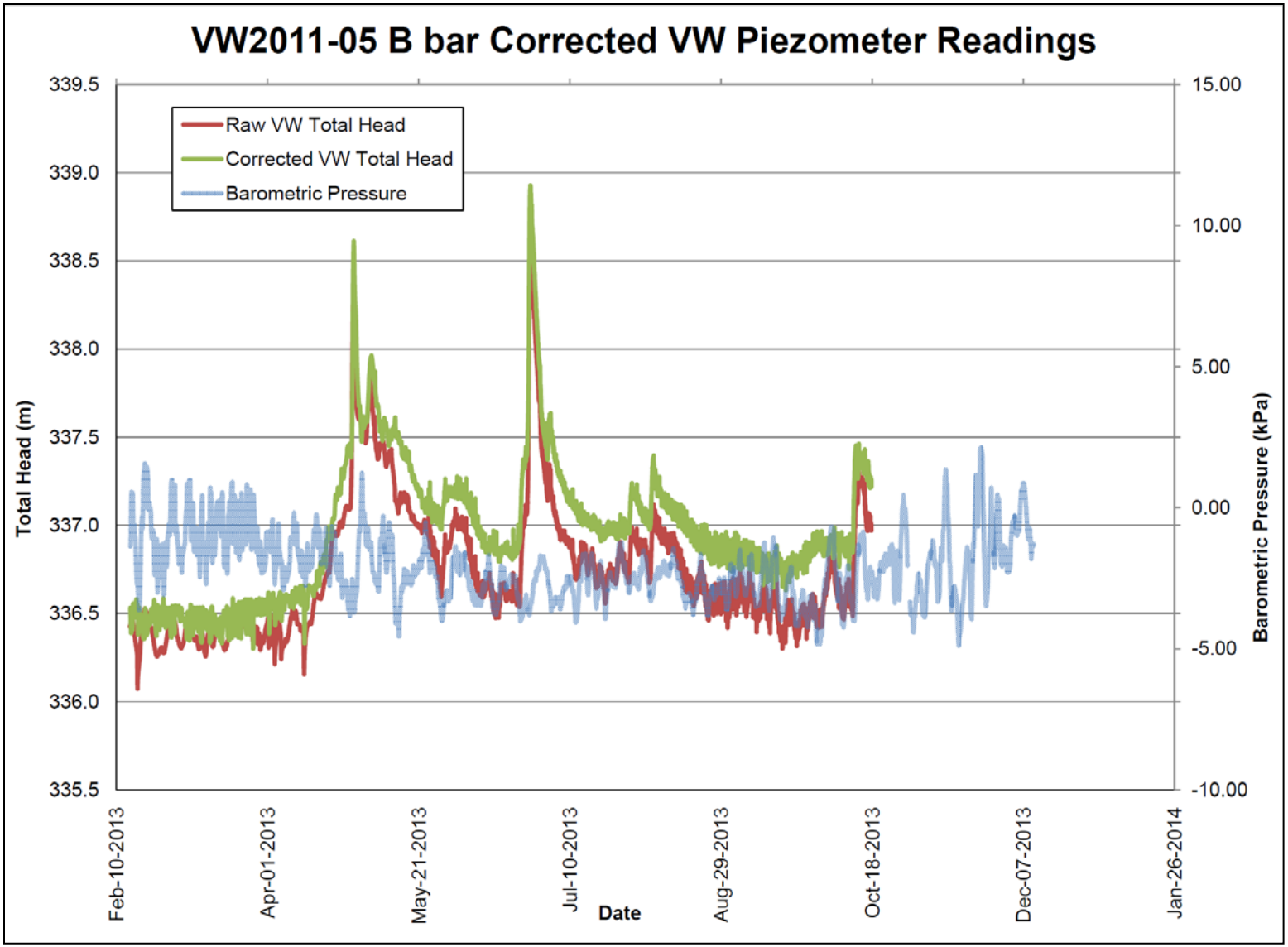

Figure 4.18 - VW2011-05 B-Corrected Piezometer Data

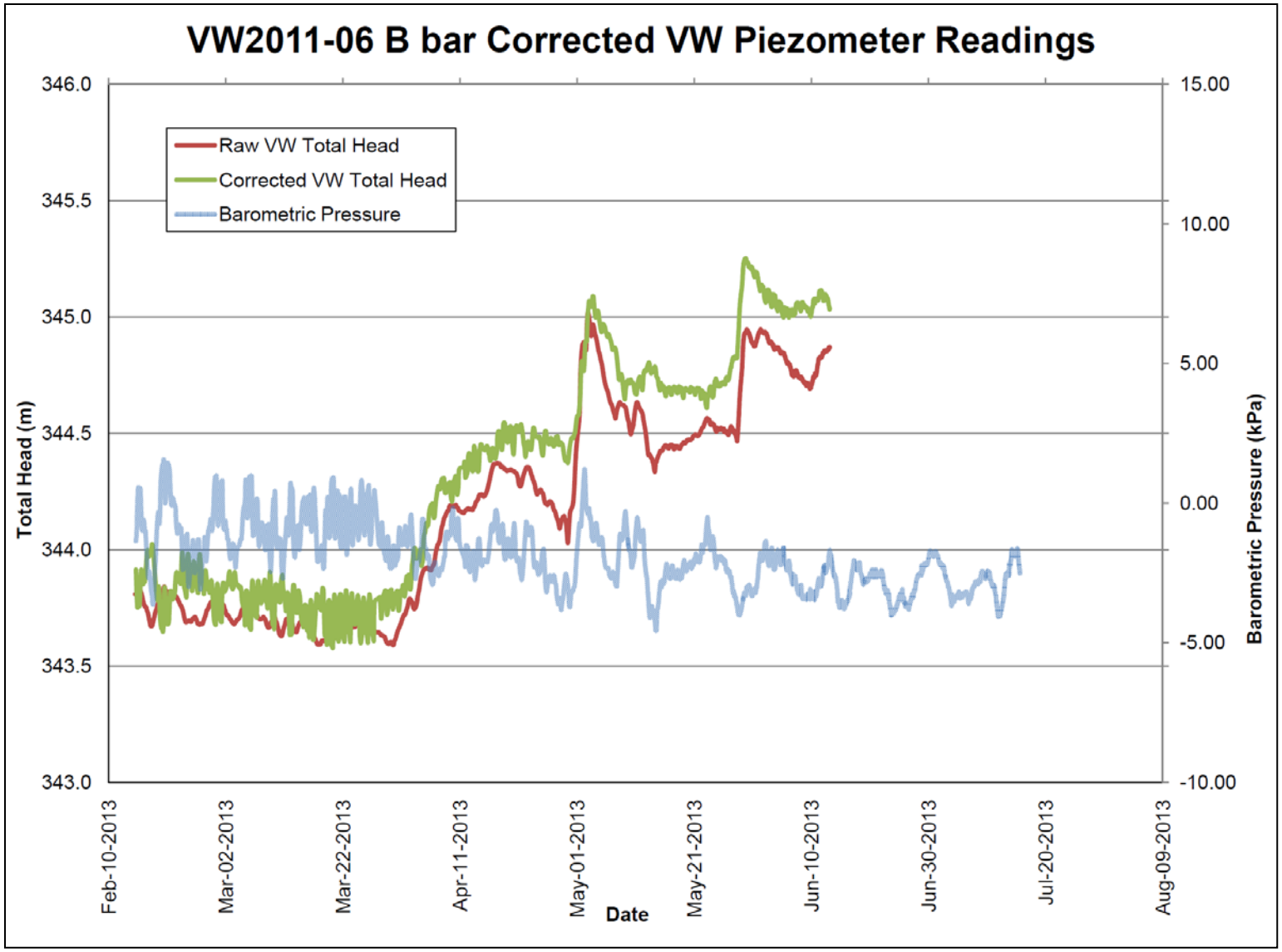

Figure 4.19 - VW2011-06 B-Corrected Piezometer Data

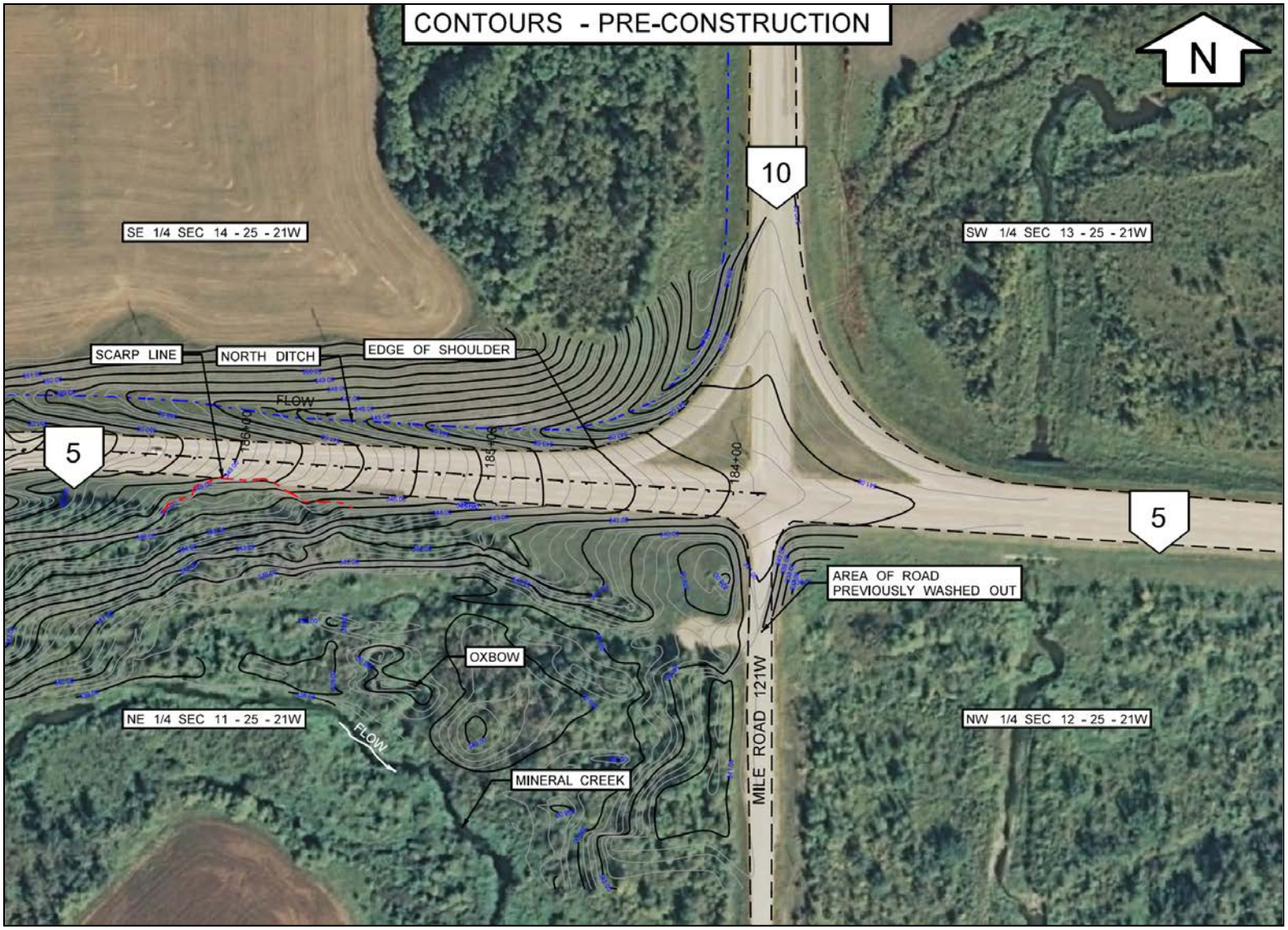

Figure 4.20 – Contour Plan of Project Area

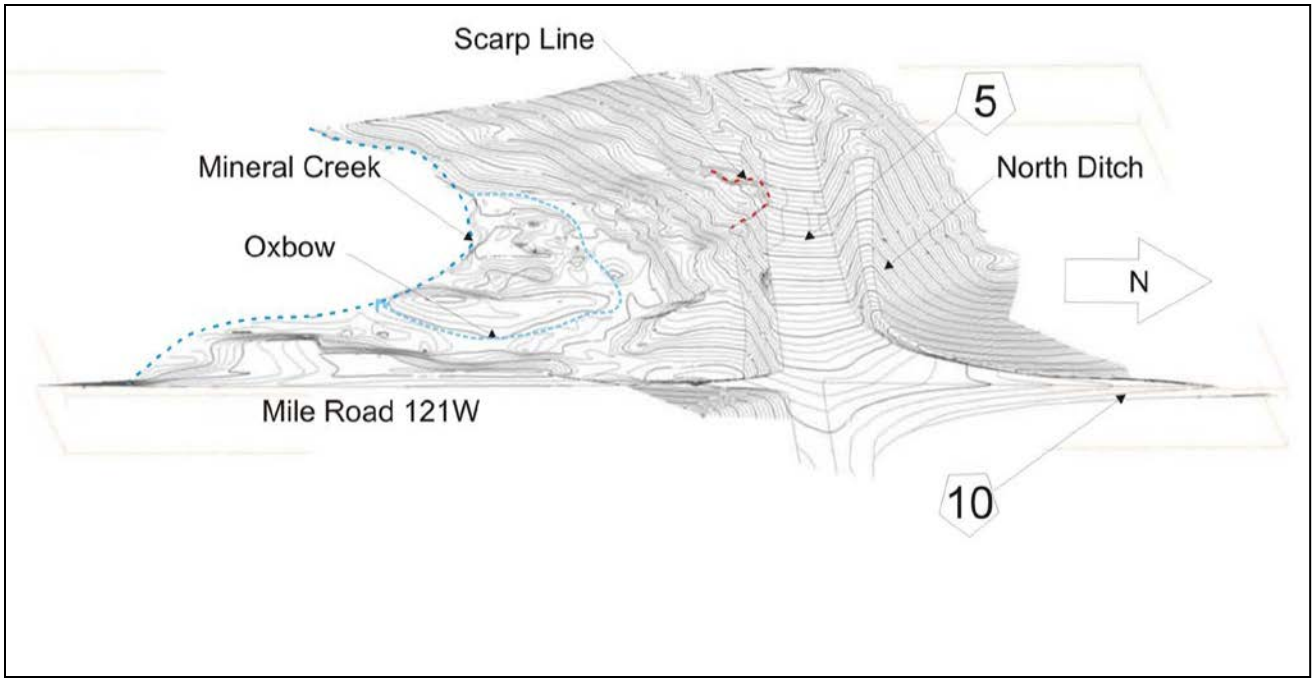

Figure 4.21 – DTM – West from PTH 10

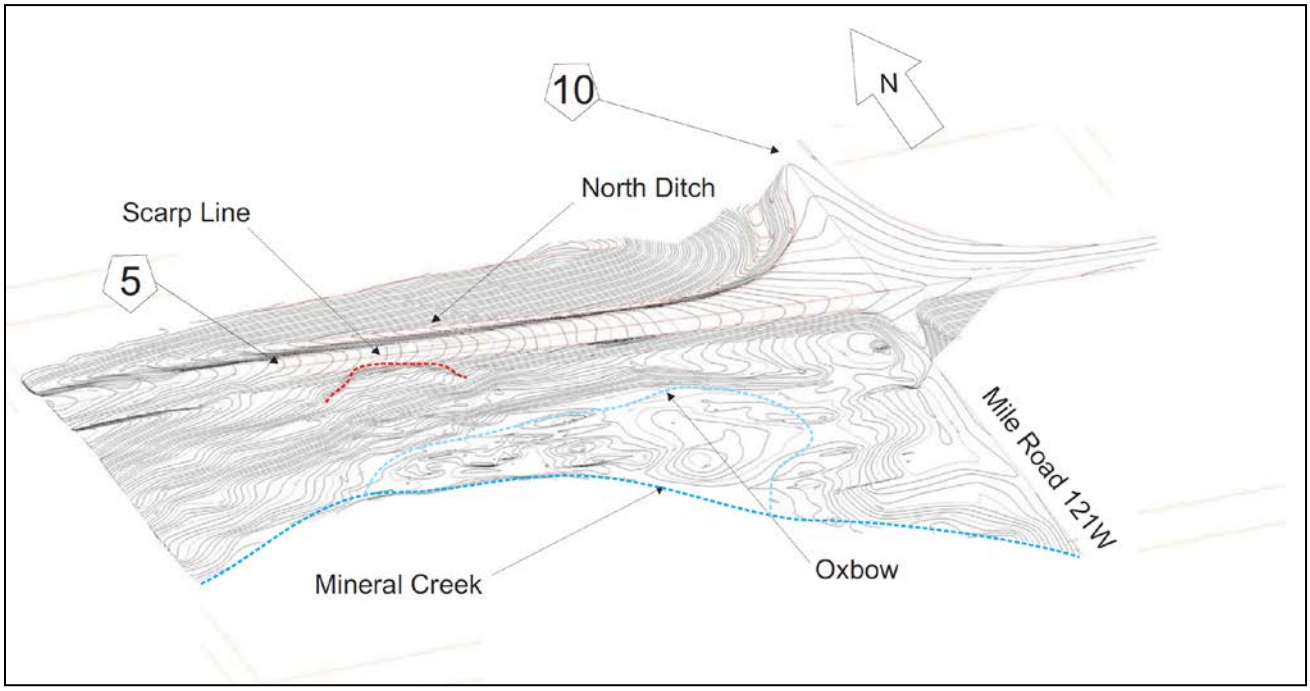

Figure 4.22 – DTM - Northeast from Mineral Creek

Chapter 5 – Laboratory Testing

5.1. Introduction

A series of laboratory tests was completed on selected samples of various materials for soil classification and advanced strength testing. Most of the testing completed for the classification of soils was done at the Materials Engineering Branch Central Lab. All advanced testing was completed at the University of Manitoba Geotechnical Laboratory, with additional soil classification testing completed on the samples selected for these tests. All testing is detailed in the following paragraphs.

5.2. Soil Classification

5.2.1. Atterberg Limits

In general, three soil types were encountered at the Ashville Junction site that are appropriate for determining Atterberg limits; till-like colluvium, clay shale and bentonite. Figure 5.1 shows a plot of plasticity index versus liquid limit, commonly referred to as the “A-line plot”. The A line generally separates clays, above the line, from organic soils and silts, below the line (Budhu, 2007). Testing was conducted in accordance with ASTM D 4318.

Specimens of colluvium selected for Atterberg limits testing had coarse particles removed, thus testing only the “fines” fraction (particles passing the 75 μm sieve). The results shown in Figure 5.1 indicate that the limits of the material are primarily at the transition between intermediate

and highly plastic. Liquid limits (w_L) vary between 35% and 64%, with a mean value of 51%. Plasticity indices (I_P) vary between 16% and 38%, with a mean value of 28.6%. The moderate limits are a reflection of considerable silt and sand content of the till-like soil. Conversely, values of w_L for the clay shale are more indicative of the clay mineralogy. The w_L varies between 48% and 75%, with a mean value of 64%. The I_P varies between 20% and 43%, with a mean value of 34%. The material is therefore highly plastic, typical of bentonitic shales in this region containing the expansive clay mineral, montmorillinite (Bamburak et al., 2004). It is common for the w_L of montmorillinite to exceed 100%, which was observed in samples of bentonite from the Ashville Junction site. The material is highly plastic with w_L varying between 83% and 185% and a mean value of 110%. The I_P vary between 47% and 134%, with a mean value of 71.6%. The Atterberg limits and moisture contents for all samples are also shown on the test hole logs in Appendix A.

5.2.2. Specific Gravity

It is common for the specific gravity (G_s) to be assumed as 2.7 with little error (Budhu, 2007). However, to ensure as much accuracy as possible, as well as identify any differences between material types, G_s was determined using ASTM D 854 for specimens on which advance strength tests were completed. Table 5.1 shows G_S as determined for each specimen.

5.2.3. Grain Size Analysis

Grain size analyses were completed on selected samples for soil classification and to assist in the interpretation of advanced strength test results. Testing was conducted in accordance with ASTM D 422. Figures 5.2a, 5.2b, 5.2c and 5.2d show typical plots of grain size distribution for

the colluvium, shale, alluvium and bentonite, respectively. All plots of grain size distribution can be found in Appendix D. Table 5.2 shows the resulting soil fractions for all material types tested.

5.3. Flexible Wall Permeameter Tests

Flexible wall permeameter tests were completed on till-like colluvium from sample T8 at effective stresses of 50 kPa and 100 kPa. The tests were conducted in accordance with ASTM D 5084. Figure 5.3 shows the flexible wall permeameter test apparatus used for this study. Following consolidation at each effective stress, permeation was completed until a constant flow rate was reached. Figures 5.4a and 5.4b show plots of volume change (as measured in the burette) versus time for effective stresses of 50 kPa and 100 kPa, respectively. In these figures, the data sets plot linearly when a constant flow rate has been reached. Using the relationships defined in ASTM D 5084, hydraulic conductivities of 6.10×10^{-9} m/s and 4.98×10^{-10} m/s were determined for the above effective stresses, respectively.

A third test was completed on a specimen of till-like colluvium combined from samples T7, T8 and T9 at M.I.T.'s Central Laboratory. This test was completed on a reconstituted specimen on which a standard Proctor test had been completed (see Appendix D). At optimum moisture content and an effective stress of 35 kPa, a hydraulic conductivity of 4.38×10^{-9} m/s was determined.

5.4. CIŪ Triaxial Tests

A series of CIŪ triaxial tests was completed on three specimens trimmed from extruded Shelby tube samples of till-like colluvium to establish some of the effective strength parameters necessary for consolidation and slope stability analysis. The tests were conducted in accordance with ASTM D 4767- 95. There was considerable difficulty in trimming the samples to the required specimen size (2:1 vertical to horizontal length ratio), due to the presence of gravel sized stones and selenite crystals (Figure 3.19).

The specimens were first sufficiently saturated to obtain the desired pore pressure parameter, B. For research purposes, this is attained when B equals 98%. Similar to Equation 2.33, the parameter, B, is defined as:

$$B = \Delta u/\Delta\sigma_3 \qquad \text{Eq. 5.1}$$

Here, Δu is the resulting change in porewater pressure in the specimen with a change in the test chamber pressure, $\Delta\sigma_3$. Figure 5.5 shows a typical specimen in the test chamber prior to axial loading.

The specimens from samples T7, T8 and T9 were then consolidated such that the effective confining stress, p'_0, for each specimen was 50 kPa, 100 kPa and 150 kPa, respectively. These confining stresses cover the range of stresses anticipated under loading of the slope during stabilization. Following consolidation of each specimen, axial loading, $\Delta\sigma_1$, was applied and the resulting stress-porewater pressure relationship, Δu, was recorded. Figure 5.6 shows the p'-q plot for each of the above specimens, and the resulting critical state strength envelope. In this

figure, each test specimen is shown to exhibit the anisotropy typically observed in natural soils as p' decreases with increasing q below the critical state line. Also of note is that each specimen exhibited signs of overconsolidation, attaining some peak strength before strain softening to failure at critical state. Figures 5.7a, 5.7b, and 5.7c show the failure surface that developed in each specimen from samples T7, T8, and T9, respectively.

Figure 5.8 shows a typical plot of q versus ε_s. All plots of q versus ε_s are shown in Appendix D. End-of test failure stresses determined from these plots of deviatoric stress versus shear strain give the critical state line with slope, M = 1.1 shown in Figure 5.6. Using Equation 2.9, the ϕ'_{cs} is then 27.7°.

The plots in Appendix D were then used to determine the initial tangent modulus, E, (Figure 2.4) for each effective confining stress, in order to establish a plot of the variability in stiffness with effective stress. Sigma/W allows the user to define the elastic stiffness as a function of vertical effective stress (Geo-Slope International Ltd., Sigma/W, 2010). To create this function, each tangent modulus was plotted against the respective effective stress, and a best fit polynomial function was applied to the series of points (Figure 5.9). The function was then imported into Slope/W for use in the linear elastic and elastic plastic constitutive models.

5.5. Oedometer Tests

A series of oedometer tests was completed on specimens trimmed from three samples of till-like colluvium. The oedometer test provides strength parameters related to one-dimensional consolidation, as well as some of the necessary input parameters for the modified Cam-Clay

constitutive model in Sigma/W. All tests were conducted in accordance with ASTM D2435-96. Figure 5.10 shows the oedometer test apparatus used for the tests.

Extruded Shelby tube samples T7, T8 and T10 were trimmed to practical lengths for trimming with the cutting ring. As with the CIŪ tests, there was difficulty in trimming the samples due to the presence of selenite crystals and gravel sized stones. Sample T10 was particularly difficult to trim as it contained significant quantities of oxidized bentonite (Figure 5.11). The resulting specimen was deemed to contain too much bentonite to be representative of the till-like colluvium. Testing was completed on the specimen for comparison, but the results have not been included in any analyses.

The loading arm applies the loads at an 11:1 ratio. Each sample was loaded and unloaded in the increments listed in Table 5.3. Figure 5.12 shows a typical plot of e versus σ'_z, with plots for each test shown in Appendix D. Figure 5.12 illustrates the relationships for the compression index, C_c, the recompression index, C_r and the effective preconsolidation pressure, σ'_{zc}. It can be seen in Figure 5.12 that σ'_{zc} is higher than the in-ground stresses, σ'_{zo}, of 60 kPa, 75 kPa and 85 kPa for samples T7, T8 and T10, respectively. As expected from the behaviour shown in the p', q plot described in the previous section, the till-like colluvium is therefore overconsolidated.

The input parameters for the modified Cam-Clay model must be defined in terms of the Critical State Model. C_c and C_r must therefore be defined in terms of λ and κ, which can be written as:

$$\lambda = C_c / \ln(10) = 0.434C_c \qquad \text{Eq. 5.2}$$

$$\kappa = C_r / \ln(10) = 0.434C_r \qquad \text{Eq. 5.3}$$

Table 5.4 summarizes all one dimensional consolidation variables obtained from the oedometer test for each sample.

As shown by Equation 2.32, the coefficient of consolidation can be used to determine the vertical hydraulic conductivity. The relationship requires that m_v is first determined, where:

$$m_v = \Delta\varepsilon_z \ / \ \Delta\sigma'_z \qquad \text{Eq. 5.4}$$

The modulus of volume compressibility, m_v, is therefore the slope of the tangent to the curve between successive measurements of vertical effective stress and vertical strain, ε_z. This parameter can then be determined from plots of this data (Budhu, 2007). Figure 5.13 shows a typical plot of σ'_z versus ε_z (plotted as volume strain).

To determine C_v, the root time method was used (Budhu, 2007). With this method, C_v is defined as:

$$C_v = 0.848H^2_{dr} / t_{90} \qquad \text{Eq. 5.5}$$

Here, H_{dr} is the length of the drainage path, calculated as 0.5 times the average height of the specimen in a particular load step, and t_{90} is the time required to achieve 90% consolidation. To determine t_{90}, the data for each load step are plotted as the square root of time versus displacement, or gauge reading. Figure 5.14 shows a typical plot of the root time method. A best-fit line is first drawn through the initial section of the curve, extending from the point where the curve intersects the vertical axis, point O, to the horizontal axis. The point at which this line crosses the horizontal axis is point A. Then t at point A is $\sqrt{t_A}$. A second point, B, is then

located on the horizontal axis where $t = 1.15\sqrt{t_A}$. If a line is extended from O to B, the point at which this line crosses the curve gives the displacement for which 90% consolidation has occurred. Table 5.5 shows the variables used in determining k_v in each load step within the applicable stress range for each sample. Figure 5.15 shows a plot of the variability of k with σ'_v from flexible wall permeameter and oedometer test results.

5.6. Direct Shear Tests

Direct shear tests were completed on specimens from three samples of clay shale. The tests were conducted in accordance with ASTM D 3080. Two specimens from sample T4, and one from sample T5, were tested at applied normal stresses of 75 kPa, 100 kPa and 150 kPa, respectively. The plasticity indices of these specimens were 31%, 31% and 39%, respectively. The range of normal stresses selected reasonably covers the range of stresses anticipated under loading of the slope during stabilization. It was assumed that applied stresses below 75 kPa would not permit adequate consolidation of the highly overconsolidated specimens prior to shearing, and may promote swelling of the specimen when water is applied to the shear box. Figure 5.16 shows a typical test in the direct shear apparatus.

Each specimen was allowed adequate time to consolidate under vertical loading, until it was observed that equilibrium had been reached. Each specimen exhibited some initial compression when the normal stress was applied, followed by some swelling as the specimen became saturated over some time in the water bath. The swelling was particularly evident under load step one (75 kPa), becoming less pronounced in steps two and three. Figures 5.17a and 5.17b show compression and swelling for load steps one and three (150 kPa) during early

time steps of the consolidation phase. Figure 5.18 shows a plot of compression (plotted as vertical strain) versus time for load step two (100 kPa) over the duration of the consolidation stage.

Following consolidation, each specimen was sheared over six cycles, with the direction of shearing being reversed after each cycle. While it is acknowledged that in some cases reaching an accurate measurement of the residual strength using the direct shear test may require significantly more cycles of shearing, six cycles were used to keep the length of testing within a manageable time frame. Figures 5.19a, 5.19b and 5.19c show the stress-strain relationship during shearing under normal stresses of 75 kPa, 100 kPa and 150 kPa, respectively. Figures 5.19a and 5.19b illustrate that the stress-strain relationship following reversal can be highly irregular, possibly from some mechanical problems with the equipment, and determining residual strengths from these plots can therefore be difficult. These irregularities appear to diminish as the load steps increase, and the shear strength from the last loading step is much easier to interpret (Figure 5.19c). Table 5.6 summarizes the values of residual shear strength interpreted from the above plots. Figure 5.20 illustrates the resulting average residual shear strength envelope. From the best fit line plotted through the residual strength values, and using the Equation 2.2 with c' = 0, ϕ'_r was determined as 10.1°.

5.7. Torsional Ring Shear Tests

Torsional ring shear tests were completed on reconstituted specimens of clay shale from sample T2, having a plasticity index of 25%. The plasticity index of this particular specimen is between 6% and 14% lower than specimens tested under direct shear. The tests were

completed in accordance with ASTM D 6467, with references made to Stark and Vettel, 1992. Reconstituted specimens were first pulverized, and then passed through a #40 sieve (425 μm). The ASTM standard recommends that materials be passed through a sieve such that the opening size is less than 10% of the original specimen height of 5 mm (500 μm). Stark and Vettel recommend passing the material through the #200 sieve, but the limited amount of sample available made this impractical, as sufficient material was needed for a minimum of two tests. Figure 5.21 shows the ring shear apparatus used for the tests.

Once the materials were passed through the sieve, they were saturated with distilled water. The ASTM standard recommends wetting the sample to around the liquid limit (approximately 62% in this case), and allowing to hydrate for a period of 24 hours. Stark and Vettel recommend wetting the sample until a liquidity index of 1.5 is reached. For the material in the author's tests, a water content of 1.25 x w_L was used, corresponding to a gravimetric moisture content of approximately 80%. For this study, samples were saturated to beyond the liquid limit and then allowed to hydrate over a period 72 hours. This is sufficient time such that hydration of cementation bonds and diffuse double layers between soil particles can occur, while maintaining pore fluid chemistry that still resembles that of the in-situ conditions[12]. After a period of 72 hours, the moisture content of the sample was reduced (evaporated) to below w_L, which is necessary for preparing the specimen inside the ring. Too much moisture can result in squeezing of the sample from between the lower and upper parts of the test cell and between the circular cell and the top platen.

Three load increments of 100 kPa, 150 kPa and 200 kPa, were applied to each of the two specimens. Each specimen was allowed to consolidate until a state of equilibrium was reached.

[12] Personal communication, Alex Man, 2014.

Stark and Vettel suggest that residual shear strength can be overestimated due to wall friction between the top platen and lower ring developing during settlement and subsequent shearing. A maximum of 0.75 mm of settlement is recommended for the multistage test procedure (see Stark and Vettel, 1992), with a maximum of 0.35 mm of settlement recorded during testing. Figure 5.22 shows a typical consolidation plot for specimens to be tested in ring shear. Each specimen was sheared at the specified load levels until the residual strength was reached. Figures 5.23a and 5.23b show plots of shear stress versus displacement for each specimen. Figures 5.24a and 5.24b show the resulting residual shear strength envelopes for specimens T2-1 and T2-2, respectively. From the best fit line plotted through the residual strength values, and using Equation 2.2 with $c' = 0$, φ'_r was determined as 9.6° and 8.1° for specimens T2-1 and T2-2, respectively, giving a mean value of 8.9°. The measured residual strength friction angle measured in torsional ring shear is therefore 1.2° lower than that measured in direct shear.

Table 5.1 – Specific Gravity by Material Type

Sample Number	Material Type	G_S
T7	Colluvium	2.72
T8a	Colluvium	2.76
T8b	Colluvium	2.67
T9	Colluvium	2.69
T2	Clay Shale	2.62
T3	Clay Shale	2.54
T4a	Clay Shale	2.55
T4b	Clay Shale	2.55
T5	Clay Shale	2.60
B25	Clay Shale	2.56
T12	Bentonite	2.76

Table 5.2 – Soil Fraction by Material Type

Sample	Soil Type	% Gravel	% Sand	% Silt	% Clay
T3	Shale	0.0	4.0	32.0	64.0
T4a	Shale	0.0	1.0	21.0	78.0
T4b	Shale	0.0	1.0	21.0	78.0
T5	Shale	0.0	1.0	18.0	81.0
B25	Shale	0.0	0.0	24.0	76.0
B37	Shale	0.0	2.0	18.0	80.0
Mean		0.0	1.5	22.3	76.2
T1	Alluvium	0.0	52.0	23.0	25.0
T7	Colluvium	2.0	11.0	22.0	65.0
T8a	Colluvium	3.0	16.0	26.0	55.0
T8b	Colluvium	0.0	6.0	31.0	63.0
T9	Colluvium	0.0	14.0	28.0	58.0
T22	Colluvium	5	22.0	20.0	53.0
T36	Colluvium	1	19.0	27.0	53.0
B2	Colluvium	2	21.0	22.0	55.0
B18	Colluvium	2	30.0	23.0	45.0
Mean		1.9	17.4	24.9	55.9
S24	Bentonite	0	7	28	65

Table 5.3 – Oedometer Test Loading Schedule

Step	Mass (kg)	Load Pressure (kPa)	Unload Pressure (kPa)
1	1.5	51.5	-
2	3.0	102.9	-
3	6.0	205.8	-
4	12.0	411.6	-
5	25.0	857.6	-
6	50.0	1715.2	-
7	25.0	-	857.6
8	12.0	-	411.6
9	25.0	857.6	-
10	50.0	1715.2	-
11	100.0	3453.0	-

Table 5.4 – Oedometer Test Results

1D Consolidation Parameter	Sample T7	Sample T8	Sample T10
C_c (λ)	0.257 (0.112)	0.246 (0.107)	0.422 (0.183)
C_r (κ)	0.0803 (0.0349)	0.0397 (0.0172)	0.104 (0.0451)
σ'_{zc} (kPa)	190	205	300
OCR = (σ'_{zc} / σ'_{zo})	3.21	2.71	3.58

Table 5.5 – Parameters Used to Determine k_z

Sample #	σ'_v (kPa)	t_{90} (s)	C_v (m^2/s)	m_v (m^2/kN)	k_z (m/s)
T7	51.5	9.6	7.6E-06	2.9E-04	2.2E-08
	102.9	25.4	2.8E-06	2.8E-04	7.8E-09
	205.8	43.4	1.6E-06	2.7E-04	4.2E-09
T8	51.5	5.4	1.4E-05	1.0E-04	1.4E-08
	102.9	21.6	3.4E-06	1.9E-04	6.3E-09
	205.8	48.6	1.5E-06	1.8E-04	2.6E-09
T10	51.5	15.0	5.0E-06	9.1E-05	4.4E-09
	102.9	25.4	2.9E-06	1.4E-04	4.0E-09
	205.8	43.4	1.7E-06	1.4E-04	2.3E-09

Table 5.6 – Clay Shale Residual Shear Strength Values

Load	Normal Stress (kPa)	Residual Shear Strength (kPa)
1	75.55	16.3
2	100.93	19.8
3	150.68	24.4

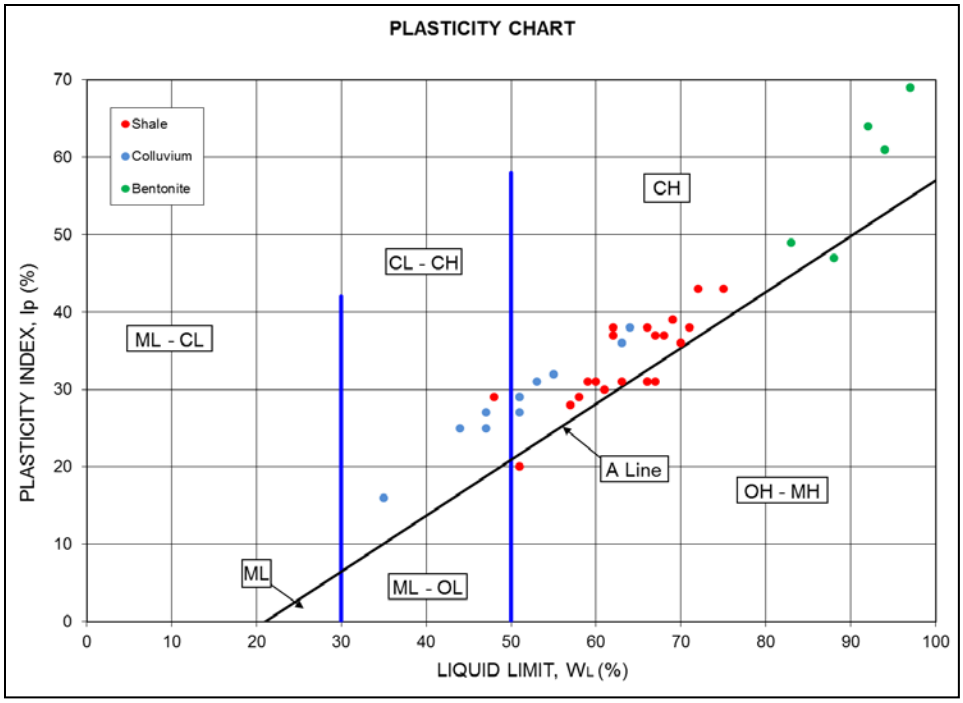

Figure 5.1 – Plasticity Chart (Modified from Budhu, 2007)

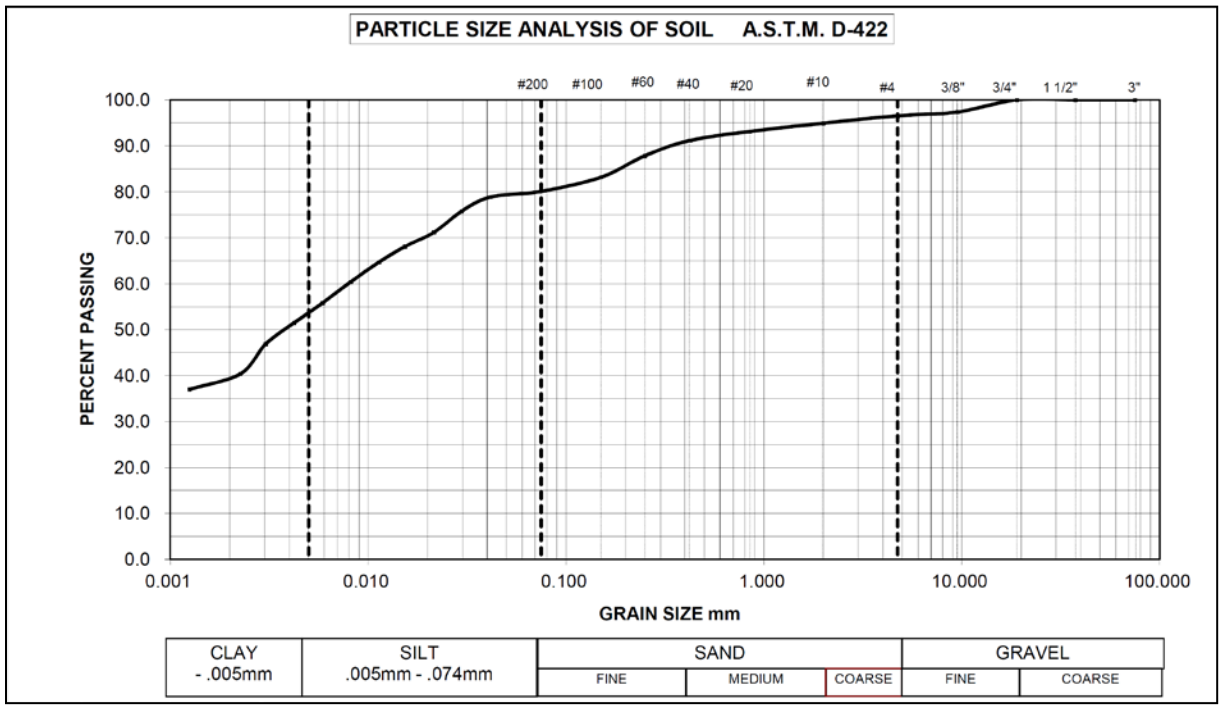

Figure 5.2a – Grain Size Distribution for Colluvium (Sample T8, TH2011-06)

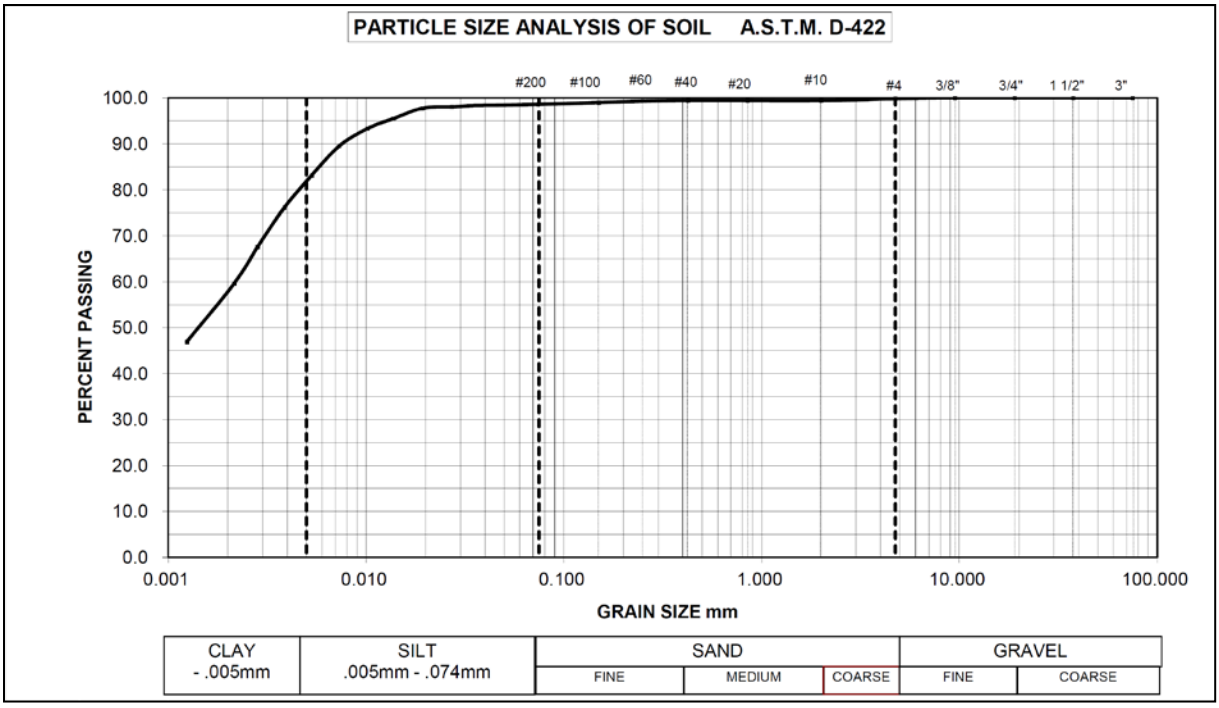

Figure 5.2b – Grain Size Distribution for Shale (Sample T5, TH2011-05)

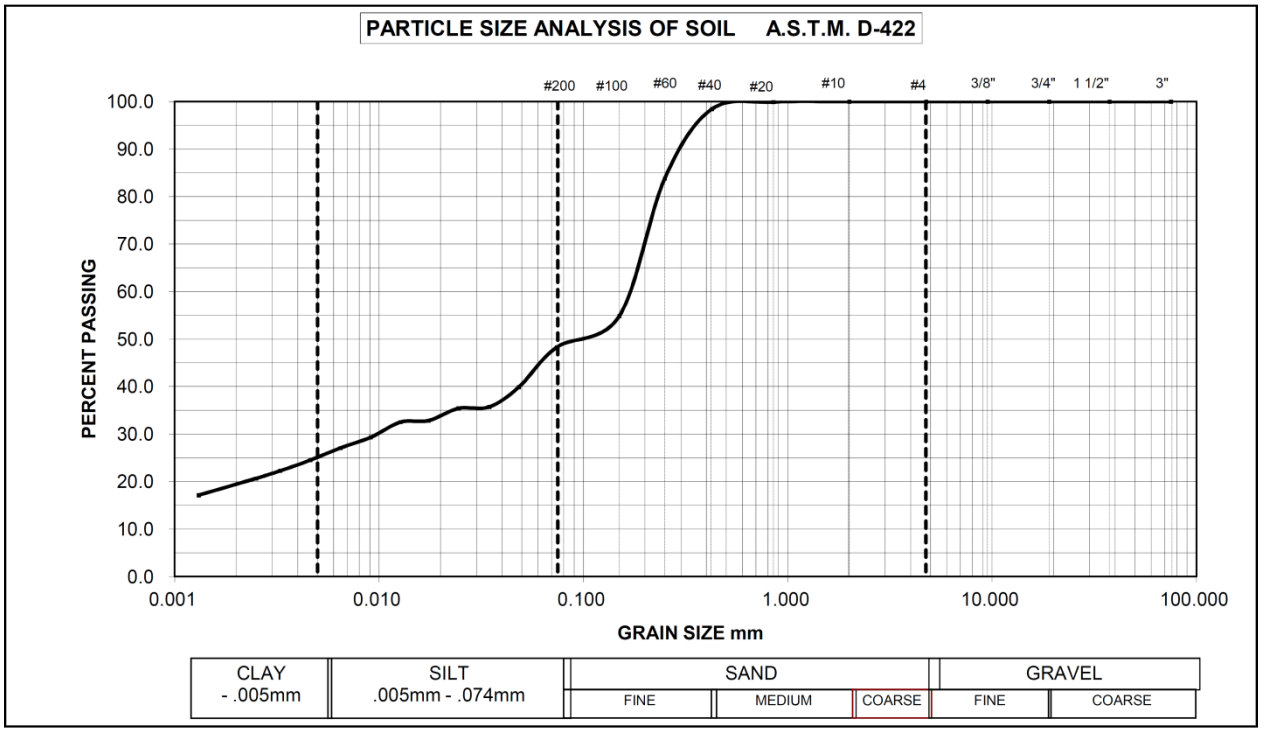

Figure 5.2c – Grain Size Distribution for Alluvium (Sample T1, TH2011-05)

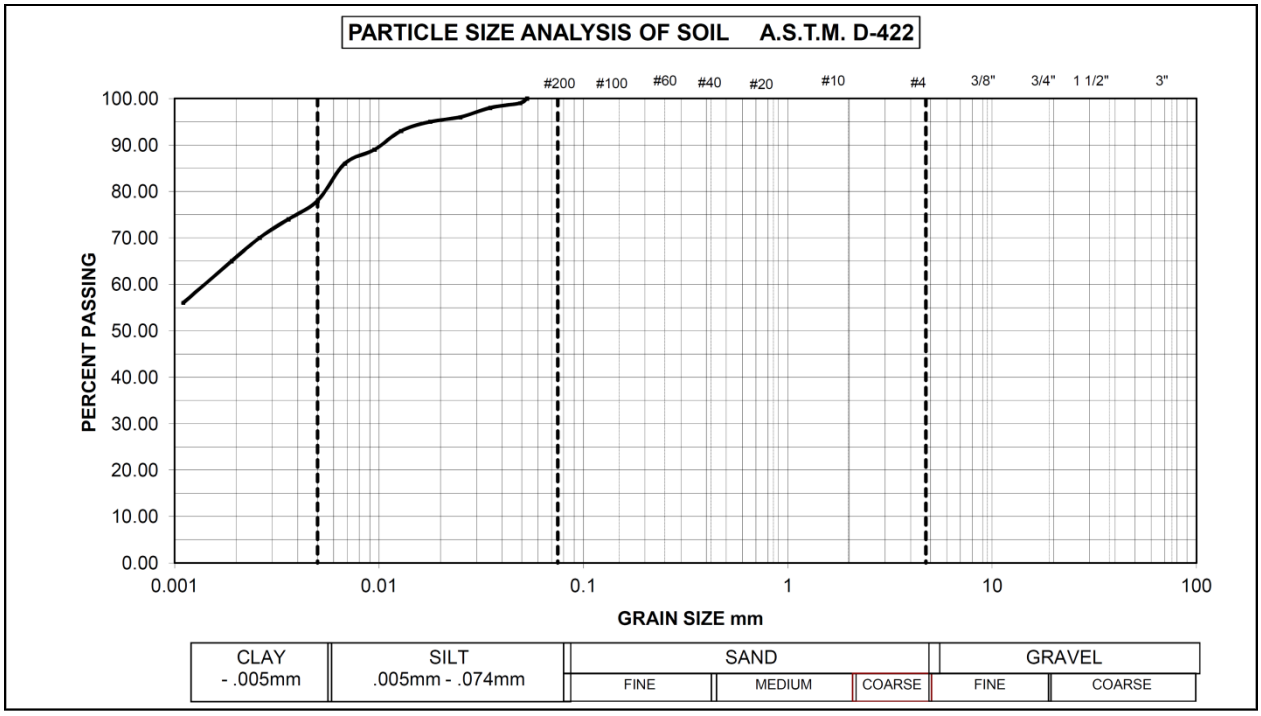

Figure 5.2d – Grain Size Distribution for Bentonite (Sample B25, TH2011-02)

Figure 5.3 – Flexible Wall Permeameter Test Apparatus

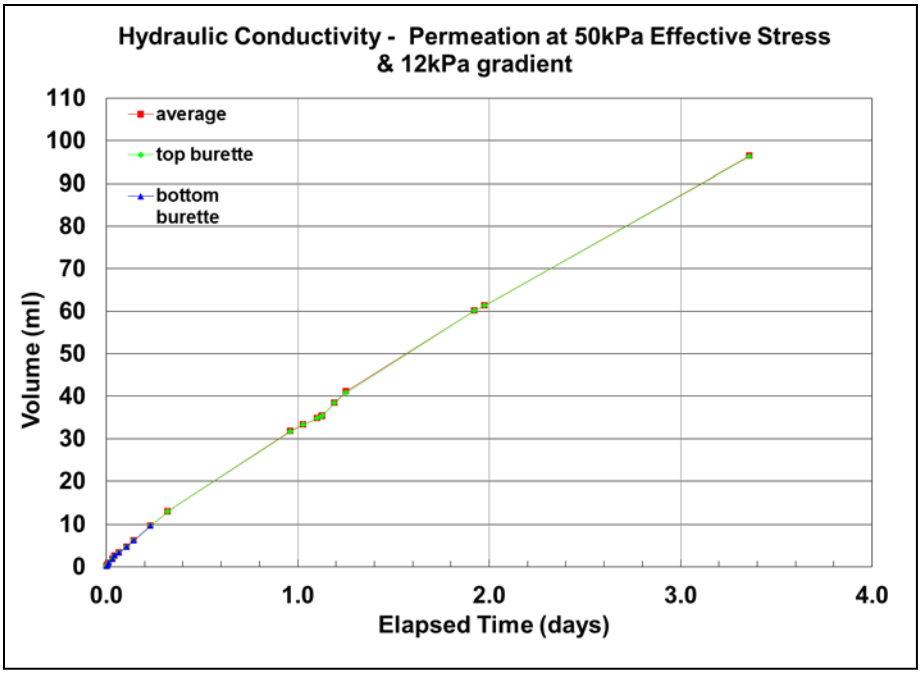

Figure 5.4a – Permeation at 50 kPa Effective Stress

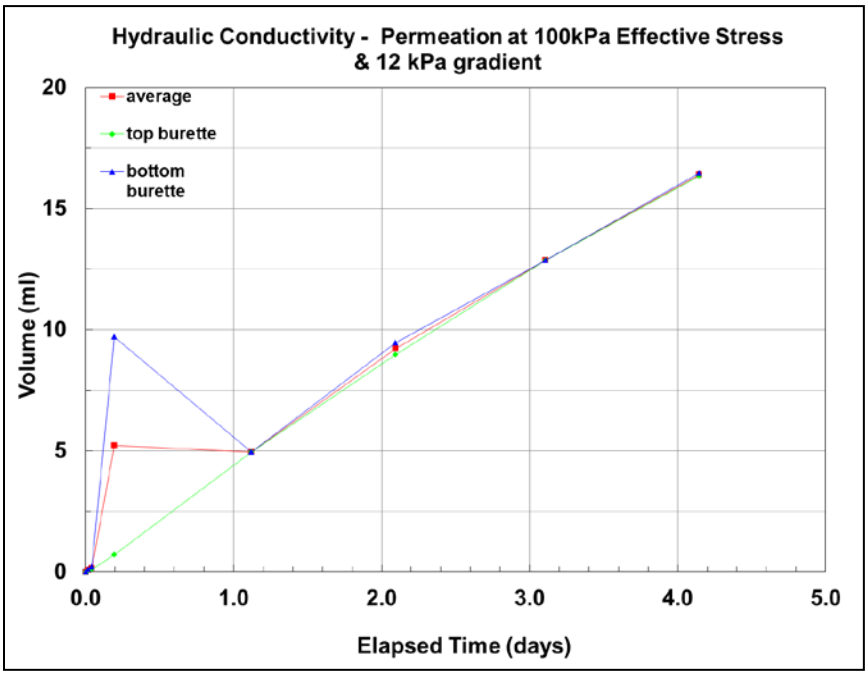

Figure 5.4b – Permeation at 100 kPa Effective Stress

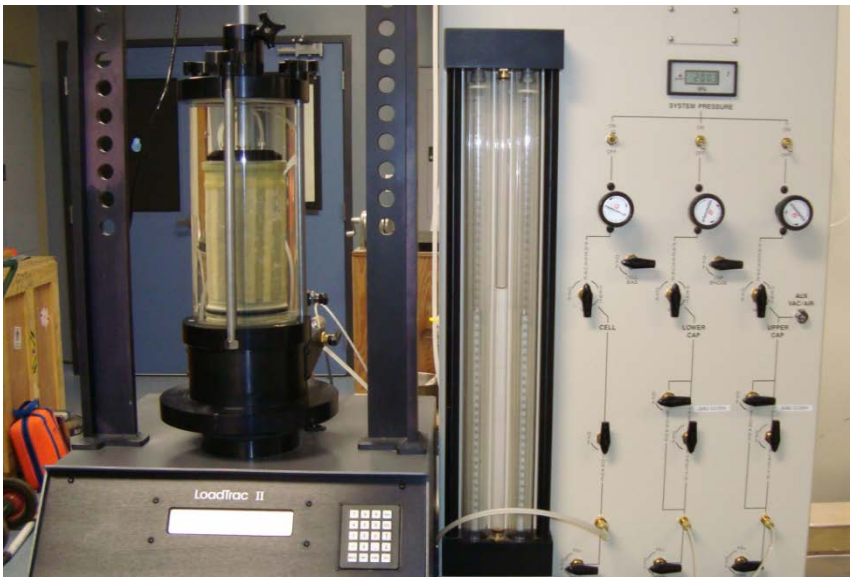

Figure 5.5 – Typical Triaxial Test Apparatus

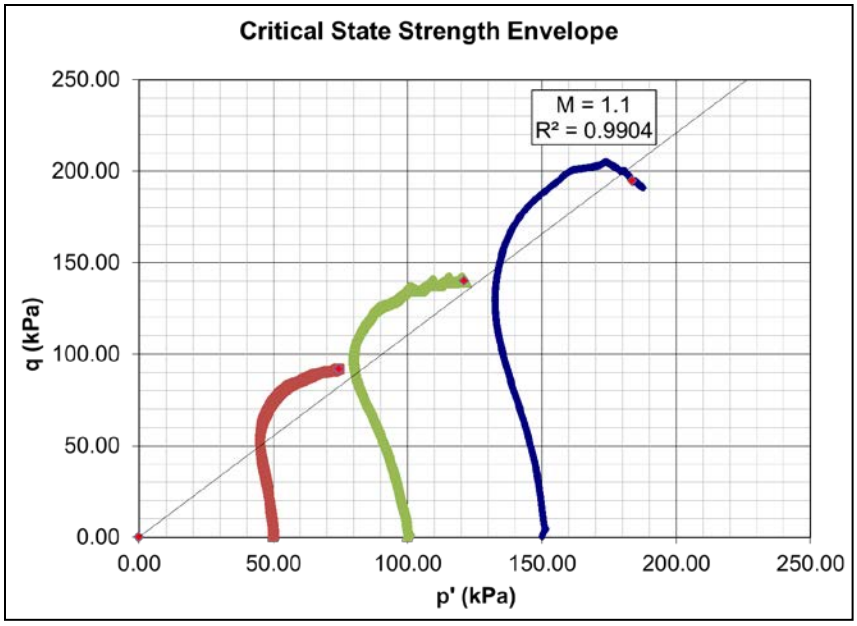

Figure 5.6 – p'-q Plot for Triaxial Tests

Figure 5.7a – Triaxial Test Failure Surface, Sample T7

Figure 5.7b – Triaxial Test Failure Surface, Sample T8

Figure 5.7c – Triaxial Test Failure Surface, Sample T9

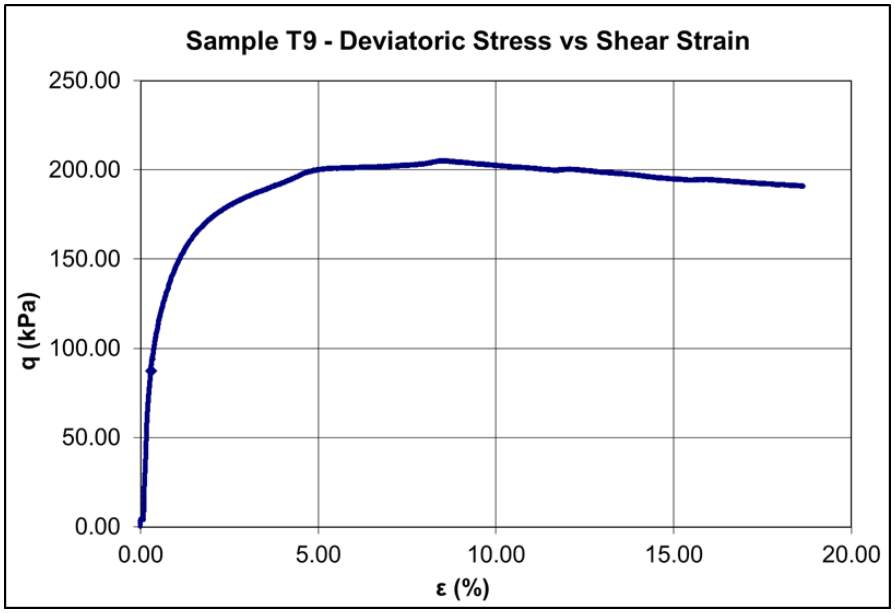

Figure 5.8 – Typical q vs ε_s Plot

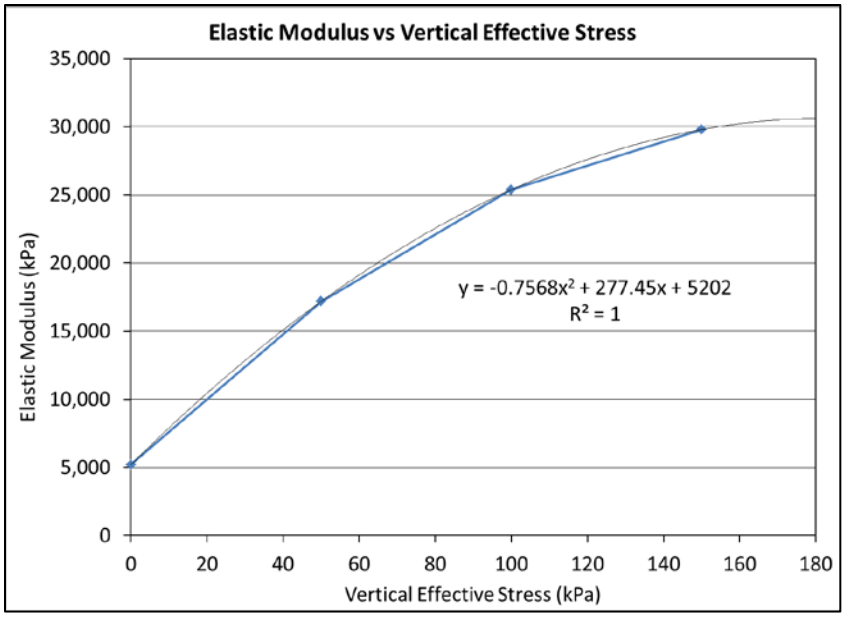

Figure 5.9 – Initial Tangent Modulus vs Y Effective Stress

Figure 5.10 – Typical Oedometer Test Apparatus

Figure 5.11 – Specimen From Sample T10 in Cutting Ring (Note the yellowish oxidized bentonite)

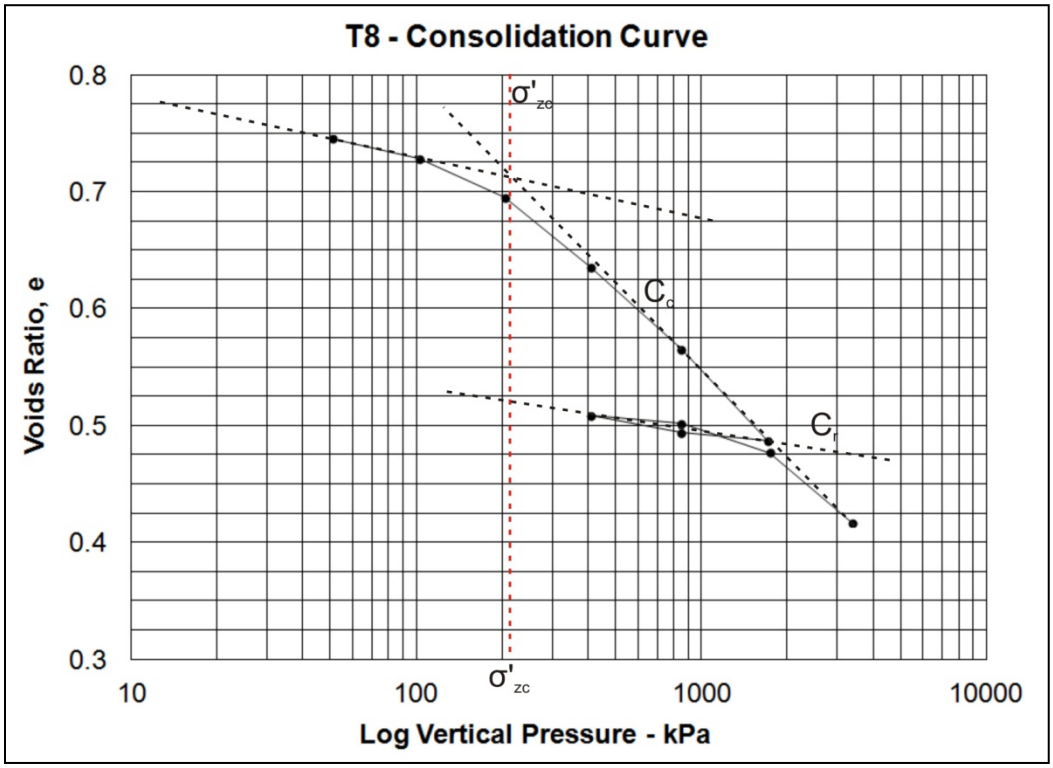

Figure 5.12 – Consolidation Curve (From Sample T8)

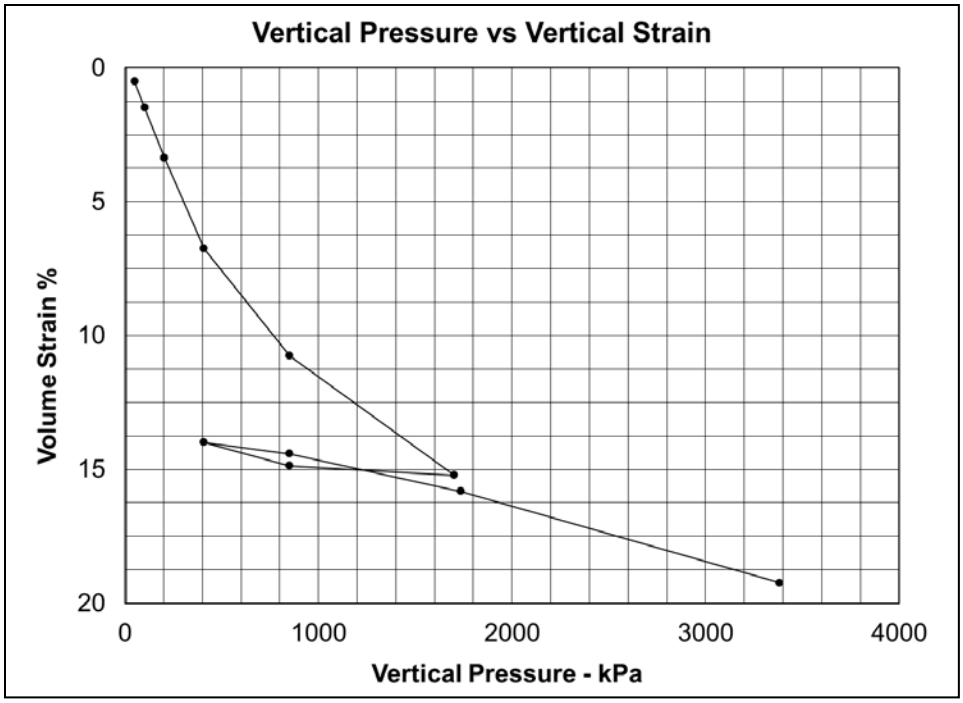

Figure 5.13 – σ'_z, ε_z Plot for Determining m_v

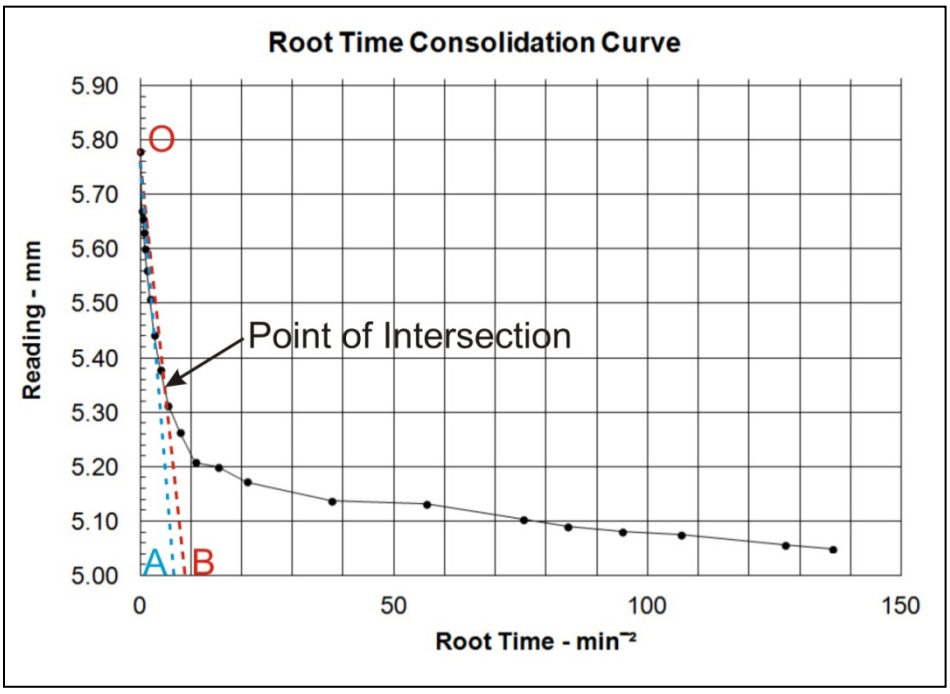

Figure 5.14 – Root Time Consolidation Curve to Determine t_{90} (T8 final load increment)

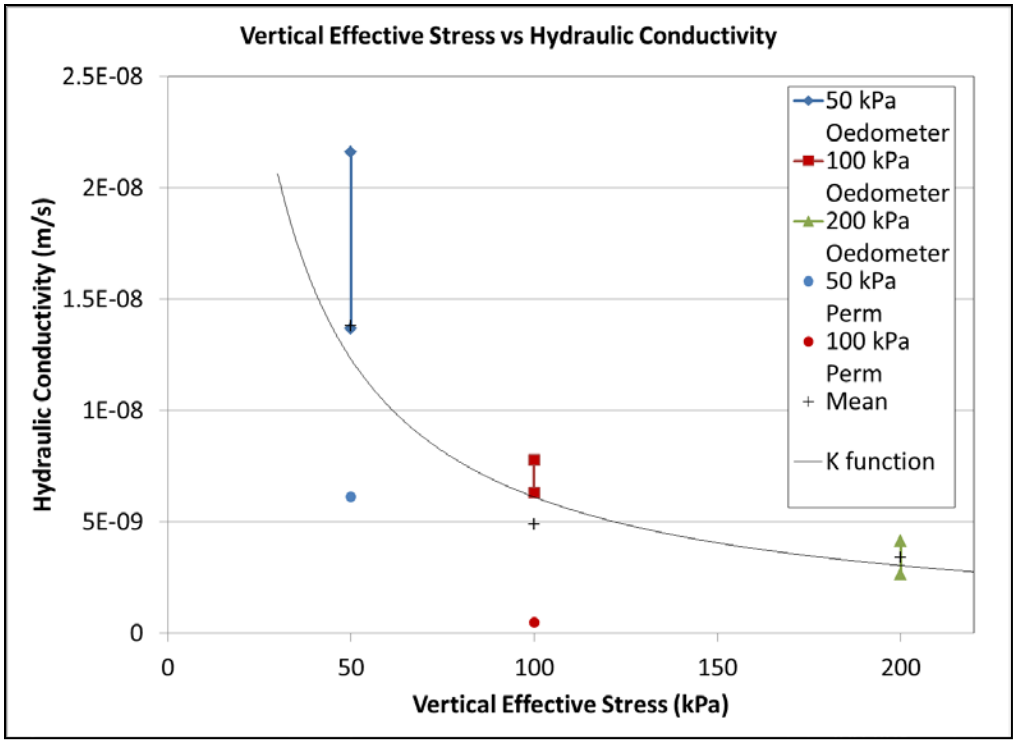

Figure 5.15 – Variability of k with σ'_v

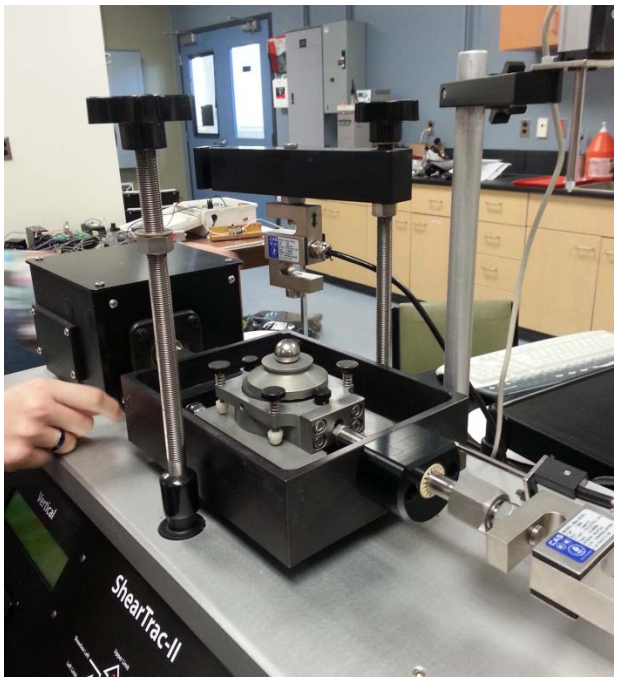

Figure 5.16 – Typical Direct Shear Test Apparatus

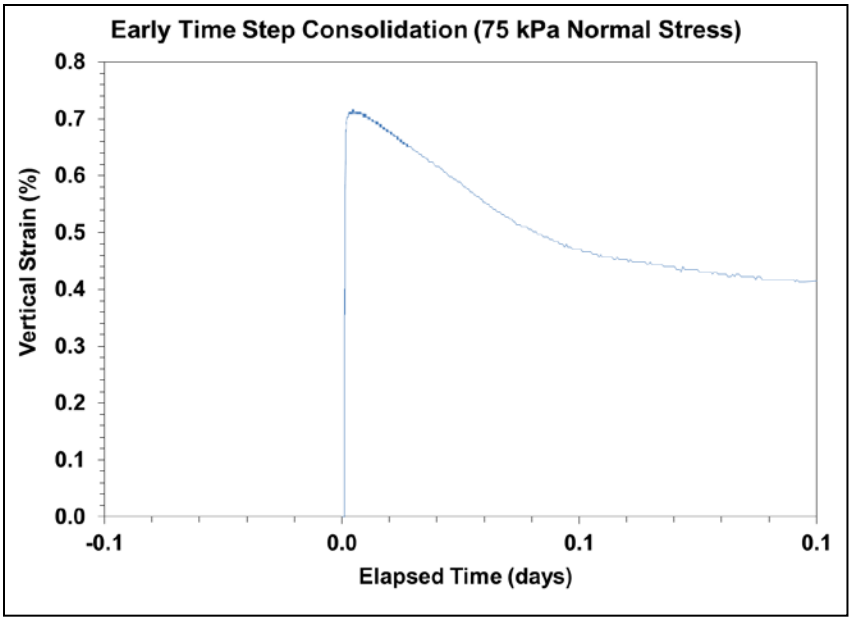

Figure 5.17a – Consolidation and Swelling, 75 kPa Normal Stress

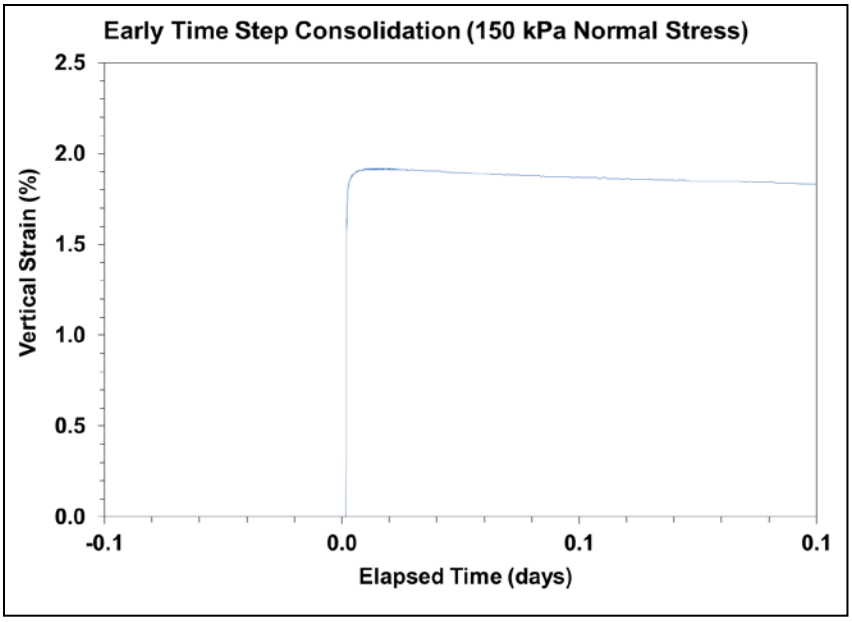

Figure 5.17b – Consolidation and Swelling, 150 kPa Normal Stress

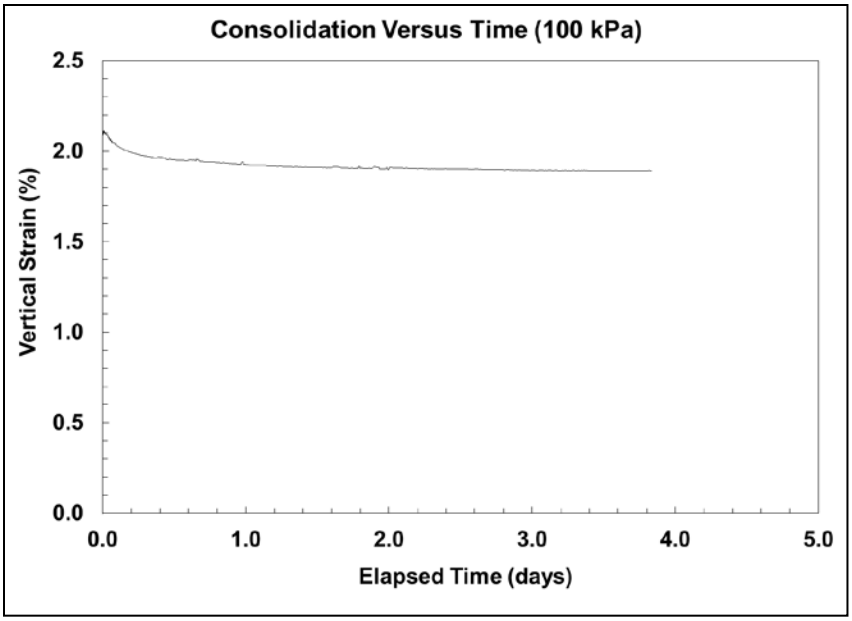

Figure 5.18 – Consolidation vs Time, 100 kPa Normal Stress

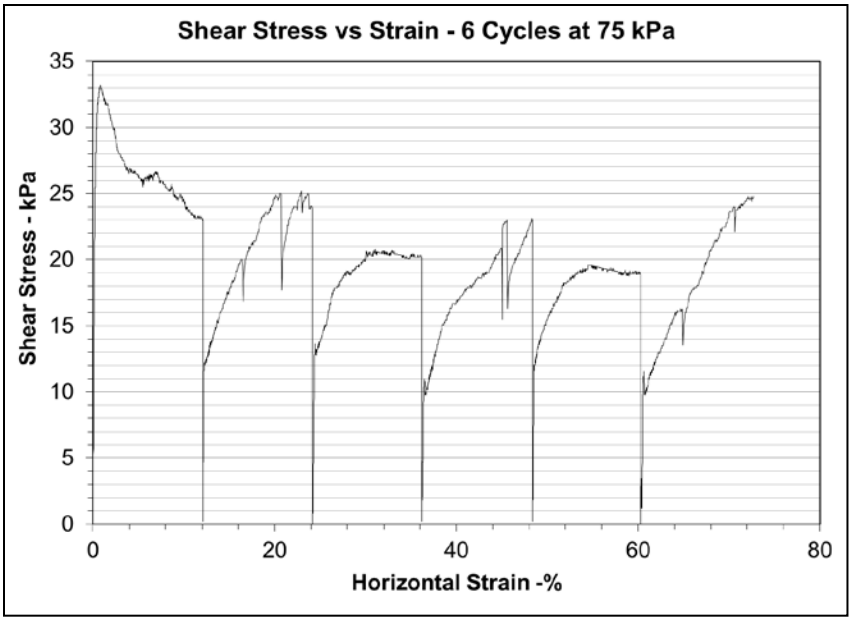

Figure 5.19a – Cyclic Stress-Strain Relationship, 75 kPa Normal Stress

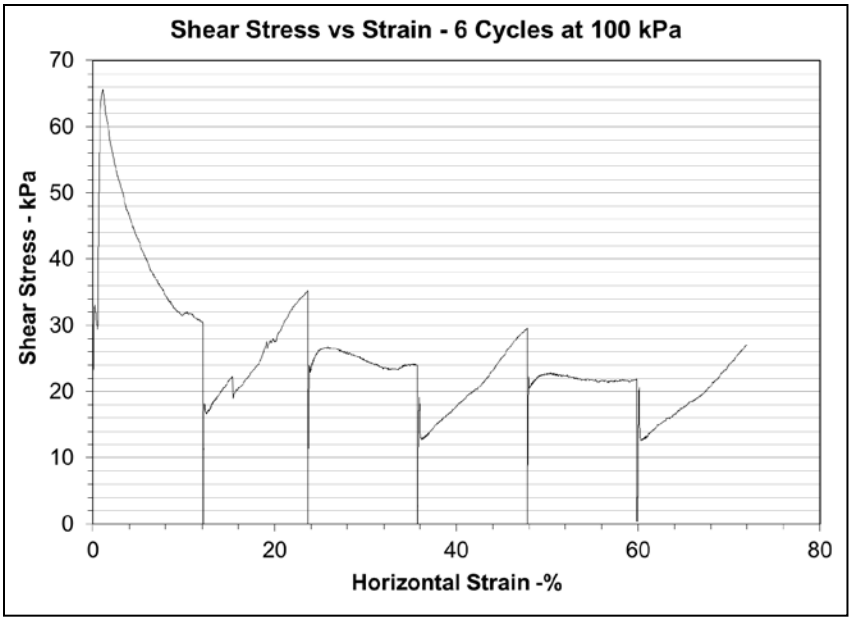

Figure 5.19b – Cyclic Stress-Strain Relationship, 100 kPa Normal Stress

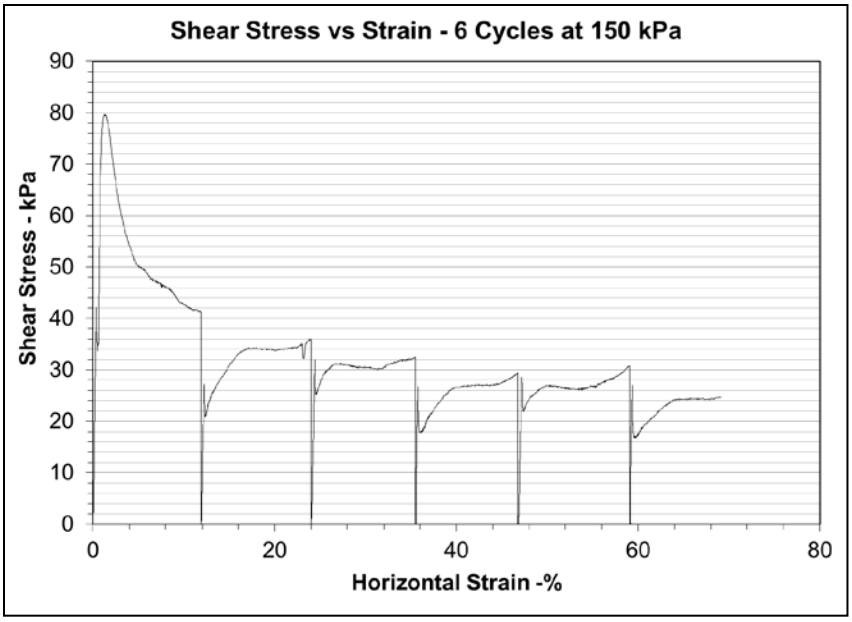

Figure 5.19c – Cyclic Stress-Strain Relationship, 150 kPa Normal Stress

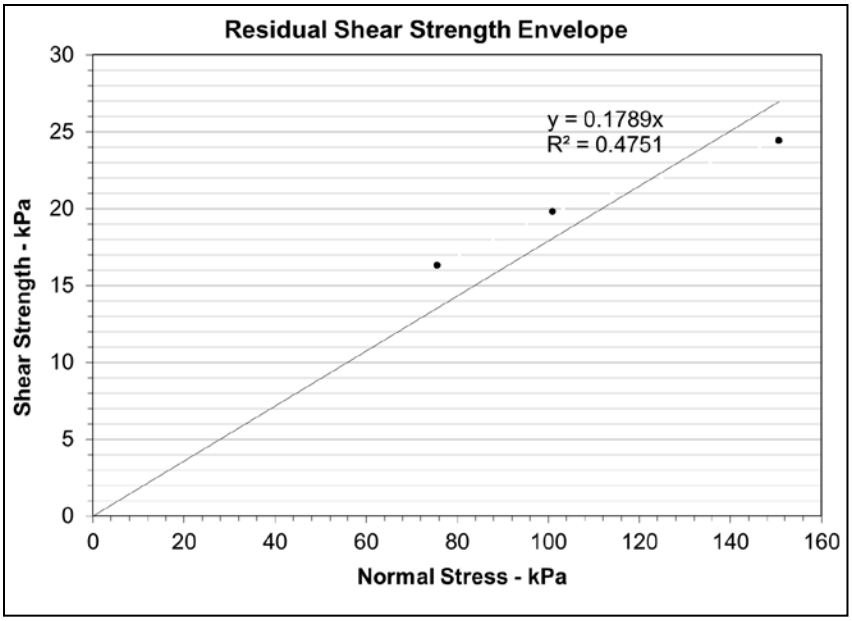

Figure 5.20 – Clay Shale Residual Shear Strength Envelope

Figure 5.21 – Ring Shear Apparatus

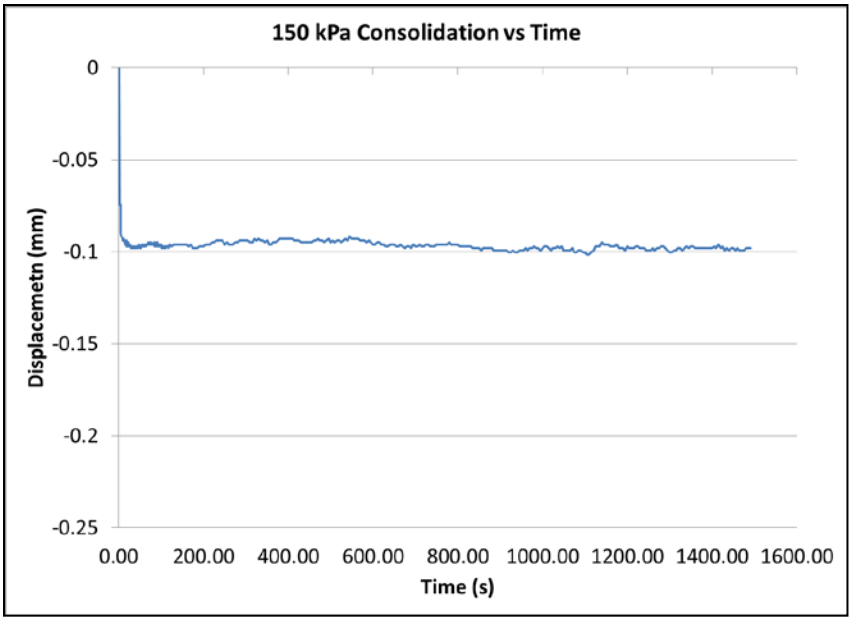

Figure 5.22 – Consolidation of Reconstituted Specimen, 150 kPa Normal Stress

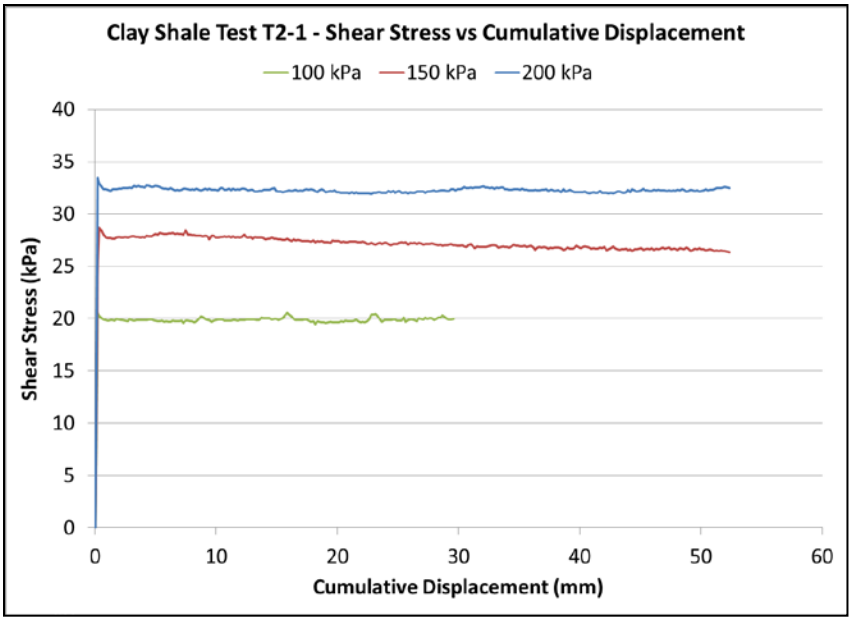

Figure 5.23a – Clay Shale Specimen 1, τ vs Displacement

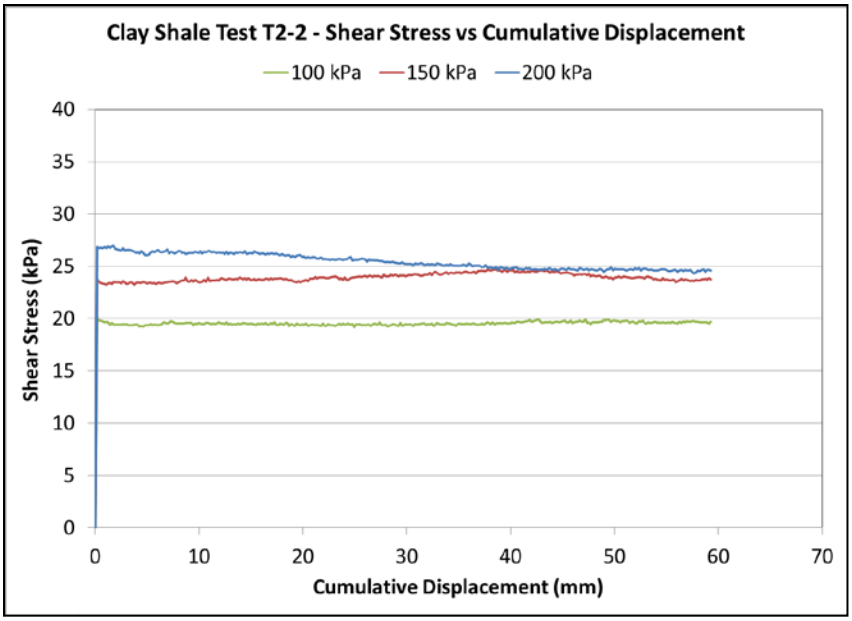

Figure 5.23b – Clay Shale Specimen 2, τ vs Displacement

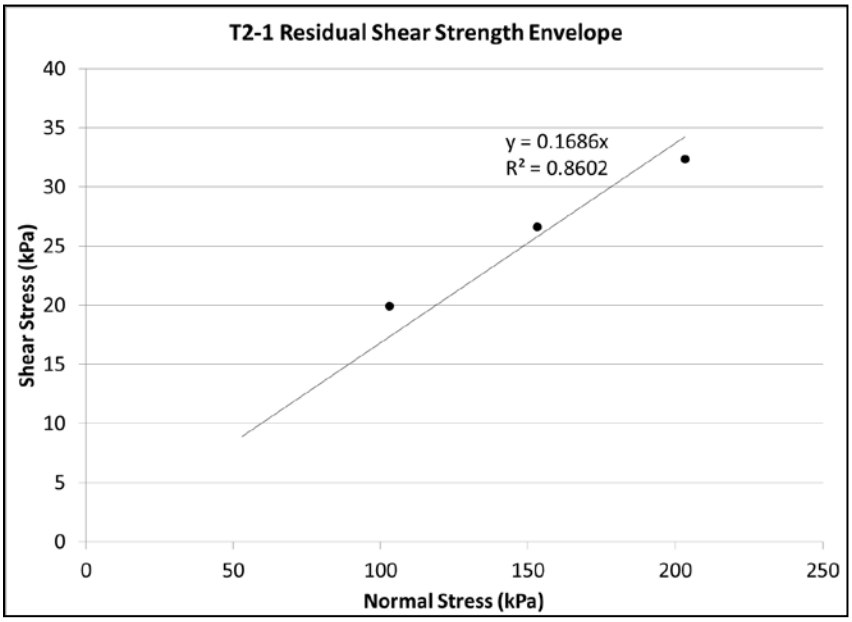

Figure 5.24a – T2-1 Residual Shear Strength Envelope

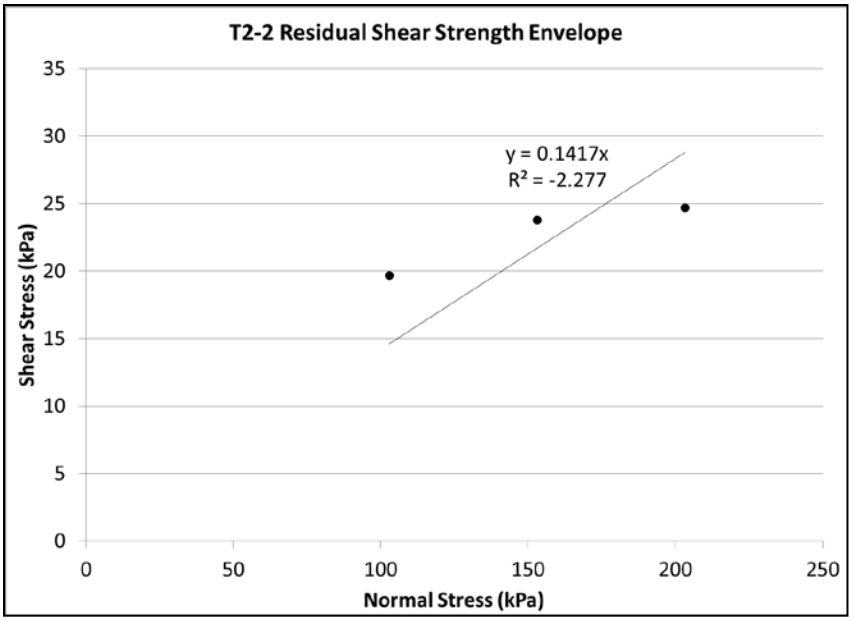

Figure 5.24b – T2-2 Residual Shear Strength Envelope

Chapter 6 – Design Alternatives

6.1. Introduction

Several design alternatives were considered for the remediation of the failed slope at the Ashville Junction. The selection of the most feasible depended on such factors as soil and groundwater conditions, constructability, material availability, and economy. The following sections describe the primary design alternatives explored, and ultimately the selection of the most feasible alternative for the Ashville Junction slide.

6.2. Soil Nails

One of the earliest considerations for slope remediation was soil nail stabilization. Once the depth of the slip surface had been determined through instrumentation, it became apparent that dynamically launched soil nails would not be possible. Launched soil nails must be driven past the failure surface such that sufficient length is fixed into competent soil to establish the required shearing resistance (United States Department of Agriculture, 1994). Drilled soil nails can typically be installed in greater lengths, and were therefore the method considered for slope stabilization.

A design-build proposal was made to M.I.T. by an external contractor to stabilize the slope using drilled soil nails. The cost to satisfy global stability was substantial and, given the imposed budget constraints of the stabilization project, only local stability at the edge of the road was considered in the proposal. Figure 6.1 shows a preliminary cross section used for the soil nail

stability analysis in Slope/W. The figure demonstrates that local stability at the road edge is satisfied with FS = 1.64, while slip surfaces with FS near or below unity still exist lower down the slope below the stabilized soil mass. There was concern that over time, continued movements of the slope below the stabilized area might eventually undermine the nails and again damage the pavement surface. Soil nail stabilization was therefore eliminated as an alternative.

6.3. Shear Key/Rock Fill Columns

Trenched shear keys have been used on several of M.I.T.'s recent slope stabilization projects, and shear key stabilization was therefore considered as an alternative for the Ashville Junction slide. However, there was concern that trenching in the marginally stable slope might induce further movement and cause significant damage to the pavement surface during construction, potentially resulting in a temporary highway closure. To avoid trenching, rock fill columns were then considered.

In Manitoba, rock fill columns are a commonly used method for riverbank stabilization (Thiessen et al. 2011). However, the equipment required is relatively large and heavy. There was concern, therefore, that the earthworks required for preparing the site for the equipment, as well as the load applied by the equipment itself, might further destabilize the slope during installation. Because of the uncertainty in constructability, as well as the substantial estimated cost, rock fill columns were not considered feasible for this particular site.

6.4. Stabilization Berm

Construction of a stabilization berm with free draining, granular fill was considered the most suitable option for both its simplicity and economy, and would not require significant excavation of the slope during construction. Furthermore, this alternative would not require any specialized equipment, and could therefore be constructed by local contractors with minimal mobilization costs. Suitable construction materials were readily available as granular fill that met the specified gradation and could be obtained from a private local pit within approximately 15 km of the project area. The proximity of the pit would therefore minimize haul distances and the associated costs. Details on the analysis of the construction and effectiveness of the stabilization berm are discussed in Chapter 7.

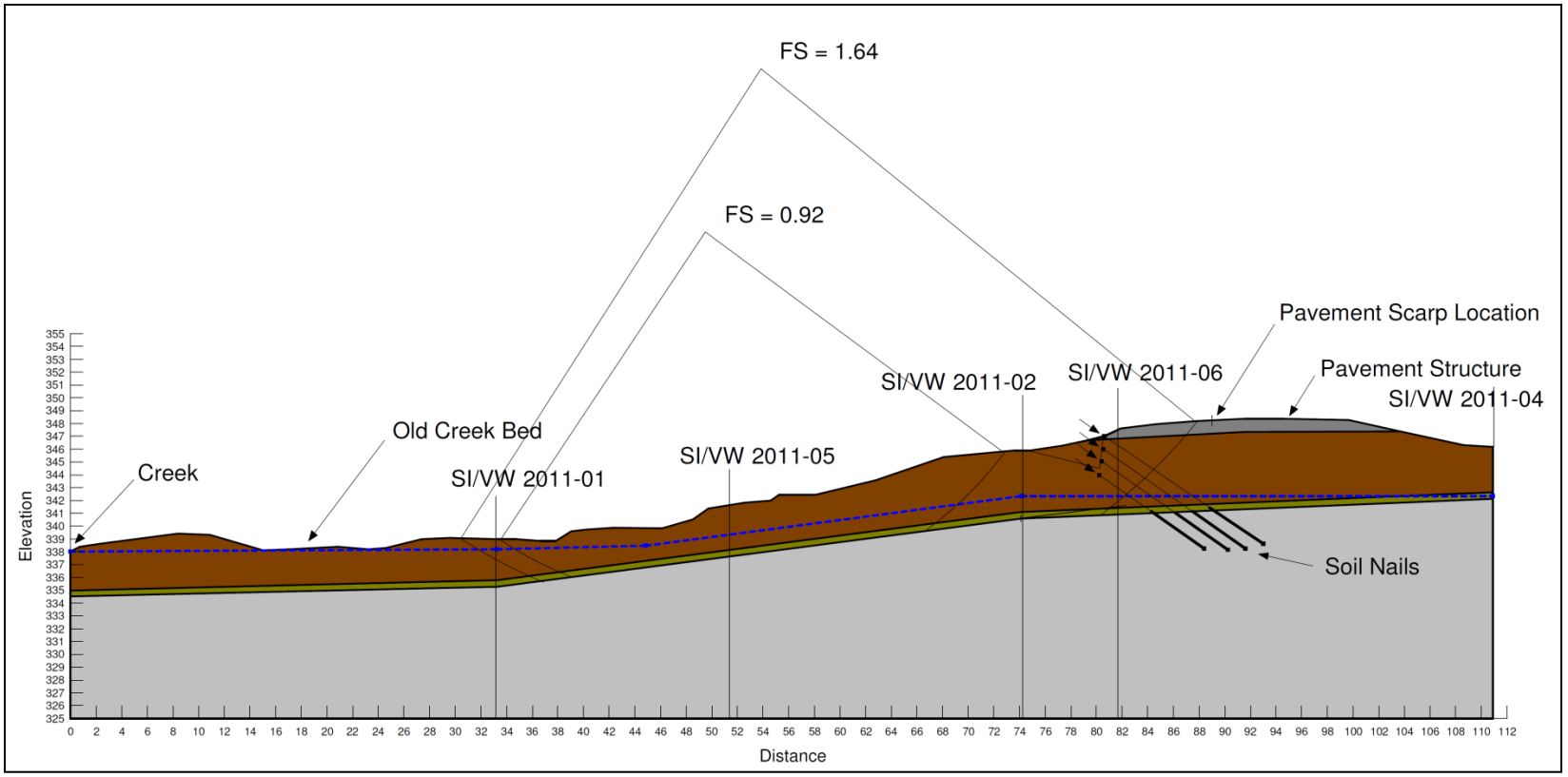

Figure 6.1 – Soil Nail Stabilization, Local Stability at Road Edge

Chapter 7 – Numerical Modeling of a Stabilization Berm

7.1. Introduction

Using the available test hole information from the 1974, 1988 and 2011 site investigations, piezometric data from the installations described in Section 4.3, and cross sections generated from the topographic survey, a model of the failed slope at the Ashville Junction was created in Seep/W. The steady state seepage model would serve as the parent analysis for subsequent slope stability and coupled stress-porewater pressure analyses. Figure 7.1 shows the cross section modeled in the steady state seepage, coupled and slope stability analyses. The details of the modeled section as it relates to each analysis are described in the following sections.

7.2. Steady State Seepage Model Calibration

A steady state seepage model was created to generate a porewater pressure distribution for the critical cross section at station 185+85 (Figure 3.3) using Seep/W. The model was calibrated using the interpreted groundwater data described in Section 4.3. Total head boundary conditions were applied to the left (H_L) and right (H_R) boundaries of the domain, with a no flow (du = 0) condition applied at the lower boundary (Figure 7.1). The right boundary was extended to a distance of approximately 400 m from the highway centerline to the divide between the Wilson River and Mineral Creek watersheds. This distance was estimated from topographic

maps of the area provided by Manitoba Infrastructure and Transportation. A constant head boundary was applied to the creek (H_C) to represent normal flow conditions at the site.

As boundary conditions were altered during calibration of the model, a no flow boundary condition with a potential seepage review was applied to the existing ground surface up to an elevation of 342.0 m. The potential seepage review was necessary if the piezometric surface was raised by changing boundary conditions during calibration such that some flow, Q, was to exit the domain over which this boundary condition was applied. In this case, Q would not then be zero as specified by the boundary condition. The iterative potential seepage review would then change the Q condition at the boundary to a head boundary condition, H, equal to the elevation at that particular node in order to reach a solution.

The right total head boundary, H_R, was modified until the piezometric surface reasonably agreed with what was observed under normal flow conditions at VW2011-04 (Figure 4.12). For steady state conditions, a constant total head of 344.5 m was assigned to H_R. The lower boundary was assigned a “no-flow” condition, which requires that no change in porewater pressure, du, can occur across this boundary. The lower boundary of the domain was extended approximately 10 m below the bottom of the deepest test hole, assuming that no significant material change occurs over this depth. This assumption was necessary to ensure that porewater pressure conditions determined at the location of VW2011-01 in the model were not significantly influenced by the assigned lower boundary condition.

An initial hydrostatic condition was applied at Mineral Creek (H_C) with a constant total head of 337.0 m, representing normal flow conditions observed in the creek. The left boundary of the domain represents the centre of the Mineral Creek valley, and the hydrostatic condition, H_C,

applied was also applied over H_L. As mentioned previously, hydrometric data is not available for Mineral Creek and the total head has therefore been estimated based on field observation and topographic survey data (Figure 4.20, Figure 7.1). With these conditions, the initial results of the model overestimated the porewater pressure observed in VW2011-01 (Section 4.3) by approximately 20 kPa. This suggests that the hydrostatic condition applied to H_C and H_L was insufficient to produce a reasonable approximation of the observed porewater pressure conditions.

As discussed in Section 4.3, no instrumentation was installed near the left boundary of the analyzed domain. Furthermore, each installation had only one VW piezometer installed. As such, limited information with respect to the vertical hydraulic gradient was available at the time of the analysis. The left boundary was modified by discretizing the porewater pressure profile such that a downward vertical gradient was established at the boundary. Using an iterative approach, the discretization was varied until porewater pressures to the right of the boundary were calibrated to what was observed in the instrumentation[13]. The installation of post-construction instrumentation was used later to validate this boundary condition assumption. Table 7.1 shows the variability of total head with depth along H_L.

Initial modeling results indicated that unsaturated flow may occur in the colluvium, clay shale, shear zone, and alluvium, requiring that a saturated/unsaturated material model be applied to these soils. This material model requires that a soil water characteristic curve (SWCC) is specified. As discussed in Section 2.3, the SWCC is determined using the Modified Kovács method. Seep/W provides an estimate of the SWCC that is also based on the Modified Kovács method, requiring the particles size diameters at 10% (D_{10}) and 60% (D_{60}) passing, the

[13] Personal Communication, J. Blatz, 2014

saturated volumetric water content and the liquid limit as input parameters (Geo-slope International Ltd., Seep/W, 2010). Figure 5.2a, 5.2b and 5.2d demonstrate that for many fine grained soils, D_{10} cannot accurately be determined, as the particles are simply too small. The method discussed in Section 2.3 uses fitting parameters to determine an equivalent particle size diameter. Both methods require assumptions, and both yield nearly identical results. Seep/W also provides a SWCC for some predefined soil types, such as clay, silty clay or sand. Figures 7.2a and 7.2b show plots comparing the different estimation methods for samples of colluvium and clay shale respectively. For simplicity, it is assumed that the shear zone (Figure 7.1) is comprised of disturbed clay shale and uses the same SWCC as the undisturbed clay shale. The saturated volumetric water contents shown on these plots for colluvium and clay shale were determined from laboratory test results.

Although limited information was obtained for the alluvium, the grain size distribution obtained from sample T1 was used to determine D_{60} and D_{10} as 0.22 mm and 0.001 mm, respectively. These values were then applied to the Modified Kovács grain size estimate of the SWCC used by Seep/W. A second estimate of the SWCC using a predefined “silty sand” material was also completed for comparison. The limited soil property data available for the alluvium could not produce a grain size estimate SWCC that could confidently be used in the analysis. The slope and air entry value for the SWCC from the “silty sand” estimate appear to better reflect the expected behavior of the alluvium, as coarse grained soils typically have steeper curves and lower air entry values than those shown on the curve plotted from grain size data (Geo-Slope International Ltd., Seep/W, 2010). Because soil property data was not available for the granular berm fill, the estimation method based on the predefined “sand” soil type was applied to this material. Figure 7.3 shows a plot of the SWCC for alluvium comparing the different estimates,

as well as the SWCC for the granular berm fill that would be used for stabilization. A saturated volumetric water content of 40% was assumed for the alluvium and granular fill.

Saturated hydraulic conductivity values for the shale (Cummings et al. 2012), alluvium (Pliakas et al. 2011) and granular fill (Budhu, 2007) are assumed within acceptable values as determined from the literature. Saturated hydraulic conductivity values for the colluvium were determined from flexible wall permeameter tests and back calculation from oedometer tests. The mean saturated vertical hydraulic conductivity (k_v) as determined through these tests was 6.3×10^{-9} m/s for the applicable stress range. This value was subsequently adjusted during calibration of the model.

In order to better reflect the groundwater conditions observed by the instrumentation, a hydraulic conductivity ratio of 0.001 was initially applied to the colluvium. The hydraulic conductivity ratio is the ratio of horizontal conductivity, k_h, and vertical conductivity, k_v. A ratio of 0.001 is likely a physically unrealistic representation of the hydraulic properties of the colluvium, as a ratio of 0.01 implies almost completely horizontal flow (Seep/W, 2010). A closer examination of the subsurface conditions was needed to determine a more realistic representation of the observed groundwater flow regime.

The 2011 site investigation revealed two thin, nearly horizontal layers of bentonite. Shelby tube samples also showed considerable fracturing, weathering and gravel-sized limestone at the interface of the shale bedrock and the Quaternary soils above, suggesting that a localized bed of relatively more highly permeable soil may exist at this location (Figures 7.4a and 7.4b). These conditions were simulated by adding lines in the model at the location of each material layer, and extending the lines across the domain (Figure 7.1, Figure 7.5). Interface elements

can then be applied to these lines, effectively creating a new region. Using the "interface" material model, assumed normal and tangential hydraulic properties can then be assigned to each respective material (Figure 7.6).

In other Cretaceous formations, head drops have been observed to occur across layers of bentonite[14]. While the mineralogy of the bentonite is such that it has an affinity for water storage (reflected in laboratory tests of moisture content), it does not have the same affinity for water flow. It can therefore be less permeable than the surrounding shale, particularly if the shale has a fractured macrostructure like that observed in core samples taken during the 2011 site investigation. Figure 7.7 shows the total head contours for the steady state seepage model used as the parent analysis.

Total head drops across the two layers of bentonite are seen in the model (Figure 7.7). Of note in the model is the development of a perched water table (Figure 7.7) near VW2011-06. The observed piezometric elevation at this location was abnormally high with respect to the other instruments, suggesting that a perched water table may exist at this location. Table 7.2 summarizes the calibrated vertical and horizontal hydraulic conductivities determined for each material used in the analysis. Figures 7.8a, 7.8b and 7.8c show the hydraulic conductivity functions used for the colluvium, clay shale and alluvium, respectively.

[14] Personal Communication, G. van der Kamp, 2014

7.3. Back Analysis Using Limit Equilibrium

Using Slope/W from Geo-Studio International, limit equilibrium was used to back analyze the critical section and evaluate shear strength parameters for the soils. Figure 7.1 shows the cross-section, the piezometric surface, and the observed slip surface used in the analysis. The Morgenstern-Price method of slices was used, with shear strength parameters being adjusted until a factor of safety near unity (FS = 1.04) was reached. A composite slip surface was analyzed, with the shale being designated as impenetrable bedrock and the remaining materials modeled using Mohr-Coulomb (c, ϕ) strengths. A shear zone of weakened shale was applied at the interface of the colluvium and shale bedrock where the failure surface was observed to occur. Table 7.3 shows the back- analyzed and mean laboratory shear strength values for colluvium and clay shale.

As mentioned in the previous section, Figure 7.1 shows the location of two bentonite seams encountered during the 2011 investigation. As discussed in Section 4.3, the previous investigations did not identify separate layers of bentonite, likely due to the limited number of test holes drilled at that time. The relatively horizontal orientation of these layers with respect to the observed failure surface suggests that they are not the primary cause of failure.

7.4. Coupled Stress/Porewater Pressure and Finite Element Method (FEM) Stability Analysis

The finite element model was created with a mesh of quadrilateral and triangular elements, with a maximum global element size of 1.0 m. A mesh-size ratio of 2.0 was applied to the global

element size at the edges of regions that would not significantly affect the results, thereby increasing the size of some elements and reducing computation times. A ratio of 0.2 was used to decrease the size of the mesh at selected areas of the domain where relatively high gradients or stress concentrations might occur, primarily between the foundation soils and the granular fill. This creates the irregular mesh pattern across the domain shown in Figure 7.9. The left and right boundaries of the domain were fixed in the x (dx = 0) direction, with the lower boundary being fixed in both the x and y (dy = 0) directions (Figure 7.1).

The initial stresses, or the stresses prior to loading, must be established for an elastic-plastic constitutive model as it uses the Mohr-Coulomb failure criterion. Stresses beyond the initial stresses will therefore bring a particular soil element closer to failure. The Modified Cam-Clay constitutive model is dependent on stress state, and therefore requires the initial stresses to be established to determine where a particular soil element lies within the defined yield locus. The in-ground stresses are first determined using an "in-situ analysis based on the user defined values for unit weight, γ (Geo-Slope International Ltd, Sigma/W, 2010). A "body load" is applied to a simple linear elastic model using the soil unit weight and the pore water pressure established in the Seep/W parent analysis. The resulting stresses can then be used in determining the stress state following the first stage of loading. Figure 7.10 shows the in-ground stress contours.

Loading from the stabilizing embankment was modeled so that uniform lifts of granular fill were placed at a frequency of one day per lift, and porewater pressures were allowed to dissipate over a period of one year following placement of the final lift. Lift heights were based on practical quantities that could reasonably be placed by a contractor in one day, based on experience from other M.I.T. earthworks projects. An elastic-plastic constitutive model was first

selected for the colluvium, while a linear elastic model was selected for the clay shale, alluvium and granular fill. A second model was then run using the Modified Cam-Clay constitutive model for the colluvium.

The elastic parameters for each material were based on laboratory and in-situ testing, as well as the literature. Young's modulus for the alluvium was assumed within acceptable values for the material type as determined from published values in Budhu (2007). Young's moduli for the colluvium and shale were determined from laboratory (Section 5.4) and in-situ testing (Section 2.5), respectively. The load response ratio (B = 0.9) discussed in Section 4.3.2 was applied to the shale; the software default value of 1.0 was applied to all other materials. Unit weights for colluvium and clay shale were determined from laboratory testing, while unit weights for the alluvium and granular fill were determined from acceptable values as determined from the literature (Budhu, 2007). Poisson's ratio for colluvium, clay shale and the shear zone were assumed at the default value in Sigma/W, while Poisson's ratio for the alluvium and granular fill was assumed within acceptable values as determined from the literature (Budhu, 2007). The critical state parameters used for the Modified Cam-Clay constitutive model were taken as the mean values obtained from laboratory testing. Table 7.4 summarizes the elastic properties used in the coupled analysis. Table 7.5 summarizes the critical state properties used in the coupled analysis.

With the in-ground stresses established, a FEM slope stability analysis was completed to establish an initial factor of safety (FS) to compare with subsequent stability analyses at various stages of loading. As discussed in Section 2.8, because limit equilibrium slope stability calculations are based only on statics, strains induced by loading of the embankment are not accounted for. Both methods resulted in values of FS near unity under post-failure conditions.

The FEM slope stability analyses were completed after every four lifts applied to the model. As the stresses change with applied loading, the stability model uses the re-calculated stresses from the parent analysis at each stage of stability analysis. A total of four analyses were completed to represent the loading process, with a fifth analysis being completed following dissipation of excess porewater pressures. This allows an assessment of stability at various stages of construction, as well as under long-term drained conditions. The excess porewater pressure response determined in the model is discussed and compared to measured values in Chapter 9.

Stability of the observed failure surface, as determined with the slope inclinometers discussed in Chapter 4, was addressed first. The failure surface was observed to have exited the slope near the toe. This was therefore the location where the highest fill was applied in the model. The granular fill material was assigned a friction angle of 32°, which is consistent with typical values as determined in the literature (Budhu, 2007).

The fill was raised to a height of approximately 4 m until the target factor of safety of 1.5 was reached for the observed failure surface. A search for other slip surfaces with FS near unity was then run. A safety map for which a range of slip surfaces near a specified FS can be produced in Seep/W, which shows a range of slip surfaces for a given range in FS. Figure 7.11 shows the safety map produced for the slope under existing conditions. The slip surfaces within the red region are those for which the FS is between 1.02 and 1.07. The green and blue regions represent slip surfaces with FS up to 1.12 and 1.17, respectively. It can be seen in Figure 7.11 that the red region of the safety map extends beyond the toe. The grade of the stabilization berm was therefore flattened until the target FS of 1.5 was reached for all slip surfaces within this region. This resulted in a slope with grade of approximately 17% (6H:1V).

With these potential slip surfaces stabilized, a grid and radius slip surface search was then run to determine any slip surfaces that may exit the slope above the stabilization berm. The slip surface search resulted in slip surfaces above the stabilization berm with FS below 1.5 (Figure 7.12). A second "tier" of stabilization berm was then added until the target factor of safety was reached (Figure 7.13). A plot of the change in FS with time during loading of the stabilization berm is shown in Figure 7.14.

Figures 7.15a, 7.15b, 7.15c and 7.15d show plots of base normal stress along the observed failure surface under existing conditions, after lift eight, after lift twelve and following dissipation of excess porewater pressure at the end of loading, respectively. The normal stress distribution for both the limit equilibrium and finite element methods are very similar under existing conditions. This is reflected in the FS determined for each method, which differ by only 2%. As loading is added, however, the disparity between the two methods becomes more evident with higher normal stresses occurring near the toe of the slope using the limit equilibrium method. Given these higher normal stresses, the limit equilibrium method gives FS of up to 19% higher than that determined using the finite element method. Figure 7.16 shows a plot of FS versus time for both the limit equilibrium and finite element methods.

Given the preconsolidation pressure of the colluvium (approximately 200 kPa) determined through oedometer tests (Section 5.5), and the relatively small load applied by the fill (approximately 80 kPa), embankment settlement was anticipated to be minimal and rapid. Using one dimensional primary consolidation theory, settlements of 27 mm were determined in the clay foundation soils. The numerical analysis using the Modified Cam-Clay and elastic-plastic constitutive models predicted settlements of 37 mm and 7 mm, respectively. Figures

7.17a and 7.17b show plots of settlement (shown as negative values) versus time for the elastic-plastic and Modified Cam-Clay models, respectively.

The elastic-plastic model appears to under-predict the anticipated settlement of the embankment. The stiffness function (Section 5.4) applied to the colluvium was interpreted from plots of triaxial test data. The initial tangent modulus determined from these plots may therefore be an over-estimate of the stiffness. Using a secant modulus, rather than the initial tangent modulus may be more appropriate, although there is some uncertainty in the measure of strain that should be used to determine this modulus from the stress-strain plot. Comparatively, the Modified Cam-Clay model used soil parameters directly measured in the laboratory and yielded results that compared relatively well with settlement values determined with one dimensional consolidation theory. Therefore, subsequent analyses aimed at examining potential failure mechanisms were conducted using this constitutive model.

Table 7.1 – Discretization of H_L

Elevation (m)	ΔL (m)	H (m)	ΔH (m)	i
337.0 – 335.5	1.5	337.0	0.2	0.13
335.5 – 334.0	1.5	336.8	0.6	0.20
334.0 – 331.0	3.0	336.2	0.6	0.20
331.0 – 328.0	3.0	335.6	0.6	0.20
328.0 – 325.0	3.0	335.0	0.6	0.20
325.0 – 322.0	3.0	334.4	0.6	0.20
322.0 – 319.0	3.0	338.8	0.6	0.20
319.0 – 316.0	3.0	333.2	0.6	0.20
316.0 – 313.0	3.0	332.8	0.4	0.13
313.0 – 311.0	2.0	332.2	0.6	0.20

Table 7.2 - Modeled Hydraulic Conductivity

Soil	k_v (m/s)	k_h (m/s)	k_v/k_h
Colluvium	$8\ e^{-8}$	$8\ e^{-07}$	0.1
Alluvium	$1\ e^{-05}$	$1\ e^{-04}$	0.1
Shale	$5\ e^{-11}$	$5\ e^{-10}$	0.1
Bentonite	$1e^{-12}$	$1e^{-11}$	0.1
Fractured Zone	$1e^{-7}$	$1e^{-5}$	0.01
Granular Fill	$1e^{-4}$	$1e^{-4}$	1

Table 7.3 - Shear Strength Parameters

Soil	ϕ'_r (DS[1])	ϕ'_r (RS[2])	ϕ'_r (BA[3])	ϕ'_{cs} (CIŪ)	c'(kPa)
Colluvium	-	-	25°	27°	0
Shale	10.1°	8.9°	8.0°	-	0

[1] direct shear
[2] ring shear (mean value)
[3] back analysis

Table 7.4 - Modeled Elastic Properties

Soil	E (kPa)	γ (kN/m^3)	ν
Colluvium[1]	varies	19.0	0.34
Shale	388,000	18.5	0.34
Weakened Shale[2]	30,000	18.5	0.34
Alluvium	40,000	20.0	0.30
Granular Fill[3]	60,000	19.0	0.30

[1]function shown in Figure 5.9
[2]applied to shear zone (Figure 7.1)
[3]dry, gravelly sand, track compacted in winter

Table 7.5 – Modeled Critical State Properties

Soil	OCR	λ	κ	e	ν	ϕ'_{cs} (°)	γ (kN/m^3)
Colluvium	2.7	0.110	0.0261	0.78	0.35	25	19

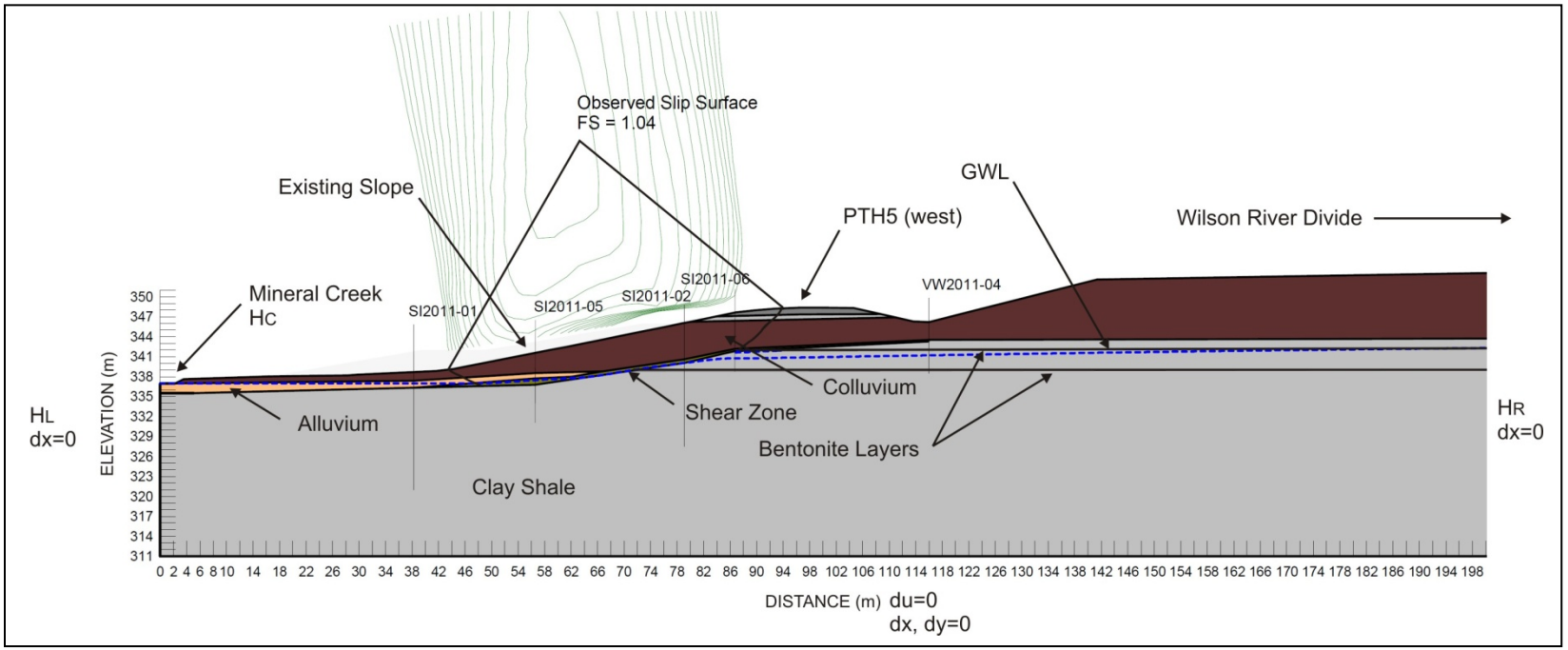

Figure 7.1 – Cross Section Used for Numerical Modeling in Geo-Studio

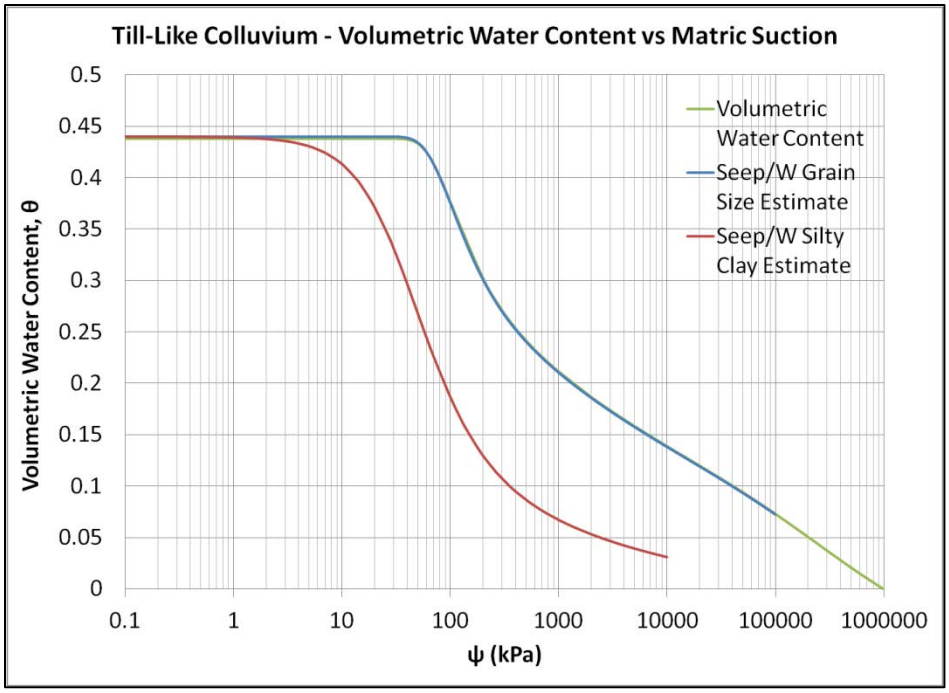

Figure 7.2a – SWCC Comparison for Colluvium

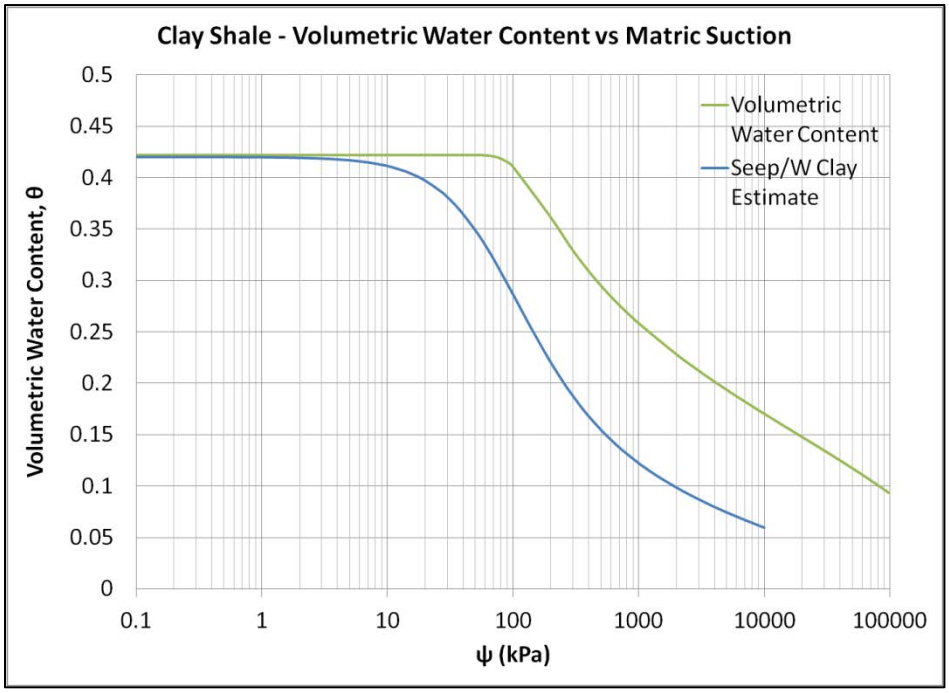

Figure 7.2b – SWCC Comparison for Clay Shale

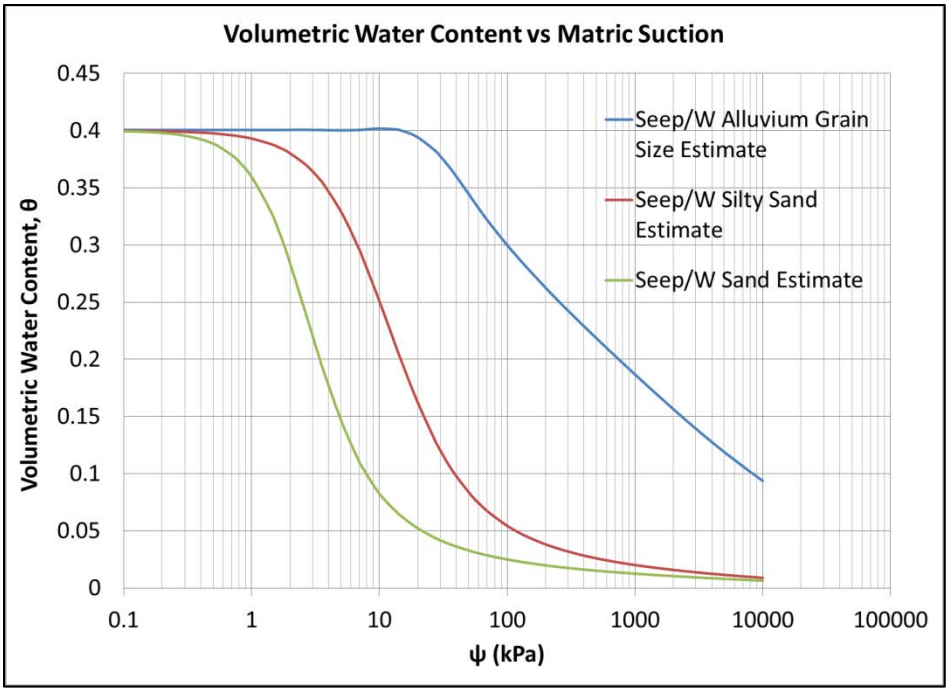

Figure 7.3 – SWCC Comparison for Alluvium and SWCC for Granular Fill (Sand)

Figure 7.4a (left) – Weathered, Fractured Clay Shale; Figure 7.4b (right) – Gravel Sized Limestone Fragments (TH2011-06, Sample T11)

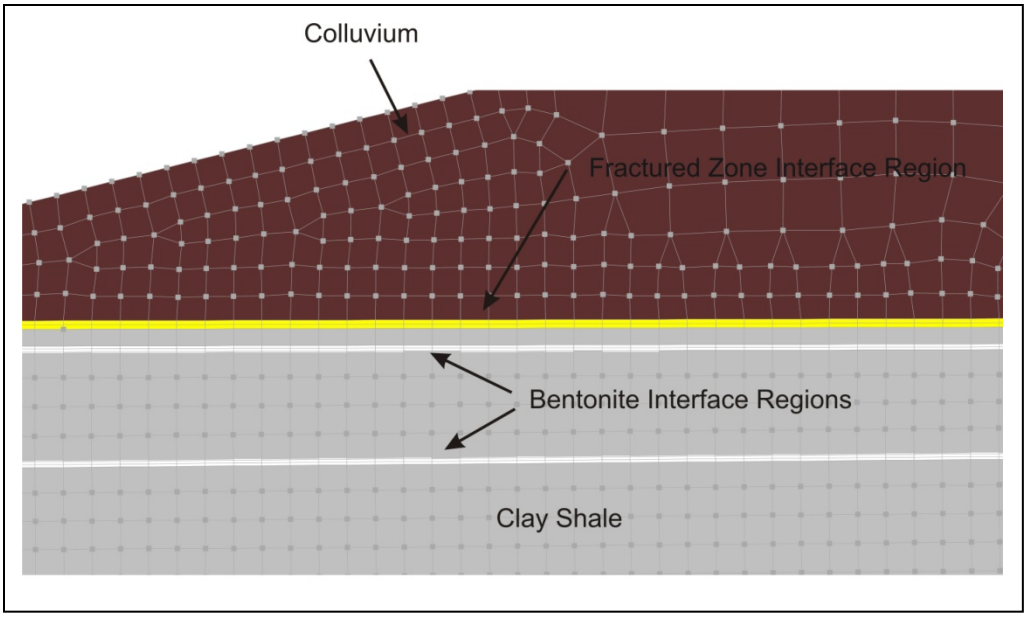

Figure 7.5 – Bentonite and Fractured Zone Interface Regions

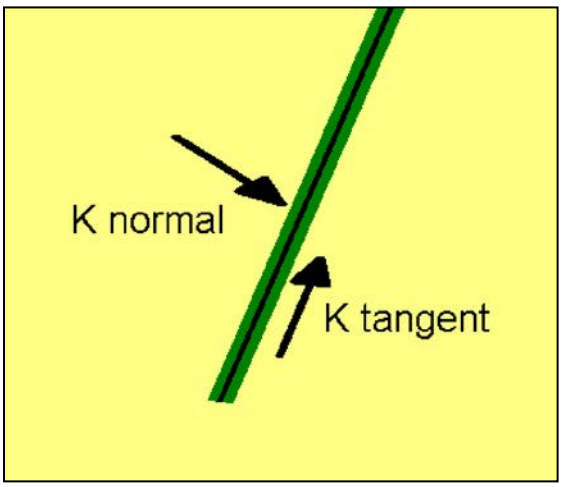

Figure 7.6 – Interface Model Applied to a Line (with permission, Geo-Slope International Ltd., Seep/W, 2010)

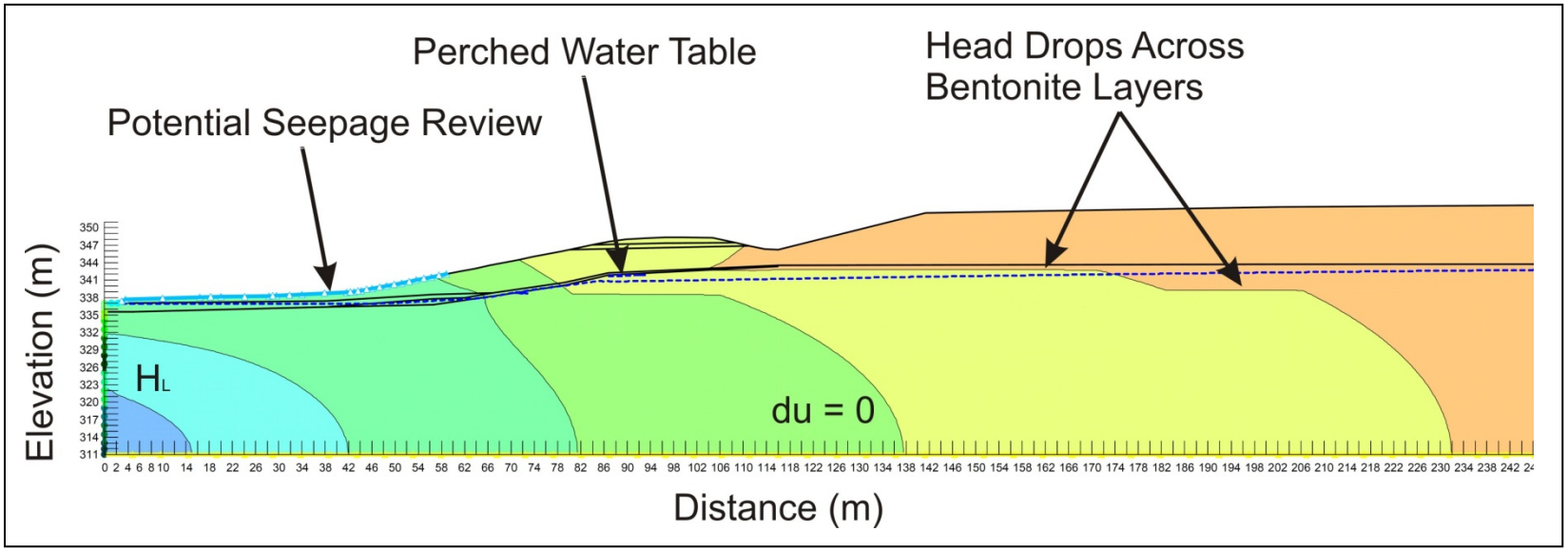

Figure 7.7 – Total Head Contours

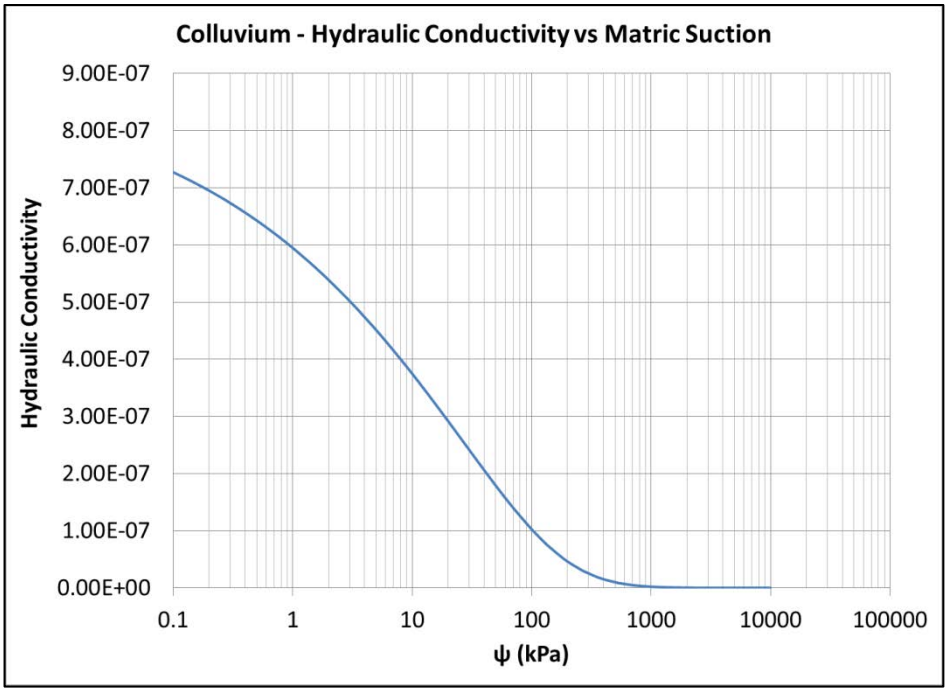

Figure 7.8a – Till-Like Colluvium k Function

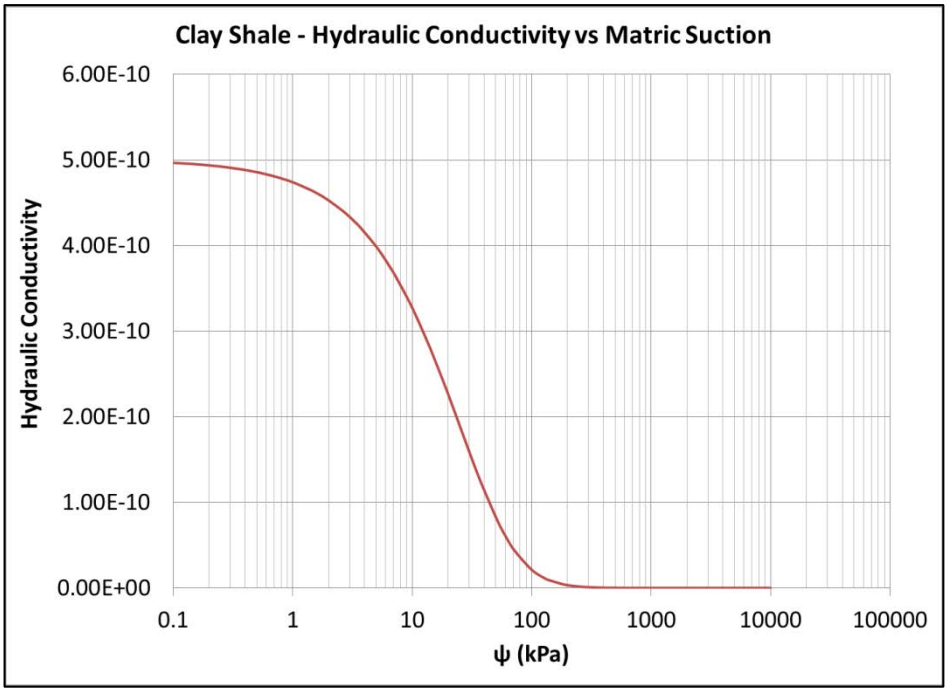

Figure 7.8b – Clay Shale k Function

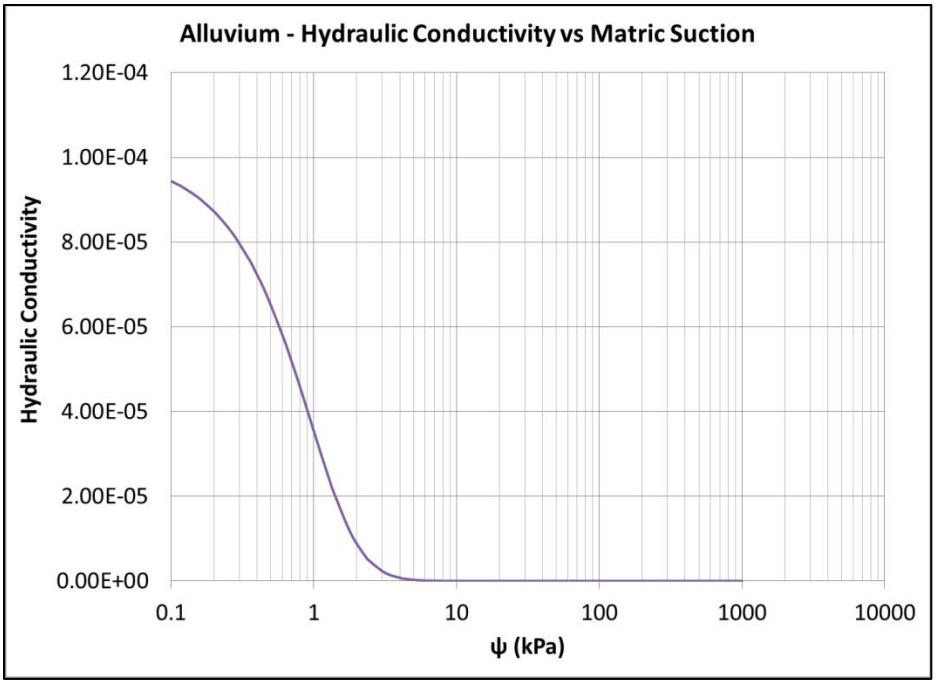

Figure 7.8c – Alluvium k Function

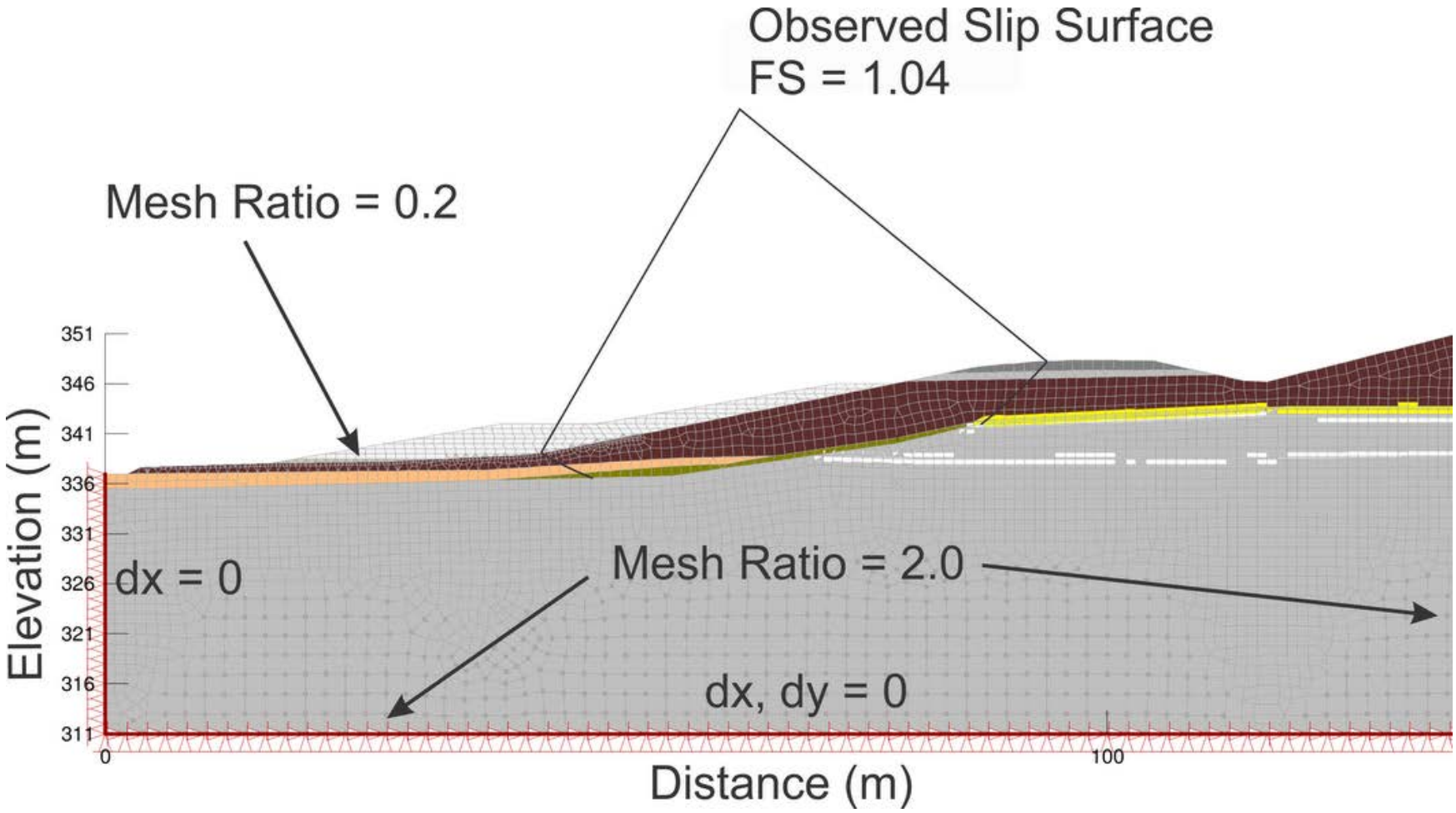

Figure 7.9 – Coupled FEM Mesh

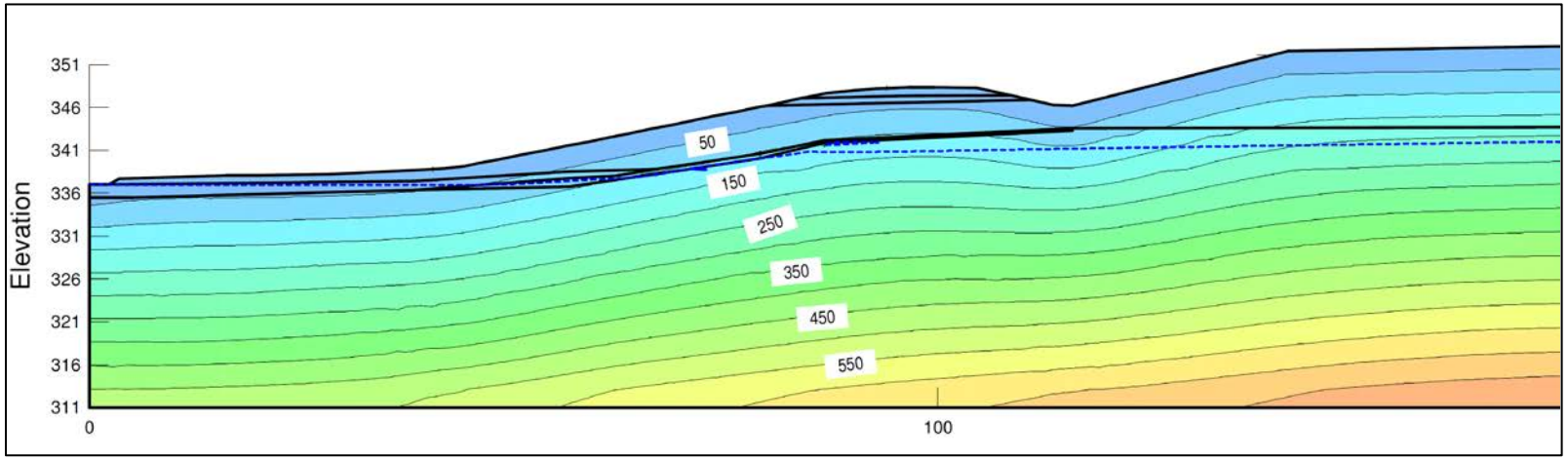

Figure 7.10 – In Ground Stress Contours (kPa)

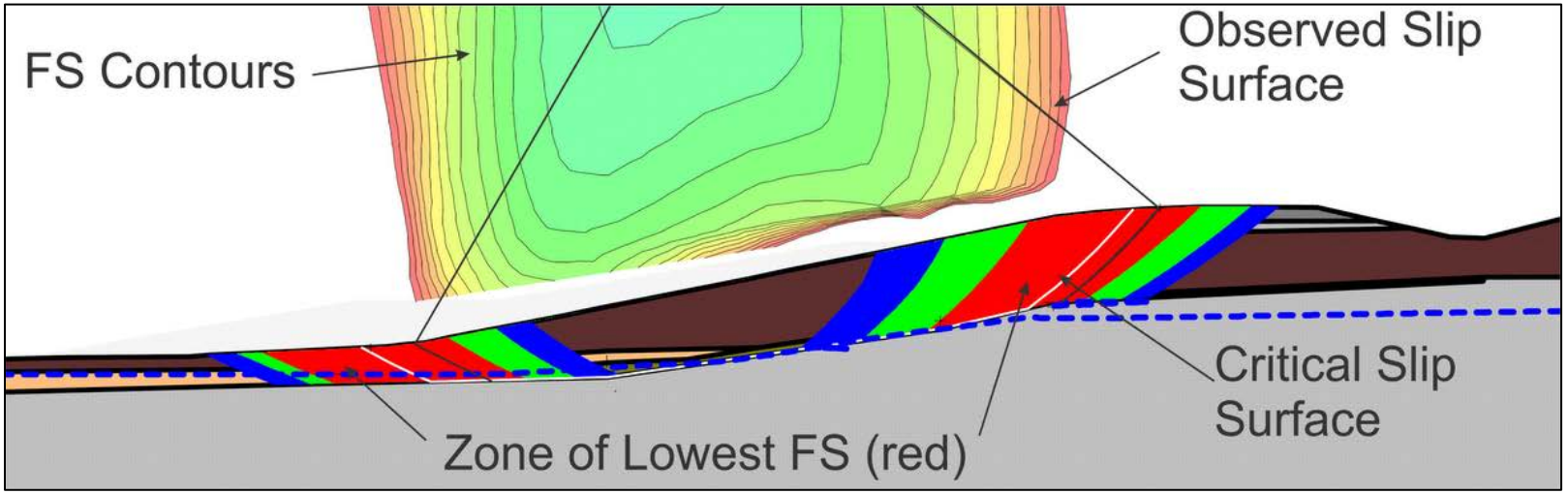

Figure 7.11 – Slope Stability Safety Map

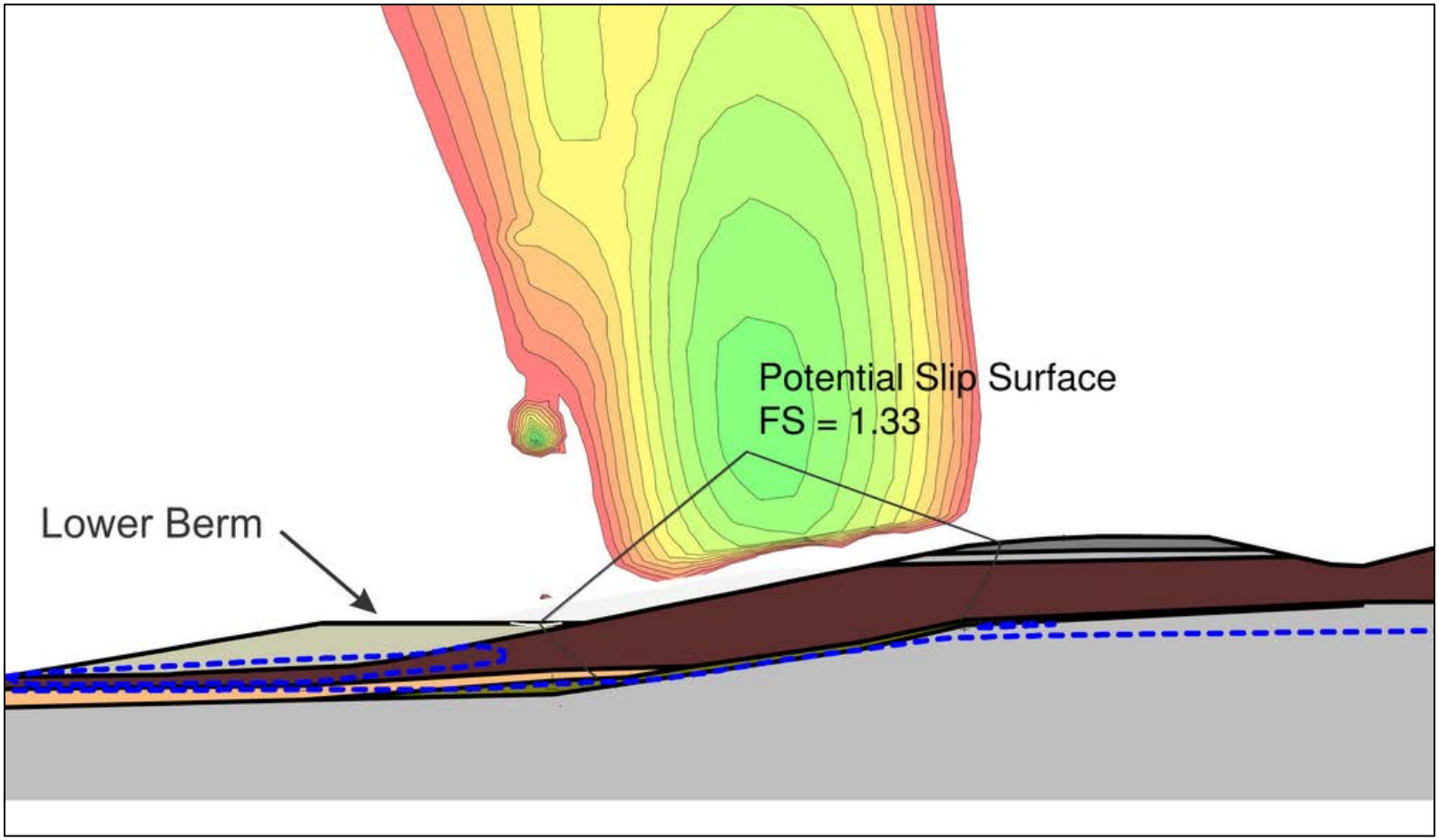

Figure 7.12 – Slip Surface Above Berm

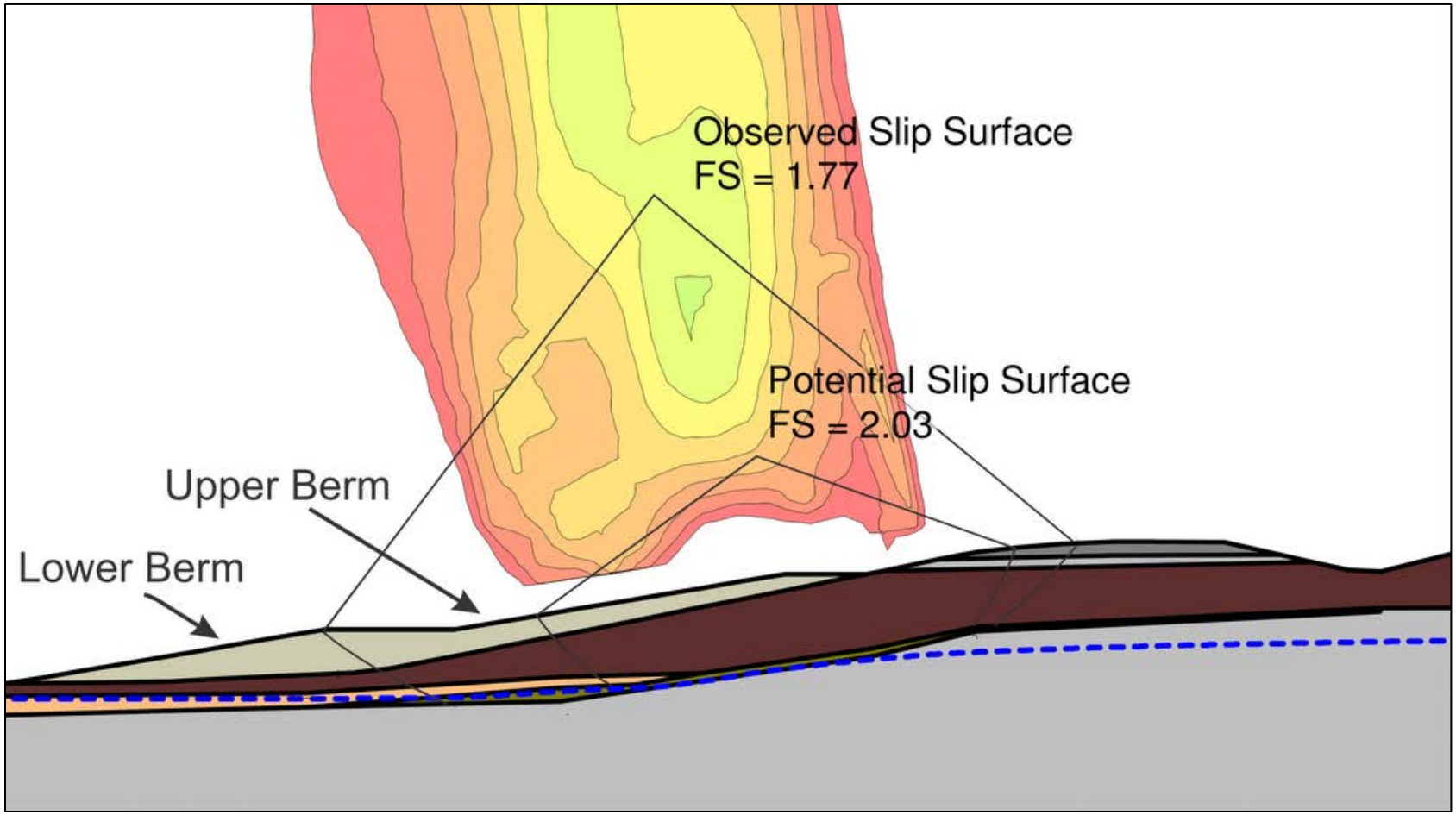

Figure 7.13 – Two Tier Stabilization Berm

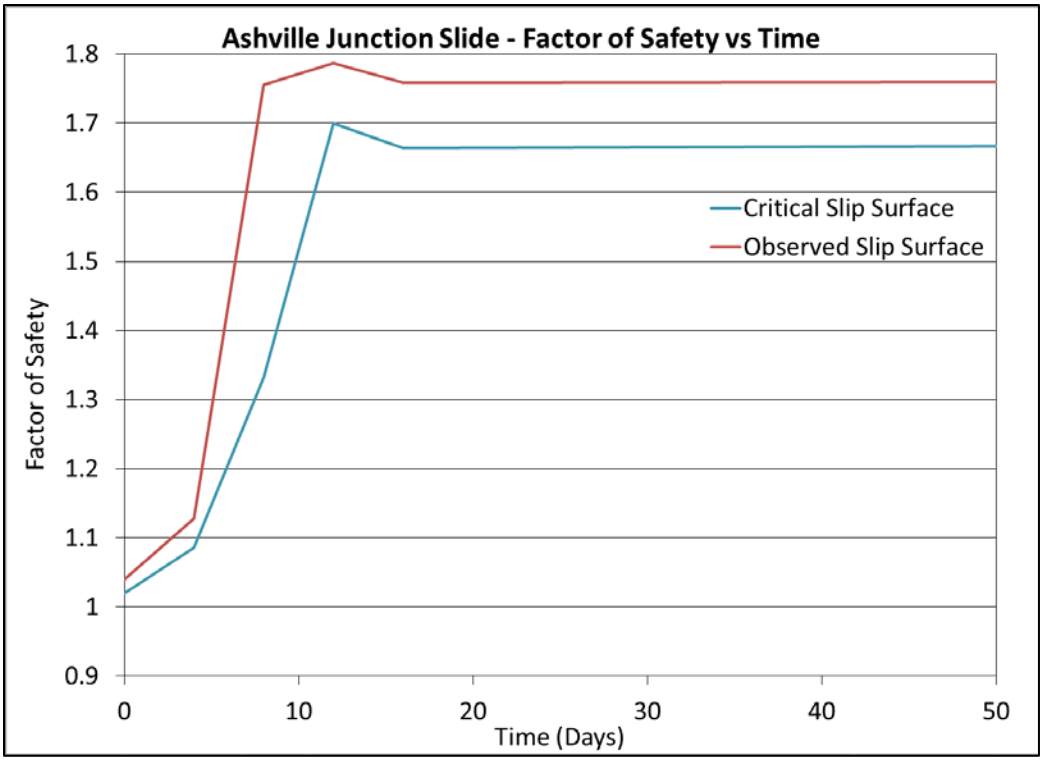

Figure 7.14 – FS vs Time for Observed and Critical Slip Surfaces

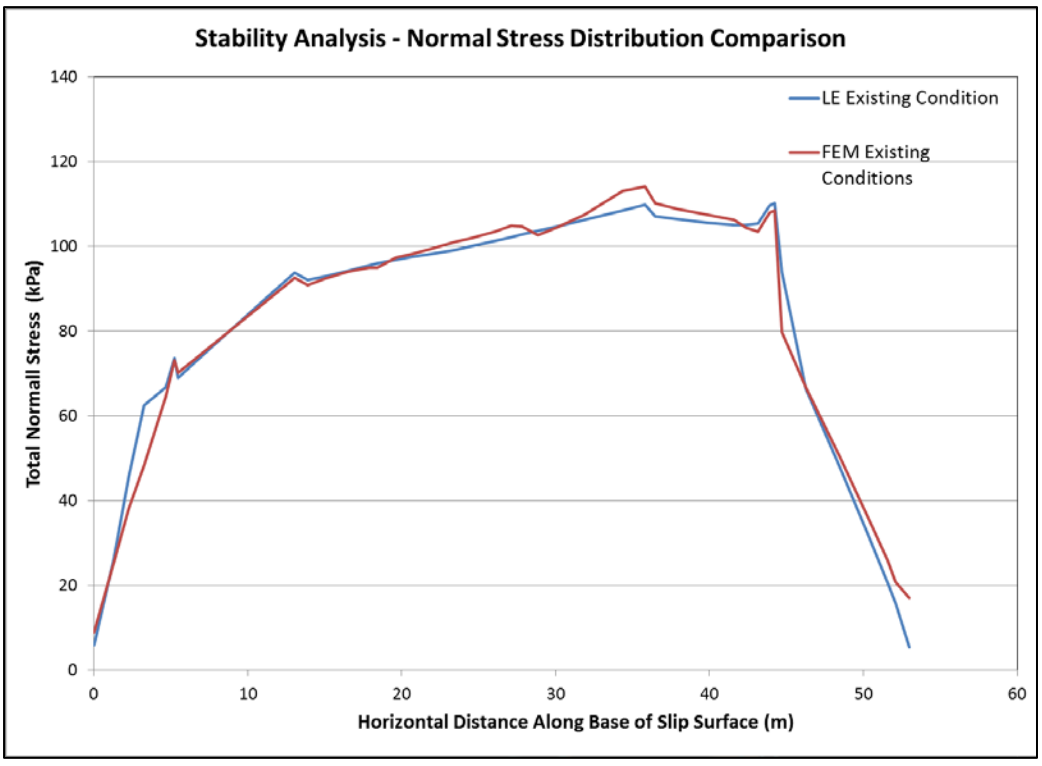

Figure 7.15a – Normal Stress Along Slip Surface, Existing Conditions

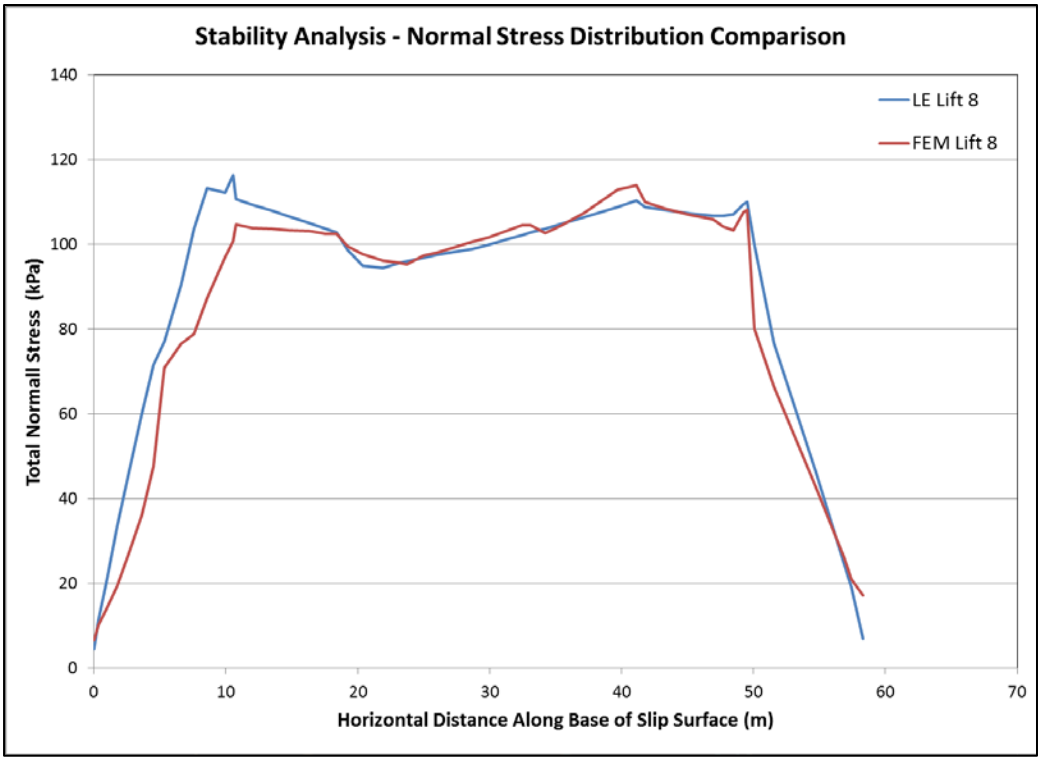

Figure 7.15b – Normal Stress Along Slip Surface, Lift 8

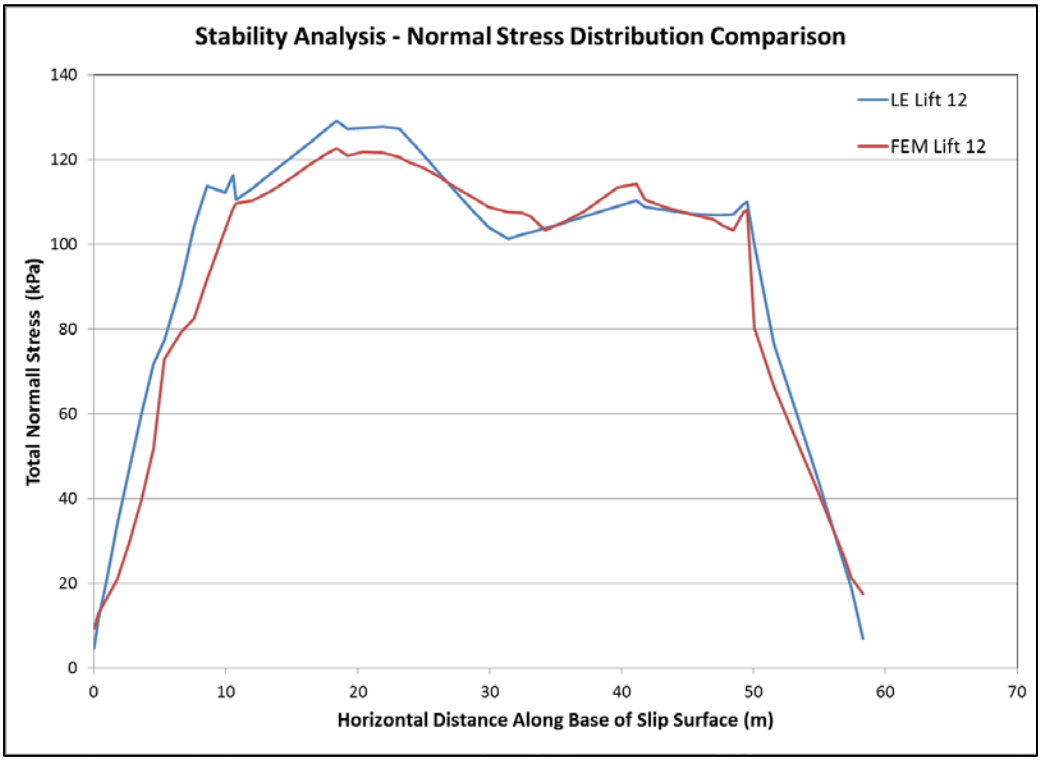

Figure 7.15c – Normal Stress Along Slip Surface, Lift 12

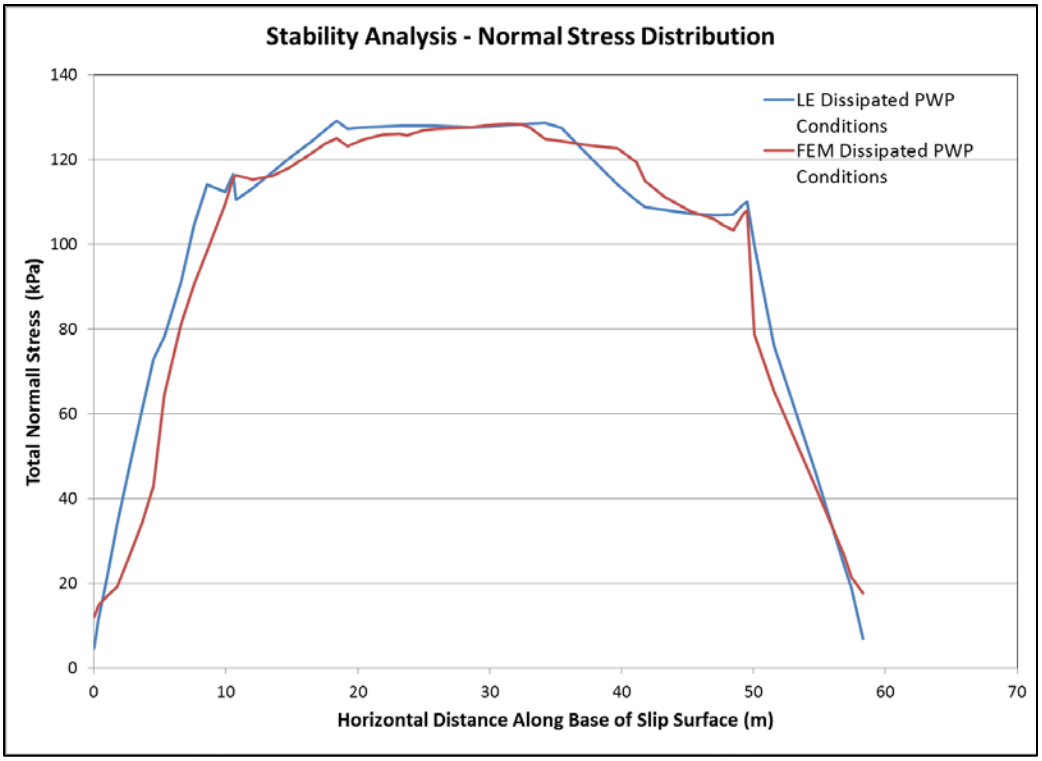

Figure 7.15d – Normal Stress Along Slip Surface, Dissipated Porewater Pressure

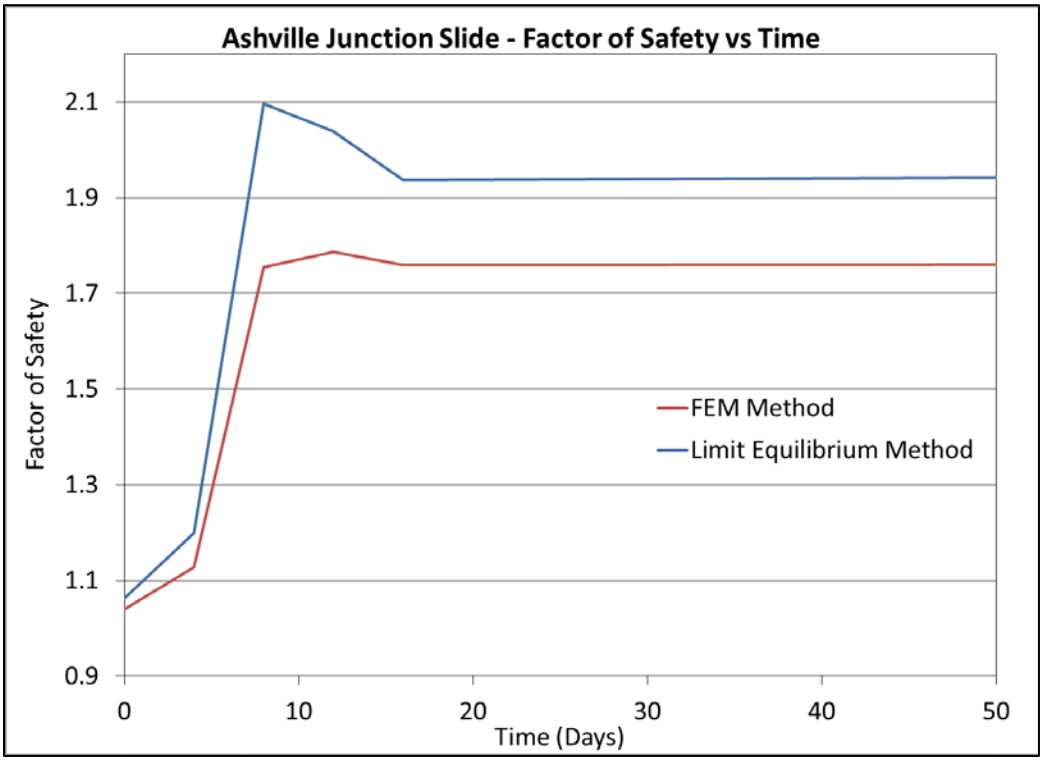

Figure 7.16 – FS vs Time for Limit Equilibrium and Finite Element Methods

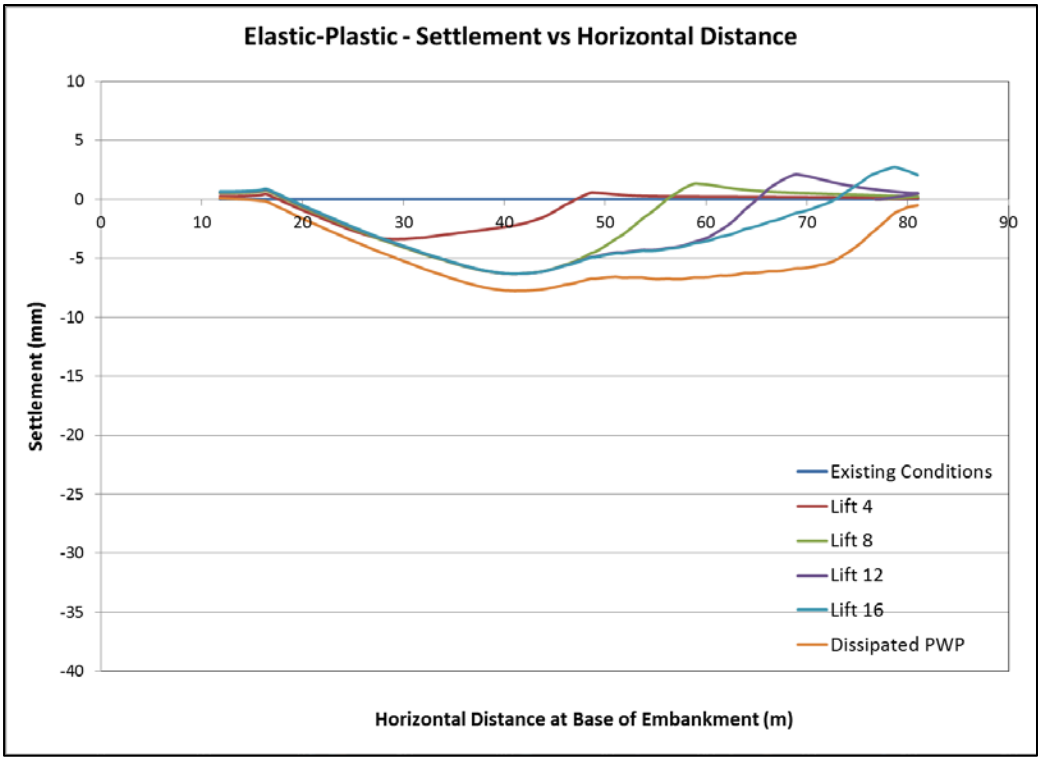

Figure 7.17a – Vertical Displacement vs Time, Elastic-Plastic Model

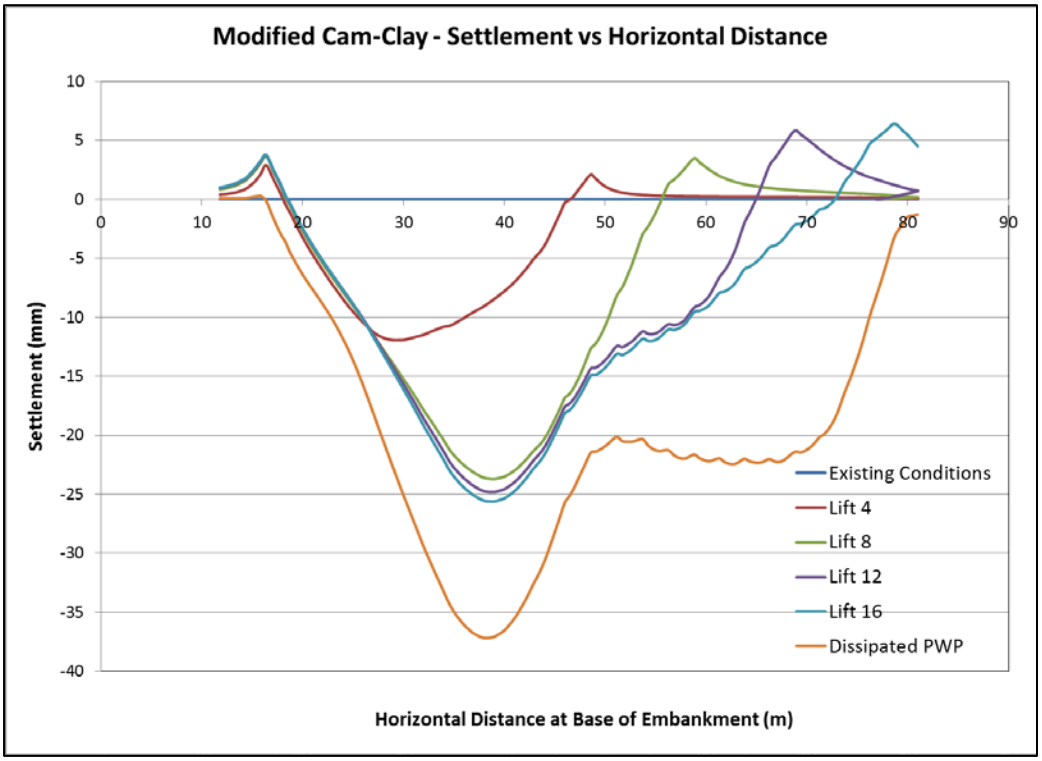

Figure 7.17b – Vertical Displacement vs Time, Modified Cam-Clay Model

Chapter 8 – Numerical Modeling of Potential Failure Mechanisms

8.1. Introduction

Since 2007, the most significant slope movements at the Ashville Junction have been observed to occur following flood events or extended periods of precipitation. A coupled stress-porewater pressure and finite element slope stability model was created to determine the effects of such occurrences on the stability of the slope. As the failure is located on the outside of a meander in the creek valley wall (Figure 1.2, Figure 4.1), it is possible that the original failure occurred some time ago following an over-steepening of the slope through erosive processes. The model does not attempt to replicate this phenomenon. For the purpose of this study, it was assumed that past movements have already brought the material in the shear zone to residual strength. The following sections examine the effects of cyclic flooding on an already weakened slope.

8.2. Modeling of Slope Response to Flooding

In 2011, significant slope movements occurred following flooding due to the spring melt; prior to any significant spring precipitation events. Flooding was therefore examined without including precipitation as a boundary condition in the analysis.

As discussed previously, hydrometric data was not available for Mineral Creek. Hydrometric data from a nearby station on the Wilson River was used to identify trends in the flow data, and these were then modified to reflect the conditions at Mineral Creek. During the June, 2013 flood event, peak water surface elevation (340.9 m) was collected in a survey of the site. The water surface elevation under "normal flow" conditions (337.0 m) had been collected prior to flooding. The Wilson River data was then modified such that the peak water surface elevation matched that of the survey data collected at Mineral Creek. However in doing so, the "normal flow" water surface elevation did not accurately reflect what was observed at Mineral Creek. The data points between the two flood events on the hydrograph were lowered so that both the peak and "normal flow" conditions reflected what was observed. This gave an estimated hydrograph that could then be used in a numerical model. Figure 8.1 shows the hydrograph (plotted as total head versus time) collected on the Wilson River, the initial modified hydrograph for Mineral Creek and the estimated hydrograph used in the model.

The estimated hydrograph was first applied as a transient, total head hydraulic boundary condition in the coupled model. Figure 8.2 illustrates that there was a limited response in the piezometers to precipitation events, and the effects of precipitation were therefore not examined in the analysis. However, this figure also shows that there was a significant porewater pressure response to the flood events recorded in 2013. As discussed in Section 4.3.2., this response is primarily due to an increase in total stress caused by the floodwater on the lower part of the slope. A transient fluid stress boundary condition function was also applied to the coupled model to represent the load applied by the water. The function converts the fluid boundary elevation to a stress based on the unit weight of water.

Figures 8.3a, 8.3b, 8.3c and 8.3d show plots of both the observed and modeled porewater pressure response to the two flood events in 2013 (plotted as total head versus time). There is a notable difference in the initial porewater pressure conditions (conditions prior to flooding) at VW2011-06 (Figure 8.3d). As discussed in Section 4.3.2, this may be due to some local anomaly in the subsurface conditions at this location affecting the measured porewater pressure. As such, the modeled response to flooding at this location is likely not representative and does not compare well with the predicted response (Figure 8.3d). The initial porewater pressure conditions between the observed and modeled data sets for the remaining piezometers compare reasonably well, giving confidence to the calibration of the steady state model.

As expected, there was little response in VW2011-04 (Figure 8.3b), as it is located at a relatively significant distance from the slope. There was a significant response observed in VW2011-01 (Figure 8.3a), and the correlation between the recorded values and modeled values of porewater pressure is reasonable. There is a difference in the peak values of approximately 15 kPa, indicating the model slightly under-predicts the porewater pressure response. This is also evident in the data for VW2011-05 (Figure 8.3c), with differences of between 15 kPa and 20 kPa for the observed and modeled values. The magnitude of the response observed in VW2011-05 is somewhat unexpected, as it is located outside of the flooding limits (installed above the peak floodwater surface elevation). It appears that the B-bar response from the load of the floodwater induced some lateral load (hydrostatic pressure) that was transferred to the installations up slope[15]. This phenomenon was reflected as straining in the up slope direction in the model. The “pulses” in porewater pressure from the two flood events can also been seen in VW2011-06, and even slightly in VW2011-04. The peak porewater pressure measured in

[15] Personal Communication, Lee Barbour, 2013

VW2011-05 suggests that perhaps the laterally induced load has also caused some shearing response to induce pressures of this magnitude. However, this would require additional testing to confirm, and is beyond the scope of this study.

Figure 8.4 illustrates the resultant X-Y direction displacement contours in the modeled slope following the two flood events. The contours show that the most significant displacements occur near the crest and the toe, which is consistent with the observed failed soil mass. Figure 8.5 illustrates that the yield conditions produced by the model occur in the shear zone. The yellow area represents all elements that have yielded. The material in the shear zone is modeled as an elastic plastic material, and yielding occurs according to the Mohr-Coulomb failure criteria detailed in Section 2.2. The yielded material is consistent with the observed failure surface; however, these figures also show that the factor of safety for the observed failure surface is virtually unchanged following the flood events.

Figure 8.6 shows plots of porewater pressure versus time and volumetric strain versus time. The data in these plots is taken from a single node, just above the shear zone, below the crest of the slope. Referring to Figure 8.4 (Node 1), this point is then in a zone of unsaturated soil. Porewater pressure at this location is decreasing with time and suction is increasing. As a result, volumetric compression is occurring (positive volumetric strain), creating the displacement contours at the crest shown in Figure 8.4. Conversely, Figure 8.7 shows the same plots for a node (Node 2) located just above the shear zone, near the toe of the slope (Figure 8.4). This plot shows increases in porewater pressure as flooding occurs. Soils in the unsaturated zone near this node then become saturated. This causes volumetric expansion near the toe, which is reflected as negative volumetric strain in the model and results in the displacement contours at the toe. Figure 8.8 shows that horizontal strains (strains in the x-

direction) measured in the shear zone at mid-slope are positive. Although the magnitude of the modeled strain values are minimal and likely insignificant, the direction indicates that the flood "pulses" induce up-slope strains. Therefore, the outputs from the coupled model do not appear to be representative of any translational down slope displacement that could lead to a landslide or slope failure.

In some instances, coupled stress-porewater pressure analyses may have difficulty coping with the non-linearity of hydraulic functions (Geo-Slope International Ltd., Seep/W, 2010). In particular, difficulty arises when hydraulic functions are relatively steep, as is the case for some of the materials in this model. The sensitivity of the model to these functions was examined; in particular to assess the occurrence of volumetric compression at the crest due to the development of suction prior to any flood "pulses" occurring. The hydraulic functions were replaced with linear functions representing the saturated hydraulic conductivity of each material. Figure 8.9 illustrates that change in porewater pressure and volumetric strain is much less, resulting in significantly less displacement at the crest. However as with the previous analysis, the strains that develop within the failed soil mass do not appear to represent the translational displacement that may be expected in landslides or slope failures.

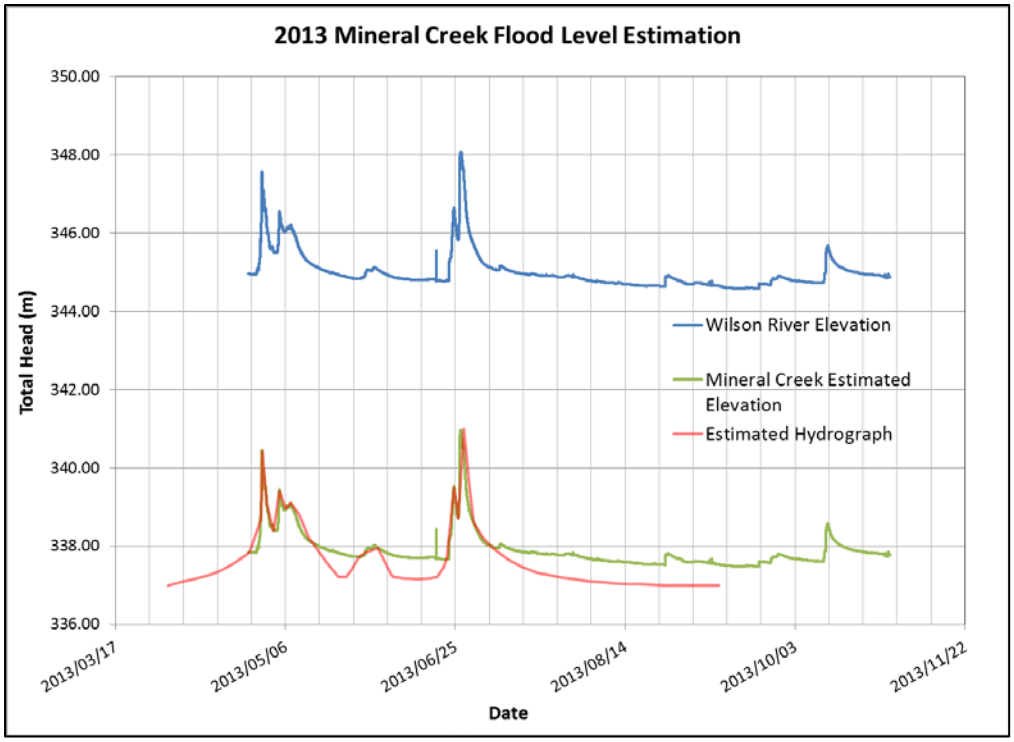

Figure 8.1 – Estimated Hydrograph from Wilson River Flow Data (Environment Canada, Wateroffice, 2013)

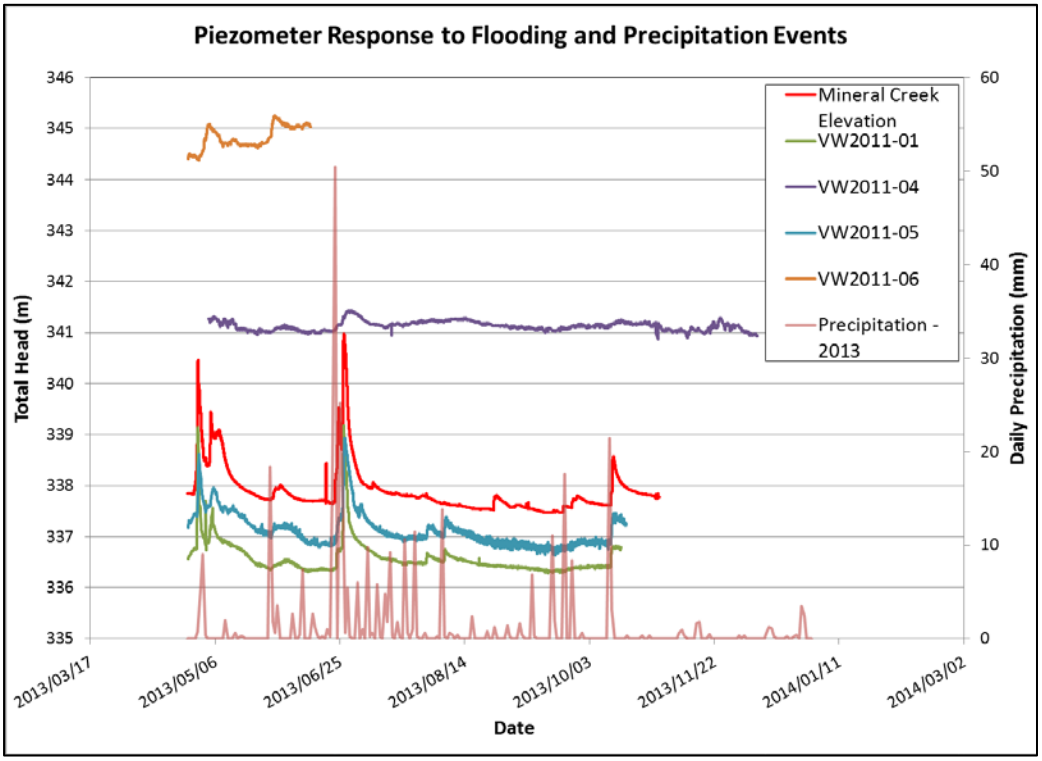

Figure 8.2 – Piezometer Response to Flooding and Precipitation

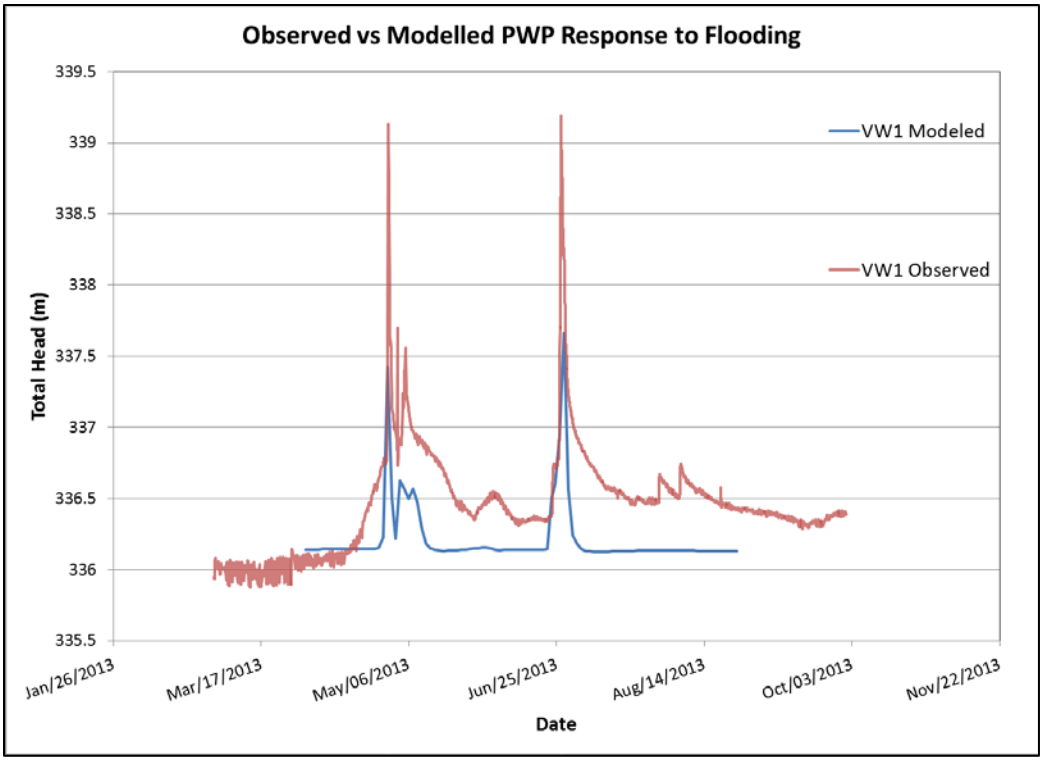

Figure 8.3a – Observed and Modeled Piezometer Response to Flood Events, VW2011-01

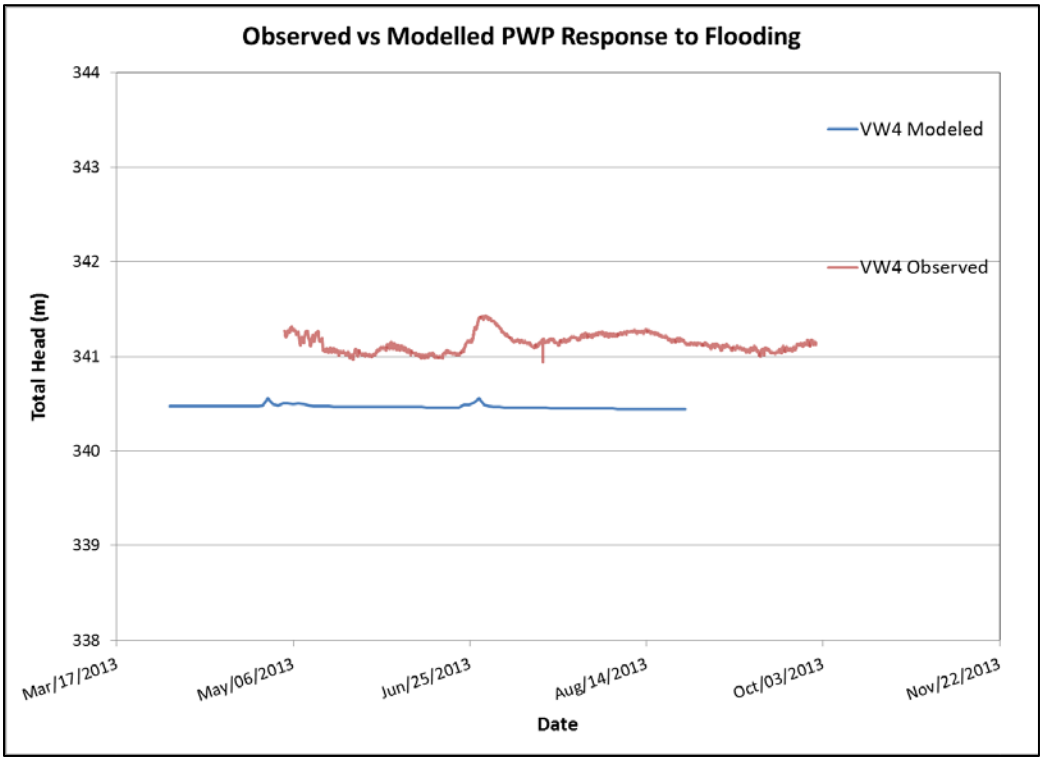

Figure 8.3b – Observed and Modeled Piezometer Response to Flood Events, VW2011-04

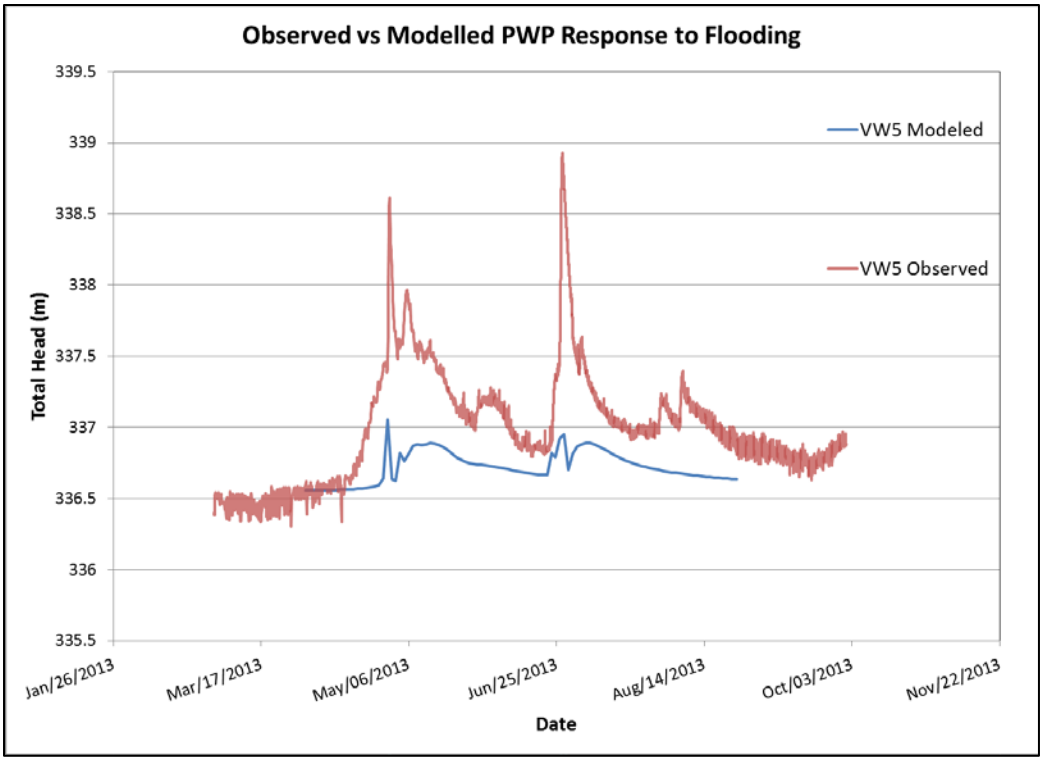

Figure 8.3c – Observed and Modeled Piezometer Response to Flood Events, VW2011-05

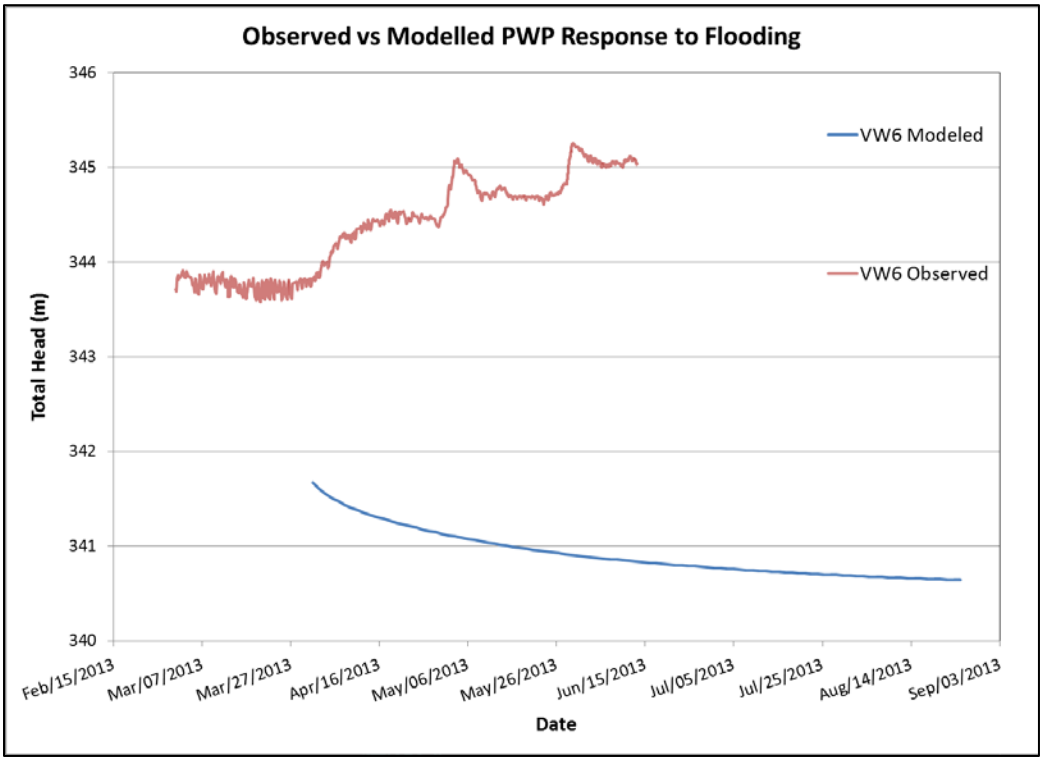

Figure 8.3d – Observed and Modeled Piezometer Response to Flood Events, VW2011-06

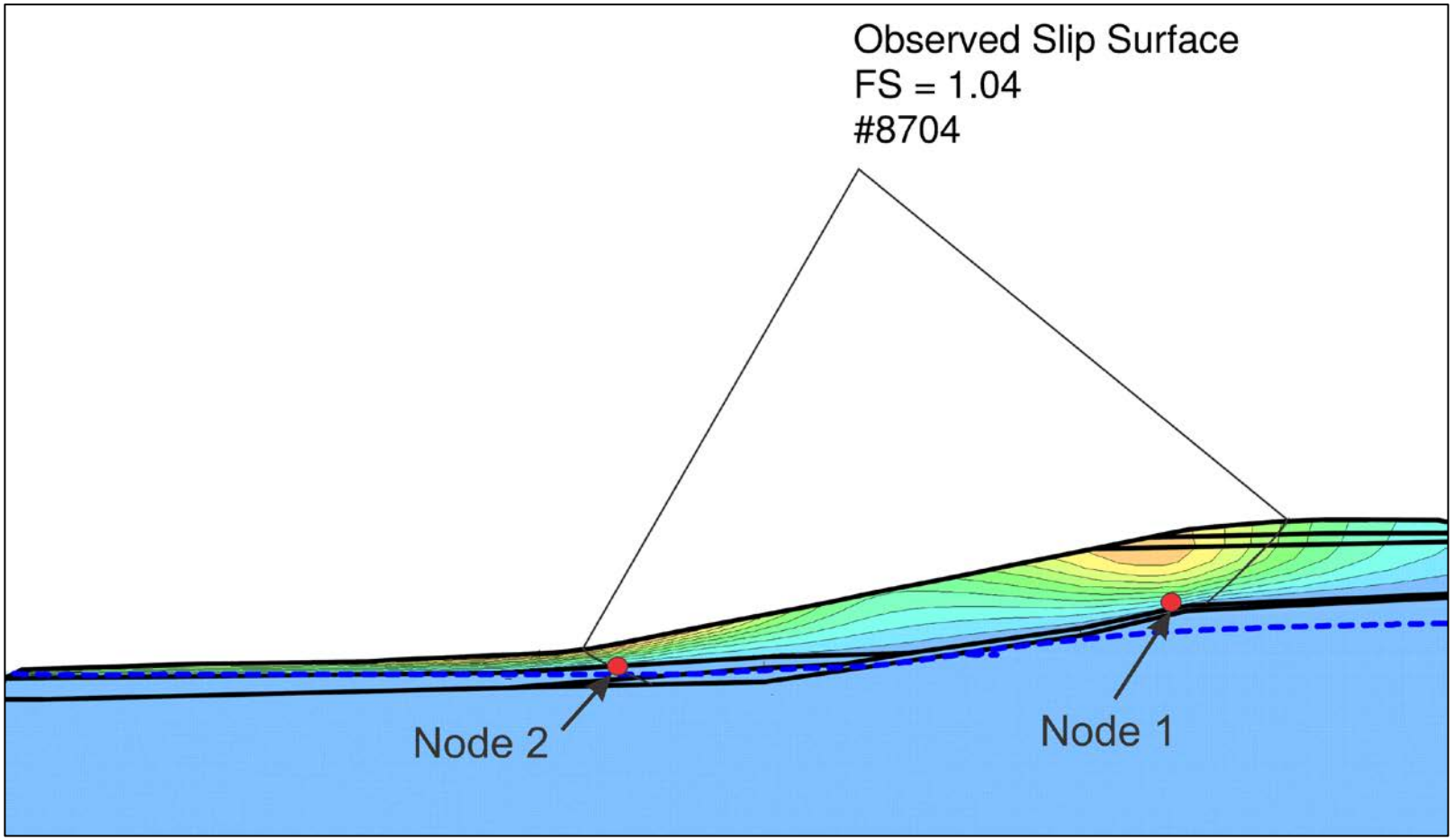

Figure 8.4 – Post-Flooding X-Y Direction Displacement Contours

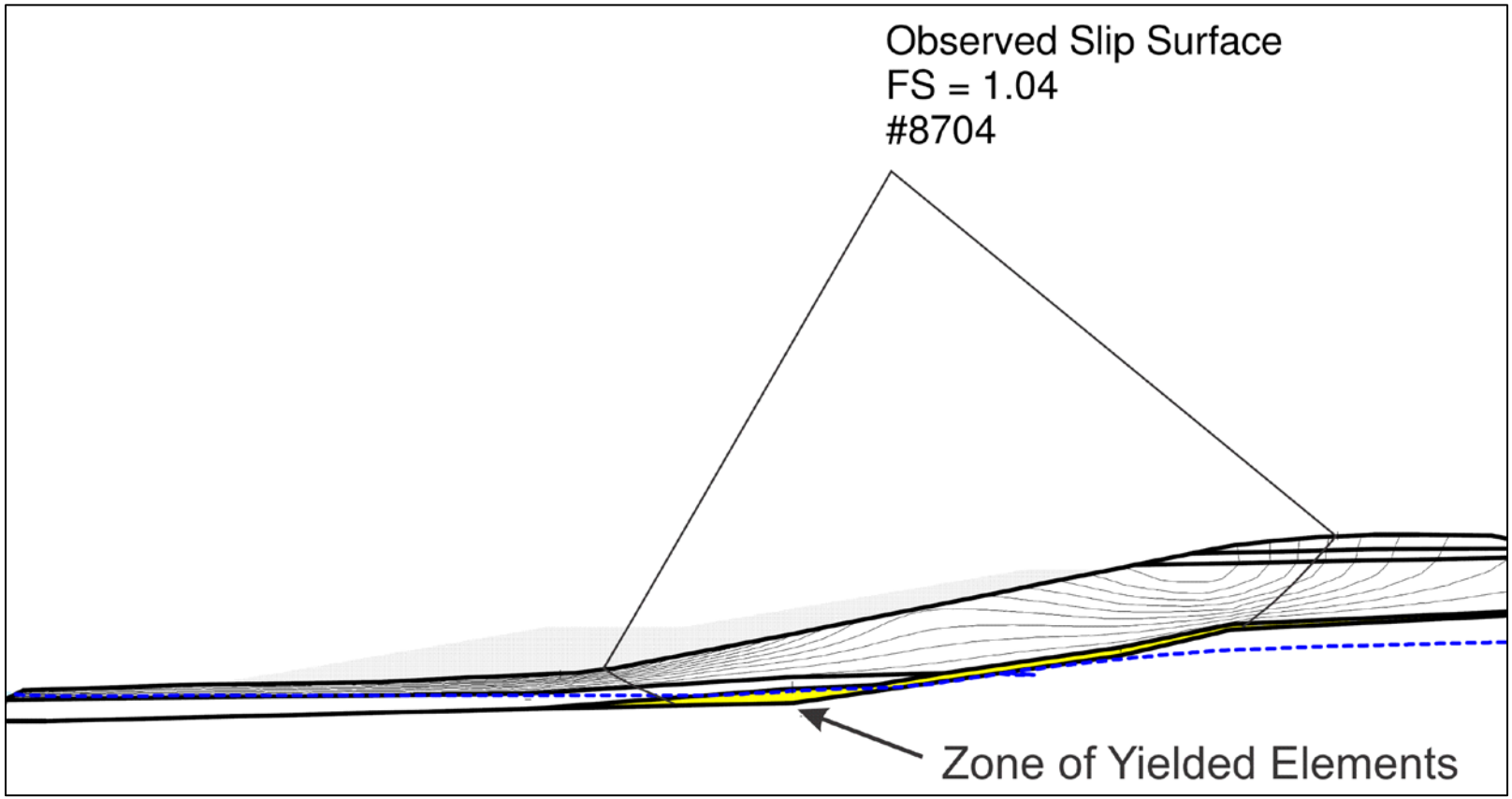

Figure 8.5 – Yielded Elements in Shear Zone

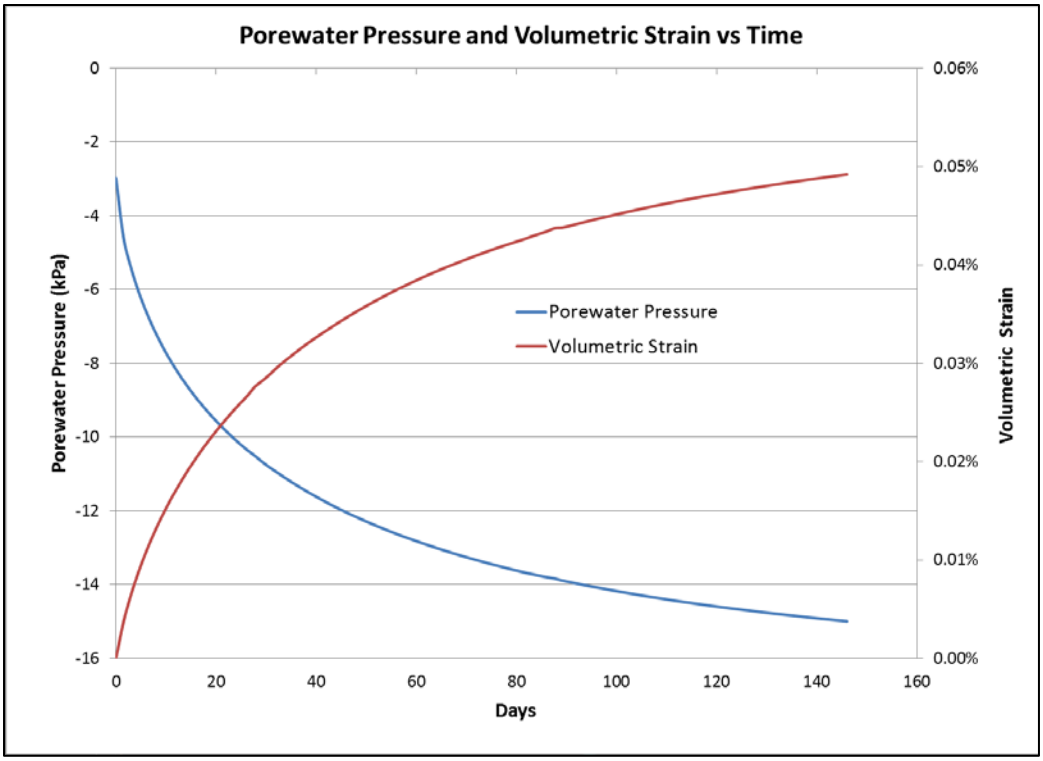

Figure 8.6 – Porewater Pressure and Volumetric Strain vs Time Near Crest

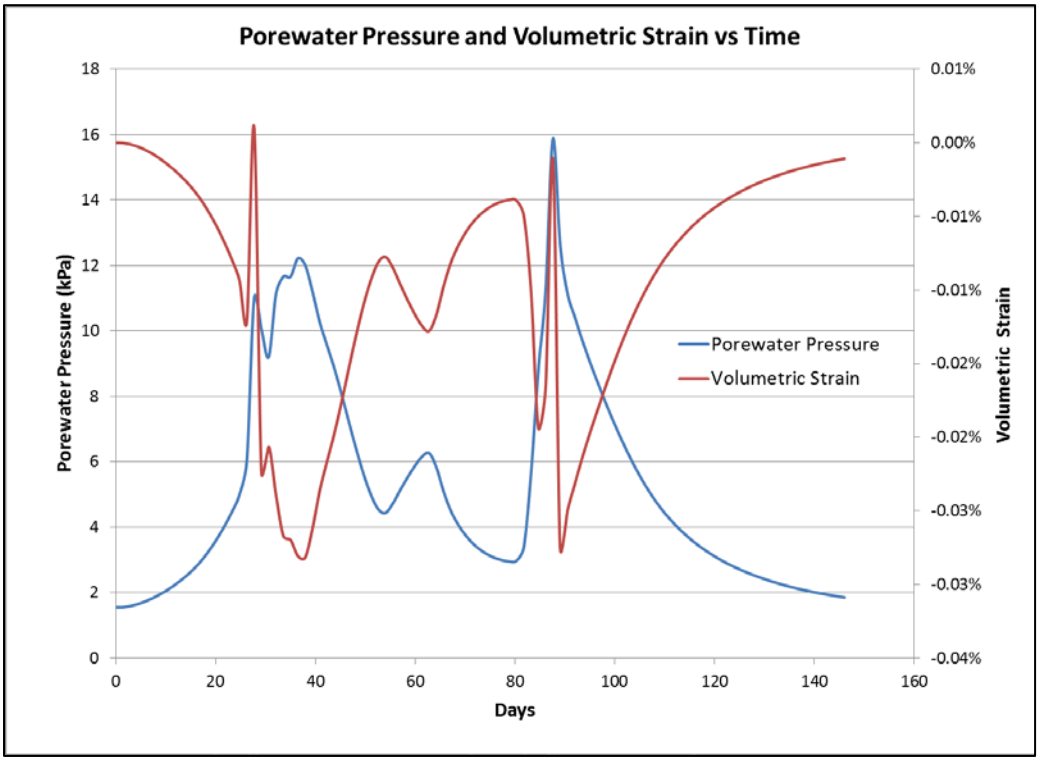

Figure 8.7 – Porewater Pressure and Volumetric Strain vs Time Near Toe

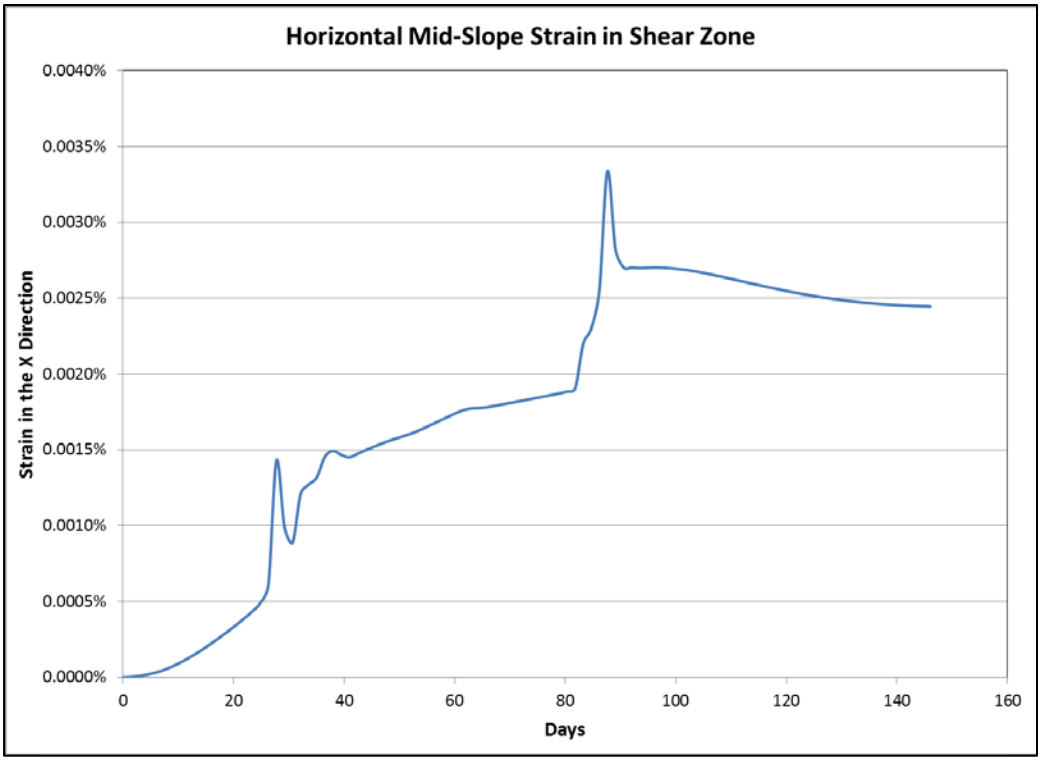

Figure 8.8 – Horizontal (X-Direction) Mid-Slope Strain

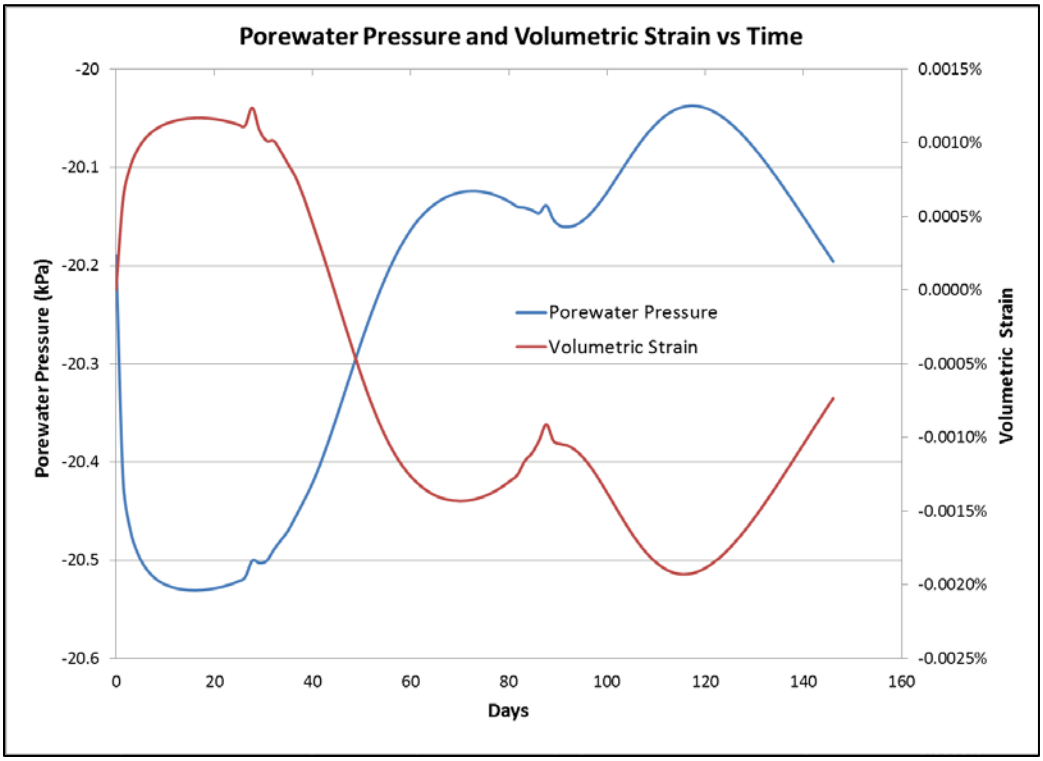

Figure 8.9 – Porewater Pressure and Volumetric Strain vs Time Near Crest, Linear k Function

Chapter 9 – Construction and Post Construction Monitoring

9.1. Berm Construction

This section discusses some aspects of construction that influenced the analysis and design of stabilization measures, but does not detail the construction of the stabilization berm. A series of photographs illustrating the construction methods are shown in Appendix B. Construction of the berm was started in mid-October, 2013. Figure 9.1 shows the design contours used in developing the cross sections used for construction (cross sections shown in Appendix E). Because of the grade of the highway, each bench was to be graded similarly, increasing in elevation from east to west.

Prior to fill placement, the area was cleared and grubbed. Following stripping of any unsuitable materials from the site, the remaining instrumentation was relocated to prevent equipment damage to the instruments during construction. Piezometer VW2011-06 had been severed by slope movements in June, 2013. When relocating the data logger at VW2011-05, it was discovered that this piezometer had also been damaged. Therefore, porewater pressure data was only available from piezometers VW2011-01 and VW2011-04 during construction.

Within hours of clearing the trees from the slope, significant slope movements of up to 450 mm began to occur at the shoulder of PTH 5. This validated concerns with the substantial equipment loads that would have been required if rock fill columns were the selected

stabilization method. Slope movements continued until a significant portion of the stabilization berm had been constructed. Local seepage was observed in the slope face at approximately mid-slope (see photo in Appendix B). Once the lower tier of the berm had been constructed to the design elevation, a trench drain was excavated perpendicular to the highway, and filled with free draining, granular material to control the seepage. After the drain was established, the upper tier of the stabilization berm was completed. Rip rap was placed along the toe of the slope to an elevation of 341.0 m; just above the peak water surface elevation recorded in 2013. The toe of the berm was graded such that runoff would be directed toward the oxbow, preventing ponding at the toe. Construction of the berm and all associated site restoration work was completed in late November, 2013.

9.2. Construction Monitoring Results

Data collected from the remaining piezometers during construction correlates reasonably well with plots generated by the coupled model. Figure 9.2 compares data sets for the observed and modeled piezometer response under embankment loading for VW2011-01 and VW2011-04. As expected, there was a minimal response observed in VW2011-04. The instrument malfunctioned in June, 2014, and no further data was recorded. The plot for VW2011-01 shows that the dissipation observed in this instrument occurred much more rapidly than the model predicted. Dissipation did not occur between load steps in the model, causing the porewater pressure to build up to approximately 12 kPa higher (el. 339.7 m) than what was observed (el. 338.2 m). The model assumes homogeneity in the shale, but it is possible that there are more permeable layers or fractured zones that facilitate a shorter drainage path, and therefore more rapid dissipation of excess porewater pressure, than is captured in the model. Thin layers such

as these could be incorporated in the model as “line regions” (see Section 7.2), but the potential locations and relative hydraulic conductivities would need to be assumed. It is the author’s opinion that the relative agreement between the observed and modeled data sets makes such assumptions unnecessary. Furthermore, the model demonstrates that stability can be maintained with porewater pressures that are higher than what was observed, giving confidence to the effectiveness of the stabilization berm.

9.3. Post-Construction Monitoring Results

As there was limited instrumentation remaining at the site following construction, additional instrumentation was installed in June, 2014. Two additional test holes were drilled along the analyzed cross section (TH2014-07 and TH2014-08), with an additional slope inclinometer and a nest of four vibrating wire piezometers (with data loggers) installed in each hole (see test hole logs in Appendix A). Test hole TH2014-07 was drilled on the upper bench of the berm, and TH2014-08 was drilled on the lower bench. Slope inclinometer plots for SI2014-07 and SI2014-08 (Appendix C) show that no significant displacement occurred post-construction as of the latest reading date (September, 2014). There are some irregular readings recorded in the B-direction for both instruments, however “checksum” plots of the data indicate that these are likely calibration errors in the B-direction for the probe used to collect the data.

The data logger that VW2011-01 and the on-site barometric piezometer were connected to was submerged following flooding in the spring of 2014. The data up to that time was retrieved, but the logger was no longer functional. Therefore, the piezometers in TH2014-07 and TH2014-08 could not be corrected for barometric affects and no measure of Young’s modulus (E) for the

shale could be made to support previous results. As discussed in Section 9.2, VW2011-04 malfunctioned in June, 2014. Figure 9.3 and Figure 9.4 show plots of total head versus time for each instrument installed in TH2014-07 and TH2014-08, respectively.

Table 9.1 and Table 9.2 show both the measured, and modeled, porewater pressure and total head for each instrument installed in test holes TH2014-07 and TH2014-08. Piezometer VW2014-7a is showing negative porewater pressure, as it is located in the unsaturated colluvium. However, positive porewater pressures were recorded at this location. As discussed in Section 9.1, there was a sand drain installed perpendicular to the road near this location, although the exact location was not surveyed in at the time of construction. It is possible that the piezometer is installed in the vicinity of this trench, which may have affected porewater pressure measurements locally that do not accurately reflect the conditions across slope at this depth. The other instruments in test hole TH2014-07 show excellent correlation between measured and modeled values of porewater pressure, giving further confidence to the calibration of hydraulic properties.

Piezometer VW2014-08a is also located in the unsaturated colluvium, and is showing negative porewater pressures that correlate well with modeled values. However, the data recorded from the remaining instruments appears somewhat erratic. Piezometers VW2014-08b and VW2014-08c are showing artesian pressures in the shale; values that are considered unreliable. The measured porewater pressure at VW2014-08c is approximately 30 kPa lower than the model predicted. As the modeled values of porewater pressure at piezometers VW2011-01 and VW2011-05 correlate well with the measured values, and are located immediately down slope and up slope of VW2014-08c, respectively, these measured values are also considered unreliable. It is possible that there is a discrepancy between the piezometers and the

appropriate ports in the data logger (ie. VW2014-8b may be connected to the port for VW2014-8b, etc.), but this could not be verified at the time the data was analyzed.

Table 9.1 – Porewater Pressure and Total Head at TH2014-07

Instrument	Modeled PWP (kPa)	Modeled Total Head (m)	Observed PWP (kPa)	Observed Total Head (m)
VW2014-7a	-21.4	339.6	9.2	342.9
VW2014-7b	2.0	339.0	2.2	339.1
VW2014-7c	63.9	338.9	62.8	339.2
VW2014-7d	117.2	339.0	116.6	338.6

Table 9.2 – Porewater Pressure and Total Head at TH2014-08

Instrument	Modeled PWP (kPa)	Modeled Total Head (m)	Observed PWP (kPa)	Observed Total Head (m)
VW2014-8a	-18.4	337.3	-24.5	336.5
VW2014-8b	16.6	337.2	68.1	342.8
VW2014-8c	50.2	337.6	22.2	334.3
VW2014-8d	153.8	337.9	192.7	342.5

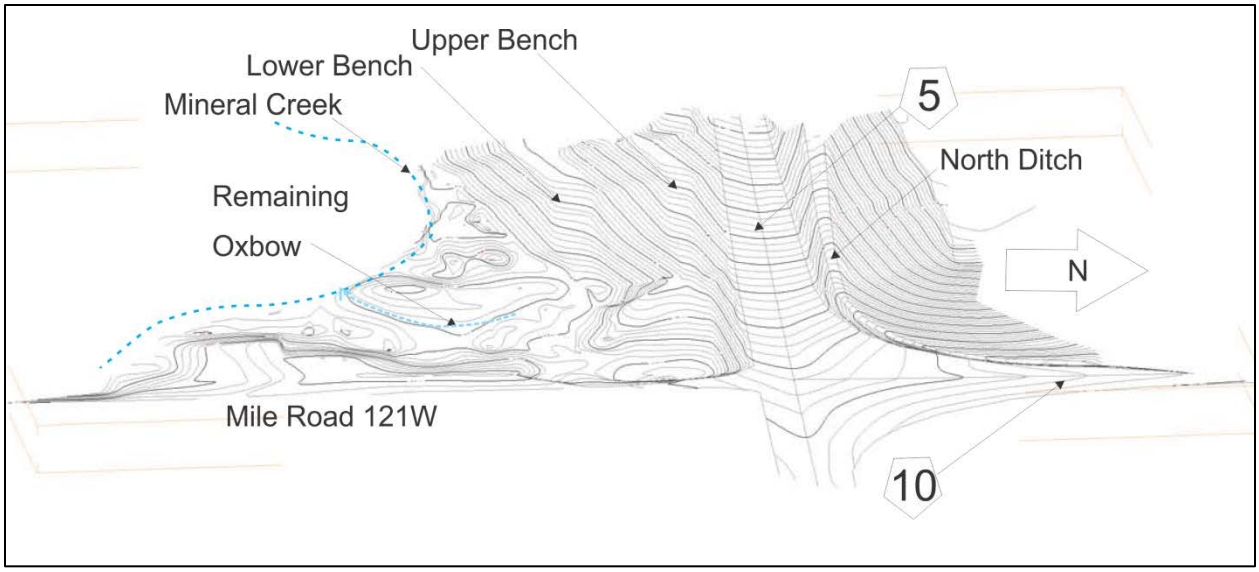

Figure 9.1 – Stabilization Berm Design Contours (East to west)

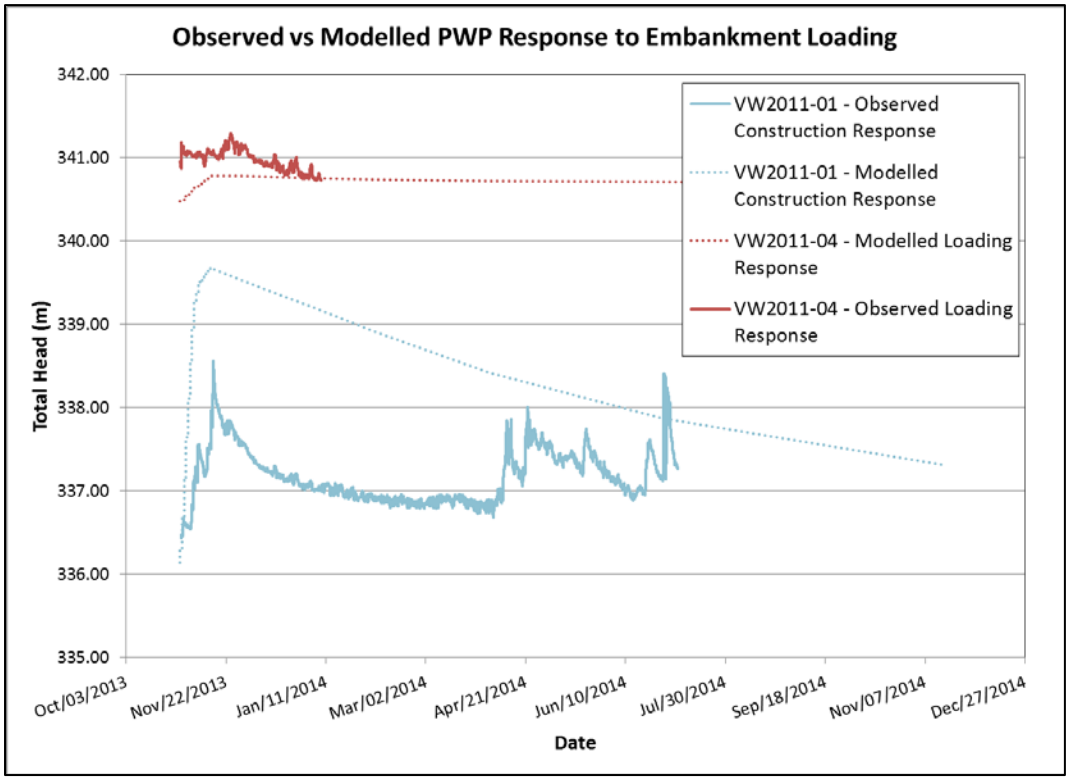

Figure 9.2 – Observed vs Modeled PWP Response to Embankment Loading

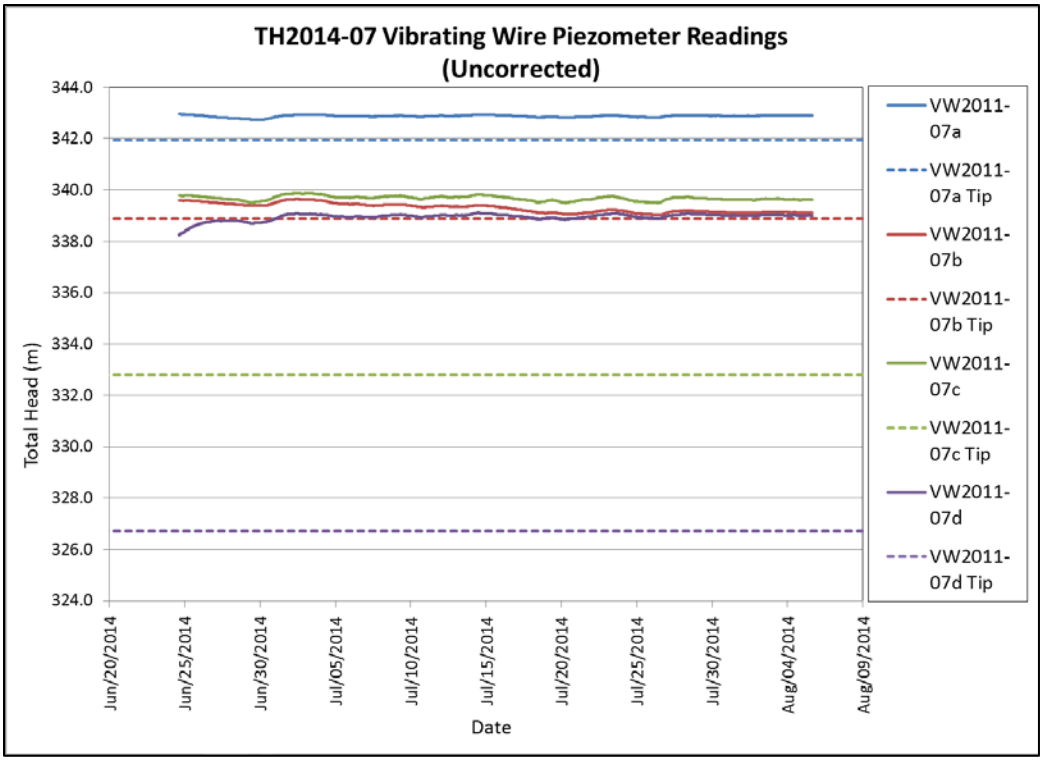

Figure 9.3 – Total Head vs Time for VW2014-07

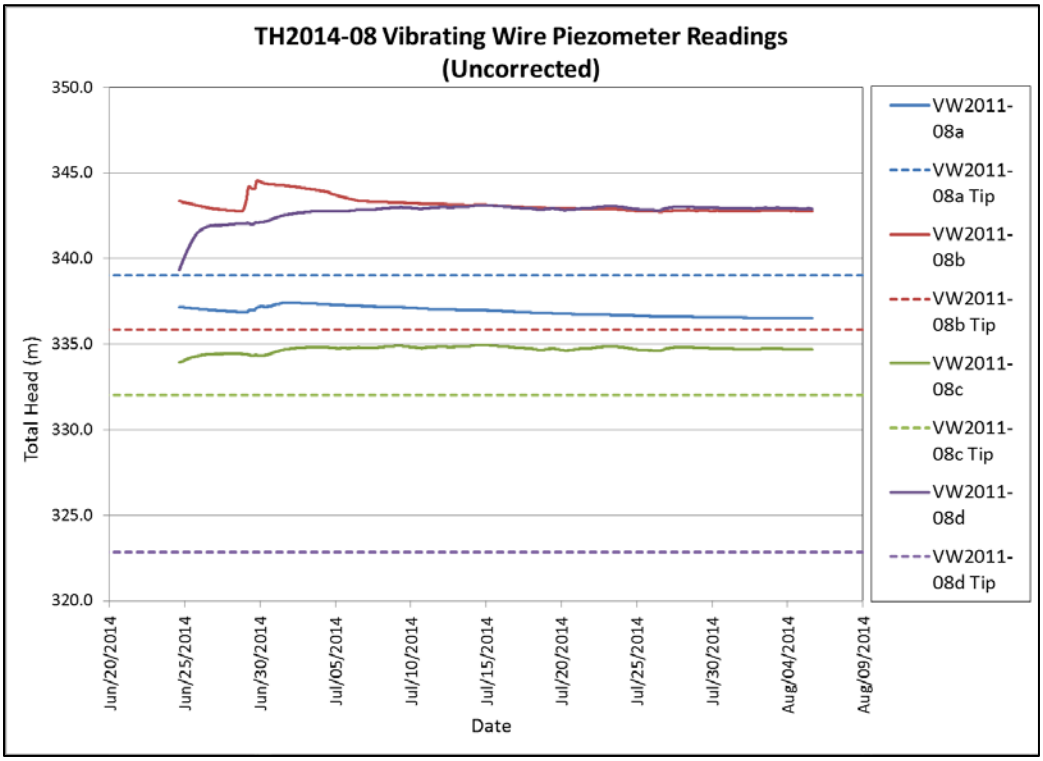

Figure 9.4 – Total Head vs Time for VW2014-08

Chapter 10 – Summary and Conclusions

10.1. Summary

The Ashville Junction slide was analyzed to determine potential failure mechanisms and explore stabilization options for remediation. Multiple site investigations were completed, and monitoring instrumentation was installed to collect porewater pressure and slope displacement data to be used in the analysis. An extensive laboratory and in-situ testing program was completed to assess material properties to be used in numerical modeling of the failure. In particular, torsional ring shear tests were completed to compare the residual shear strength of fine grained soils with back analyzed and direct shear test results; the latter of which is common local practice. Data collected from vibrating wire piezometers installed during the site investigations was interpreted to determine an in-situ measurement Young's modulus for the highly overconsolidated clay shale encountered. To the author's knowledge, this is a new procedure in Manitoba. Using this data, numerical models were used to design stabilization measures and examine the effects of cyclic flash flood events on the stability of the slope. Following construction, the results of modeled loading conditions were compared to values recorded in-situ.

10.2. Limitations

The remoteness of the Ashville Junction meant that data collection for the slope inclinometers could only be completed periodically. Not long after installation, only two sets of readings were taken at SI-2011-02 before the instrument was sheared by slope movements. The analysis of

cyclic flood events as a potential failure mechanism would probably have been made easier with real time displacement data, and the analysis was therefore limited in this regard. Shape Accel Array (SAA) inclinometers can provide displacement data in real time, which would have allowed for better correlation with the available hydrometric, piezometric and precipitation data used in the analysis.

The torsional ring shear tests were the last tests conducted for the study, and time constraints limited the number of tests that could be completed. Early results are promising in terms of the ability of the ring shear test to accurately and quickly determine the residual shear strength of fine grained soils. The results compared better with back analyzed values than results from direct shear tests. However, a larger statistical sample size would likely be required to validate the test as a viable replacement for the more common direct shear test.

For many geotechnical projects, the extent of laboratory testing is often limited by budget or time constraints, and material availability. For this study, the materials tested were often difficult to trim, which limited the number of specimens available for oedometer tests and direct shear tests. Furthermore, budget constraints limited the number of test holes that could be drilled to obtain samples.

10.3. Conclusions

The site of the Ashville Junction slide is one of relatively complex geology and porewater pressure conditions, with variable seasonal surface water conditions that add further complexity to a numerical analysis. The material that comprises the surface stratum at the site is a highly

heterogeneous soil deposit that contains many voids due to roots and boulders left following glaciation. Modeling the effect of such abnormalities is very difficult, as they may influence such material properties as hydraulic conductivity, water storage, soil saturation, and likely consolidation. Additionally, it became apparent during construction of the stabilization berm that the stability of the slope failure at limiting equilibrium depended highly on the vegetation for shear strength; a phenomenon that is very difficult to model and quantify.

The measure of Young's modulus determined for the clay shale is in relative agreement with values as determined in the literature. It was anticipated that this value could be validated by interpreting the data from the instruments installed post-construction, but as discussed in Chapter 9, the logger collecting local barometric data was damaged following flooding. Where feasible, any future work that may be done using the elastic theory and barometric correction to obtain Young's modulus should attempt to obtain laboratory measured values of this parameter for comparison. In the study of this site, the model was not particularly sensitive to Young's modulus, provided the value remained within generally acceptable limits. A sensitivity analysis showed that lowering the value from 388,000 kPa to 100,000 kPa had a very minimal effect on consolidation and the associated plots of excess porewater pressure.

Conversely, calibration of the steady state seepage model showed that the model was sensitive to selected values of hydraulic conductivity and the ratio of horizontal to vertical hydraulic conductivity. There is good agreement between the modeled and observed values of porewater pressure, both at steady state and following the dissipation of excess porewater pressure after loading. Having in situ measurements of the horizontal hydraulic gradient and hydraulic conductivity could provide an excellent basis for comparison.

Finite element analysis has proven to be a very useful tool in the analysis of geotechnical problems. There are, however, limits to the kind of information a numerical model can provide for a given problem. Given the relative complexity of the site, and the many variables that may have contributed to the instabilities observed, the model could not definitively demonstrate the hypothesized failure mechanism. The discrepancy between the observed and modeled porewater pressure response to flood events, particularly for VW2011-01 and VW2011-05, may be attributed to an underestimate of the function used to model the flood events. It is possible that Mineral Creek crested prior to obtaining a geodetic elevation of the high water level. In spite of the model's inability to confirm the suspected failure mechanism due to these flood events, results did compare well with porewater pressure measurements recorded during construction of the stabilization berm.

The factor of safety (1.77) produced by the model for the stabilized slope is admittedly conservative. This conservatism is the reflection of a design process that evolved over time, and involved improving geometry, obtaining reliable measurements of material properties and re-calibration of the numerical model as more data became available. These processes continued, even after construction began. Early models of the Ashville Junction Slide produced a factor of safety much closer to the target value of 1.5.

An example of the geometry used in an early analysis of the failure was shown in Figure 6.1. In this figure, the shear zone extends the full length of the model. The rationale behind this is that although SI2011-01 did not show any displacement during data collection, there was still some uncertainty with respect to the original geometry of the slope. If slope movements had occurred in the past, it is possible that the failure may have previously extended further down slope, reducing those soils to residual strength. Also of note in this figure is the absence of the

alluvium. Although a small layer of silty sand had been observed in TH2011-05, it was uncertain if the layer was continuous and extended toward Mineral Creek. It was not until the instruments were relocated once construction had started that the alluvium was confirmed as a continuous layer. Hand augered holes were drilled near the toe of the berm to install the mounting post for the data logger. These holes confirmed shallow alluvium comprised of sands and gravels, with groundwater approximately 300mm below existing ground level. The addition of this layer to the model facilitated better drainage, and therefore faster dissipation of excess porewater pressure. Furthermore, it replaced the assumed low strength shear zone with a higher strength material. The evolution of the model over the duration of this study is an excellent example of how having a complete set of quality geotechnical data for a particular project can help minimize conservatism due to risk and the associated cost of the project.

References

Anochikwa, C.I., van der Kamp, G., Barbour, S.L. 2012. Interpreting pore-water pressure changes induced by water table fluctuations and mechanical loading due to soil moisture changes. Canadian Geotechnical Journal **49**: pp. 357-366.

Aubertin, M., Mbonimpa, M., Bussiere, B., Chapuis, R.P. 2003. A model to predict the water retention curve from basic geotechnical properties. Canadian Geotechnical Journal **40**: pp. 1104-1122.

Bamburak, J.D., Christopher, J.E. 2004. Mesozoic Stratigraphy of the Manitoba Escarpment. Manitoba Geological Survey, Saskatchewan Geological Survey.

Blatz, J.A., Ferreira, N.J., and Graham, J. 2004. Effects of near-surface environmental conditions on instability of an unsaturated soil slope. Canadian Geotechnical Journal **41**: pp. 1111-1126.

Budhu, M. 2007. Soil Mechanics and Foundations. 2nd Ed. John Wiley & Sons Inc. Hoboken, N.J.

Craig, R.F. 2004. Craig's Soil Mechanics. 7th ed. Spoon Press. New York.

Environment Canada. Climate (Precipitation Data, 2013). http://climate.weather.gc.ca.

Environment Canada. Wateroffice (Historical Hydrometric Data Search, 2013). http://www.wsc.ec.gc.ca.

Fredlund, D.G., Krahn, J. 1977. Comparison of slope stability methods of analysis. Canadian Geotechnical Journal **14**: pp. 429-439.

Fredlund, D.G., Morgenstern, N.R. 1977. Stress State Variables for Unsaturated Soils. ASCE **103**: pp. 447-464.

Fredlund, D.G., Xing, A. 1994. Equations for the soil-water characteristic curve. Canadian Geotechnical Journal **31**: pp. 521-532.

Freeze, R. A., Cheery, J. A. 1979. Groundwater. Prentice-Hall Inc. Englewood Cliffs, N.J.

Geo-Slope International Ltd. 2010. Seepage Modeling with Seep/W: An engineering methodology. 4th ed.

Geo-Slope International Ltd. 2010. Stability Modeling with Slope/W: An engineering methodology. 4th ed.

Geo-Slope International Ltd. 2010. Stress-Deformation Modeling with Sigma/W: An engineering methodology. 4th ed.

Graham, J., Houlsby, G.L. 1983. Anisotropic elasticity of a natural clay. Geotechnique **33**: pp. 165-180.

Graham, J. 1984 Methods of stability analysis. Chapter 6 in "Slope Instability", Ed. D.Brunsden and D.B.Prior, Wiley Interscience, London, pp.171-215.

Graham, J., Crooks, J.H.A., Lau, S.L.K. 1988. Yield envelopes: identification and geometric properties. Geotechnique **38**: pp. 125-134.

Graham, J. 2006. The 2003 R. M. Hardy Lecture: Soil parameters for numerical analysis in clay. Canadian Geotechnical Journal **43**: pp. 187-2009.

Josh, M., Esteban, L., Delle Piane, C., Sarout, J., Dewhurst, D.N., Clennell, M.B. 2012. Laboratory characterization of shale properties. Journal of Petroleum Science and Engineering **88-89**: pp. 107-124.

Keller, C.K., van der Kamp, G., Cherry, J.A. 1989. A Multiscale Study of the Permeability of a Thick Clayey Till. Water Resources Research **25**: pp. 2299-2317.

Kelly, A.J., Sauer, E.K., Christiansen, E.A., Barbour, S.L. 1995. Deformation of the deer creek bridge by an active landslide in clay shale. Canadian Geotechnical Journal **32**: pp. 701-724.

Klassen, R.W. 1979. Pleistocene Geology and Geomorphology of the Riding Mountain and Duck Mountain Areas, Manitoba-Saskatchewan. Geological Survey of Canada. Memoir **396**.

Krahn, J. 2003. The 2001 R.M. Hardy Lecture: The limits of limit equilibrium analyses. Canadian Geotechnical Journal **40**: pp. 643-660.

Manitoba Water Stewardship. 2011. Dauphin Lake Integrated Watershed Management Plan: Surface Water Hydrology Report. Government of Manitoba.

Matile, G.L.D., Keller, G.R. 2004. Surficial Geology Compilation Map Series: SG-62N. Manitoba Industry, Economic Development and Mines. Manitoba Geological Survey.

Matile, G.L.D., Keller, G.R. 2007. Surficial Geology of Manitoba, Surficial Geology Compilation Map Series: SG-MB. Manitoba Science, Technology, Energy and Mines.

Matile, G.L.D., Keller, G.R. 2012. Subsurface Phanerozoic geology of southern Manitoba, Transect 49 (5670870N). Manitoba Innovation, Energy and Mines, Manitoba Geological Survey, Stratigraphic Map SM2012-1.

Matile, G. and Keller, G. 2013. Sand & Gravel Deposits along the Assiniboine Spillway: Sand and Gravel Deposits Image 1; Manitoba Geological Survey. http://www.manitoba.ca/iem/mrd/geo/demsm/sandgravel1.html

Manitoba Infrastructure and Transportation. 2013. Shell River Slide Field Program Report. Internal Document. Materials Engineering Branch.

McNeil, D.H. 1977: The Cretaceous System in the Manitoba Escarpment; Ph.D. thesis, University of Saskatchewan.

Moe, K.W.S., Cruden, D.M., Martin, C.D., and Lewycky, D. 2009. Mechanisms and kinematics of three translational slides along the North Saskatchewan River Valley, Edmonton. Proc. Canadian Geotechnical Society Conference, Halifax. pp. 390-397.

Mogenstern, N. Price, V.E. 1965. The analysis of the stability of generalized slip surfaces. Geotechnique **15**: pp. 79-93.

Neuzil, C. E. 1994. How permeable are clays and shales? Water Resource Research. **30, 2**: pp. 145-150. American Geophysical Union.

Pliakas, F., Petalas, C. 2011. Determination of hydraulic conductivity of unconsolidated river alluvium from permeameter tests, empirical formulas and statistical parameters effect analysis. Water Resource Manage **25**: pp. 2877-2899.

Sauer, E.K. 1983. The Denholm landslide, Saskatchewan. Part II: analysis. Canadian Geotechnical Journal **20**: pp. 208-220.

Sauer, E.K., Christiansen, E.A. 1987. The Denholm landslide, Saskatchewan, Canada, an update. Canadian Geotechnical Journal **24**: pp. 163-168.

Skempton, A. W. 1964. Long-term stability of clay slopes. Geotechnique **14**: pp. 77-102.

Stark, T.D., Eid, H.T. 1994. Drained residual strength of cohesive soils. Journal of Geotechnical Engineering **120, 5**: pp. 856-871.

Stark, T.D. Vettel, J.J. 1992. Bromhead ring shear test procedure. Geotechnical Testing Journal **15**: pp. 24-32. American Society for Testing and Materials. Philadelphia, PA.

Terzaghi, K., Peck, R.B., Mesri, G. 1996. Soil mechanics in engineering practice, 3rd ed., John Wiley and Sons, Inc., New York.

Thiessen, K.J., Alfaro, M.C. and Blatz, J.A. 2011. Measuring the load-deformation response of rockfill columns by a full-scale field test on a natural riverbank. Canadian Geotechnical Journal **48**: 1032-1043.

Turner, A.K., Schuster, R.L. (Transportation Research Board, National Research Council). 1996. Landslides: Investigation and Mitigation. National Academy Press. Washington, D.C.

Tutkaluk, J., Blatz, J., Graham, J. and Wingrove, T. 2002. A generic study of the influence of a confined aquifer on slope stability in lacustrine clay slopes. Proc. 55th Canadian Geotechnical Conference, Niagara Falls ON, October 2002. pp. 1185-1190.

United States Department of Agriculture, Forest Service. 1994. Application guide for launched soil nails. Vol. **1**.

Van Genuchten, M. Th. 1980. A closed-form equation for predicting the hydraulic conductivity of unsaturated soils. Soil Science Society of America Journal **44**: 892-898.

Wood, D.M. 1990. Soil Behaviour and Critical State Soil Mechanics. Cambridge University Press. Cambridge.

Wykeham Farrance International. WF25850 Bromhead Ring Shear (User Manual). Berks, England. Date Unknown.

Appendix A – Test Hole Logs

PROJECT: PTH 5 & 10 Grade Slope Failure	CLIENT: Region 4	TESTHOLE NO: **SI/VW-2011-01**
UTM: 5667874.839m N 409067.838m E		PROJECT NO.: 2010-4G
CONTRACTOR: Paddock Drilling Ltd	METHOD: 170mm HSA	ELEVATION (m): 338.978

SAMPLE TYPE: GRAB | SHELBY TUBE | SPLIT SPOON | BULK | NO RECOVERY | CORE

BACKFILL TYPE: GROUT | GRAVEL | SLOUGH | BENTONITE | CUTTINGS | SAND

DEPTH (m)	SOIL DESCRIPTION	SAMPLE TYPE	SAMPLE #	SPT (N)	COMMENTS	ELEVATION (m)
0	CLAY and SILT - some organics -dark brown, moist, soft -organic odour					
1	CLAY (alluvium) - silty, sandy, trace organics (rootlets) -grey with brown lenses, moist to wet, soft -intermediate plastic		B1			338
2	Below ~1.7m: trace to some gravel -dark grey, moist, firm, high plastic -minor seepage observed at ~ 1.8m Sample B2: Gravel - 2%, Sand - 21%, Silt - 22%, Clay - 55%		B2			337
3	CLAY SHALE - some silt, trace silt lenses -dark grey, moist, stiff -high plastic, blocky structure		T3			336
4	- trace silt, very stiff to hard		B4			335
5	-occasional silt and fine sand lenses between ~4.9m and 6.1m		S5	60		334
6			B6			333
7			T7			332
8			S8	72		331
9			T9			330
10			B10			329
11			S11	81		328
12	dry, hard silty shale encountered at ~ 12.2m to end of hole		T12			327
13						326
14			S13	202		325
15						

QU (Su) (kPa) 50 100 150 200 | Total Unit Wt (kN/m³) 17 19 21 23 | SPT (Standard Pen Test) (Blows/300mm) 20 40 60 80 | PLASTIC M.C. LIQUID 20 40 60 80

LOG OF TESTHOLE REVISED (OLD) PTH 5 ASHVILLE JUNCTION TEST HOLE LOGS 2013-12-20.GPJ MIT.GDT 14-8-28

Manitoba

LOGGED BY: Ken Kalynuk	COMPLETION DEPTH: 18.29 m
REVIEWED BY: J. Fiebelkorn	COMPLETION DATE: 11-6-8
PROJECT ENGINEER: Jeremy Fiebelkorn	Page 1 of 2

PROJECT: PTH 5 & 10 Grade Slope Failure	CLIENT: Region 4	TESTHOLE NO: **SI/VW-2011-01**
UTM: 5667874.839m N 409067.838m E		PROJECT NO.: 2010-4G
CONTRACTOR: Paddock Drilling Ltd	METHOD: 170mm HSA	ELEVATION (m): 338.978

SAMPLE TYPE: GRAB | SHELBY TUBE | SPLIT SPOON | BULK | NO RECOVERY | CORE

BACKFILL TYPE: GROUT | GRAVEL | SLOUGH | BENTONITE | CUTTINGS | SAND

DEPTH (m)	SLOPE INCLINOMETER / VW PIEZOMETER	SOIL SYMBOL	SOIL DESCRIPTION	SAMPLE TYPE	SAMPLE #	SPT (N)	QU (Su) (kPa) 50 100 150 200 / Total Unit Wt (kN/m³) 17 19 21 23 / SPT (Standard Pen Test) (Blows/300mm) 20 40 60 80 / PLASTIC M.C. LIQUID 20 40 60 80	COMMENTS	ELEVATION (m)
15			SPT 14 - Refusal after 300mm		S14	90/ 150mm	>>		
16									323
17					S15	110/ 150mm	→		322
18					B16				321
19			END HOLE AT 18.3m IN CLAY SHALE						320
20			Notes: 1. Seepage observed at various depths, hole wet upon completion; 2. No sloughing observed; 3. SI-2011-01 installed to 18.3m below existing ground level (el. 320.7m) -approximately 40 gallons grout used -above ground steel casing installed 4. VW-2011-01 installed to 17.4m below existing ground level (el. 321.6m at tip)						319
21									318
22									317
23									316
24									315
25									314
26									313
27									312
28									311
29									310
30									

LOG OF TESTHOLE REVISED (OLD) PTH 5 ASHVILLE JUNCTION TEST HOLE LOGS 2013-12-20.GPJ MIT.GDT 14-8-28

Manitoba

LOGGED BY: Ken Kalynuk	COMPLETION DEPTH: 18.29 m
REVIEWED BY: J. Fiebelkorn	COMPLETION DATE: 11-6-8
PROJECT ENGINEER: Jeremy Fiebelkorn	Page 2 of 2

PROJECT: PTH 5 & 10 Grade Slope Failure	CLIENT: Region 4	TESTHOLE NO: **SI/VW-2011-02**
UTM: 5667916.01m N 409065.335m E		PROJECT NO.: 2010-4G
CONTRACTOR: Paddock Drilling Ltd	METHOD: 170mm HSA	ELEVATION (m): 345.897

SAMPLE TYPE: GRAB | SHELBY TUBE | SPLIT SPOON | BULK | NO RECOVERY | CORE

BACKFILL TYPE: GROUT | GRAVEL | SLOUGH | BENTONITE | CUTTINGS | SAND

DEPTH (m)	SOIL DESCRIPTION	SAMPLE TYPE	SAMPLE #	SPT (N)	ELEVATION (m)
0	CLAY (fill) - some silt, some organics, trace sand, trace gravel -brown, moist, firm -intermediate to high plastic				345
1			B17		
	CLAY (till-like) - some silt, some sand -brown, moist, firm to stiff -high plastic		B18		
2	Sample B18: Gravel - 2%, Sand - 30%, Silt - 23%, Clay - 45%		B19		344
3	-trace gravel, trace silt lenses		T20		343
4			B21		342
5	Sample T22: Gravel - 5%, Sand - 22%, Silt - 20%, Clay - 53%		T22		341
	CLAY SHALE - silty -dark grey/black, hard -high plastic		B23		
6	-light grey colour observed at ~5.3m (bentonite)		S24	29	340
7	-dark grey/black colour below ~6.7m		B25		339
8			S26	86	338
9			S27	50	337
10					336
11			S28	69	335
12					334
13			S29	60	333
14			S30	87	332
15					331

SLOPE INCLINOMETER | VW PIEZOMETER | SOIL SYMBOL

■ Total Unit Wt ■ (kN/m³) 17 19 21 23

◆ SPT (Standard Pen Test) ◆ (Blows/300mm) 20 40 60 80

PLASTIC M.C. LIQUID 20 40 60 80

× QU (Su) × (kPa) 50 100 150 200

△ Pocket Pen. (Su) △ (kPa) 50 100 150 200

COMMENTS

121

LOG OF TESTHOLE REVISED (OLD) PTH 5 ASHVILLE JUNCTION TEST HOLE LOGS 2013-12-20.GPJ MIT.GDT 14-8-28

Manitoba

LOGGED BY: Ken Kalynuk	COMPLETION DEPTH: 18.29 m
REVIEWED BY: J. Fiebelkorn	COMPLETION DATE: 11-6-9
PROJECT ENGINEER: Jeremy Fiebelkorn	Page 1 of 2

PROJECT: PTH 5 & 10 Grade Slope Failure	CLIENT: Region 4	TESTHOLE NO: **SI/VW-2011-02**
UTM: 5667916.01m N 409065.335m E		PROJECT NO.: 2010-4G
CONTRACTOR: Paddock Drilling Ltd	METHOD: 170mm HSA	ELEVATION (m): 345.897

SAMPLE TYPE: GRAB | SHELBY TUBE | SPLIT SPOON | BULK | NO RECOVERY | CORE

BACKFILL TYPE: GROUT | GRAVEL | SLOUGH | BENTONITE | CUTTINGS | SAND

DEPTH (m)	SLOPE INCLINOMETER / VW PIEZOMETER	SOIL SYMBOL	SOIL DESCRIPTION	SAMPLE TYPE	SAMPLE #	SPT (N)	Total Unit Wt (kN/m³) 17 19 21 23 / SPT (Standard Pen Test) (Blows/300mm) 20 40 60 80 / PLASTIC M.C. LIQUID 20 40 60 80	QU (Su) (kPa) 50 100 150 200 / Pocket Pen. (Su) (kPa) 50 100 150 200	COMMENTS	ELEVATION (m)
15										
16										330
17					S31	98				329
18					S32	127				328
19					B33					327
20										326
21										325
22										324
23										323
24										322
25										321
26										320
27										319
28										318
29										317
30										316

END HOLE AT 18.3m IN CLAY SHALE

Notes:
1. No sloughing observed;
2. Seepage observed, hole wet upon completion (uncertain of seepage location);
3. SI-2011-02 installed to 18.3m below existing ground level (el. 327.6m);
-approximately 40 gallons of grout used
-above ground steel casing installed
4. VW-2011-02 installed to 9.75m below existing ground level (el. 336.2m at tip);
5. SP-2011-03 installed ~2m east of SI/VW-2011-02.

Manitoba

LOGGED BY: Ken Kalynuk	COMPLETION DEPTH: 18.29 m
REVIEWED BY: J. Fiebelkorn	COMPLETION DATE: 11-6-9
PROJECT ENGINEER: Jeremy Fiebelkorn	Page 2 of 2

LOG OF TESTHOLE REVISED (OLD) PTH 5 ASHVILLE JUNCTION TEST HOLE LOGS 2013-12-20.GPJ MIT.GDT 14-8-28

PROJECT: PTH 5 & 10 Grade Slope Failure	CLIENT: Region 4	TESTHOLE NO: **VW2011-04**
UTM: 5667953.169m N 409060.962m E		PROJECT NO.: 2010-4G
CONTRACTOR: Paddock Drilling Ltd	METHOD: 170mm HSA	ELEVATION (m): 346.518

SAMPLE TYPE: GRAB | SHELBY TUBE | SPLIT SPOON | BULK | NO RECOVERY | CORE

BACKFILL TYPE: GROUT | GRAVEL | SLOUGH | BENTONITE | CUTTINGS | SAND

DEPTH (m)	SOIL DESCRIPTION	SAMPLE TYPE	SAMPLE #	SPT (N)	COMMENTS	ELEVATION (m)
0	CLAY (till-like) - some silt to silty, trace to some sand, trace gravel -brown, moist, stiff -high plastic					346
1			B34			345
2			B35			344
3	Sample T36: Gravel - 1%, Sand - 19%, Silt - 27%, Clay - 53%		T36			343
4	CLAY SHALE - silty -dark grey, dry to moist, stiff -blocky structure -silty, light grey colour to ~4.4m (bentonite) Sample B37: Gravel - 0%, Sand - 2%, Silt 18%, Clay - 80%		B37		127	342
5			T38			
	-hard below ~5.2m		B39			341
6			S40	39		
7	-some silt lenses -dry		B41			340
	-light grey colour observed at ~7.5m (bentonite)		B42		185	339
8			B43			
	END HOLE AT 8.1m IN CLAY SHALE					338
9	Notes: 1. No seepage observed; 2. No sloughing observed; 3. VW-2011-04 installed to 7.92m below existing ground level (el. 338.6m at tip)					337
10						336
11						335
12						334
13						333
14						332
15						

△ Pocket Pen. (Su) △ (kPa) 50 100 150 200

◆ SPT (Standard Pen Test) ◆ (Blows/300mm) 20 40 60 80

PLASTIC M.C. LIQUID 20 40 60 80

Manitoba

LOGGED BY: Ken Kalynuk	COMPLETION DEPTH: 8.08 m
REVIEWED BY: J. Fiebelkorn	COMPLETION DATE: 11-6-9
PROJECT ENGINEER: Jeremy Fiebelkorn	Page 1 of 1

LOG OF TESTHOLE REVISED (OLD) PTH 5 ASHVILLE JUNCTION TEST HOLE LOGS 2013-12-20.GPJ MIT.GDT 14-8-28

PROJECT: PTH 5 & 10 Grade Slope Failure	CLIENT: Region 4	TESTHOLE NO: **SI/VW-2011-05**
UTM: 5667893.541m N 409066.921m E		PROJECT NO.: 2010-4G
CONTRACTOR: Paddock Drilling Ltd	METHOD: 170mm HSA, NQ Core	ELEVATION (m): 342.002

SAMPLE TYPE: GRAB | SHELBY TUBE | SPLIT SPOON | BULK | NO RECOVERY | CORE

BACKFILL TYPE: GROUT | GRAVEL | SLOUGH | BENTONITE | CUTTINGS | SAND

DEPTH (m)	SOIL DESCRIPTION	SAMPLE TYPE	SAMPLE #	PLASTIC / M.C. / LIQUID (20 40 60 80)	COMMENTS	ELEVATION (m)
0	TOPSOIL - rootlets throughout -black, moist					
1	CLAY (till-like) - silty, trace sand, trace gravel -brown, moist, firm -intermediate plastic					341
2						340
3						339
4	SAND (alluvial deposit) - silty, clayey, poorly graded -brown/grey, moist, trace oxidation Sample T1: Gravel-0%, Sand-52%, Silt-23%, Clay-25%		T1			338
5	CLAY (till-like) - silty, trace sand, trace gravel -brown, moist, firm, intermediate to high plastic		T2			337
6	CLAY SHALE - trace silt, trace find sand -dark grey/black, dry to moist, stiff -high plastic, blocky structure -laminated structure below ~5.2m, trace sulfates (gypsum), hard, horizontally fractured at ~10mm to 15mm intervals -fractures becoming less frequent below ~5.8m (20mm to 40mm intervals)		T3 T4 T5			336
7						335
8	-occasional silt and fine sand seams		C1			334
9			C2			333
10			C3			332
11	END HOLE AT 10.8m IN CLAY SHALE					331
12	Notes: 1. Sloughing observed in till; 2. No seepage observed; 3. SI-2011-05 installed to 10.80m below existing ground level (el. 331.2m); -approximately 40 gallons of grout used -above ground steel casing installed 4. VW-2011-05 installed to 7.01m below existing ground level (el. 335.0m at tip).					330
13						329
14						328
15						

LOG OF TESTHOLE REVISED (OLD) PTH 5 ASHVILLE JUNCTION TEST HOLE LOGS 2013-12-20.GPJ MIT.GDT 14-8-28

Manitoba

LOGGED BY: Ken Kalynuk	COMPLETION DEPTH: 10.80 m
REVIEWED BY: J. Fiebelkorn	COMPLETION DATE: 11-11-8
PROJECT ENGINEER: Jeremy Fiebelkorn	Page 1 of 1

PROJECT: PTH 5 & 10 Grade Slope Failure	CLIENT: Region 4	TESTHOLE NO: **SI/VW-2011-06**
UTM: 5667923.703m N 409064.874m E		PROJECT NO.: 2010-4G
CONTRACTOR: Paddock Drilling Ltd	METHOD: 170mm HSA, NQ Core	ELEVATION (m): 347.939

SAMPLE TYPE: GRAB | SHELBY TUBE | SPLIT SPOON | BULK | NO RECOVERY | CORE

BACKFILL TYPE: GROUT | GRAVEL | SLOUGH | BENTONITE | CUTTINGS | SAND

DEPTH (m)	SOIL DESCRIPTION	SAMPLE TYPE	SAMPLE #	SPT (N)	COMMENTS	ELEVATION (m)
0	GRAVEL (recycled asphalt fill)					
1	CLAY (fill) - silty, some sand, some gravel -brown, moist, firm -high plastic					347
2						346
3	CLAY (till-like) - silty, trace to some sand, trace gravel -brown mottled grey, moist, firm to stiff -intermediate to high plastic, trace oxidation Sample T7: Gravel-2%, Sand-11%, Silt-22%, Clay-65%		T6 T7			345
4			T8			344
5	-trace sulfates Sample T9: Gravel-0%, Sand-14%, Silt-28%, Clay-58% -light grey/yellow oxidized bentonite seam from ~4.8m to 5.4m		T9 T10			343
6	CLAY SHALE - trace silt, occasional fine sand seams -dark grey/black, dry to moist, stiff becoming hard with depth, high plastic		T11			342
	CLAY (bentonite) - some silt -light blue/grey, moist, firm, high plastic		T12 G14		102	
7	CLAY SHALE - trace silt, occasional fine sand seams -dark grey/black, dry to moist, hard -high plastic		S13			341
8			C15			340
9						339
10			C16	45		338
11	END HOLE AT 11.0m IN CLAY SHALE					337
12	Notes: 1. Sloughing observed in fill; 2. No seepage observed; 3. SI2011-06 installed to 10.97m below existing ground level (el. 339.96m); -approximately 40 gallons of grout used -above ground steel casing installed 4. VW2011-06 installed to 6.10m below existing ground level (el. 341.84m at tip).					336
13						335
14						334
15						

Total Unit Wt (kN/m³): 17 19 21 23

SPT (Standard Pen Test) (Blows/300mm): 20 40 60 80

PLASTIC M.C. LIQUID: 20 40 60 80

LOG OF TESTHOLE REVISED (OLD) PTH 5 ASHVILLE JUNCTION TEST HOLE LOGS 2013-12-20.GPJ MIT.GDT 14-8-28

Manitoba

LOGGED BY: Ken Kalynuk	COMPLETION DEPTH: 10.13 m
REVIEWED BY: J. Fiebelkorn	COMPLETION DATE: 11-11-9
PROJECT ENGINEER: Jeremy Fiebelkorn	Page 1 of 1

PROJECT: PTH 5 & 10 Grade Slope Failure	CLIENT: Region 4	TESTHOLE NO: **SI/VW-2014-07**
UTM: 5667909.970m N 409060.450m E		PROJECT NO.: 2010-4G
CONTRACTOR: Maple Leaf Drilling Ltd	METHOD: 170mm HSA	ELEVATION (m): 346.221

SAMPLE TYPE: GRAB | SHELBY TUBE | SPLIT SPOON | BULK | NO RECOVERY | CORE

BACKFILL TYPE: GROUT | GRAVEL | SLOUGH | BENTONITE | CUTTINGS | SAND

DEPTH (m)	SLOPE INCLINOMETER	VW PIEZOMETER	SOIL SYMBOL	SOIL DESCRIPTION	SAMPLE TYPE	SAMPLE #	COMMENTS	ELEVATION (m)
0				Granular Berm Fill - sand and gravel				346
1								345
2				CLAY (till-like) - silty, trace sand, trace gravel -brown, moist, firm -intermediate plastic				344
3								343
4								342
5								341
6				CLAY SHALE - trace silt, occasional fine sand seams -dark grey/black, dry to moist, stiff becoming hard with depth, high plastic -blue/white bentonite observed to ~ 9m				340
7								339
8								338
9								337
10								336
11								335
12								334
13								333
14								332
15								

LOG OF TESTHOLE REVISED (OLD) PTH 5 ASHVILLE JUNCTION TEST HOLE LOGS 2013-12-20.GPJ MIT.GDT 14-8-28

Manitoba

LOGGED BY: Andre Dupuis
REVIEWED BY: J. Fiebelkorn
PROJECT ENGINEER: Jeremy Fiebelkorn

COMPLETION DEPTH: 19.81 m
COMPLETION DATE: 14-6-21

PROJECT: PTH 5 & 10 Grade Slope Failure	CLIENT: Region 4	TESTHOLE NO: **SI/VW-2014-07**
UTM: 5667909.970m N 409060.450m E		PROJECT NO.: 2010-4G
CONTRACTOR: Maple Leaf Drilling Ltd	METHOD: 170mm HSA	ELEVATION (m): 346.221

SAMPLE TYPE: GRAB | SHELBY TUBE | SPLIT SPOON | BULK | NO RECOVERY | CORE

BACKFILL TYPE: GROUT | GRAVEL | SLOUGH | BENTONITE | CUTTINGS | SAND

DEPTH (m)	SLOPE INCLINOMETER / VW PIEZOMETER	SOIL SYMBOL	SOIL DESCRIPTION	SAMPLE TYPE	SAMPLE #	COMMENTS	ELEVATION (m)
15							331
16							330
17							329
18							328
19							327
20			END HOLE AT 19.8m IN CLAY SHALE				326
21							325
22							324
23							323
24							322
25							321
26							320
27							319
28							318
29							317
30							

Notes:
1. No sloughing observed (HSA);
2. Seepage observed between 10.7m and 13.7m;
3. SI2014-07 installed to 19.81m below existing ground level (el. 326.41m);
-hole grouted to surface
-above ground steel casing installed
4. VW2014-07a (#1305040) installed to 4.27m below existing ground level (el. 341.95m at tip);
5. VW2014-07b (#1305037) installed to 7.32m below existing ground level (el. 338.90m at tip);
6. VW2014-07c (#1305038) installed to 13.41m below existing ground level (el. 332.81m at tip);
7. VW2014-07d (#1305041) installed to 19.51m below existing ground level (el. 326.71m at tip).

Manitoba

LOGGED BY: Andre Dupuis	COMPLETION DEPTH: 19.81 m
REVIEWED BY: J. Fiebelkorn	COMPLETION DATE: 14-6-21
PROJECT ENGINEER: Jeremy Fiebelkorn	Page 2 of 2

LOG OF TESTHOLE REVISED (OLD) PTH 5 ASHVILLE JUNCTION TEST HOLE LOGS 2013-12-20.GPJ MIT.GDT 14-8-28

PROJECT: PTH 5 & 10 Grade Slope Failure			CLIENT: Region 4			TESTHOLE NO: **SI/VW-2014-08**	
UTM: 5667885.99m N 409060.520m E						PROJECT NO.: 2010-4G	
CONTRACTOR: Maple Leaf Drilling Ltd			METHOD: 170mm HSA			ELEVATION (m): 342.375	
SAMPLE TYPE	GRAB	SHELBY TUBE	SPLIT SPOON	BULK	NO RECOVERY	CORE	
BACKFILL TYPE	GROUT	GRAVEL	SLOUGH	BENTONITE	CUTTINGS	SAND	

DEPTH (m)	SLOPE INCLINOMETER	VW PIEZOMETER	SOIL SYMBOL	SOIL DESCRIPTION	SAMPLE TYPE	SAMPLE #	COMMENTS	ELEVATION (m)
0				Granular Berm Fill - sand and gravel				342
1								341
2								340
3				CLAY (till-like) - silty, trace sand, trace gravel -brown, moist, firm -intermediate plastic				339
4								338
5								337
6								336
7				CLAY SHALE - trace silt, occasional fine sand seams -dark grey/black, dry to moist, stiff becoming hard with depth, high plastic -blue/white bentonite observed to ~ 9m				335
8								334
9								333
10								332
11								331
12								330
13								329
14								328
15								

LOG OF TESTHOLE REVISED (OLD) PTH 5 ASHVILLE JUNCTION TEST HOLE LOGS 2013-12-20.GPJ MIT.GDT 14-8-28

Manitoba

LOGGED BY: Andre Dupuis	COMPLETION DEPTH: 19.81 m
REVIEWED BY: J. Fiebelkorn	COMPLETION DATE: 14-6-22
PROJECT ENGINEER: Jeremy Fiebelkorn	Page 1 of 2

PROJECT: PTH 5 & 10 Grade Slope Failure	CLIENT: Region 4	TESTHOLE NO: **SI/VW-2014-08**
UTM: 5667885.99m N 409060.520m E		PROJECT NO.: 2010-4G
CONTRACTOR: Maple Leaf Drilling Ltd	METHOD: 170mm HSA	ELEVATION (m): 342.375

SAMPLE TYPE: GRAB | SHELBY TUBE | SPLIT SPOON | BULK | NO RECOVERY | CORE

BACKFILL TYPE: GROUT | GRAVEL | SLOUGH | BENTONITE | CUTTINGS | SAND

DEPTH (m)	SLOPE INCLINOMETER / VW PIEZOMETER	SOIL SYMBOL	SOIL DESCRIPTION	SAMPLE TYPE	SAMPLE #	COMMENTS	ELEVATION (m)
15							327
16							326
17							325
18							324
19							323
20			END HOLE AT 19.8m IN CLAY SHALE				322
21							321
22							320
23							319
24							318
25							317
26							316
27							315
28							314
29							313
30							

Notes:
1. No sloughing observed (HSA);
2. Seepage observed between 6.1m and 9.1m;
3. SI2014-08 installed to 19.81m below existing ground level (el. 326.41m);
-hole grouted to surface
-above ground steel casing installed
4. VW2014-08a (#1305068) installed to 3.35m below existing ground level (el. 339.025m at tip);
5. VW2014-08b (#1305045) installed to 6.55m below existing ground level (el. 335.83m at tip);
6. VW2014-08c (#1305039) installed to 10.36m below existing ground level (el.332.02m at tip);
7. VW2014-08d (#1305044) installed to 19.51m below existing ground level (el. 322.87m at tip).

Manitoba

LOGGED BY: Andre Dupuis	COMPLETION DEPTH: 19.81 m
REVIEWED BY: J. Fiebelkorn	COMPLETION DATE: 14-6-22
PROJECT ENGINEER: Jeremy Fiebelkorn	Page 2 of 2

LOG OF TESTHOLE REVISED (OLD) PTH 5 ASHVILLE JUNCTION TEST HOLE LOGS 2013-12-20.GPJ MIT.GDT 14-8-28

PROJECT: PTH 5 & 10 Grade Slope Failure	CLIENT: Region 4	TESTHOLE NO: **TH1974-01**
UTM: STA 7+43 (ft), 52' s of CL		PROJECT NO.: 2010-4G
CONTRACTOR: Unknown	METHOD: Power Auger	ELEVATION (m): 346.86

SAMPLE TYPE: GRAB | SHELBY TUBE | SPLIT SPOON | BULK | NO RECOVERY | CORE

DEPTH (m)	SOIL SYMBOL	SOIL DESCRIPTION	SAMPLE TYPE	SAMPLE #	QU (Su) (kPa) 50 100 150 200 / PLASTIC M.C. LIQUID 20 40 60 80	COMMENTS	ELEVATION (m)
0		CLAY (till) - silty, some sand, numerous pebbles -soft, intermediate plasticity					346
1							
2							345
3				T1			344
4				T2			343
		CLAY (bentonite) -light grey, soft, highly plastic		T3	105		
5		CLAY SHALE -black, stiff becoming very stiff with depth		T4			342
6							341
		END HOLE AT 6.25m in CLAY SHALE					
7		Notes: 1. Tube damaged; 2. Seepage observed at ~3.7m below EGL on June 5, 1974.					340
8							339
9							338
10							337
11							336
12							335
13							334
14							333
15							332

Manitoba

LOGGED BY:	COMPLETION DEPTH: 6.25 m
REVIEWED BY: RVC	COMPLETION DATE: 74-6-5
PROJECT ENGINEER: Jeremy Fiebelkorn	Page 1 of 1

LOG OF TESTHOLE REVISED (OLD) PTH 5 ASHVILLE JUNCTION TEST HOLE LOGS 2013-12-20.GPJ MIT.GDT 14-8-28

PROJECT: PTH 5 & 10 Grade Slope Failure	CLIENT: Region 4	TESTHOLE NO: **TH1974-02**
UTM: STA 7+41 (ft), 91' s of CL		PROJECT NO.: 2010-4G
CONTRACTOR: Unknown	METHOD: Power Auger	ELEVATION (m): 345.95

SAMPLE TYPE: GRAB | SHELBY TUBE | SPLIT SPOON | BULK | NO RECOVERY | CORE

DEPTH (m)	SOIL DESCRIPTION	SAMPLE TYPE	SAMPLE #	COMMENTS	ELEVATION (m)
0	CLAY - silty, trace of sand -soft, intermediate plasticity				345
1			T5		344
2			T6		343
3			T7		342
4			T8		341
5	CLAY (bentonite) -blue-grey, numerous oxide streaks		T9		340
6	CLAY SHALE -black, stiff		T10		339
7			T11		338
8					337
9	END OF HOLE IN CLAY SHALE Notes: 1. Seepage observed at 2.7m below EGL.				336
10					335
11					334
12					333
13					332
14					
15					

QU (Su) (kPa): 50 100 150 200
Total Unit Wt (kN/m³): 17 19 21 23
PLASTIC M.C. LIQUID: 20 40 60 80

LOG OF TESTHOLE REVISED (OLD) PTH 5 ASHVILLE JUNCTION TEST HOLE LOGS 2013-12-20.GPJ MIT.GDT 14-8-28

Manitoba

LOGGED BY:	COMPLETION DEPTH: 8.84 m
REVIEWED BY: RVC	COMPLETION DATE: 74-5-11
PROJECT ENGINEER: Jeremy Fiebelkorn	Page 1 of 1

PROJECT: PTH 5 & 10 Grade Slope Failure	CLIENT: Region 4	TESTHOLE NO: **TH1974-03**
UTM: STA 7+25 (ft), 159' s of CL		PROJECT NO.: 2010-4G
CONTRACTOR: Unknown	METHOD: Power Auger	ELEVATION (m): 340.16

SAMPLE TYPE: GRAB | SHELBY TUBE | SPLIT SPOON | BULK | NO RECOVERY | CORE

DEPTH (m)	SOIL SYMBOL	SOIL DESCRIPTION	SAMPLE TYPE	SAMPLE #	QU (Su) (kPa) 50 100 150 200 / Total Unit Wt (kN/m³) 17 19 21 23 / PLASTIC M.C. LIQUID 20 40 60 80	COMMENTS	ELEVATION (m)
0		CLAY -soft, grey					340
1		-brown					339
2							338
3		SAND		T12			337
4		CLAY -soft, brown					336
5		CLAY SHALE -black, hard		T13			335
6							334
7				T14			333
8				T15			332
9							331
10							330
11							329
12							328
13							327
14							326
15							

LOG OF TESTHOLE REVISED (OLD) PTH 5 ASHVILLE JUNCTION TEST HOLE LOGS 2013-12-20.GPJ MIT.GDT 14-8-28

Manitoba

LOGGED BY:	COMPLETION DEPTH: 8.84 m
REVIEWED BY: RVC	COMPLETION DATE: 74-5-13
PROJECT ENGINEER: Jeremy Fiebelkorn	Page 1 of 1

SOIL LOG & DESCRIPTION

SUMMARY OF SAMPLING & TESTING

DEPTH METRES	SOIL DESCRIPTION	CLASSIFICATION	SAMPLE NUMBER	SAMPLE TYPE	GRAIN SIZE ANALYSIS % PASSING mm / um (425, 75)	PP T.S.F.	SPT N VALUE
0.0	TOPSOIL						
	VERY STIFF BROWN PEBBLY SANDY SILTY CLAY						
	•tr. odd gravel mix, some sand mix approx 10%, some light brown silt specks & lenses	CI	24	B		3.3 3.8	23
	•as above	CI	25	B		3.9	
3.0	•tr. odd gravel (4.76mm) mix, some sand mix approx 10%, tr. mica crystals, some silt lenses & specks	CI	26	B		3.4	17
4.0	•tr. odd gravel (9.52mm), some sand mix approx 10%, as above	CI	27	B		1.6	
	•as above	CH	28	B		1.8 2.2	14.5
5.0	•tr. gravel (9.52mm), some sand mix approx 15%, as above	CH	29	B		0.1 2.2	
	•tr. gravel (19.1mm) mix, some sand mix approx 10%, tr. mica, some silt lenses & specks	CI	30	B		3.3	
6.0	FIRM-STF BRN & BLK PEBBLY SANDY SILTY CLAY •tr. odd gravel (9.52mm) some sand mix approx 10%, some silt lenses & specks	CI	31	B		1.4 1.6	17
	V. STF. BLACKISH PEBBLY SANDY SILTY CLAY	CI	32	B		3.1 3.8	
7.0	•w/some gravel mix (9.52mm) approx 8%, some sand mix approx 15%, tr. mica, tr. silt lenses	CI	33	B		1.35 1.8	
	•as above	CI	34	B		3.8	20
8.0	•as above	CI	35	B		2.4	
	HARD BLACK SHALE CLAY	MH	36	B		3.8	
	•tr. mica crystal specks, tr. yellowish brn. silt lenses	MH	37	B			32
	•as above	MH	38	B		>5.0	
10.0	•as above	MH	39	B			
	•as above	MH	40	B			
11.0	•as above	MH	41	B			
12.0	•as above	MH	42	B			
13.0	HARD GREY BENTONITE •hard light grey bentonitic shale	MH	43	B	W_L=127%		
14.0							

REMARKS :-

Manitoba Highways and Transportation

GEOTECHNICAL SOILS REPORT

PROJECT ASHVILLE JUNCTION

LOCATION PTH 5 & PTH 10

HOLE No. 2 FIELD BOOK No. 5880

CO-ORDINATES STA 165+28.4 ; 41.1 m. NORTH OF ℄

ELEVATIONS

GROUND SURFACE 352.1

BOTTOM OF HOLE 338.1

BEDROCK SURFACE

STATIC WATER LEVEL DATE

DRY HOLE WHILE DRILLING

ADDITIONAL TESTING

C - CONSOLIDATION
DS - DIRECT SHEAR
PP - POCKET PENETROMETER
QU - UNCONFINED COMPRESSION TEST
SPT - STANDARD PENETRATION TEST
VS - VANE SHEAR (INSITU)

SOIL SYMBOLS

ORGANIC SOILS
SAND
SILT
GRAVEL
CLAY
SHALE

SAMPLE TYPE

A - AUGER
B BAG SAMPLE
C - CORE BARREL
D DISCARDED
L - BLOCK SAMPLE
P - PISTON SAMPLER
S - SPLIT TUBE
T - THIN WALL TUBE
W - WASH
X - WAXED

MATERIALS AND RESEARCH SECTION

DATE SAMPLED MAY 25, 1988

DATE DRAWN JANUARY 16, 1989

DRAWN RP

CHECKED KRB

SHEET 2 OF 3

SOIL LOG & DESCRIPTION

SUMMARY OF SAMPLING & TESTING

DEPTH METRES	SOIL LOG	SOIL DESCRIPTION	CLASSIFICATION	SAMPLE NUMBER	SAMPLE TYPE	γ_w kg/m³	GRAIN SIZE ANALYSIS % PASSING mm 425 um 75 um	PP TSF	SPT N VALUE
0.0		FIRM BRN PEBBLY SANDY SILTY CLAY • w/some gravel (9.52mm) approx 10% some sand mix approx 15%, num silt tr. shale gravel & shale sand mix	CI	44	B			1.4	
1.0		STIFF BRN PEBBLY SANDY SILTY CLAY • as above approx 20% sand mix	CI	45	B			2.0	
		• tr. gravel mix (9.52mm), some sand mix approx 20%, some silt lenses, tr. organic	CH	46	B			2.25	12
		WET GRAVEL							
		WASH SHALE CLAY WITH BENTONITE SEAMS • silty clay & bentonite, silt & tr. bentonite lenses, tr. organic, tr. odd gravel	CI MH	47	B				
3.0		STIFF BLK PEBBLY SILTY CLAY • tr. gravel mix (9.52mm), some sand mix & approx 20%, tr. shale gravel & shale sand mixture	CI	48	B			2.6	25
		VERY STIFF BLACK SHALE CLAY • tr. odd gravel & sand mix (4.76mm)	MH	49	B			3.75	
4.0		• fragmented, as above	MH	50	B			2.8	
		STIFF BLACK SHALE CLAY • black, fragmented shale clay, tr. salt lenses, tr. oxides	MH	51	B			1.6	12
5.0		• as above, w/some grey silt seams tr. oxides	MH	52	B			1.7	
		• as above	MH	53	B				
6.0		DENSE BLACK SHALE CLAY • w/some grey silt seams, tr. oxides	MH	54	B			>5.0	60
7.0									

ATTERBERG LIMITS MOISTURE CONTENT % — w_p w_n w_L (10 20 30 40 50 60)

w_L = 100%

REMARKS :-

▼ WATER LNTERS HOLE.

NOTE: CLAY & BENTONITIC SILT WERE SEPARATED FOR A/L (SAMPLE 47)

Manitoba Highways and Transportation

GEOTECHNICAL SOILS REPORT

PROJECT ASHVILLE JUNCTION

LOCATION PTH 5 & PTH 10

HOLE No. 3 FIELD BOOK No. 5880

CO-ORDINATES STA 164+07.7 ; 17.4m NORTH OF ℄

ELEVATIONS

GROUND SURFACE 340.6

BOTTOM OF HOLE 334.1

BEDROCK SURFACE

STATIC WATER LEVEL 339.5 DATE MAY 28, 1988

ADDITIONAL TESTING

C - CONSOLIDATION
DS - DIRECT SHEAR
PP - POCKET PENETROMETER
QU - UNCONFINED COMPRESSION TEST
SPT - STANDARD PENETRATION TEST
VS - VANE SHEAR (INSITU)

SOIL SYMBOLS

ORGANIC SOILS · SAND · SILT · GRAVEL · CLAY · SHALE

SAMPLE TYPE

A - AUGER
B BAG SAMPLE
C - CORE BARREL
D DISCARDED
L - BLOCK SAMPLE
P - PISTON SAMPLER
S - SPLIT TUBE
T - THIN WALL TUBE
W - WASH
X - WAXED

MATERIALS AND RESEARCH SECTION

DATE SAMPLED MAY 25, 1988
DATE DRAWN JANUARY 18, 1989
DRAWN RP
CHECKED KRB
SHEET 3 OF 3

SOIL LOG & DESCRIPTION

SUMMARY OF SAMPLING & TESTING

DEPTH METRES	SOIL DESCRIPTION	CLASSIFICATION	SAMPLE NUMBER	SAMPLE TYPE	γ_w kg/m³	GRAIN SIZE ANALYSIS % PASSING mm 19.0	mm 4.75	um 425	um 75	PP T.S.F.	SPT N VALUE
0.0	TOPSOIL										
	FIRM BUFF STONEY SANDY SILTY CLAY • w/Tr. gravel mix 9.52mm ϕ max, some sand mix, approx 35%, some oxides, Tr. mica crystal	CL	1	B		100	90.0	82.0	59.3		≈ 12
	VERY STIFF BRN PEBBLY SANDY SILTY CLAY • w/Tr. gravel mix 19.1mm ϕ max, some sand mix, approx 20%, num. silt lenses Tr. brn sand lenses. • gravel 9.52 mm max, 8%, Sand mix approx 20%, as above	CH	2	B						3.8	
		CH	3	B						4.1	
3.0	VERY STIFF BRN SILTY CLAY & WASH SAND • Tr. add gravel, sand mix 10%, some silt lenses	CH	4	B						2.8	18
	VERY STIFF BRN PEBBLY SILTY CLAY • w/Tr. gravel, sand mix approx 10%	CI	5	B						3.6	
	• w/some gravel, 9.52mm ϕ approx 8% sand mix approx 15%, some silt lenses and specks, Tr. shale gravel & shale sand • as above, approx 15% sand, Tr. add gravel	CI	6	B						3.6	
5.0		CI	7	B						2.3-2.7	21
	COMPACT BUFF TILL • w/some gravel mix approx 10%, some sand mix approx 30%	CL	8	B		100	92.5	80.0	63.8		
6.0	VERY STIFF BLACK SHALE (slight Tr. of bentonite) • w/some yellowish brown silt lenses	MH	9	B							27
	• w/Tr. yellowish brown silt lenses, Tr. mica crystals, some shale fragments	MH	10	B						3.8	
7.0	HARD BLACK SHALE CLAY • w/yellowish brown silt lenses, some portions fragmented.	MH	11	B						4.4	
	• as above	MH	12	B						4.0	35
8.0	• as above	MH	13	B							
	• as above	MH	14	B						>5.0	
	• as above	MH	15	B							32
	• as above, w/some salt accumulations in fissures	MH	16	B							
10.0	• as above	MH	17	B							
	WET CRUNCHY SEAM										
11.0	HARD GREY BENTONITE • bentonite shale w/Tr. oxides	MH	18	B							30
	• as above	MH	19	B							
	CRUNCHY SEAM										
12.0	DENSE BLACK SHALE CLAY • w/Tr. light grey silt lenses	MH	20	B							
	• as above	MH	21	B							99
	• fragmented, as above	MH	22	B							
13.0	• fragmented, as above	MH	23	B							
14.0											

ATTERBERG LIMITS MOISTURE CONTENT % — 10 20 30 40 50 60 — w_p + — w_n o — w_L x

w_L = 113%

w_L = 119%

WATER ENTERS HOLE

REMARKS :-

Manitoba Highways and Transportation

GEOTECHNICAL SOILS REPORT

PROJECT ASHVILLE JUNCTION

LOCATION PTH 5 & PTH 10

HOLE No. 1 FIELD BOOK No. 5880

CO-ORDINATES STA 164+45.6 & 44.2 m N. OF ℄

ELEVATIONS

GROUND SURFACE 350.3

BOTTOM OF HOLE 336.7

BEDROCK SURFACE

STATIC WATER LEVEL 341.6 DATE MAY 25, 1988

ADDITIONAL TESTING

C - CONSOLIDATION
DS - DIRECT SHEAR
PP - POCKET PENETROMETER
QU - UNCONFINED COMPRESSION TEST
SPT - STANDARD PENETRATION TEST
VS - VANE SHEAR (INSITU)

SOIL SYMBOLS

ORGANIC SOILS, SAND, SILT, GRAVEL, CLAY, SHALE

SAMPLE TYPE

A - AUGER
B BAG SAMPLE
C - CORE BARREL
D DISCARDED
L - BLOCK SAMPLE
P - PISTON SAMPLER
S - SPLIT TUBE
T - THIN WALL TUBE
W - WASH
X - WAXED

MATERIALS AND RESEARCH SECTION

DATE SAMPLED MAY 24, 1988
DATE DRAWN JANUARY 18, 1989
DRAWN RP
CHECKED KRB
SHEET 1 OF 3

Appendix B – Photos

Photo 1a – TH2011-05, Sample T1 (Upper Portion in Colluvium)

Photo 1b – TH2011-05, Sample T1 (Lower Portion in Alluvium)

Photo 2 – TH2011-05, Sample T2

Photo 3 – TH2011-05, Sample T3

Photo 4 – TH2011-05, Sample T4

Photo 5 – TH2011-05, Sample T5

Photo 6a to Photo 6c – TH2011-05 Core Sample (Top of Run #1 on Top Left, End of Run #2 Lower Right)

Photo 7 – TH2011-06, Sample T7

Photo 8 – TH2011-06, Sample T8

Photo 9 – TH2011-06, Sample T9

Photo 10 – TH2011-06, Sample T10

Photo 11 – TH2011-06, Sample T11

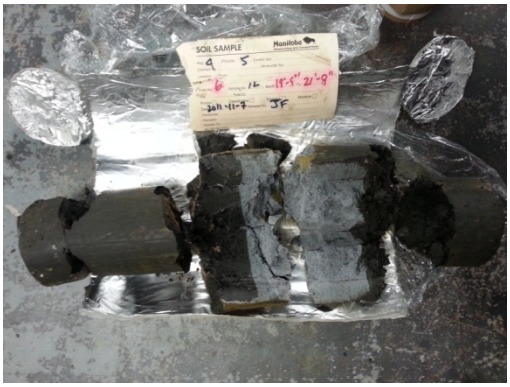

Photo 12 – TH2011-06, Sample T12

Photo 13a to Photo 13c – TH2011-06 Core Sample (Top of Run #1 on Top Left)

Photo 14 – Clearing and Grubbing of the Site

Photo 15 – Slope Movements Following Clearing and Grubbing

Photo 16 – Seepage from Slope Face at Mid-Slope

Photo 17 – Compaction Prior to Fill Placement (Conduit for Instrument Relocation shown in Centre)

Photo 18 – Grading at Toe of Lower Berm Prior to Fill Placement

Photo 19 – First Lifts of Lower Berm

Photo 20 – Grading of Lower Berm

Photo 21 – Fill Placement on Lower Berm

Photo 22 – Lower Berm at Design Elevation

Photo 23 – Bench Cuts Prior to Fill Placement for Upper Berm

Photo 24 – Fill Placement for Upper Berm

Photo 25 – Berm at Design Grade Following Rip Rap and Erosion Control Blanket Placement

Photo 26 – Re-vegetated Ashville Junction Site

Appendix C – Slope Inclinometer Plots

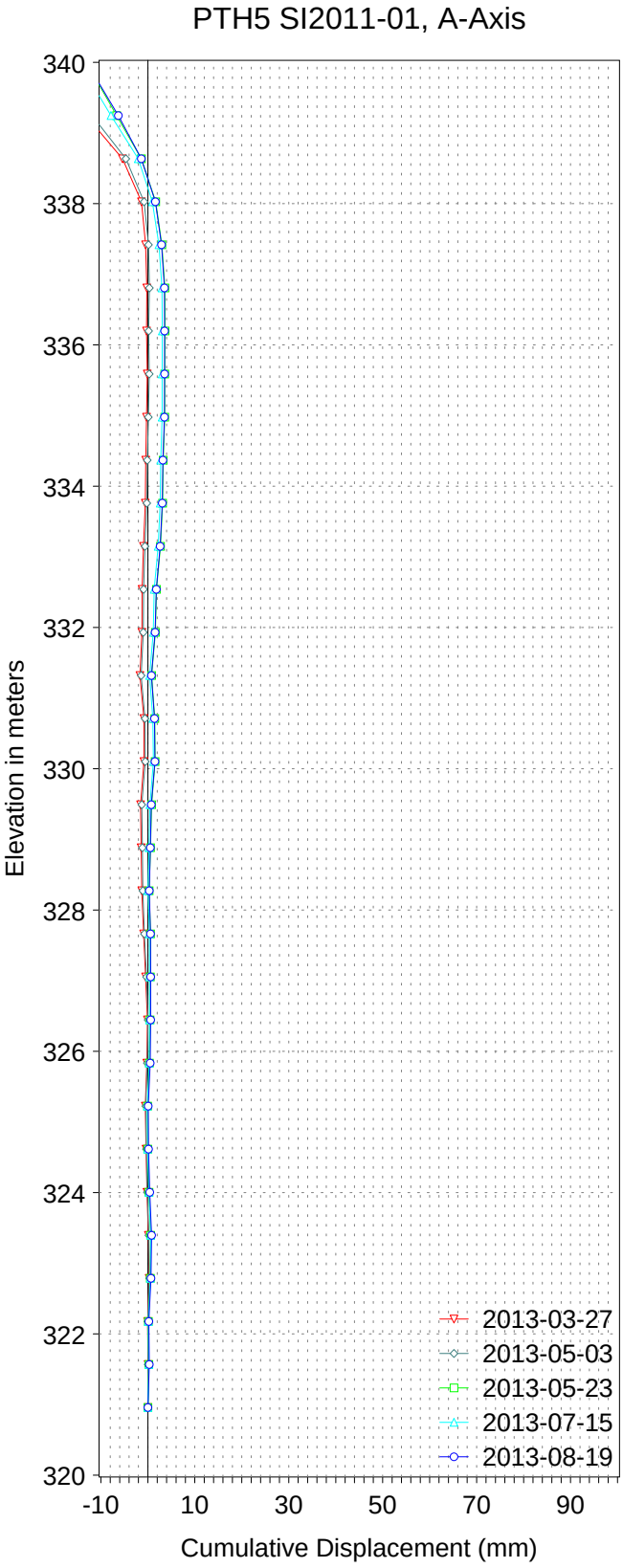

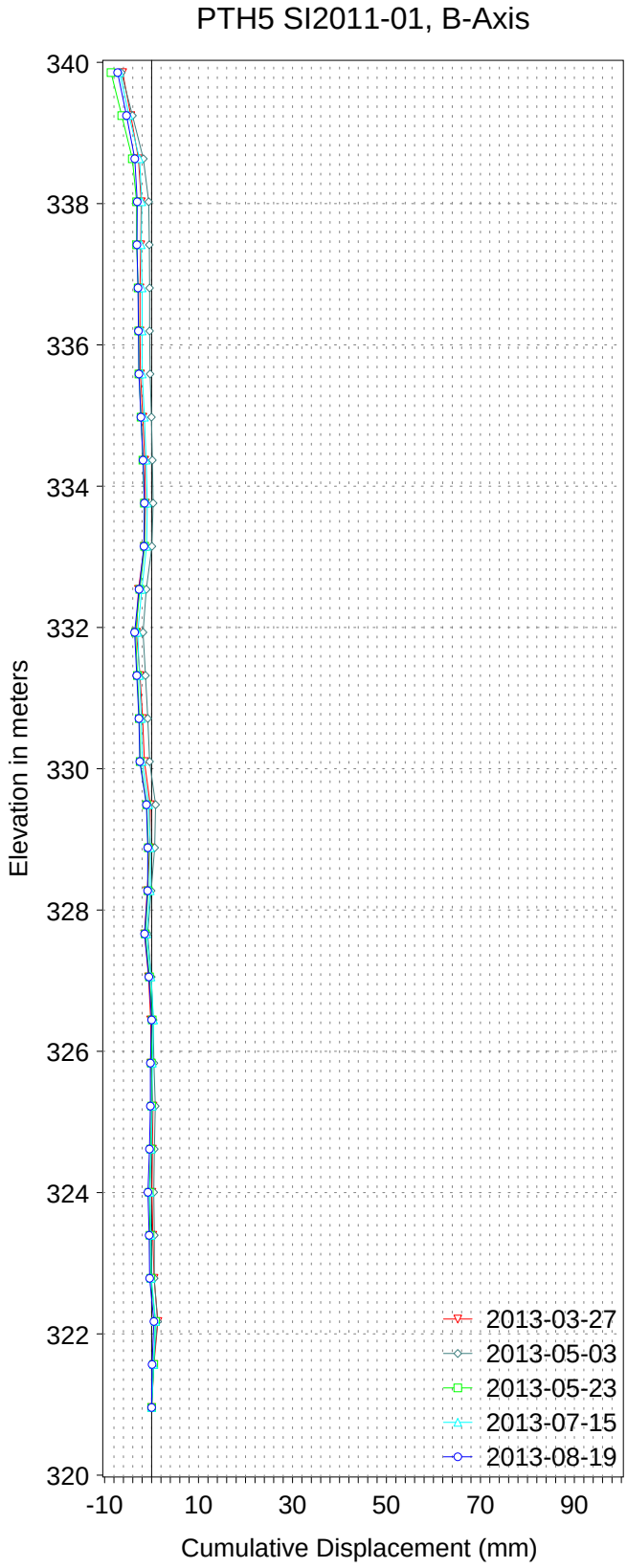

Ashville Junction Slope Stabilization
Cumulative Displacement vs Elevation
TH2011-01

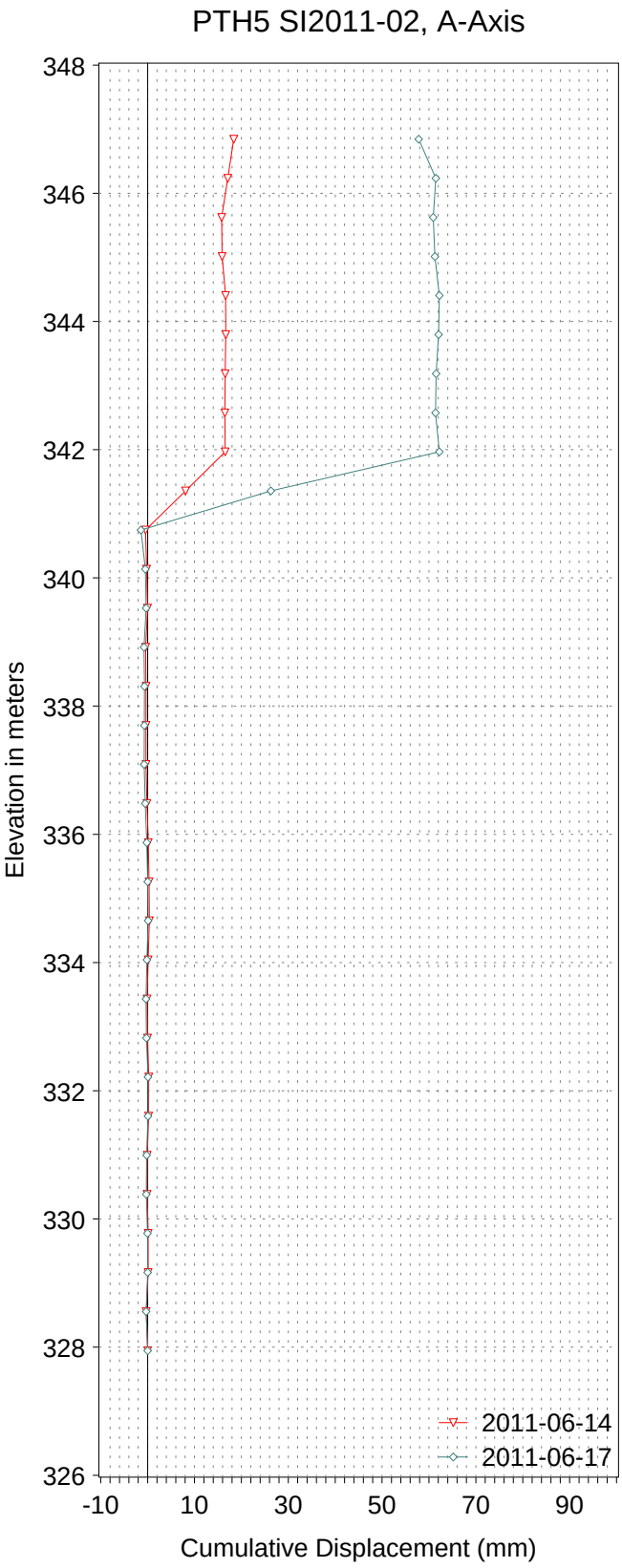

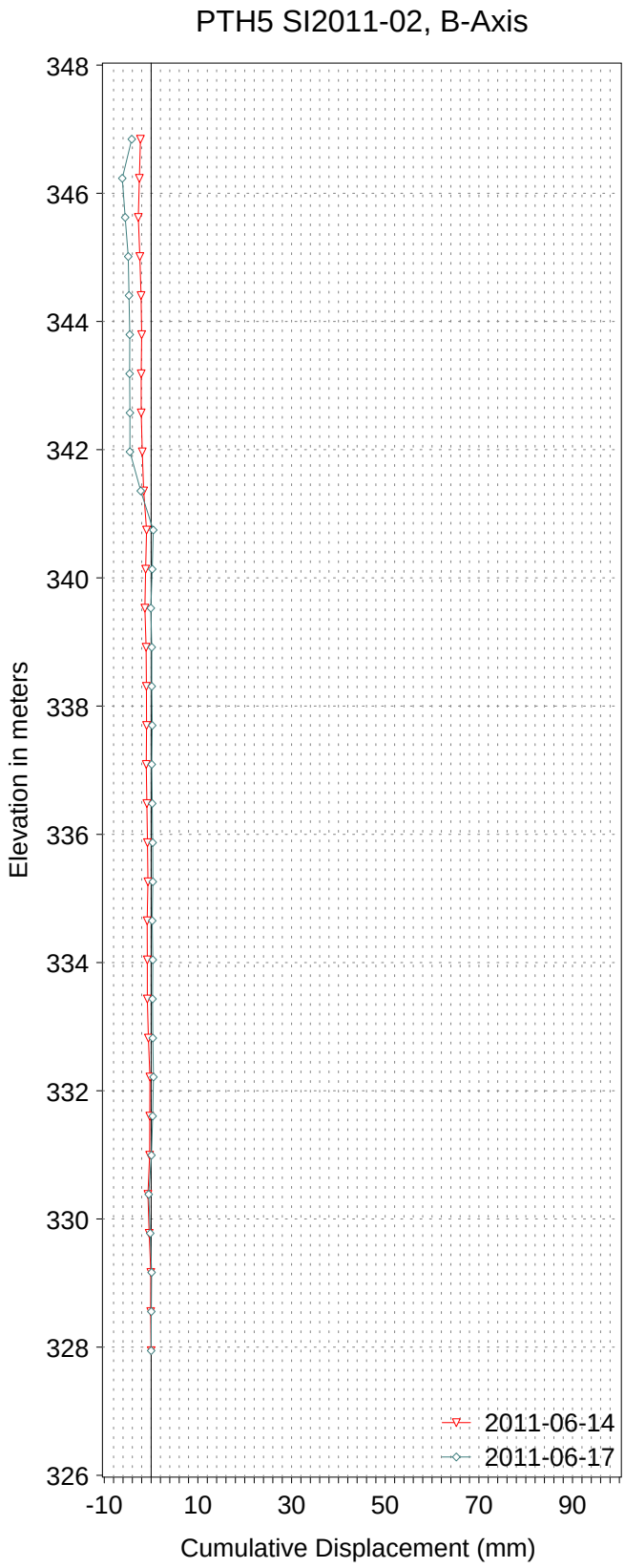

Ashville Junction Slope Stabilization
Cumulative Displacement vs Elevation
TH2011-02

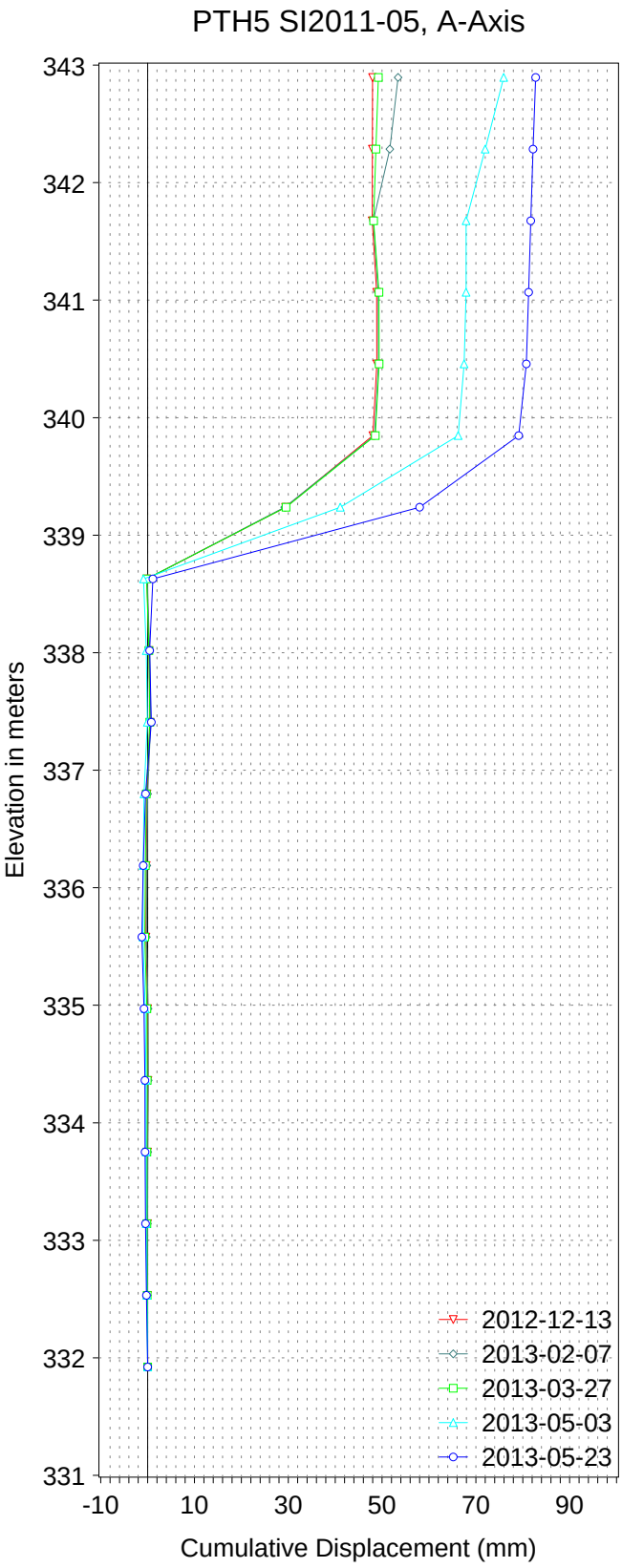

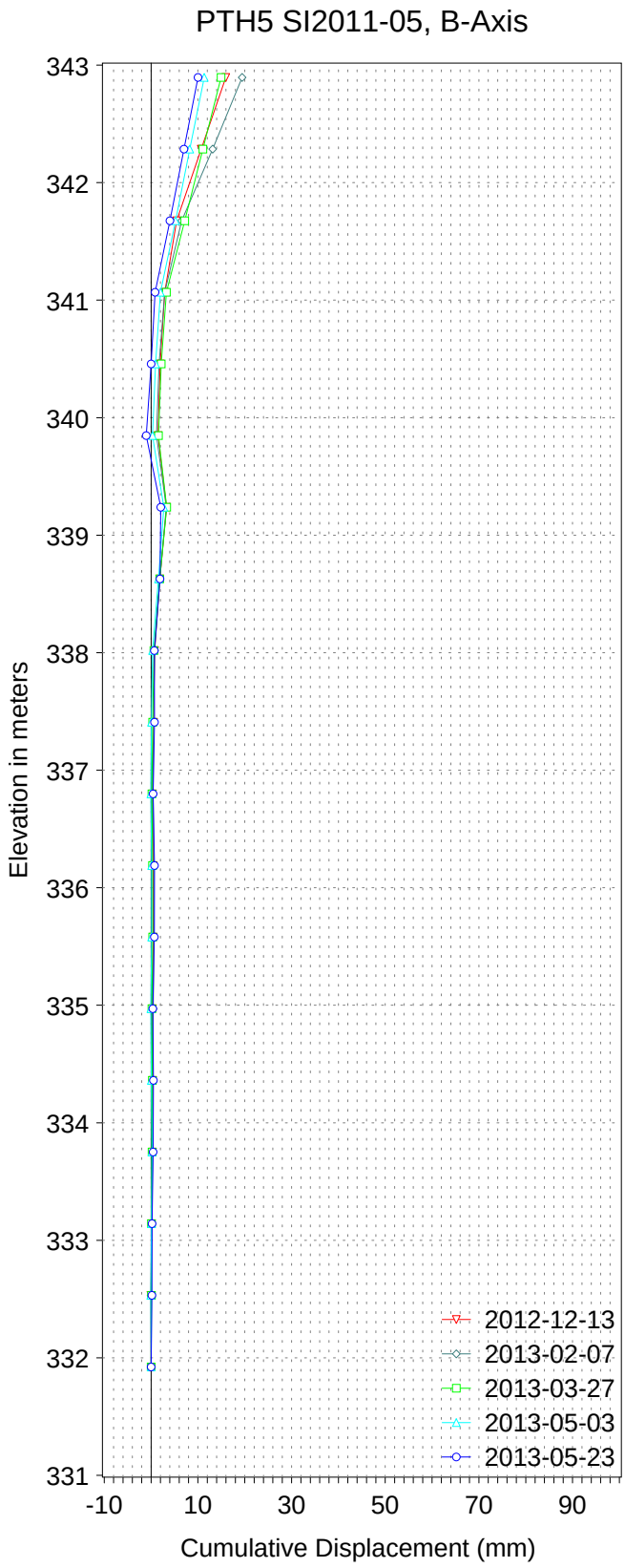

Ashville Junction Slope Stabilization
Cumulative Displacement vs Elevation
TH2011-05

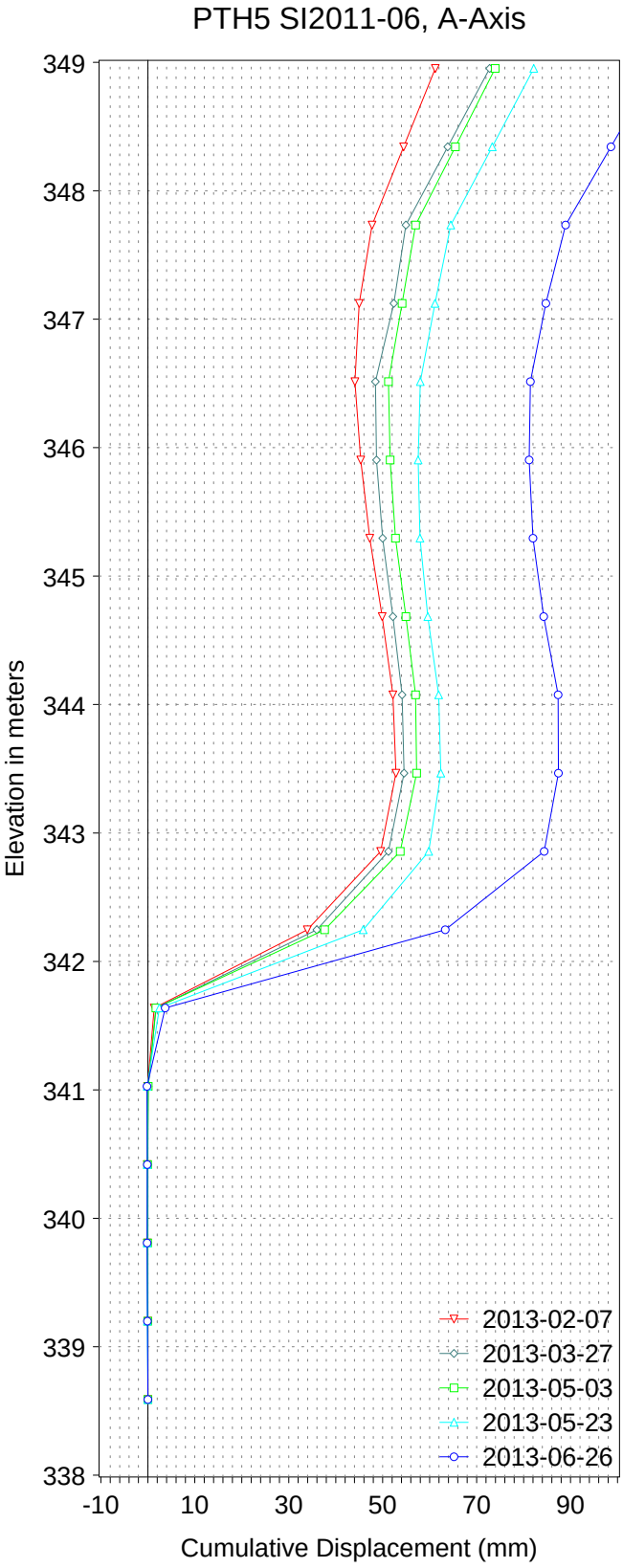

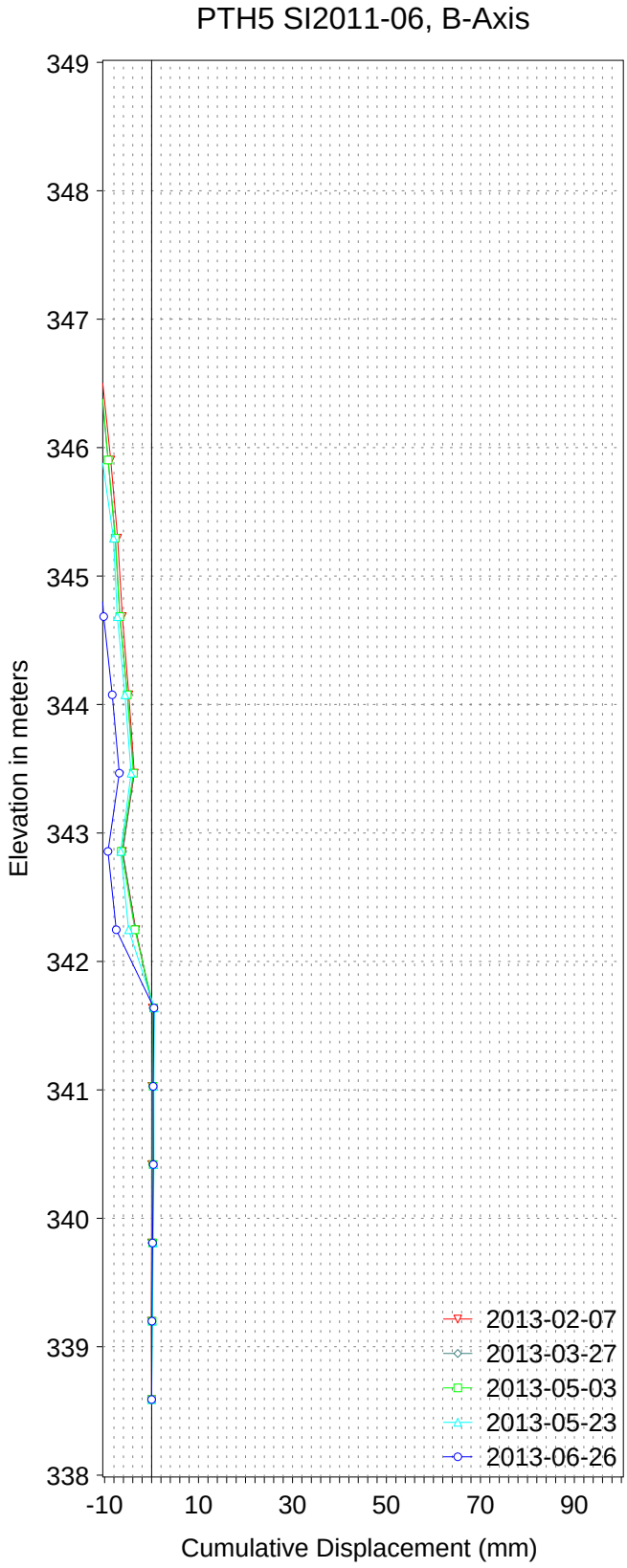

Ashville Junction Slope Stabilization
Cumulative Displacement vs Elevation
TH2011-06

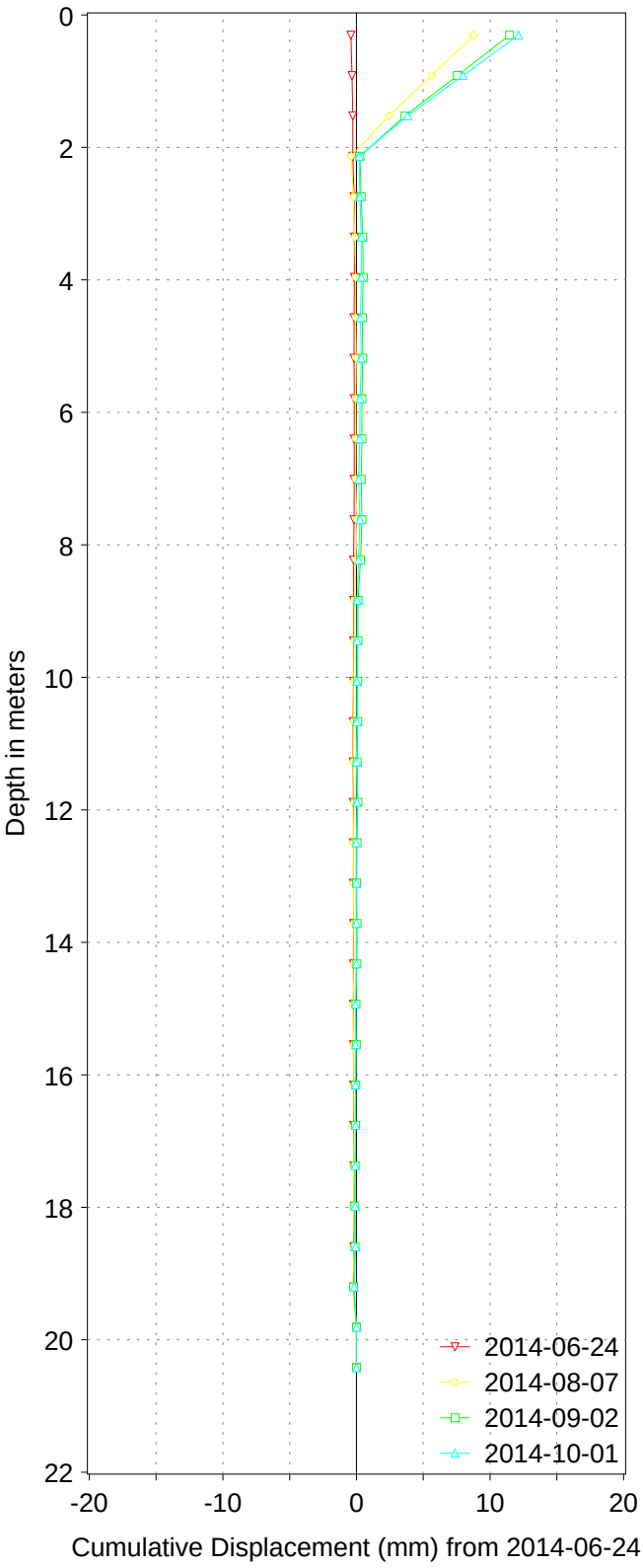
5 2014 SI7, A-Axis
Depth in meters
0
2
4
6
8
10
12
14
16
18
20
22
-20
-10
0
10
20
Cumulative Displacement (mm) from 2014-06-24
2014-06-24
2014-08-07
2014-09-02
2014-10-01

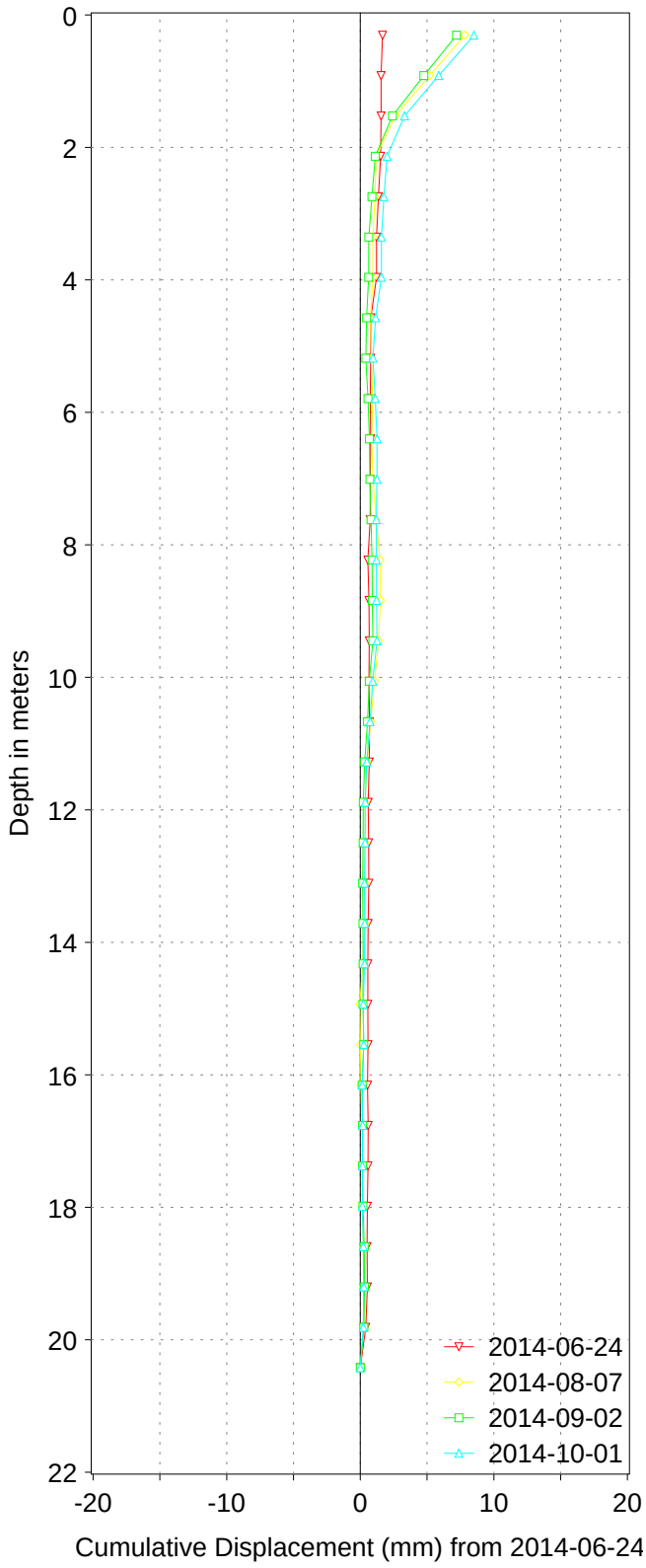
5 2014 SI7, B-Axis
Depth in meters
0
2
4
6
8
10
12
14
16
18
20
22
-20
-10
0
10
20
Cumulative Displacement (mm) from 2014-06-24
2014-06-24
2014-08-07
2014-09-02
2014-10-01

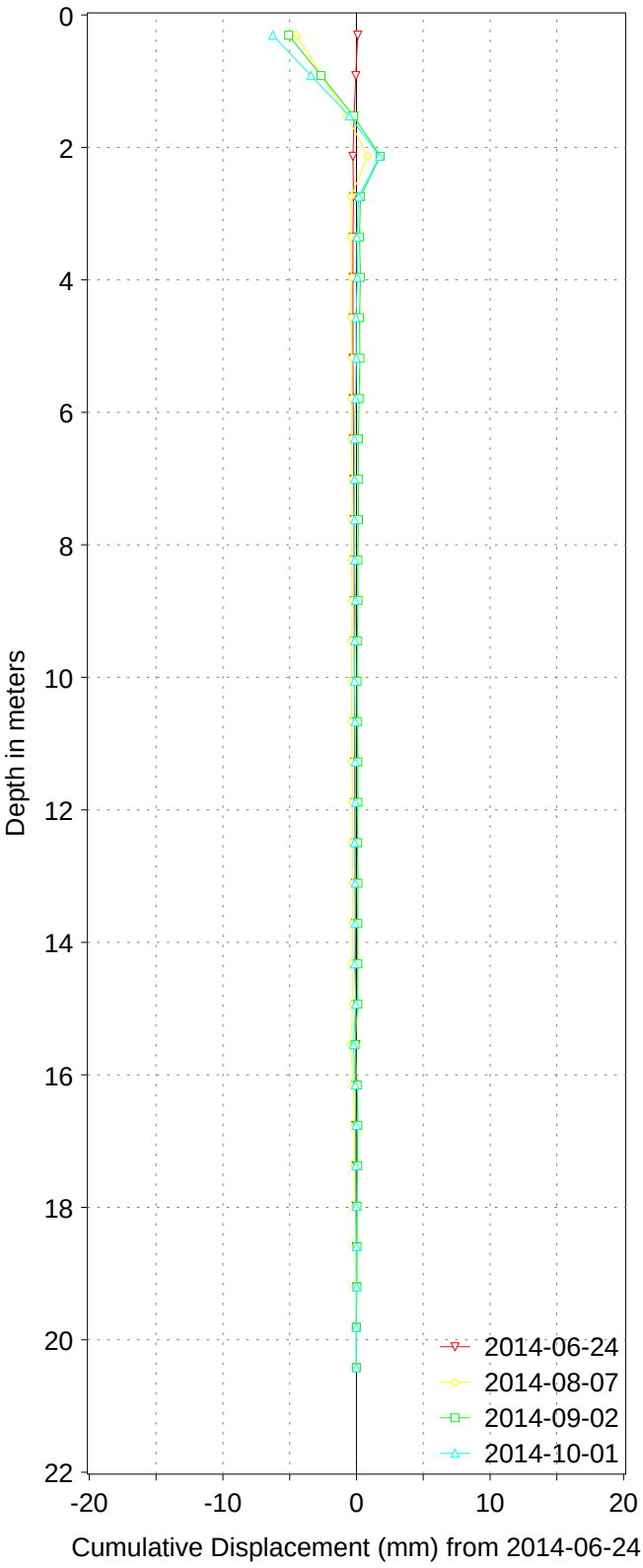
5 2014 SI8, A-Axis
Depth in meters
0
2
4
6
8
10
12
14
16
18
20
22
-20
-10
0
10
20
Cumulative Displacement (mm) from 2014-06-24
2014-06-24
2014-08-07
2014-09-02
2014-10-01

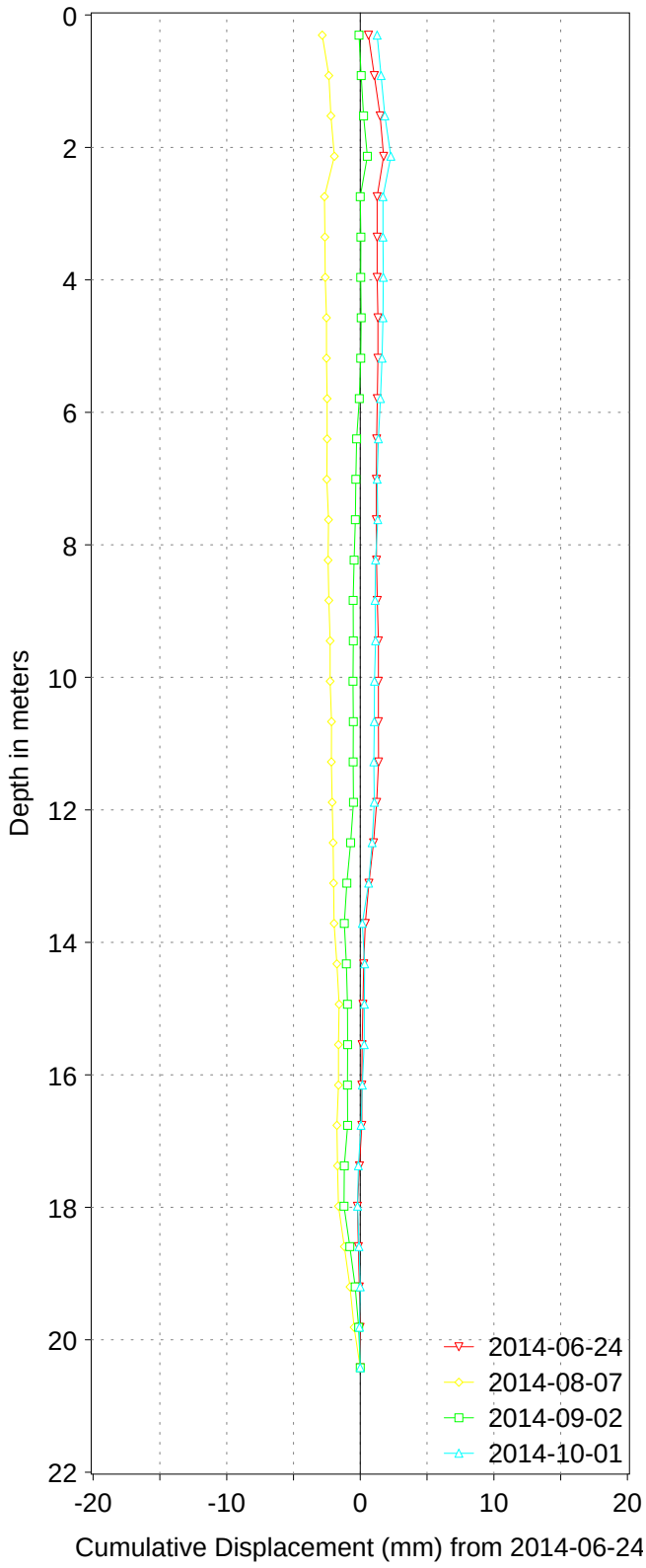
5 2014 SI8, B-Axis
Depth in meters
0
2
4
6
8
10
12
14
16
18
20
22
-20
-10
0
10
20
Cumulative Displacement (mm) from 2014-06-24
2014-06-24
2014-08-07
2014-09-02
2014-10-01

Appendix D – Laboratory Test Results

MANITOBA INFRASTRUCTURE and TRANSPORTATION

MATERIALS ENGINEERING BRANCH

CENTRAL LAB

PARTICLE SIZE ANALYSIS of SOILS A.S.T.M. D-422

PROJECT: PTH 5 - South Grade Slope Slide — **TESTED BY:** J.H.
LOCATION: PTH 5 - 0.5km West of PTH 10 Ashville Junction — **CHECKED:** G.J.

LAB.NO. WGT110505 FIELD NO. B37 HOLE NO. VW-2011-04 DEPTH (m) 3.96-4.27

SIEVE ANALYSIS			HYDROMETER ANALYSIS				
SIEVE U.S. STANDARD	DIAMETER (mm)	% PASSING	TIME MINUTES	HYDROMETER READING R_O	HYDROMETER READING R_C	DIAMETER (mm)	% PASSING
3.00 in	75.00	100.0	1	32.4	29.3	0.0394	97.5
1.50 in	37.50	100.0	2	32.0	28.9	0.0280	96.2
0.75 in	19.00	100.0	4	31.3	28.2	0.0200	93.9
0.375 in	9.50	100.0	8	30.8	27.7	0.0142	92.2
NO.4	4.75	100.0	15	29.9	26.8	0.0105	89.2
10	2.00	100.0	30	28.9	25.8	0.0076	85.9
20	850um	100.0	60	27.5	24.4	0.0054	81.2
40	425um	100.0	120	26.1	23.0	0.0039	76.5
60	250um	99.5	240	24.6	21.5	0.0028	71.5
100	150um	98.7	356	23.6	20.5	0.0023	68.2
200	75um	97.7	1467	20.9	17.8	0.0012	59.2

% GRAVEL	% SAND	% SILT	% CLAY
	2	18	80

PARTICLE SIZE ANALYSIS OF SOIL A.S.T.M. D-422

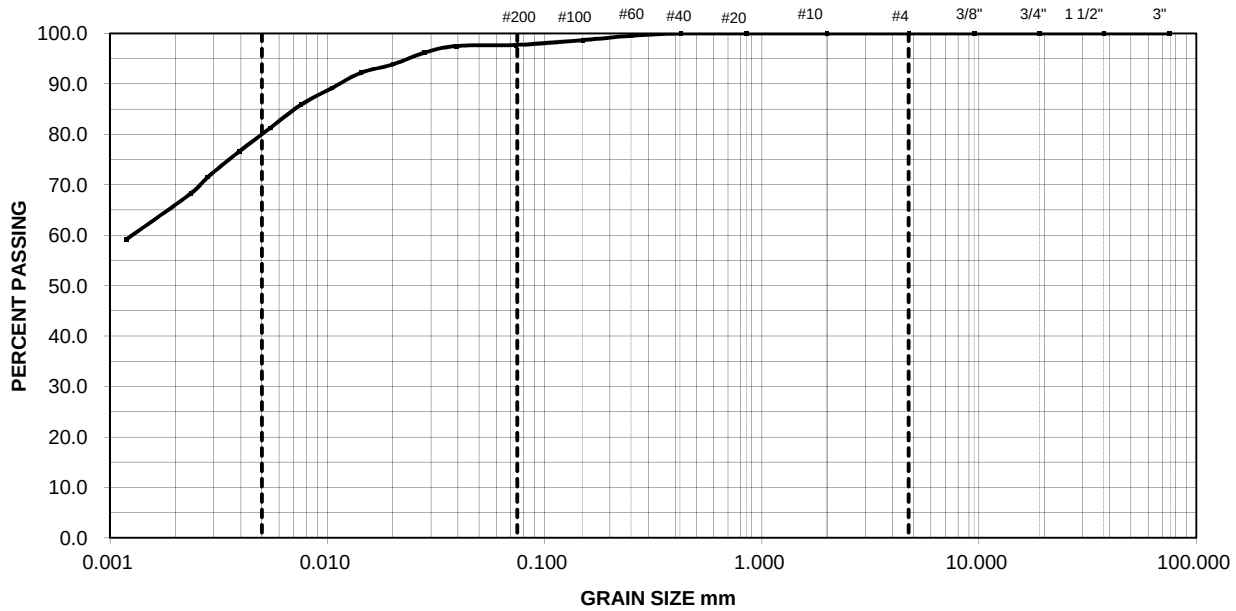

MANITOBA INFRASTRUCTURE and TRANSPORTATION
MATERIALS ENGINEERING BRANCH - CENTRAL LAB

PARTICLE SIZE ANALYSIS of SOILS - ASTM D 422

PROJECT: PTH 5 - South Grade Slope Slide **Technician:**
LOCATION: PTH 5 - 0.5km West of PTH 10 Ashville Junction **Checked By:** GK

LAB.NO. WGT110493 FIELD NO. B25 HOLE NO. SI/VW-2011-02 DEPTH (m) 7.01-7.32

SIEVE ANALYSIS			HYDROMETER ANALYSIS				
SIEVE U.S. STANDARD	DIAMETER (mm)	% PASSING	TIME MINUTES	HYDROMETER READING R_O	HYDROMETER READING R_C	DIAMETER (mm)	% PASSING
3.00	75.0	100.0	1	54.2	49.9	0.0350	98%
1.50	37.5	100.0	2	53.3	49.0	0.0250	96%
0.75	19.0	100.0	4	52.8	48.5	0.0178	95%
0.375	9.5	100.0	8	52.0	47.7	0.0128	93%
#4	4.75	100.0	15	50.0	45.7	0.0095	89%
#10	2.00	100.0	30	48.0	43.7	0.0068	86%
#20	0.850	100.0	60	44.3	40.0	0.0050	78%
#40	0.425	100.0	120	42.0	37.7	0.0036	74%
#60	0.250	100.0	240	40.0	35.7	0.0026	70%
#100	0.150	100.0	360	37.5	33.2	0.0019	65%
#200	0.075	100.0	1440	33.1	28.8	0.0011	56%

% GRAVEL	% SAND	% SILT	% CLAY
0	0	24	76

PARTICLE SIZE ANALYSIS OF SOIL A.S.T.M. D-422

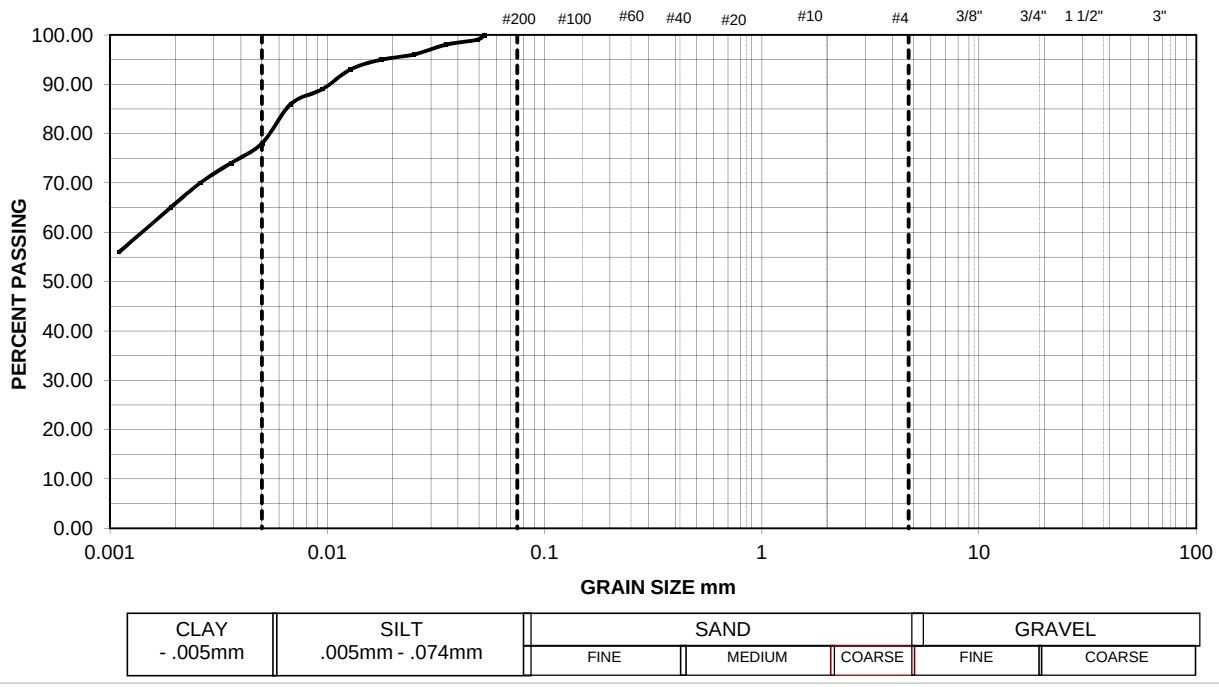

MANITOBA INFRASTRUCTURE and TRANSPORTATION

MATERIALS ENGINEERING BRANCH

CENTRAL LAB

PARTICLE SIZE ANALYSIS of SOILS A.S.T.M. D-422

PROJECT: PTH 5 - South Grade Slope Slide — **TESTED BY:** P.M.
LOCATION: PTH 5 - 0.5km West of PTH 10 Ashville Junction — **CHECKED:** G.J.

LAB.NO. WGT110504 FIELD NO. T36 HOLE NO. VW-2011-04 DEPTH (m) 3.05-3.35

SIEVE ANALYSIS			HYDROMETER ANALYSIS				
SIEVE U.S. STANDARD	DIAMETER (mm)	% PASSING	TIME MINUTES	HYDROMETER READING R_O	HYDROMETER READING R_C	DIAMETER (mm)	% PASSING
3.00 in	75.00	100.0	1	27.0	23.9	0.0424	75.7
1.50 in	37.50	100.0	2	26.5	23.4	0.0302	74.1
0.75 in	19.00	100.0	4	25.5	22.4	0.0216	71.0
0.375 in	9.50	99.7	8	24.4	21.3	0.0155	67.5
NO.4	4.75	98.8	15	23.2	20.1	0.0115	63.7
10	2.00	98.0	30	22.2	19.1	0.0082	60.5
20	850um	97.2	60	20.7	17.6	0.0059	55.7
40	425um	95.9	120	19.3	16.2	0.0042	51.3
60	250um	89.6	240	17.4	14.3	0.0031	45.3
100	150um	83.3	360	16.2	13.1	0.0025	41.5
200	75um	80.2	1471	13.8	10.7	0.0013	33.9

% GRAVEL	% SAND	% SILT	% CLAY
1	19	27	53

PARTICLE SIZE ANALYSIS OF SOIL A.S.T.M. D-422

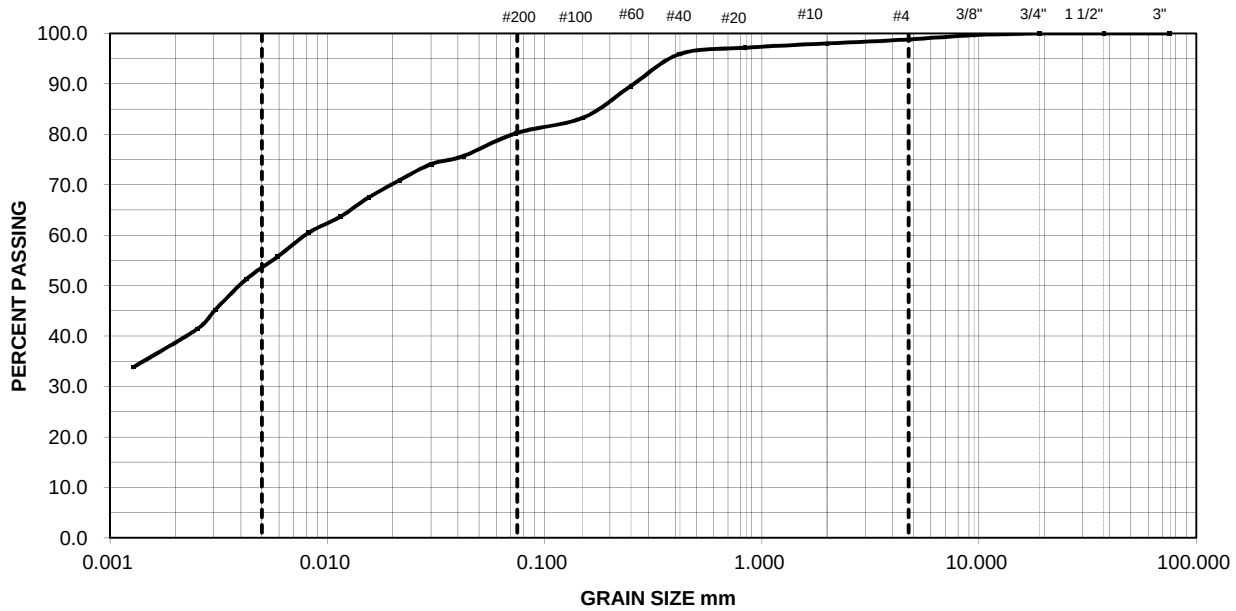

CLAY	SILT	SAND			GRAVEL	
- .005mm	.005mm - .074mm	FINE	MEDIUM	COARSE	FINE	COARSE

MANITOBA INFRASTRUCTURE and TRANSPORTATION

MATERIALS ENGINEERING BRANCH

CENTRAL LAB

PARTICLE SIZE ANALYSIS of SOILS A.S.T.M. D-422

PROJECT: PTH 5 - South Grade Slope Slide — **TESTED BY:** J.H.,P.M.
LOCATION: PTH 5 - 0.5km West of PTH 10 Ashville Junction — **CHECKED:** G.J.

LAB.NO. WGT110762 FIELD NO. T1 HOLE NO. SI/VW-2011-01 DEPTH (m) 3.05-3.66

SIEVE ANALYSIS			HYDROMETER ANALYSIS				
SIEVE U.S. STANDARD	DIAMETER (mm)	% PASSING	TIME MINUTES	HYDROMETER READING R_O	HYDROMETER READING R_C	DIAMETER (mm)	% PASSING
3.00 in	75.00	100.0	1	15.4	12.5	0.0483	39.9
1.50 in	37.50	100.0	2	14.1	11.2	0.0346	35.7
0.75 in	19.00	100.0	4	14.0	11.1	0.0245	35.4
0.375 in	9.50	100.0	8	13.2	10.3	0.0174	32.8
NO.4	4.75	100.0	15	13.1	10.2	0.0127	32.5
10	2.00	100.0	30	12.1	9.2	0.0091	29.3
20	850um	99.9	60	11.4	8.5	0.0065	27.1
40	425um	98.4	120	10.6	7.7	0.0046	24.5
60	250um	83.8	240	9.9	7.0	0.0033	22.3
100	150um	54.9	416	9.4	6.5	0.0025	20.7
200	75um	48.3	1550	8.3	5.4	0.0013	17.2

% GRAVEL	% SAND	% SILT	% CLAY
	52	23	25

PARTICLE SIZE ANALYSIS OF SOIL A.S.T.M. D-422

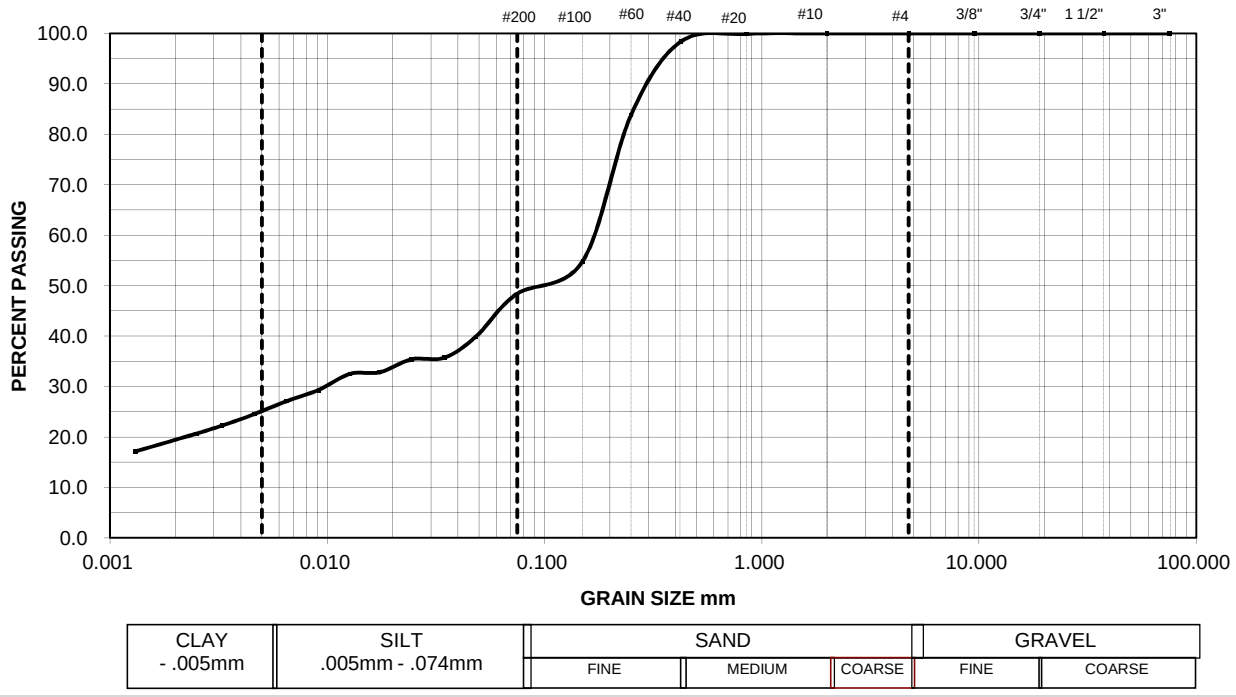

MANITOBA INFRASTRUCTURE and TRANSPORTATION
MATERIALS ENGINEERING BRANCH - CENTRAL LAB

PARTICLE SIZE ANALYSIS of SOILS - ASTM D 422

PROJECT: PTH 5 - South Grade Slope Slide **Technician:** JF
LOCATION: PTH 5 - 0.5km West of PTH 10 Ashville Junction **Checked By:**

LAB.NO. WGT110493 FIELD NO. T2 HOLE NO. SI/VW-2011-02 DEPTH (m) 7.01-7.32

SIEVE ANALYSIS			HYDROMETER ANALYSIS				
SIEVE U.S. STANDARD	DIAMETER (mm)	% PASSING	TIME MINUTES	HYDROMETER READING R_O	HYDROMETER READING R_C	DIAMETER (mm)	% PASSING
3.00	75.0	Not Tested	1	40.5	37.4	0.0342	82%
1.50	37.5	Not Tested	2	39.5	36.4	0.0247	78%
0.75	19.0	Not Tested	4	39.0	35.9	0.0176	75%
0.375	9.5	Not Tested	8	38.8	35.7	0.0125	73%
#4	4.75	Not Tested	15	38.3	35.2	0.0092	72%
#10	2.00	Not Tested	30	37.2	34.1	0.0066	71%
#20	0.850	Not Tested	60	35.8	32.7	0.0048	70%
#40	0.425	Not Tested	120	32.9	29.8	0.0036	68%
#60	0.250	Not Tested	240	28.2	25.1	0.0027	65%
#100	0.150	Not Tested	360	20.5	17.4	0.0024	60%
#200	0.075	Not Tested	1440	11.1	8.0	0.0013	50%

% GRAVEL	% SAND	% SILT	% CLAY
0	18	16	66

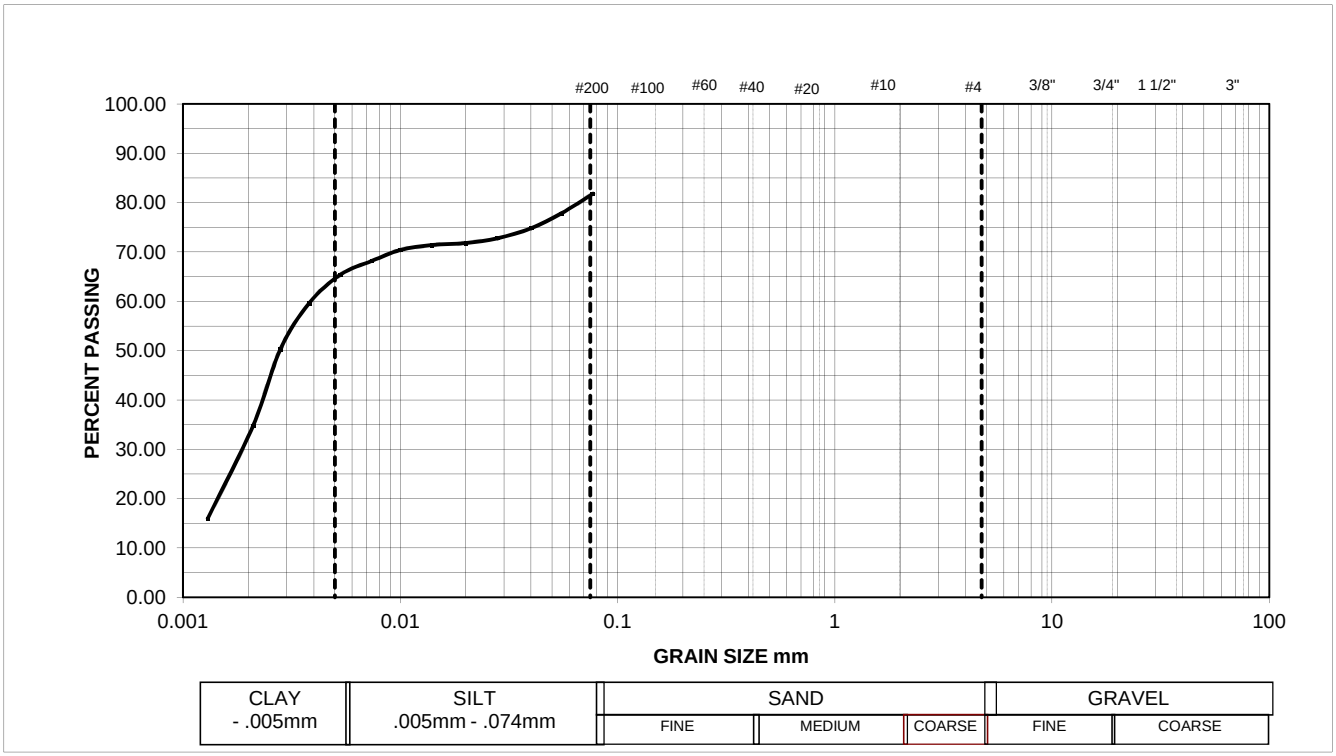

MANITOBA INFRASTRUCTURE and TRANSPORTATION

MATERIALS ENGINEERING BRANCH

CENTRAL LABORATORY

PARTICLE SIZE ANALYSIS of SOILS A.S.T.M. D-422

PROJECT: PTH 5 - South Grade Slope Slide — **TESTED BY:** M.J.
LOCATION: PTH 5 - 0.5km West of PTH 10 Ashville Junction — **CHECKED:** G.J.

LAB.NO. WGT110764 FIELD NO. T3 HOLE NO. SI/VW-2011-05 DEPTH (m) 5.18-5.78

SIEVE ANALYSIS			HYDROMETER ANALYSIS				
SIEVE U.S. STANDARD	DIAMETER (mm)	% PASSING	TIME MINUTES	HYDROMETER READING R_O	HYDROMETER READING R_C	DIAMETER (mm)	% PASSING
3.00 in	75.00	100.0	1	30.1	27.5	0.0404	86.5
1.50 in	37.50	100.0	2	28.8	26.2	0.0291	82.4
0.75 in	19.00	100.0	4	28.2	25.6	0.0208	80.5
0.375 in	9.50	100.0	8	27.3	24.7	0.0149	77.6
NO.4	4.75	99.9	15	27.0	24.4	0.0109	76.7
10	2.00	99.0	30	25.5	22.9	0.0078	72.0
20	850um	98.9	60	23.8	21.2	0.0057	66.6
40	425um	98.8	120	22.2	19.6	0.0041	61.6
60	250um	98.2	240	20.1	17.5	0.0030	55.0
100	150um	96.9	427	18.2	15.6	0.0023	49.0
200	75um	96.1	1472	15.5	12.9	0.0013	40.5

% GRAVEL	% SAND	% SILT	% CLAY
0	4	32	64

PARTICLE SIZE ANALYSIS OF SOIL A.S.T.M. D-422

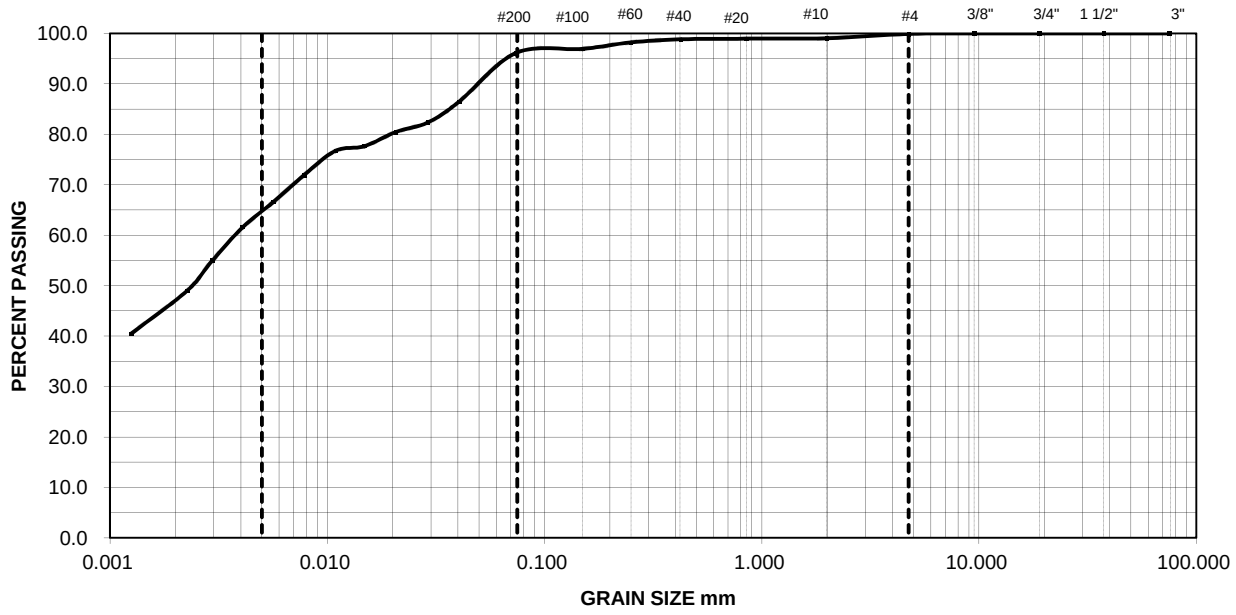

CLAY	SILT	SAND			GRAVEL	
- .005mm	.005mm - .074mm	FINE	MEDIUM	COARSE	FINE	COARSE

MANITOBA INFRASTRUCTURE and TRANSPORTATION

MATERIALS ENGINEERING BRANCH

CENTRAL LABORATORY

PARTICLE SIZE ANALYSIS of SOILS A.S.T.M. D-422

PROJECT: PTH 5 - South Grade Slope Slide — **TESTED BY:** M.J.
LOCATION: PTH 5 - 0.5km West of PTH 10 Ashville Junction — **CHECKED:** G.J.

LAB.NO. WGT110765 FIELD NO. T4 HOLE NO. SI/VW-2011-05 DEPTH (m) 5.79-6.39

SIEVE ANALYSIS			HYDROMETER ANALYSIS				
SIEVE U.S. STANDARD	DIAMETER (mm)	% PASSING	TIME MINUTES	HYDROMETER READING R_O	HYDROMETER READING R_C	DIAMETER (mm)	% PASSING
3.00 in	75.00	100.0	1	33.5	30.9	0.0384	98.4
1.50 in	37.50	100.0	2	33.0	30.4	0.0274	96.8
0.75 in	19.00	100.0	4	32.7	30.1	0.0195	95.9
0.375 in	9.50	100.0	8	32.1	29.5	0.0139	94.0
NO.4	4.75	100.0	15	31.4	28.8	0.0102	91.7
10	2.00	100.0	30	29.5	26.9	0.0074	85.7
20	850um	100.0	60	27.8	25.2	0.0054	80.2
40	425um	100.0	120	25.6	23.0	0.0039	73.2
60	250um	99.8	240	23.2	20.6	0.0029	65.6
100	150um	99.5	422	20.9	18.3	0.0022	58.2
200	75um	99.1	1468	17.6	15.0	0.0012	47.7

% GRAVEL	% SAND	% SILT	% CLAY
	1	21	78

PARTICLE SIZE ANALYSIS OF SOIL A.S.T.M. D-422

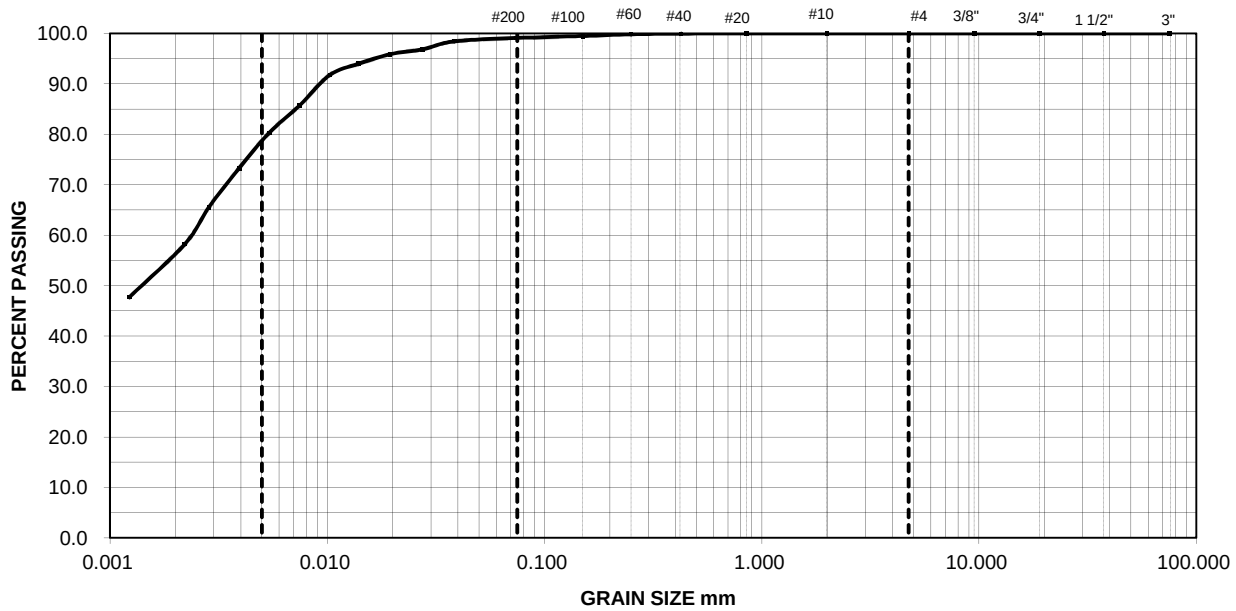

CLAY	SILT	SAND			GRAVEL	
- .005mm	.005mm - .074mm	FINE	MEDIUM	COARSE	FINE	COARSE

MANITOBA INFRASTRUCTURE and TRANSPORTATION

MATERIALS ENGINEERING BRANCH

CENTRAL LABORATORY

PARTICLE SIZE ANALYSIS of SOILS A.S.T.M. D-422

PROJECT: PTH 5 - South Grade Slope Slide — **TESTED BY:** M.J.
LOCATION: PTH 5 - 0.5km West of PTH 10 Ashville Junction — **CHECKED:** G.J.

LAB.NO. WGT110766 FIELD NO. T5 HOLE NO. SI/VW-2011-05 DEPTH (m) 6.40-7.00

SIEVE ANALYSIS			HYDROMETER ANALYSIS				
SIEVE U.S. STANDARD	DIAMETER (mm)	% PASSING	TIME MINUTES	HYDROMETER READING R_O	HYDROMETER READING R_C	DIAMETER (mm)	% PASSING
3.00 in	75.00	100.0	1	33.6	31.0	0.0384	98.4
1.50 in	37.50	100.0	2	33.5	30.9	0.0272	98.1
0.75 in	19.00	100.0	4	33.4	30.8	0.0192	97.8
0.375 in	9.50	100.0	8	32.7	30.1	0.0138	95.5
NO.4	4.75	99.9	15	32.0	29.4	0.0102	93.3
10	2.00	99.4	30	30.8	28.2	0.0073	89.5
20	850um	99.4	60	28.8	26.2	0.0053	83.1
40	425um	99.4	120	26.6	24.0	0.0039	76.1
60	250um	99.3	240	23.9	21.3	0.0028	67.6
100	150um	99.0	438	21.4	18.8	0.0022	59.6
200	75um	98.6	1440	17.4	14.8	0.0012	46.9

% GRAVEL	% SAND	% SILT	% CLAY
0	1	18	81

PARTICLE SIZE ANALYSIS OF SOIL A.S.T.M. D-422

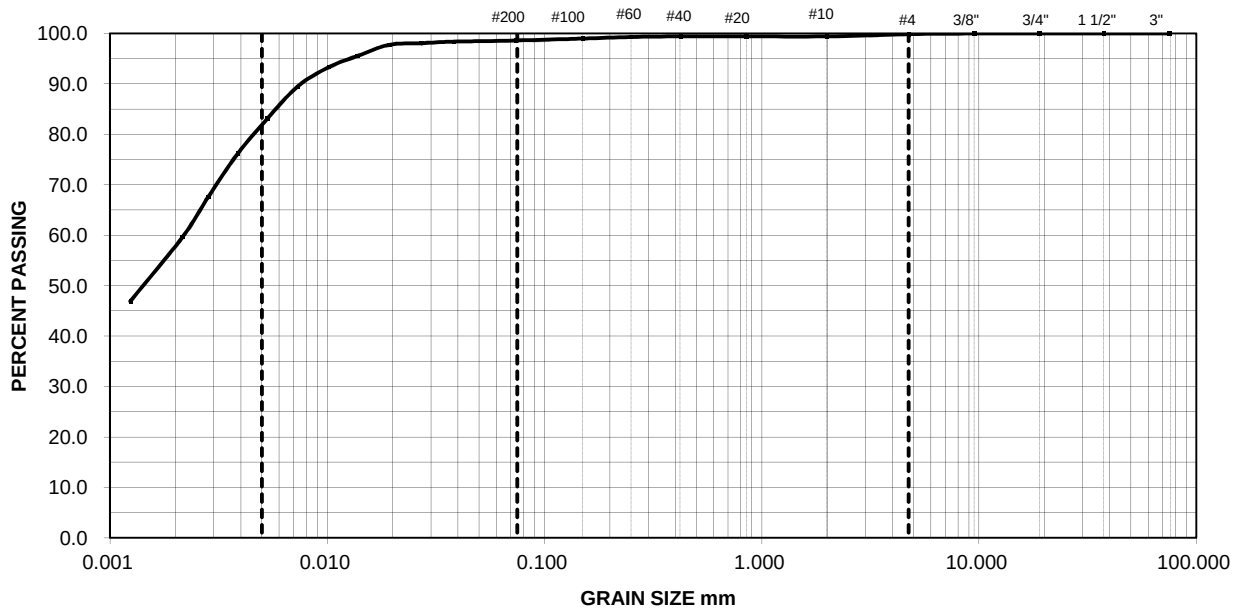

CLAY	SILT	SAND			GRAVEL	
- .005mm	.005mm - .074mm	FINE	MEDIUM	COARSE	FINE	COARSE

MANITOBA INFRASTRUCTURE and TRANSPORTATION

MATERIALS ENGINEERING BRANCH

CENTRAL LAB

PARTICLE SIZE ANALYSIS of SOILS A.S.T.M. D-422

PROJECT: PTH 5 - South Grade Slope Slide — **TESTED BY:** J.H.,P.M.
LOCATION: PTH 5 - 0.5km West of PTH 10 Ashville Junction — **CHECKED:** G.J.

LAB.NO. WGT110771 FIELD NO. T7 HOLE NO. SI/VW-2011-02 DEPTH (m) 3.05-3.50

SIEVE ANALYSIS			HYDROMETER ANALYSIS				
SIEVE U.S. STANDARD	DIAMETER (mm)	% PASSING	TIME MINUTES	HYDROMETER READING R_O	HYDROMETER READING R_C	DIAMETER (mm)	% PASSING
3.00 in	75.00	100.0	1	30.8	27.9	0.0402	86.6
1.50 in	37.50	100.0	2	29.8	26.9	0.0288	83.5
0.75 in	19.00	100.0	4	29.2	26.3	0.0206	81.6
0.375 in	9.50	98.9	8	28.1	25.2	0.0148	78.2
NO.4	4.75	97.6	15	27.1	24.2	0.0109	75.1
10	2.00	96.7	30	26.0	23.1	0.0078	71.7
20	850um	96.1	60	24.3	21.4	0.0057	66.4
40	425um	95.1	120	22.8	19.9	0.0041	61.7
60	250um	92.9	240	21.1	18.2	0.0029	56.4
100	150um	89.9	420	20.0	17.1	0.0022	53.0
200	75um	86.9	1552	17.2	14.3	0.0012	44.3

% GRAVEL	% SAND	% SILT	% CLAY
2	11	22	65

PARTICLE SIZE ANALYSIS OF SOIL A.S.T.M. D-422

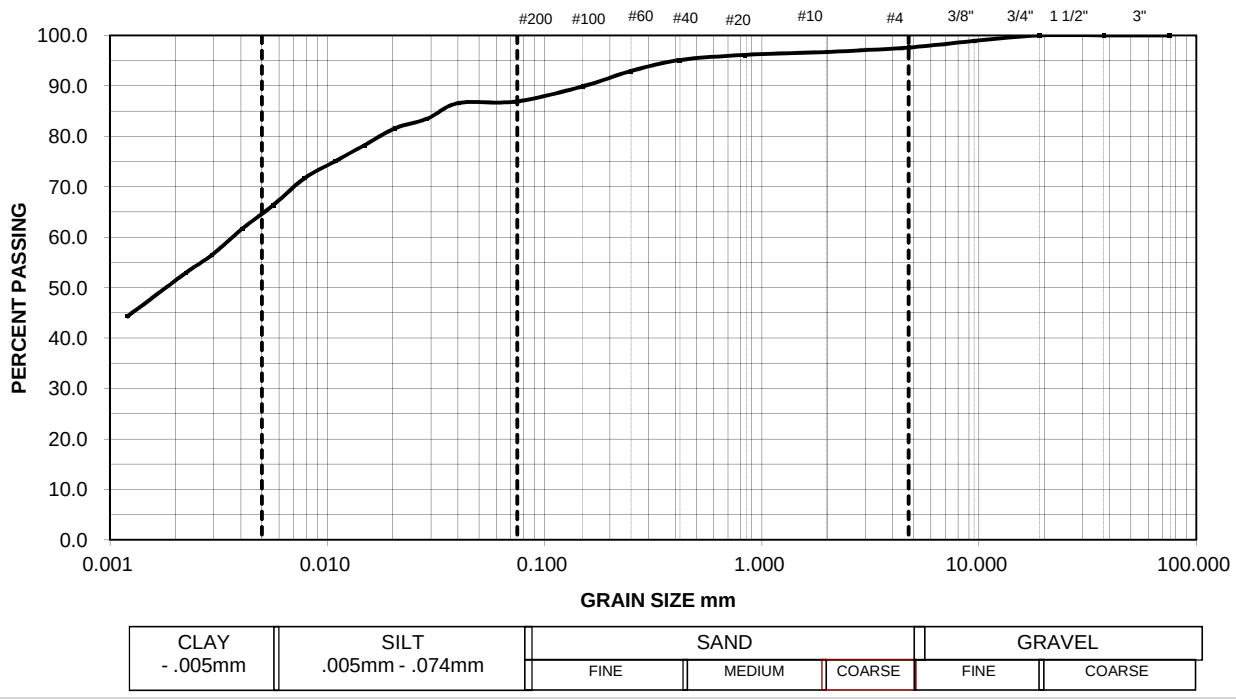

MANITOBA INFRASTRUCTURE and TRANSPORTATION
MATERIALS ENGINEERING BRANCH - CENTRAL LAB

PARTICLE SIZE ANALYSIS of SOILS - ASTM D 422

PROJECT: PTH 5 - South Grade Slope Slide **Technician:** JF
LOCATION: PTH 5 - 0.5km West of PTH 10 Ashville Junction **Checked By:**

LAB.NO. N/A FIELD NO. T8 HOLE NO. SI/VW2011-06 DEPTH (m) 3.9m

SIEVE ANALYSIS			HYDROMETER ANALYSIS				
SIEVE U.S. STANDARD	DIAMETER (mm)	% PASSING	TIME MINUTES	HYDROMETER READING R_O	HYDROMETER READING R_C	DIAMETER (mm)	% PASSING
3.00	75.0	100.0	1	46.8	43.8	0.0370	94%
1.50	37.5	100.0	2	45.5	42.5	0.0264	91%
0.75	19.0	100.0	4	44.0	41.0	0.0190	87%
0.375	9.5	100.0	8	42.0	39.0	0.0137	85%
#4	4.75	100.0	15	40.3	37.3	0.0101	82%
#10	2.00	100.0	30	37.0	34.0	0.0073	78%
#20	0.850	100.0	60	34.9	31.9	0.0053	74%
#40	0.425	Not Tested	120	32.1	29.1	0.0038	68%
#60	0.250	Not Tested	240	30.1	27.1	0.0027	64%
#100	0.150	Not Tested	360	27.1	24.1	0.0020	58%
#200	0.075	Not Tested	1440	24.3	21.3	0.0012	54%

% GRAVEL	% SAND	% SILT	% CLAY
0	6	31	63

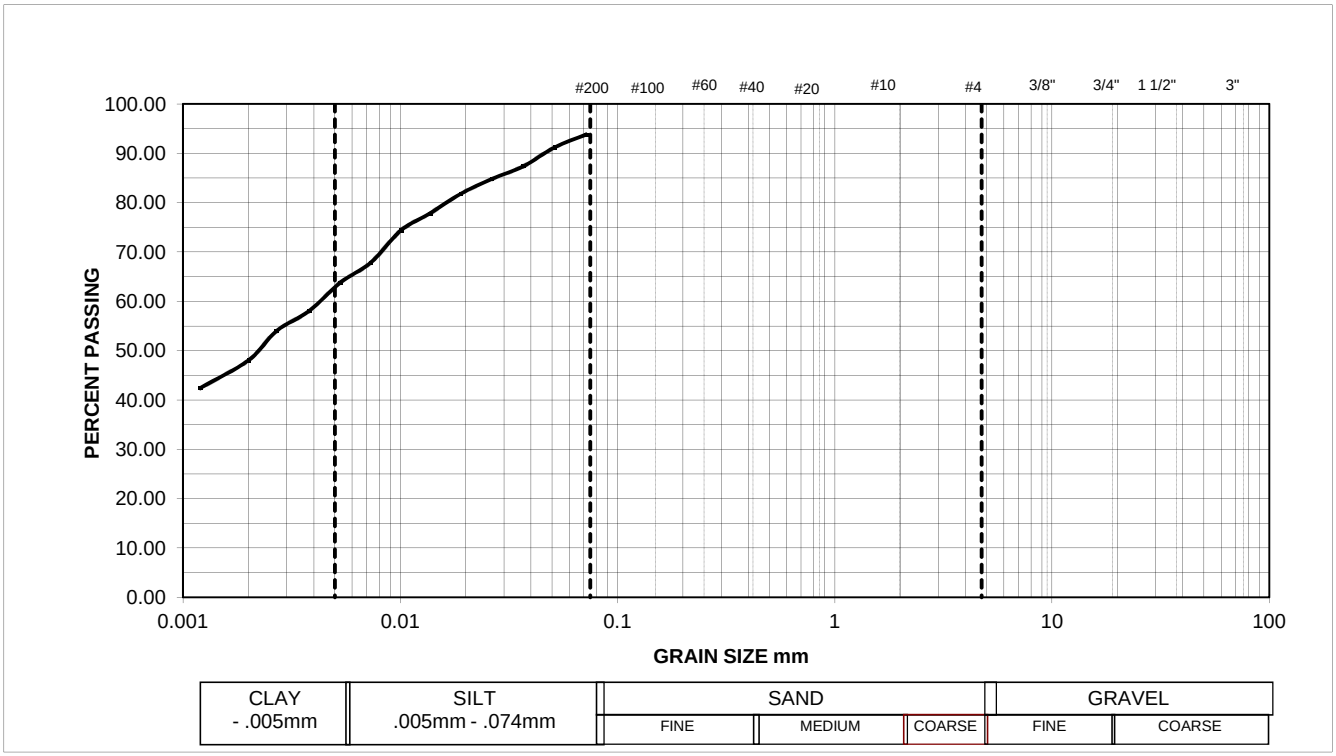

MANITOBA INFRASTRUCTURE and TRANSPORTATION

MATERIALS ENGINEERING BRANCH

CENTRAL LABORATORY

PARTICLE SIZE ANALYSIS of SOILS A.S.T.M. D-422

PROJECT: PTH 5 - South Grade Slope Slide — **TESTED BY:** M.J.
LOCATION: PTH 5 - 0.5km West of PTH 10 Ashville Junction — **CHECKED:** G.J.

LAB.NO. WGT110772 FIELD NO. T8 HOLE NO. SI/VW-2011-06 DEPTH (m) 3.66-4.06

SIEVE ANALYSIS			HYDROMETER ANALYSIS				
SIEVE U.S. STANDARD	DIAMETER (mm)	% PASSING	TIME MINUTES	HYDROMETER READING R_O	HYDROMETER READING R_C	DIAMETER (mm)	% PASSING
3.00 in	75.00	100.0	1	28.5	25.6	0.0415	78.9
1.50 in	37.50	100.0	2	27.5	24.6	0.0297	75.8
0.75 in	19.00	100.0	4	26.0	23.1	0.0214	71.2
0.375 in	9.50	97.4	8	25.0	22.1	0.0153	68.1
NO.4	4.75	96.5	15	23.9	21.0	0.0114	64.7
10	2.00	94.9	30	22.5	19.6	0.0082	60.4
20	850um	93.1	60	21.0	18.1	0.0059	55.8
40	425um	91.2	120	19.6	16.7	0.0042	51.5
60	250um	87.8	240	18.1	15.2	0.0030	46.9
100	150um	83.2	450	16.0	13.1	0.0023	40.4
200	75um	80.0	1500	14.9	12.0	0.0013	37.0

% GRAVEL	% SAND	% SILT	% CLAY
3	16	26	55

PARTICLE SIZE ANALYSIS OF SOIL A.S.T.M. D-422

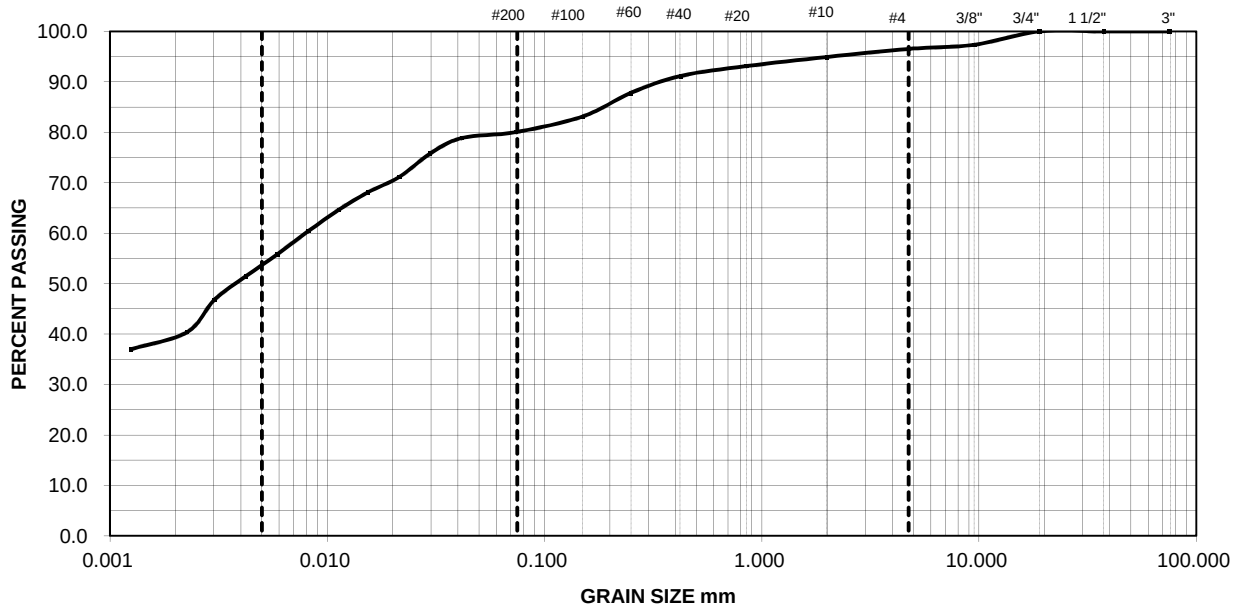

CLAY	SILT	SAND			GRAVEL	
- .005mm	.005mm - .074mm	FINE	MEDIUM	COARSE	FINE	COARSE

MANITOBA INFRASTRUCTURE and TRANSPORTATION

MATERIALS ENGINEERING BRANCH

CENTRAL LAB

PARTICLE SIZE ANALYSIS of SOILS A.S.T.M. D-422

PROJECT: PTH 5 - South Grade Slope Slide — **TESTED BY:** J.H.,P.M.
LOCATION: PTH 5 - 0.5km West of PTH 10 Ashville Junction — **CHECKED:** G.J.

LAB.NO. WGT110773 FIELD NO. T9 HOLE NO. SI/VW-2011-02 DEPTH (m) 4.27-4.62

SIEVE ANALYSIS			HYDROMETER ANALYSIS				
SIEVE U.S. STANDARD	DIAMETER (mm)	% PASSING	TIME MINUTES	HYDROMETER READING R_O	HYDROMETER READING R_C	DIAMETER (mm)	% PASSING
3.00 in	75.00	100.0	1	29.0	26.1	0.0412	84.4
1.50 in	37.50	100.0	2	28.0	25.1	0.0295	81.2
0.75 in	19.00	100.0	4	27.0	24.1	0.0212	77.9
0.375 in	9.50	100.0	8	26.0	23.1	0.0152	74.7
NO.4	4.75	100.0	15	24.8	21.9	0.0112	70.8
10	2.00	100.0	30	23.3	20.4	0.0081	65.9
20	850um	100.0	60	21.8	18.9	0.0058	61.1
40	425um	100.0	120	20.3	17.4	0.0042	56.2
60	250um	96.0	240	19.0	16.1	0.0030	52.0
100	150um	90.9	412	18.0	15.1	0.0023	48.8
200	75um	86.5	1546	15.3	12.4	0.0012	40.0

% GRAVEL	% SAND	% SILT	% CLAY
	14	28	58

PARTICLE SIZE ANALYSIS OF SOIL A.S.T.M. D-422

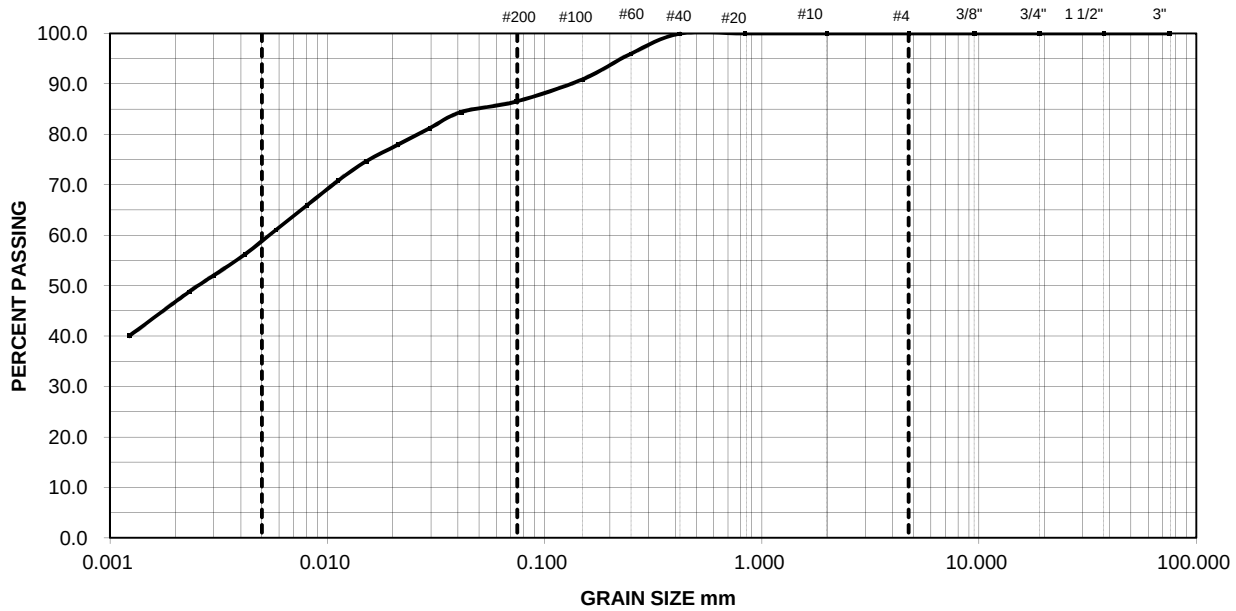

CLAY	SILT	SAND			GRAVEL	
- .005mm	.005mm - .074mm	FINE	MEDIUM	COARSE	FINE	COARSE

MANITOBA INFRASTRUCTURE and TRANSPORTATION

MATERIALS ENGINEERING BRANCH

CENTRAL LABORATORY

PARTICLE SIZE ANALYSIS of SOILS A.S.T.M. D-422

PROJECT: PTH 5 - South Grade Slope Slide — **TESTED BY:**
LOCATION: PTH 5 - 0.5km West of PTH 10 Ashville Junction — **CHECKED:**

LAB.NO. WGT110490 FIELD NO. T22 HOLE NO. SI/VW-2011-02 DEPTH (m) 4.72-5.07

SIEVE ANALYSIS			HYDROMETER ANALYSIS				
SIEVE U.S. STANDARD	DIAMETER (mm)	% PASSING	TIME MINUTES	HYDROMETER READING R_O	HYDROMETER READING R_C	DIAMETER (mm)	% PASSING
3.00 in	75.00	100.0	1	26.3	23.2	0.0428	69.7
1.50 in	37.50	100.0	2	25.4	22.3	0.0306	67.0
0.75 in	19.00	97.2	4	25.0	21.9	0.0218	65.8
0.375 in	9.50	95.9	8	24.1	21.0	0.0156	63.1
NO.4	4.75	94.6	15	23.3	20.2	0.0115	60.7
10	2.00	93.2	30	22.7	19.6	0.0082	58.9
20	850um	92.3	60	21.5	18.4	0.0059	55.3
40	425um	90.8	120	20.0	16.9	0.0042	50.8
60	250um	84.5	240	18.3	15.2	0.0030	45.7
100	150um	77.2	347	17.3	14.2	0.0025	42.6
200	75um	72.9	1459	15.1	12.0	0.0013	36.0

% GRAVEL	% SAND	% SILT	% CLAY
5	22	20	53

PARTICLE SIZE ANALYSIS OF SOIL A.S.T.M. D-422

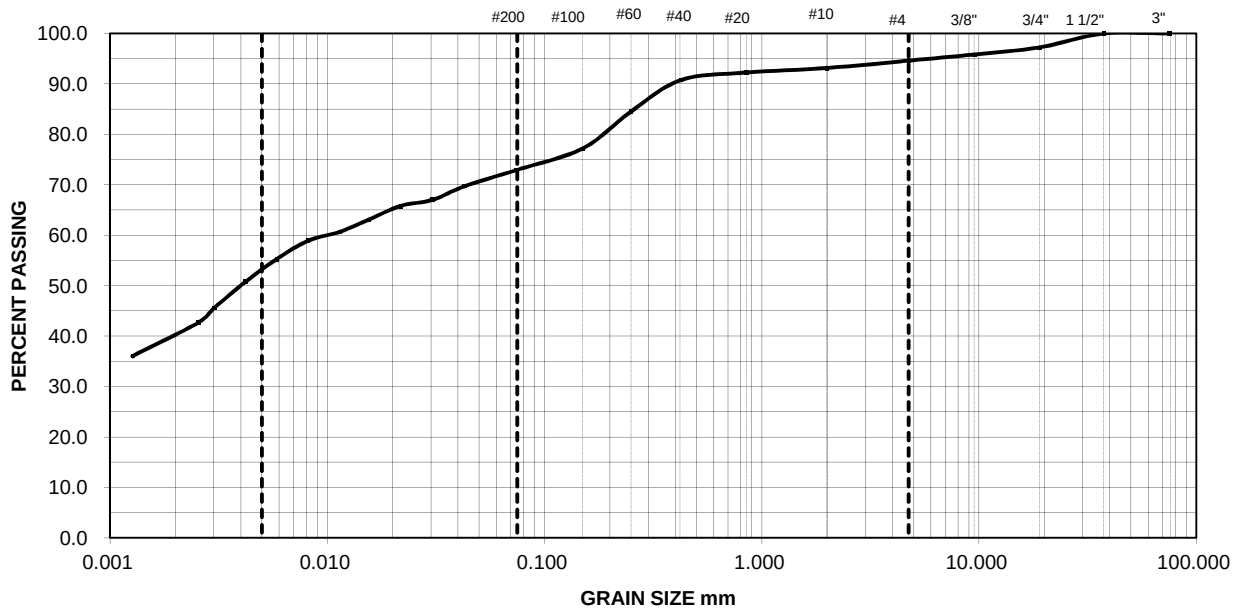

CLAY	SILT	SAND			GRAVEL	
- .005mm	.005mm - .074mm	FINE	MEDIUM	COARSE	FINE	COARSE

MANITOBA INFRASTRUCTURE AND TRANSPORTATION
MATERIALS ENGINEERING BRANCH
CENTRAL LAB - WINNIPEG

HYDRAULIC CONDUCTIVITY OF SATURATED SOILS USING A FLEX WALL PERMEAMETER

Client:	Region 4	**Report To:**	Jery Zihrul, Jeff Tallin, Jeremy Fiebelkorn
Project:	PTH 5 South Grade Slope Slide	**Project #**	2010-4G
Location/Plan:	0.5 km West of PTH 10	**Internal Order #**	200034112
Date Sampled:	2012-06-08	**Lab #:**	WGT110771-773
Sampled By:	Ken Kalynuk	**Hole #**	2011-06
Date Started:	2012-07-16	**Field Sample #:**	T7, T8, T9
Date Finished:	2012-09-17	**Depth (m):**	3.05-4.88
Tested By:	KH, GK	**Date Reported:**	2012-10-05

Sample Moisture Content	**Start**	**End**
Mass Tare and Sample Wet (g)	231.2	359.58
Mass Tare and Sample Dry (g)	210.1	292.1
Mass of Water (g)	21.1	67.5
Mass of Tare (g)	105.8	53.12
Mass Dry Sample (g)	104.3	238.9
Moisture Content (%)	20.2	28.3
Sample Weight	**Start**	**End**
	592.43	628.1
Sample Dimensions	**Start**	**End**
Sample Diameter (cm)	7.27	7.43
Sample Height (cm)	7.31	7.31
Sample Area (cm^2)	41.52	43.40
Volume (cm^3)	303.67	317.13
Specific Gravity (assumed)	2.70	2.70
Volume of Solids (cm^3)	182.55	181.37
Volume of Voids (cm^3)	121.12	135.76
Void Ratio	0.66	0.75
Degree of Saturation	82.18	101.95
Dry Density (kg/m^3)	1623	1544

Moisture Density Proctor Results	
Maximum Dry Density (kg/m3):	1621
Optimum Moisture Content (%):	20.8

Test Parameters		
Liquid Used	Deaired Water	
Cell Pressure (kPa)	379.21	(55 psi)
Back Pressure (kPa)	344.74	(50 psi)
Hydraulic Gradient	10.00	
Effective Stress (kPa)	34.48	
Max., effluent end (psi)	50.00	
Max., effluent end (kPa)	344.74	
Min., influent end (psi)	51.00	
Min., influent end (kPa)	351.63	

Classification Results:	
Liquid Limit (%):	56
Plastic Limit (%):	25
Plasticity Index:	31
Gravel %:	3
Sand (%):	13
Silt (%):	21
Clay (%):	63
Unified Classification:	CH

Temp (^oC)	Time (minutes)	In Flow (cm^3)	Out Flow (cm^3)	Hydraulic Head (cm)	K (cm/sec)	K_{20} (cm/sec)
19	1400	1.52	1.37	70.3	4.31E-08	4.57E-08
19	1490	1.40	1.39	70.3	3.91E-08	4.15E-08
19	1443	1.26	1.29	70.3	3.69E-08	3.91E-08
19	1423	1.62	1.52	70.3	4.61E-08	4.89E-08
					Average Permeability	**4.38E-08 (cm/sec)**

Remarks: Field samples T7, T8 and T9 were combined for this test. A Moisture Density (proctor) test was performed to determine the maximum dry density and optimum moisture content. A sample was prepared at the optimum moisture content from which a Hydraulic Conductivity test specimen was obtained.

Per: *Gord Konzelman*

LOG P' - ε_v CURVE

Test Frame Number =	**3**	
Load Multiplication Factor =	**11**	
Specimen Diameter	**63.29**	**mm**
# of Load Increments =	**9**	
# of Unloading Points =	**2**	

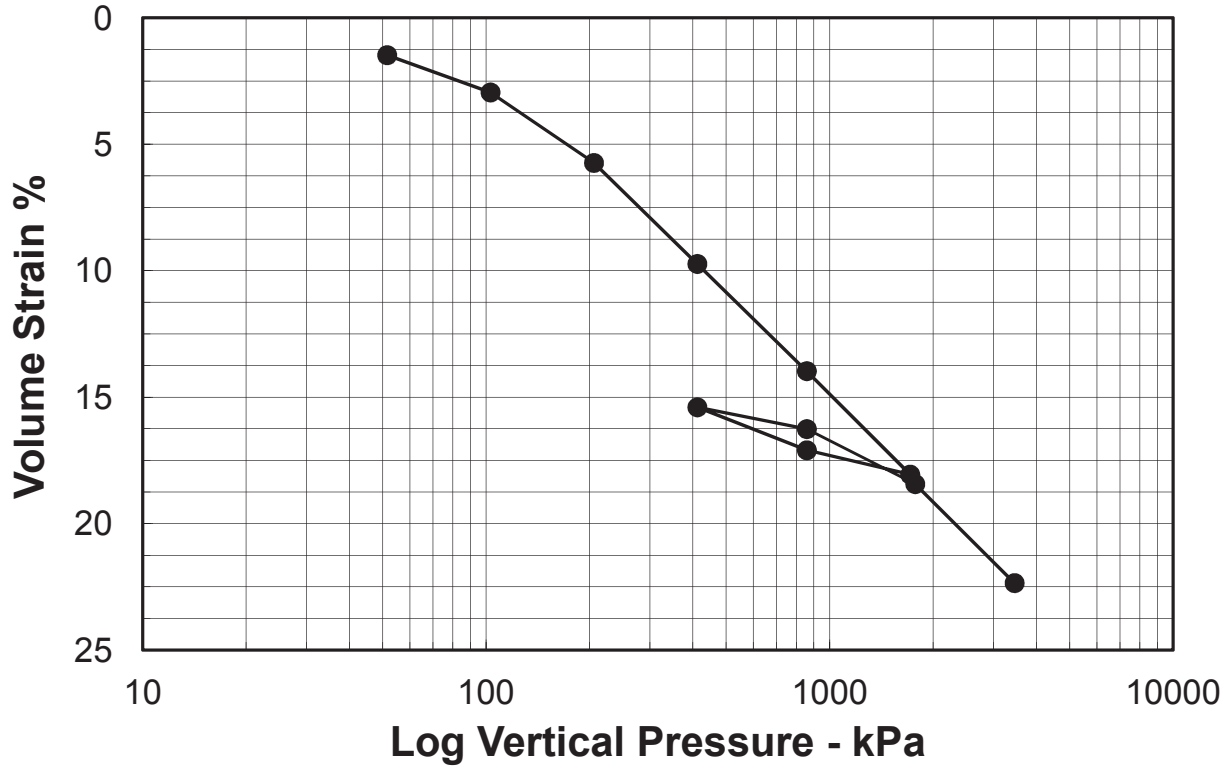

Client:	Region 4		
Project:	PTH 5 & 10 Grade Slope Failure		
Sample #	T7	**Hole #**	SI/VW-2011-06
Location:	Dauphin, Mb	**Depth:**	3.25m
Technician:	J. Fiebelkorn	**Date:**	12-Jan-12

σ' - εv CURVE

Test Frame Number =	**3**	
Load Multiplication Factor =	**11**	
Specimen Diameter	**63.29**	**mm**
# of Load Increments =	**9**	
# of Unloading Points =	**2**	

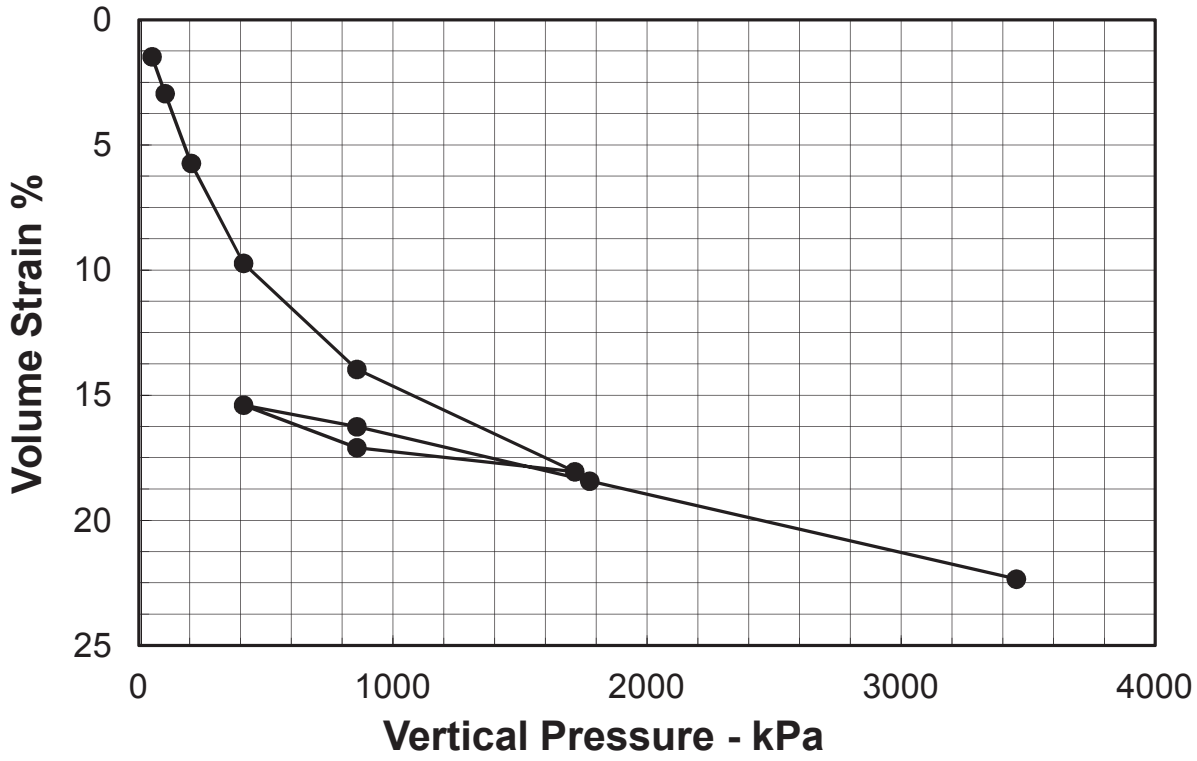

Client:	Region 4		
Project:	PTH 5 & 10 Grade Slope Failure		
Sample #	T7	**Hole #**	SI/VW-2011-06
Location:	Dauphin, Mb	**Depth:**	3.25m
Technician:	J. Fiebelkorn	**Date:**	12-Jan-12

GEOTECHNICAL LABORATORY

DEPARTMENT OF CIVIL AND

GEOLOGICAL ENGINEERING

UNIVERSITY OF MANITOBA

Winnipeg, MB R3T 5V6

Telephone # 474 - 9241

LOG P' - e CURVE

Test Frame Number =	**3**	
Load Multiplication Factor =	**11**	
Specimen Diameter	**63.29**	**mm**
# of Load Increments =	**9**	
# of Unloading Points =	**2**	

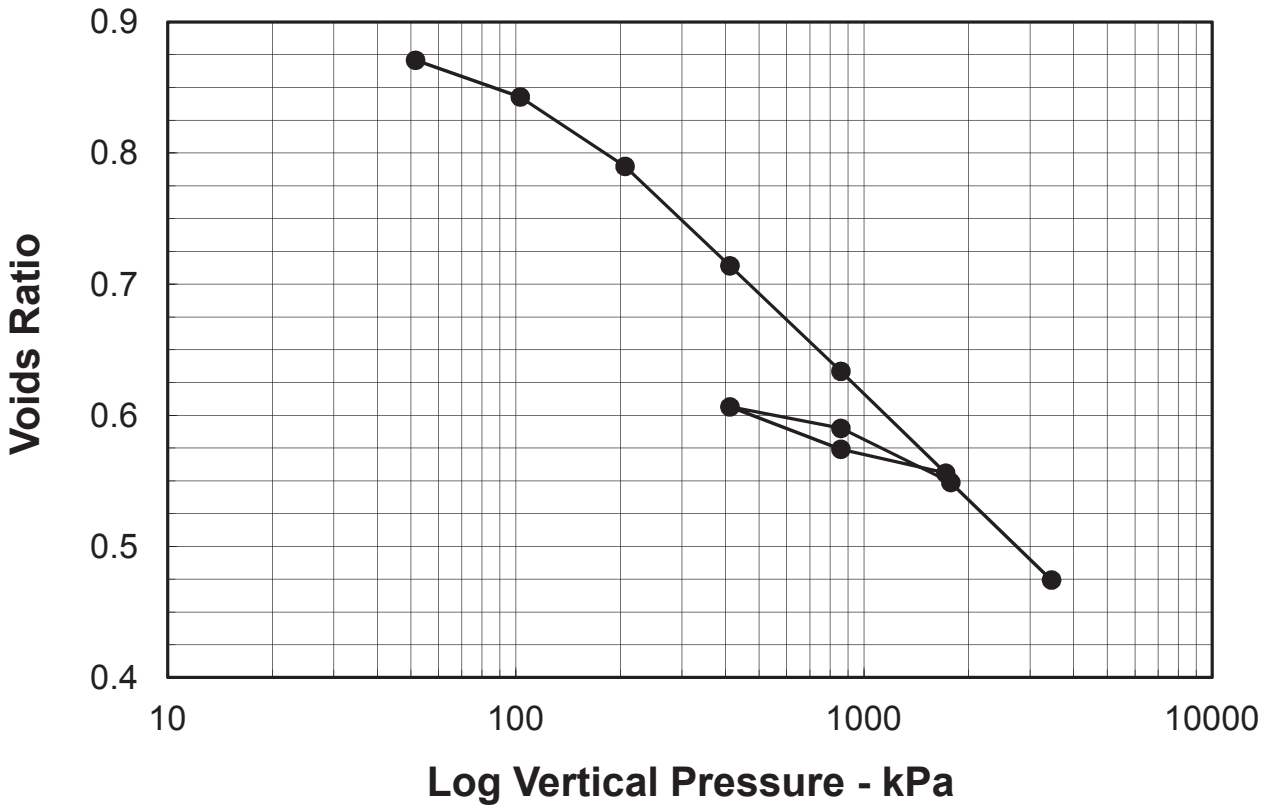

Client:	Region 4		
Project:	PTH 5 & 10 Grade Slope Failure		
Sample #	T7	**Hole #**	SI/VW-2011-06
Location:	Dauphin, Mb	**Depth:**	3.25m
Technician:	J. Fiebelkorn	**Date:**	12-Jan-12

GEOTECHNICAL LABORATORY

DEPARTMENT OF CIVIL AND

GEOLOGICAL ENGINEERING

UNIVERSITY OF MANITOBA

Winnipeg, MB R3T 5V6

Telephone # 474 - 9241

SUMMARY DATA SHEET - CONSOLIDATION TEST RESULTS

Client:	Region 4	**Ring # =**	3		**Initial Bulk Density =**	1.84	Mg/m^3
Project:	PTH 5 & 10 Grade Slope Failure	**Load Frame # =**	3		**Final Bulk Density =**	2.20	Mg/m^3
Location:	Dauphin, Mb	**Dead Load =**	474.51	g	**Initial Dry Density =**	1.43	Mg/m^3
Hole #	SI/VW-2011-06	**Ring Height =**	19.85	mm	**Final Dry Density =**	1.78	Mg/m^3
Sample #	T7	**Ring Diameter =**	63.29	mm	**Height of Solids, Hs =**	7.95	mm
Depth:	3.25m	**Ring Area =**	3.15E-03	m^2	**Volume of Solids =**	2.52E-05	m^3
Sample Description:	Clay till, silty, trace sand, trace gravel,	**Initial Water Content =**	28.5%		**Initial Saturation =**	86.2%	
	trace silt inclusions, trace gypsum, brown	**Final Water Content =**	23.3%		**Final Saturation =**	120.1%	
	moist, firm to stiff, intermediate to high plastic	**Gs =**	2.72		**Initial Voids Ratio =**	0.899	
Lab No.					**Final Voids Ratio =**	0.527	
Technician:	J. Fiebelkorn **Date:** 2012-01-11						

Date mm/dd/yr	Scale Load N	Applied Pressure kPa	Final Dial mm	Total Dial Change mm	Final Height mm	Average Height H_{avg}, mm	D = H_{avg} / 2 mm	Change in Voids Ratio Δe	Voids Ratio e	Average Voids Ratio e_{avg}	t_{90} s	Coeff of Cons. c_v, m2 / s	Hydraulic Conductivity k, m / s
Loading													
01-12-12	0	0	8.666		18.723		9.361	0.000	0.899	0.899			
01-12-12	14.72	51.47	8.390	0.276	18.447	18.585	9.292	0.035	0.864	0.881	9.6	7.6E-06	2.7E-08
01-12-12	29.43	102.91	8.114	0.552	18.171	18.309	9.154	0.069	0.829	0.847	25.4	2.8E-06	9.8E-09
01-12-12	58.86	205.82	7.568	1.099	17.624	17.897	8.949	0.138	0.761	0.795	43.4	1.6E-06	5.4E-09
01-12-12	117.72	411.64	6.845	1.822	16.901	17.263	8.631	0.229	0.670	0.715	60.0	1.1E-06	2.4E-09
01-12-12	245.25	857.58	6.051	2.615	16.108	16.504	8.252	0.329	0.570	0.620	117.6	4.9E-07	5.7E-10
01-12-12	490.50	1715.17	5.285	3.381	15.342	15.725	7.862	0.425	0.473	0.522	540.0	9.7E-08	5.6E-11
01-12-12	987.47	3452.97	4.482	4.184	14.539	14.940	7.470	0.527	0.372	0.423	600.0	7.9E-08	2.4E-11
Unloading													
01-12-12	245.25	857.58	5.465	3.201	15.522	15.432	7.716	0.403	0.496	0.485			
01-12-12	117.72	411.64	5.784	2.883	15.840	15.681	7.840	0.363	0.536	0.516			

LOG P' - εv CURVE

Test Frame Number =	**2**	
Load Multiplication Factor =	**11**	
Specimen Diameter	**63.54**	**mm**
# of Load Increments =	**9**	
# of Unloading Points =	**2**	

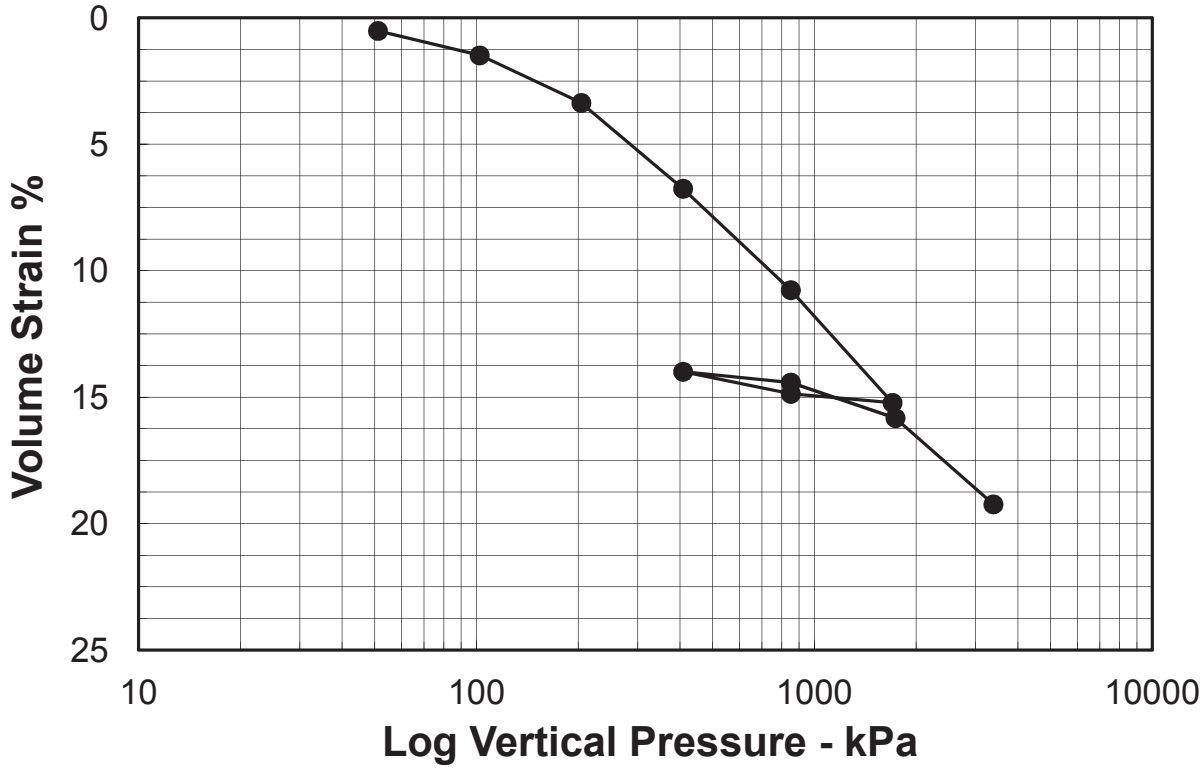

Client:	Region 4		
Project:	PTH 5 & 10 Grade Slope Failure		
Sample #	T8	**Hole #**	SI/VW-2011-06
Location:	Dauphin, Mb	**Depth:**	3.80m
Technician:	J. Fiebelkorn	**Date:**	12-Jan-12

LOG P' - e CURVE

Test Frame Number =	**2**	
Load Multiplication Factor =	**11**	
Specimen Diameter	**63.54**	**mm**
# of Load Increments =	**9**	
# of Unloading Points =	**2**	

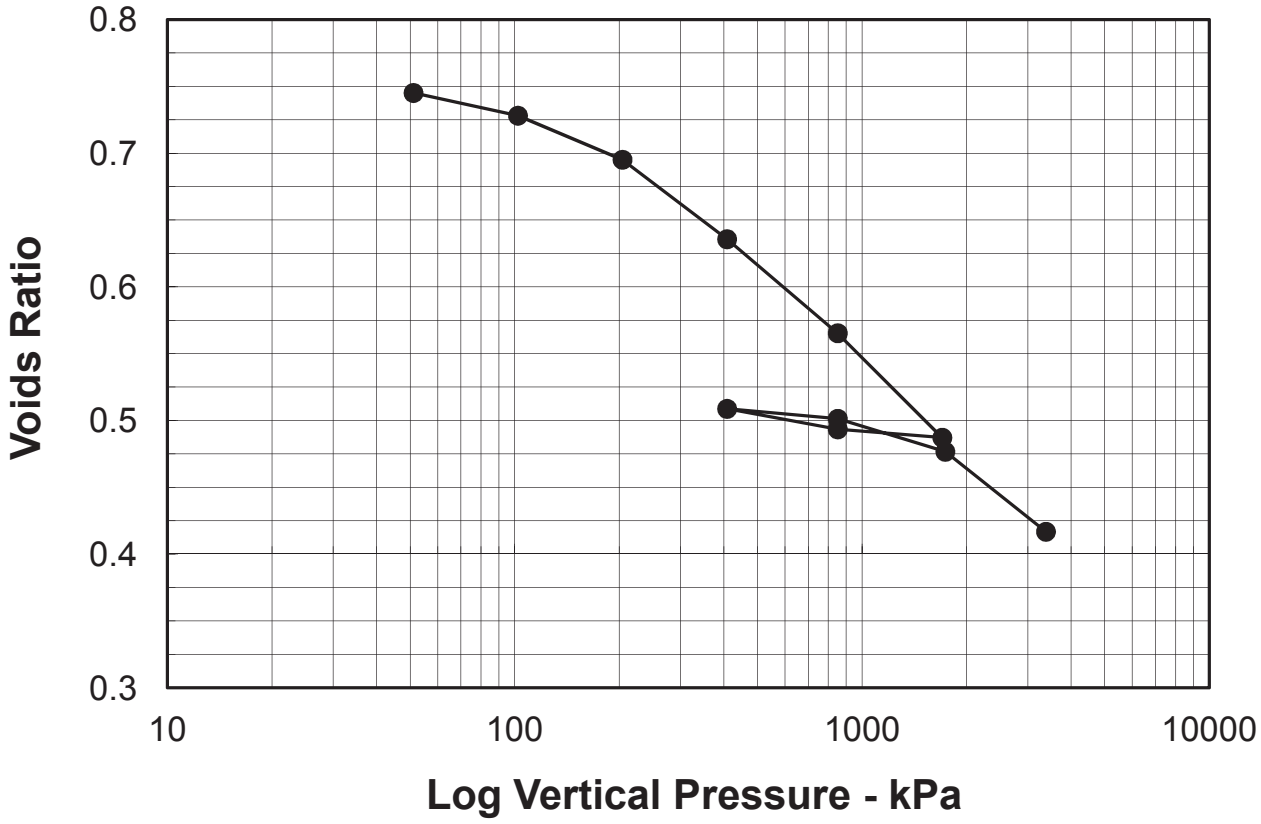

Client:	Region 4		
Project:	PTH 5 & 10 Grade Slope Failure		
Sample #	T8	**Hole #**	SI/VW-2011-06
Location:	Dauphin, Mb	**Depth:**	3.80m
Technician:	J. Fiebelkorn	**Date:**	=

σ' - εv CURVE

Test Frame Number =	**2**	
Load Multiplication Factor =	**11**	
Specimen Diameter	**63.54**	**mm**
# of Load Increments =	**9**	
# of Unloading Points =	**2**	

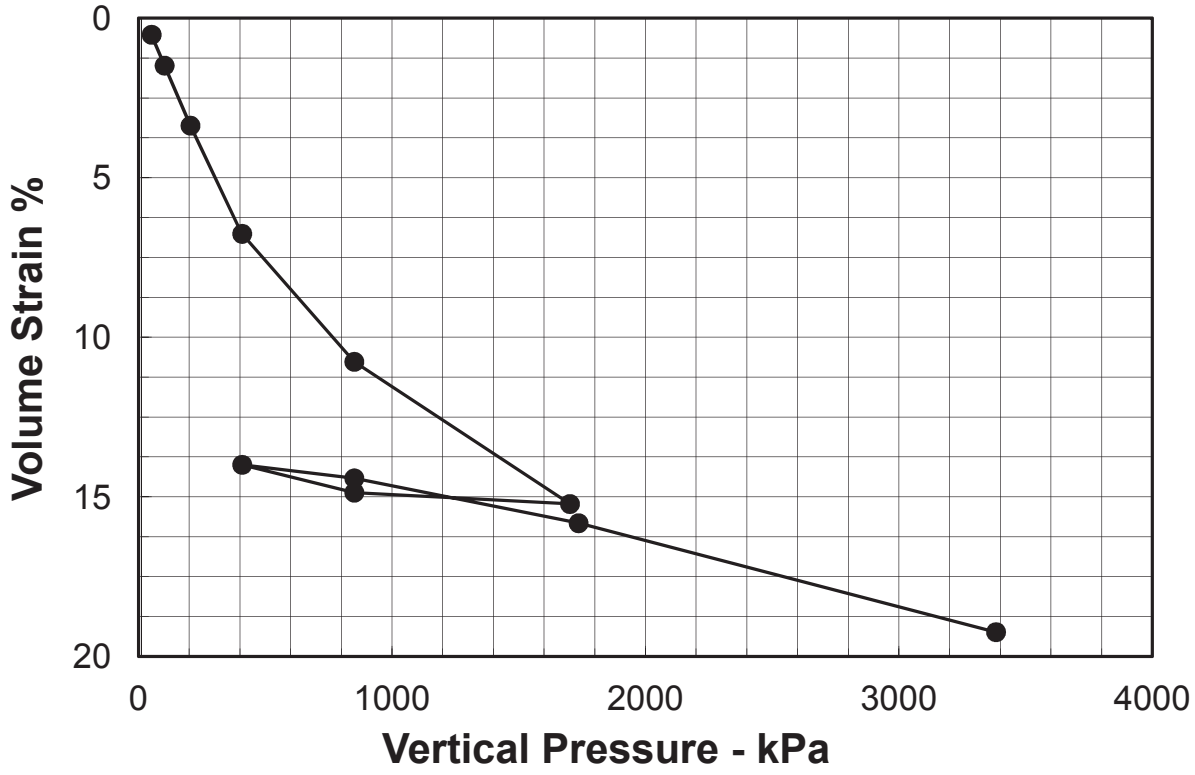

Client:	Region 4		
Project:	PTH 5 & 10 Grade Slope Failure		
Sample #	T8	**Hole #**	SI/VW-2011-06
Location:	Dauphin, Mb	**Depth:**	3.80m
Technician:	J. Fiebelkorn	**Date:**	12-Jan-12

SUMMARY DATA SHEET - CONSOLIDATION TEST RESULTS

Client:	Region 4	**Ring # =**	2		**Initial Bulk Density =**	1.96	Mg/m^3
Project:	PTH 5 & 10 Grade Slope Failure	**Load Frame # =**	2		**Final Bulk Density =**	2.29	Mg/m^3
Location:	Dauphin, Mb	**Dead Load =**	474.51	g	**Initial Dry Density =**	1.55	Mg/m^3
Hole #	SI/VW-2011-06	**Ring Height =**	19.91	mm	**Final Dry Density =**	1.94	Mg/m^3
Sample #	T8	**Ring Diameter =**	63.54	mm	**Height of Solids, Hs =**	7.95	mm
Depth:	3.80m	**Ring Area =**	3.17E-03	m^2	**Volume of Solids =**	2.52E-05	m^3
Sample Description:	Clay till, silty, trace sand, trace gravel,	**Initial Water Content =**	26.2%		**Initial Saturation =**	94.4%	
	trace silt inclusions, trace gypsum, brown	**Final Water Content =**	18.1%		**Final Saturation =**	122.4%	
	moist, firm to stiff, intermediate to high plastic	**Gs =**	2.72		**Initial Voids Ratio =**	0.754	
Lab No.					**Final Voids Ratio =**	0.403	
Technician:	J. Fiebelkorn **Date:** 2012-01-11						

Date mm/dd/yr	Scale Load N	Applied Pressure kPa	Final Dial mm	Total Dial Change mm	Final Height mm	Average Height H_{avg}, mm	D = H_{avg} / 2 mm	Change in Voids Ratio Δe	Voids Ratio e	Average Voids Ratio e_{avg}	t_{90} s	Coeff of Cons. c_v, m2 / s	Hydraulic Conductivity k, m / s
Loading													
01-12-12	0	0	8.750		18.783		9.391	0.000	0.754	0.754			
01-12-12	14.72	51.06	8.653	0.097	18.686	18.734	9.367	0.012	0.742	0.748	5.4	1.4E-05	1.8E-08
01-12-12	29.43	102.09	8.471	0.279	18.504	18.595	9.297	0.035	0.719	0.731	21.6	3.4E-06	8.5E-09
01-12-12	58.86	204.19	8.096	0.654	18.129	18.316	9.158	0.082	0.672	0.696	48.6	1.5E-06	3.8E-09
01-12-12	117.72	408.37	7.481	1.269	17.514	17.821	8.911	0.160	0.595	0.633	72.6	9.3E-07	2.0E-09
01-12-12	245.25	850.78	6.728	2.022	16.761	17.137	8.569	0.254	0.500	0.547	93.8	6.6E-07	8.0E-10
01-12-12	490.50	1701.56	5.891	2.859	15.924	16.342	8.171	0.360	0.394	0.447	470.4	1.2E-07	8.3E-11
01-12-12	975.20	3383.00	5.137	3.613	15.170	15.547	7.773	0.455	0.300	0.347	960.0	5.3E-08	1.7E-11
Unloading													
01-12-12	245.25	850.78	5.958	2.792	15.991	15.957	7.979	0.351	0.403	0.399			
01-12-12	117.72	408.37	6.122	2.628	16.155	16.073	8.036	0.331	0.424	0.413			

Log p' - εv CURVE

Test Frame Number =	**1**	
Load Multiplication Factor =	**11**	
Specimen Diameter	**63.49**	**mm**
# of Load Increments =	**9**	
# of Unloading Points =	**2**	

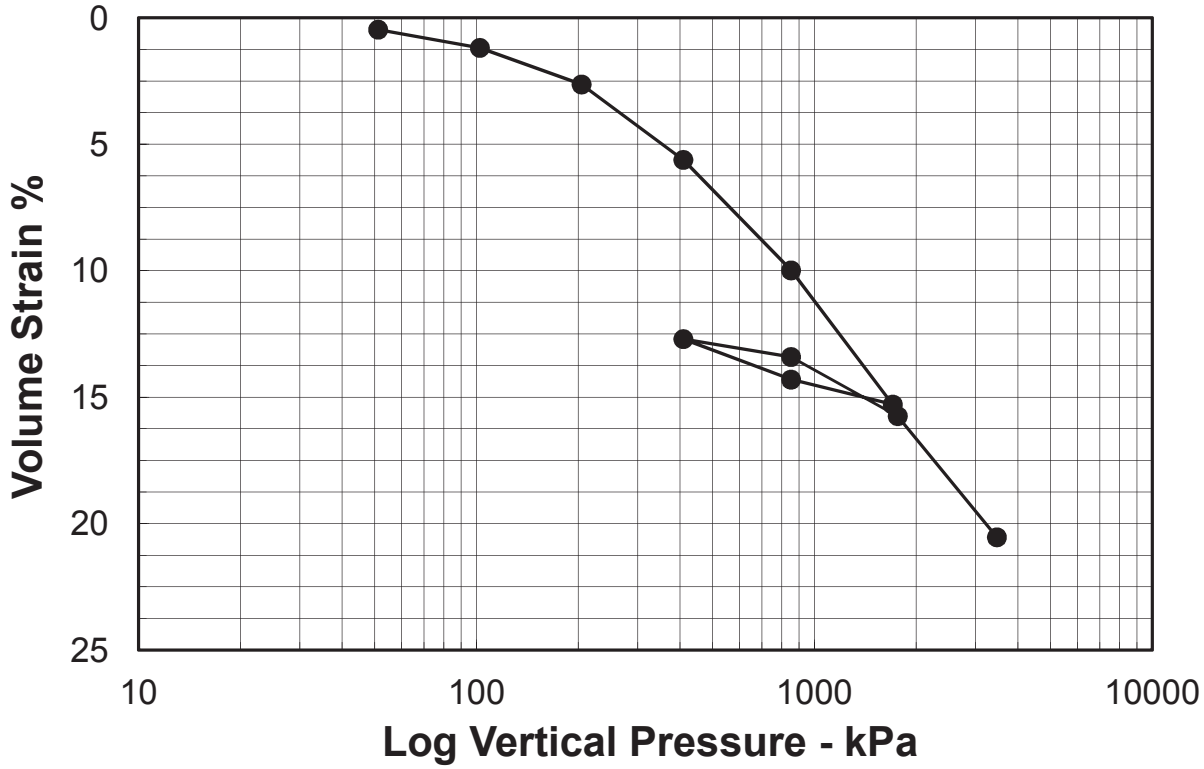

Client:	Region 4		
Project:	PTH 5 & 10 Slope Failure		
Sample #	T10	**Hole #**	SI/VW-2011-06
Location:	Dauphin, Mb	**Depth:**	5.05m
Technician:	J. Fiebelkorn	**Date:**	12-Jan-12

LOG P' - e CURVE

Test Frame Number =	**1**	
Load Multiplication Factor =	**11**	
Specimen Diameter	**63.49**	**mm**
# of Load Increments =	**9**	
# of Unloading Points =	**2**	

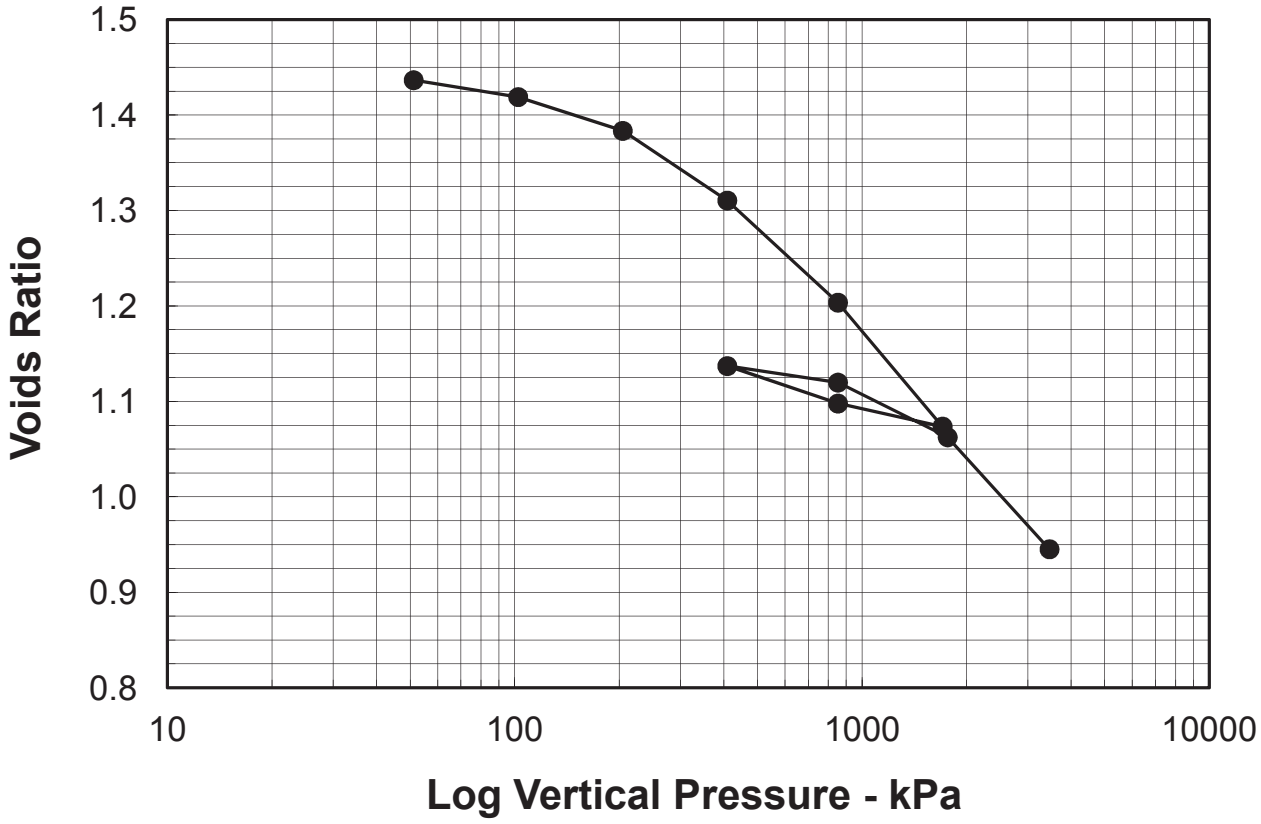

Client:	Region 4		
Project:	5 & 10 Slope Failure		
Sample #	T10	**Hole #**	SI/VW-2011-06
Location:	Dauphin, Mb	**Depth:**	5.05m
Technician:	J. Fiebelkorn	**Date:**	12-Jan-12

σ' - εv CURVE

Test Frame Number =	**1**	
Load Multiplication Factor =	**11**	
Specimen Diameter	**63.49**	**mm**
# of Load Increments =	**9**	
# of Unloading Points =	**2**	

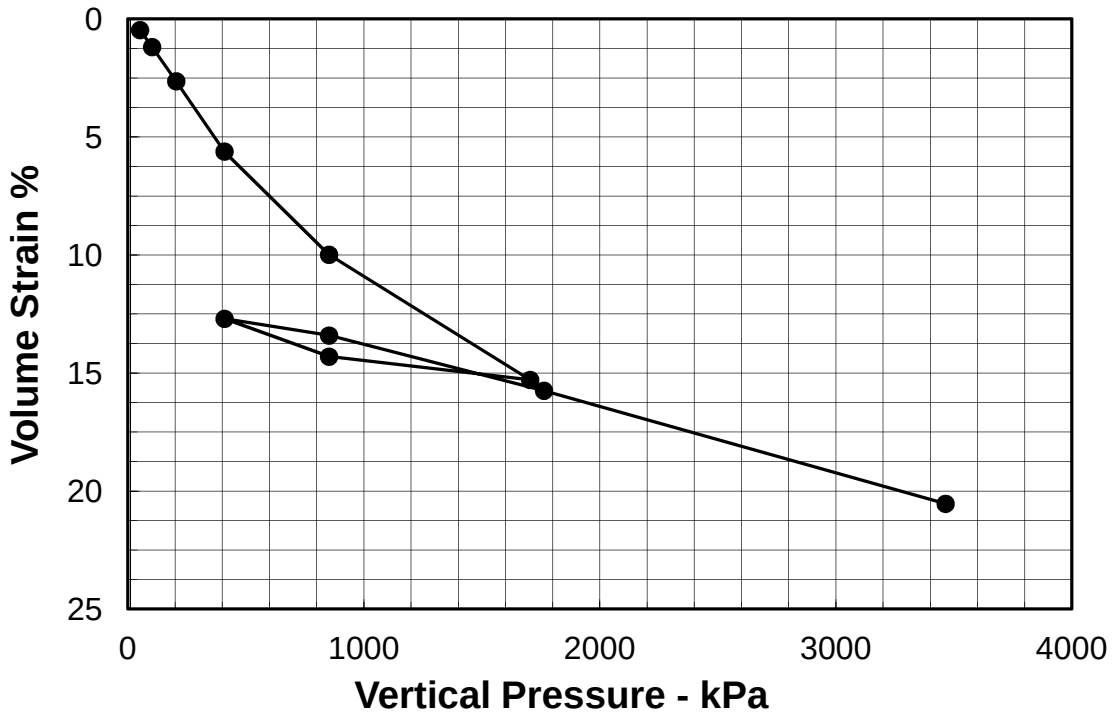

Client:	Region 4		
Project:	PTH 5 & 10 Slope Failure		
Sample #	T10	**Hole #**	SI/VW-2011-06
Location:	Dauphin, Mb	**Depth:**	5.05m
Technician:	J. Fiebelkorn	**Date:**	12-Jan-12

SUMMARY DATA SHEET - CONSOLIDATION TEST RESULTS

Client:	Region 4	**Ring # =**	1		**Initial Bulk Density =**	1.68	Mg/m^3
Project:	PTH 5 & 10 Slope Failure	**Load Frame # =**	1		**Final Bulk Density =**	1.93	Mg/m^3
Location:	Dauphin, Mb	**Dead Load =**	474.51	g	**Initial Dry Density =**	1.11	Mg/m^3
Hole #	SI/VW-2011-06	**Ring Height =**	19.94	mm	**Final Dry Density =**	1.38	Mg/m^3
Sample #	T10	**Ring Diameter =**	63.49	mm	**Height of Solids, Hs =**	7.95	mm
Depth:	5.05m	**Ring Area =**	3.17E-03	m^2	**Volume of Solids =**	2.52E-05	m^3
Sample Description:	Clay till, silty, trace sand, trace gravel,	**Initial Water Content =**	50.9%		**Initial Saturation =**	95.6%	
	trace silt inclusions, trace gypsum, brown	**Final Water Content =**	40.5%		**Final Saturation =**	112.7%	
	moist, firm to stiff, intermediate to high plastic,	**Gs =**	2.72		**Initial Voids Ratio =**	1.448	
Lab No.	mixed with yellow/white high plastic silt seam				**Final Voids Ratio =**	0.978	
Technician:	J. Fiebelkorn **Date:** 2012-01-11						

Date mm/dd/yr	Scale Load N	Applied Pressure kPa	Final Dial mm	Total Dial Change mm	Final Height mm	Average Height H_{avg}, mm	D = H_{avg} / 2 mm	Change in Voids Ratio Δe	Voids Ratio e	Average Voids Ratio e_{avg}	t_{90} s	Coeff of Cons. c_v, m2 / s	Hydraulic Conductivity k, m / s
Loading													
01-12-12	0	0	8.506		18.808		9.404	0.000	1.448	1.448			
01-12-12	14.72	51.12	8.419	0.088	18.720	18.764	9.382	0.011	1.437	1.442	15.0	5.0E-06	4.3E-09
01-12-12	29.43	102.25	8.283	0.223	18.585	18.652	9.326	0.028	1.420	1.428	25.4	2.9E-06	3.9E-09
01-12-12	58.86	204.49	8.002	0.505	18.303	18.444	9.222	0.063	1.385	1.402	43.4	1.7E-06	2.3E-09
01-12-12	117.72	408.99	7.450	1.056	17.752	18.027	9.014	0.133	1.315	1.350	79.4	8.7E-07	1.2E-09
01-12-12	245.25	852.05	6.628	1.878	16.930	17.341	8.670	0.236	1.212	1.263	583.8	1.1E-07	1.0E-10
01-12-12	490.50	1704.11	5.631	2.876	15.932	16.431	8.215	0.362	1.086	1.149	1552.3	3.7E-08	2.2E-11
01-12-12	997.18	3464.43	4.644	3.863	14.945	15.439	7.719	0.486	0.962	1.024	5440.5	9.3E-09	2.6E-12
Unloading													
01-12-12	245.25	852.05	5.816	2.690	16.118	16.025	8.012	0.339	1.109	1.098			
01-12-12	117.72	408.99	6.118	2.389	16.419	16.268	8.134	0.301	1.147	1.128			

GEOTECHNICAL LABORATORY
DEPARTMENT OF CIVIL AND GEOLOGICAL ENGINEERING
UNIVERSITY OF MANITOBA
Winnipeg, MB R3T 5V6
Telephone # 474 - 9241, Fax # 261 - 9534

Remarks:

University of Manitoba
Geotechnical Laboratory

T7 - p' vs q

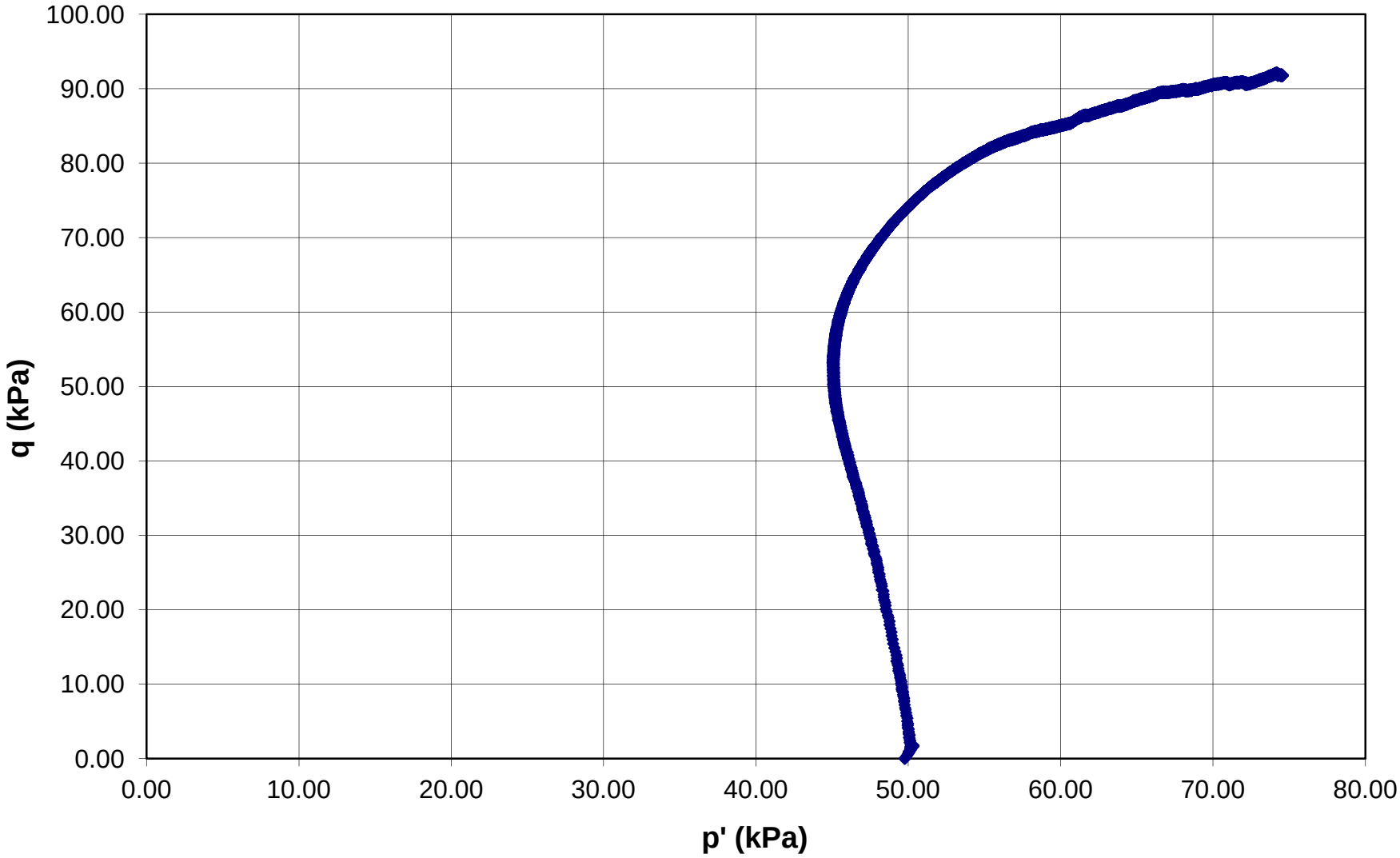

University of Manitoba
Geotechnical Laboratory

T7 -Deviatoric Stress vs Strain

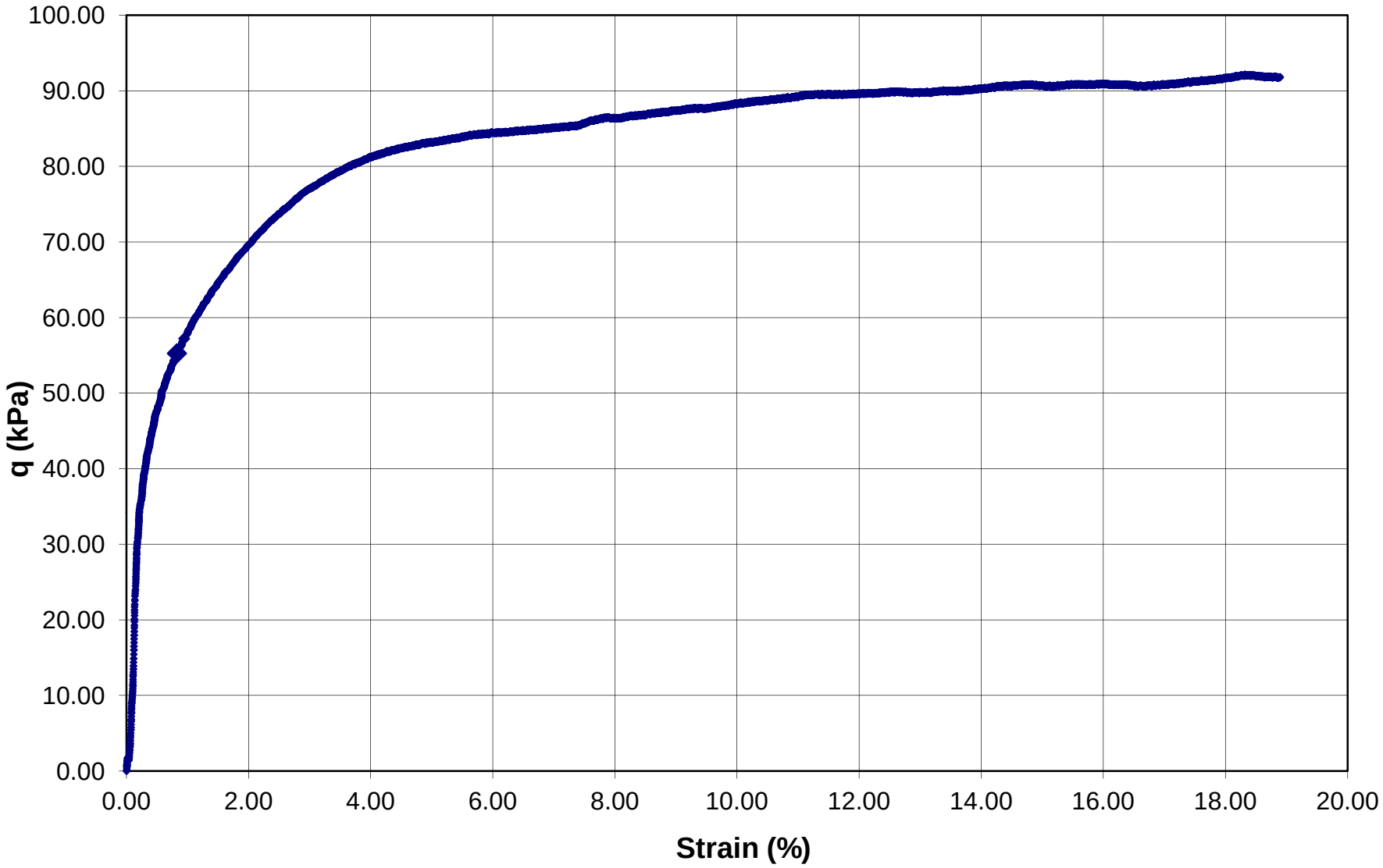

TRIAXIAL TESTING

Date Received:	**2012-01-12**
Date Tested:	
Date Completed:	
Client:	**MIT Region 4**
Project:	**PTH 5 & 10 Slope Stabilization**
Location:	**Dauphin, Mb**
Sample #	**T7**
Hole #	**SI/VW2011-06**
Depth:	**3.25 m**
Tested By:	**J Fiebelkorn**

Material Description

Material:	**Clay Till**
Color:	**Brown mottled grey**
Composition:	**Silty, trace sand, trace gravel, trace oxidation,**
	trace to some sulfates
Odor:	**Nil**
Structure:	**Random**
Consistency:	**Firm to stiff**

REMARKS: **Some stones and gypsum crystals removed, voids filled with cuttings**

Initial Water Content

Container No.	T7	
Wet+Tare:	**132.27**	g
Dry+Tare	**110.45**	g
Wt. Water	21.82	g
Tare:	**31.63**	g
Wt. Dry:	78.82	g
Water Cont.	27.68%	
Avg. Water Content =		

Initial Density Measurements

Wt. sample wet **1221.13** g.

Diam. (mm.)	**73.42**	**73.58**	**73.44**	**73.60**	Avg.=	73.51	mm.
Length (mm)	**149.12**	**149.02**	**149.02**	**149.06**	Avg.=	149.06	mm.

Area=	42.42	cm^2	Gs =	**2.72**
Volume=	632.28	cm^3	e =	0.798
Wet Density=	1.931	Mg/m^3	Sr =	
Dry Density=	1.513	Mg/m^3	n =	

Final Water Content

Container No.	T7TA	
Wet+Tare:	**119.72**	g
Dry+Tare	**98.45**	g
Wt. Water	21.27	g
Tare:	**18.66**	g
Wt. Dry:	79.79	g
Water Cont.	26.66%	
Avg. Water Content=		

Final Density Measurements

Wt. sample wet **1233.65** g.

Diam. (mm.)	**75.32**	**86.04**	**75.10**	**81.78**	Avg.=	79.56	mm.
Length (mm)	**149.12**	**122.86**	**123.02**	**122.66**	Avg.=	129.42	mm.

Area =	49.69	cm^2	Gs =	**2.72**
Volume =	643.05	cm^3	e =	0.796
Wet Density =	1.918	Mg/m^3	Sr =	
Dry Density =		Mg/m^3	n =	

Notes:

University of Manitoba
Geotechnical Laboratory

T8 - Deviatoric Stress vs Strain

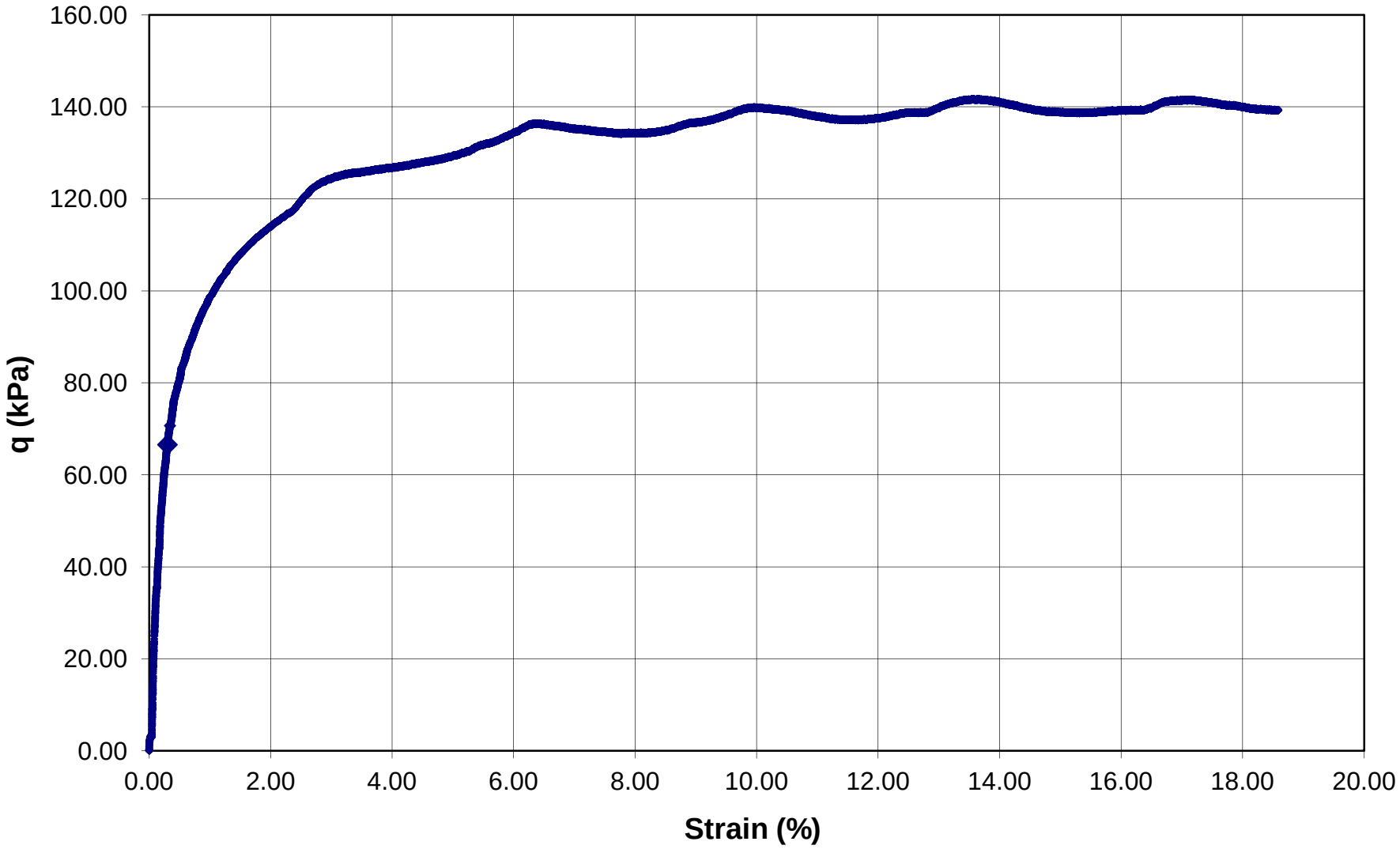

TRIAXIAL TESTING

Date Received:	**2012-01-12**
Date Tested:	
Date Completed:	
Client:	**MIT Region 4**
Project:	**PTH 5 & 10 Slope Stabilization**
Location:	**Dauphin, Mb**
Sample #	**T8**
Hole #	**SI/VW2011-06**
Depth:	**3.8m**
Tested By:	**J Fiebelkorn**

Material Description

Material:	**Clay Till**
Color:	**Brown mottled grey**
Composition:	**Silty, trace sand, trace gravel, trace oxidation, trace to some sulfates**
Odor:	**Nil**
Structure:	**Random**
Consistency:	**Firm to stiff**

REMARKS: **Some stones and gypsum crystals removed, voids filled with cuttings**

Initial Water Content

Container No.	T8	
Wet+Tare:	**96.73**	g
Dry+Tare	**83.08**	g
Wt. Water	13.65	g
Tare:	**30.96**	g
Wt. Dry:	52.12	g
Water Cont.	26.19%	
Avg. Water Content =		

Initial Density Measurements

Wt. sample wet **1169.7** g.

Diam. (mm.)	**72.96**	**72.24**	**72.48**	**72.86**	Avg.=	72.64	mm.
Length (mm)	**142.96**	**143.08**	**143.10**	**143.22**	Avg.=	143.09	mm.

Area=	41.42	cm^2	Gs =	**2.72**
Volume=	592.61	cm^3	e =	0.739
Wet Density=	1.974	Mg/m^3	Sr =	
Dry Density=	1.564	Mg/m^3	n =	

Final Water Content

Container No.	T8TA	
Wet+Tare:	**137.43**	g
Dry+Tare	**110.77**	g
Wt. Water	26.66	g
Tare:	**23.85**	g
Wt. Dry:	86.92	g
Water Cont.	30.67%	
Avg. Water Content=		

Final Density Measurements

Wt. sample wet **1171.69** g.

Diam. (mm.)	**85.76**	**73.86**	**83.68**	**79.44**	Avg.=	80.69	mm.
Length (mm)	**116.30**	**117.48**	**116.56**	**116.30**	Avg.=	116.66	mm.

Area =	51.10	cm^2	Gs =	**2.72**
Volume =	596.18	cm^3	e =	0.808
Wet Density =	1.965	Mg/m^3	Sr =	
Dry Density =		Mg/m^3	n =	

Notes:

University of Manitoba
Geotechnical Laboratory

Sample T9 - Deviatoric Stress vs Strain

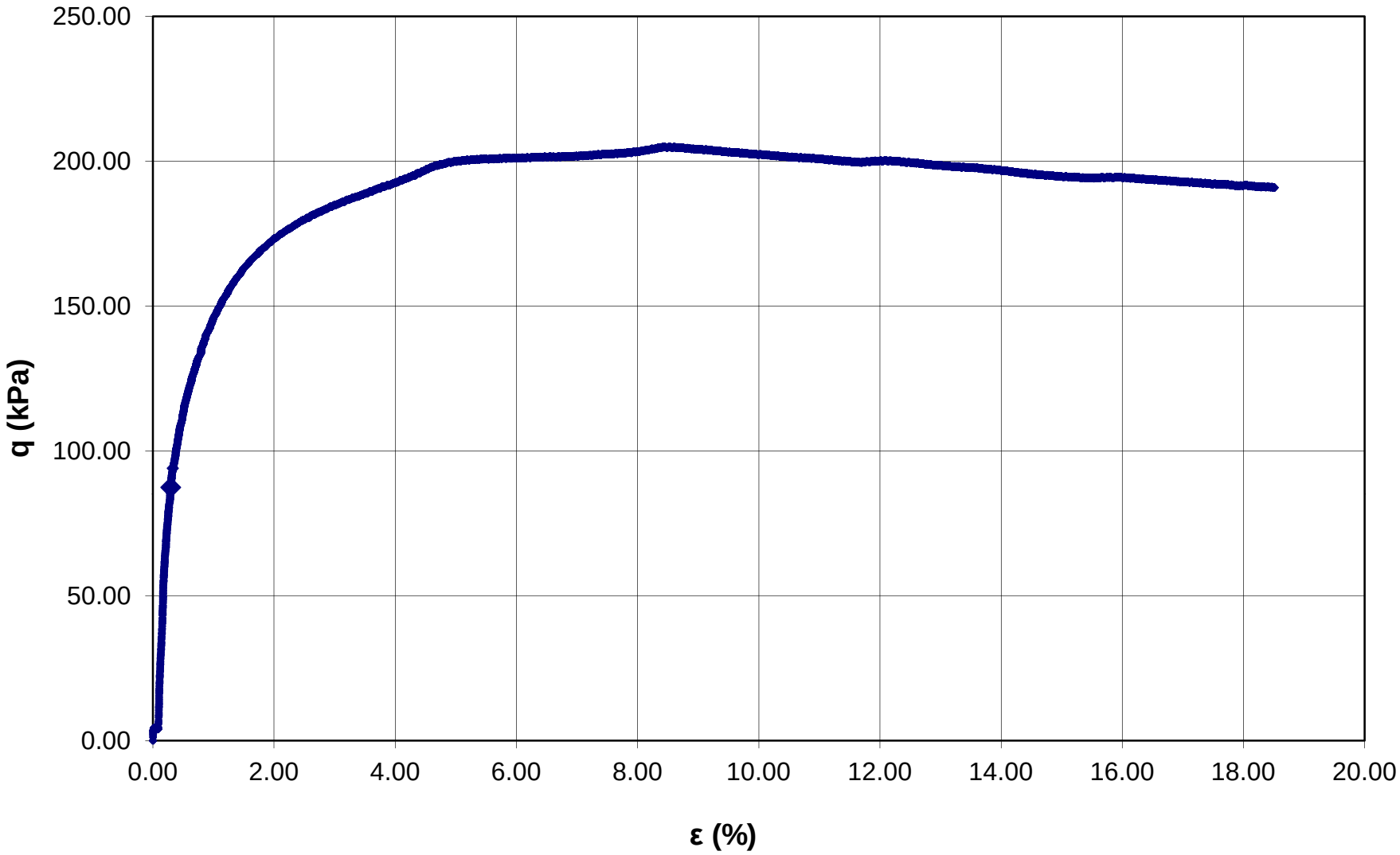

TRIAXIAL TESTING

Date Received:	**2012-01-12**
Date Tested:	
Date Completed:	
Client:	**MIT Region 4**
Project:	**PTH 5 & 10 Slope Stabilization**
Location:	**Dauphin, Mb**
Sample #	**T9**
Hole #	**SI/VW2011-06**
Depth:	**4.45**
Tested By:	**J Fiebelkorn**

Material Description

Material: **Clay Till**
Color: **Brown mottled grey**
Composition: **Silty, trace sand, trace gravel, trace oxidation, trace to some sulfates**
Odor: **Nil**
Structure: **Random**
Consistency: **Firm to stiff**

REMARKS: **Some stones and gypsum crystals removed, difficult to trim, voids filled with cuttings**

Initial Water Content

Container No.	T9	
Wet+Tare:	**94.58**	g
Dry+Tare	**77.78**	g
Wt. Water	16.8	g
Tare:	**18.63**	g
Wt. Dry:	59.15	g
Water Cont.	28.40%	
Avg. Water Content =		

Initial Density Measurements

Wt. sample wet **1183.34** g.

Diam. (mm.)	**73.14**	**71.50**	**72.42**	**72.80**	Avg.=	72.47 mm.
Length (mm)	**143.48**	**142.98**	**143.24**	**143.02**	Avg.=	143.18 mm.

Area=	41.22	cm^2	Gs =	**2.72**
Volume=	590.21	cm^3	e =	0.742
Wet Density=	2.005	Mg/m^3	Sr =	
Dry Density=	1.561	Mg/m^3	n =	

Final Water Content

Container No.	T9	
Wet+Tare:	**97.78**	g
Dry+Tare	**80.02**	g
Wt. Water	17.76	g
Tare:	**18.64**	g
Wt. Dry:	61.38	g
Water Cont.	28.93%	
Avg. Water Content=		

Final Density Measurements

Wt. sample wet **1191.79** g.

Diam. (mm.)	**85.62**	**74.92**	**77.76**	**85.24**	Avg.=	80.89 mm.
Length (mm)	**117.56**	**118.04**	**117.88**	**118.14**	Avg.=	117.91 mm.

Area =	51.36	cm^2	Gs =	**2.72**
Volume =	605.53	cm^3	e =	0.782
Wet Density =	1.968	Mg/m^3	Sr =	
Dry Density =		Mg/m^3	n =	

Notes:

Appendix E – Design Cross Sections

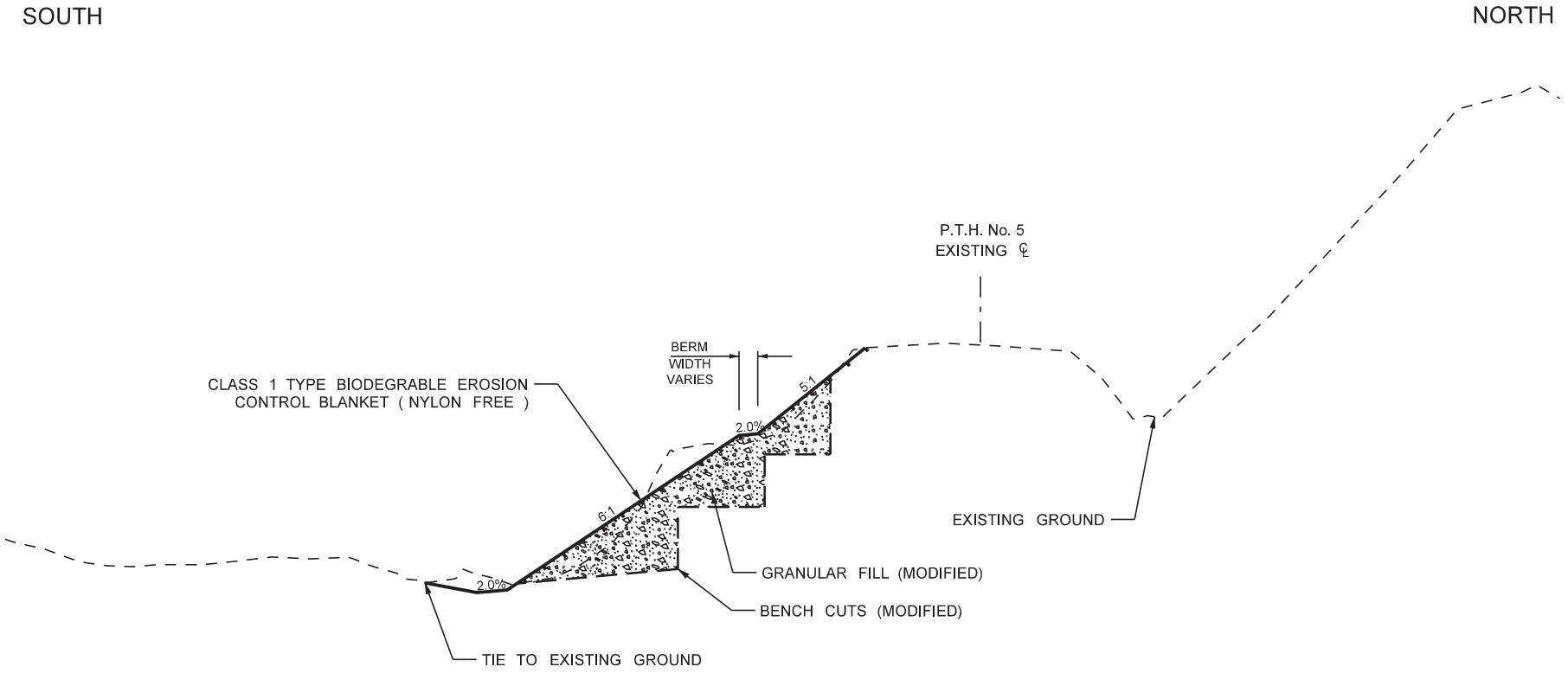

CROSS SECTION DETAIL

P.T.H. No. 5

@ STA. 185+00.000

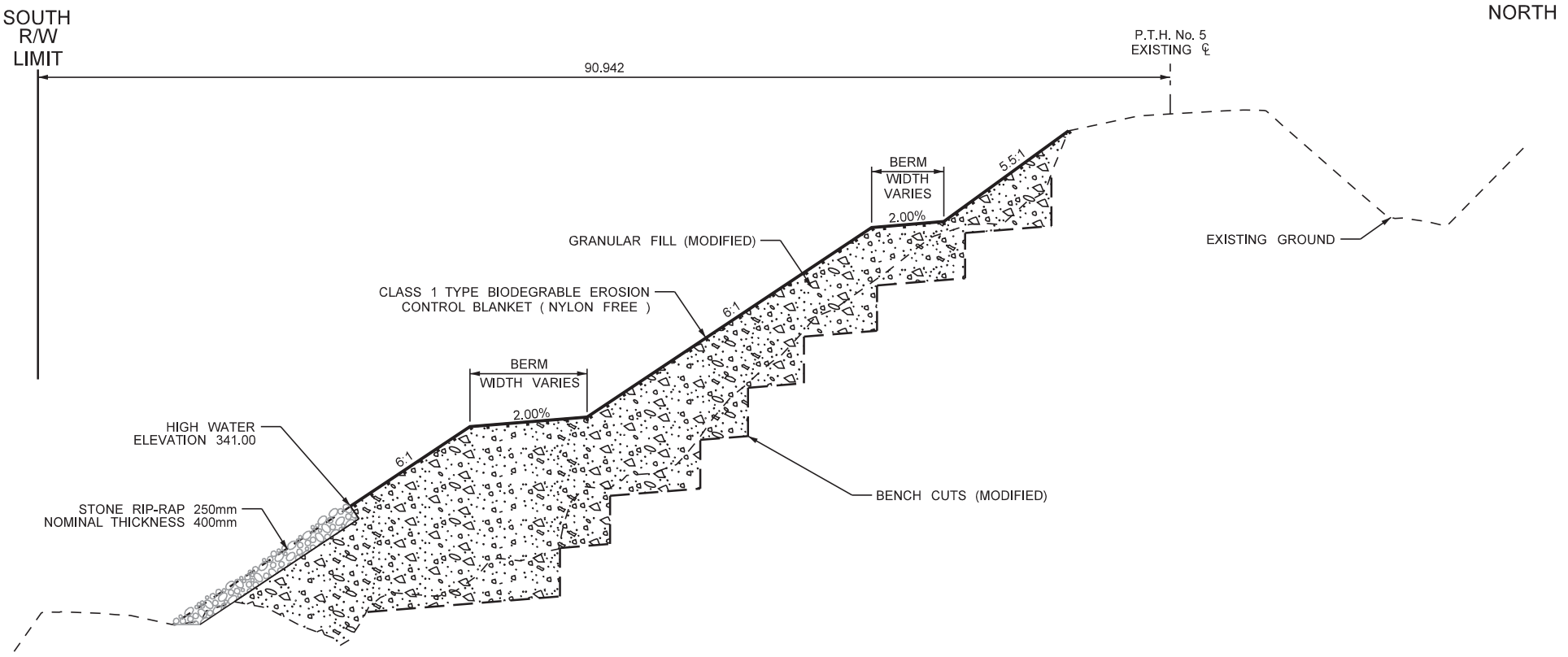

CROSS SECTION DETAIL

P.T.H. No. 5

@ STA. 185+85.000

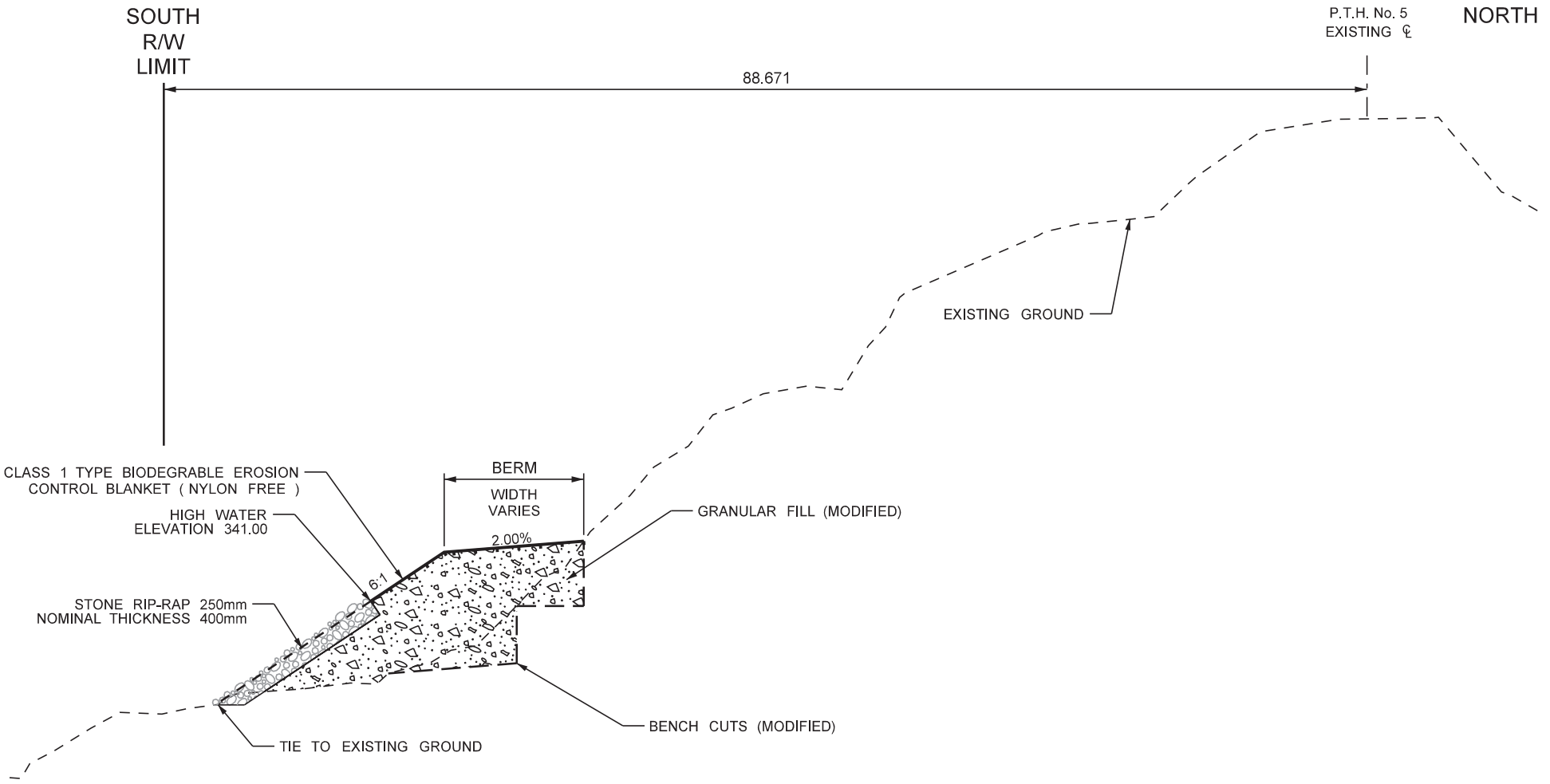

CROSS SECTION DETAIL

P.T.H. No. 5

@ STA. 186+50.000